AEDC-TR-78-4
AFATL-TR-77-110

cy.2

RESULTS OF A WIND TUNNEL AND FLIGHT TEST PROGRAM TO DEVELOP A MAXIMUM VOLUME BOMB (MVB) CONFIGURATION FOR MULTIPLE CARRIAGE AND SEPARATION FROM TACTICAL AIRCRAFT AT MACH NUMBERS FROM 0.50 TO 1.10

David W. Hill, Jr.
ARO, Inc., a Sverdrup Corporation Company

PROPULSION WIND TUNNEL FACILITY
ARNOLD ENGINEERING DEVELOPMENT CENTER
AIR FORCE SYSTEMS COMMAND
ARNOLD AIR FORCE STATION, TENNESSEE 37389

May 1978

Final Report for Period February 4, 1975 - May 21, 1976

Approved for public release; distribution unlimited.

Prepared for

AIR FORCE ARMAMENT LABORATORY/DLJC
EGLIN AFB, FLORIDA 32542

NOTICES
When U. S. Government drawings, specifications, or other data are used for any purpose other than a definitely related Government procurement operation, the Government thereby incurs no responsibility nor any obligation whatsoever, and the fact that the Government may have formulated, furnished, or in any way supplied the said drawings, specifications, or other data, is not to be regarded by implication or otherwise, or in any manner licensing the holder or any other person or corporation, or conveying any rights or permission to manufacture, use, or sell any patented invention that may in any way be related thereto.
Qualified users may obtain copies of this report from the Defense Documentation Center.
References to named commerical products in this report are not to be considered in any sense as an indorsement of the product by the United States Air Force or the Government.

This report has been reviewed by the Information Office (OI) and is releasable to the National Technical Information Service (NTIS). At NTIS, it will be available to the general public, including foreign nations.

APPROVAL STATEMENT

This report has been reviewed and approved.

James M. McGee

JAMES M. McGEE, 2d Lt, USAF
Test Director, PWT Division
Directorate of Test Operations

Approved for publication:

FOR THE COMMANDER

Chauncey D. Smith, Jr.

CHAUNCEY D. SMITH, JR, Lt Colonel, USAF
Director of Test Operations
Deputy for Operations

REPORT DOCUMENTATION PAGE	READ INSTRUCTIONS BEFORE COMPLETING FORM
1 REPORT NUMBER AEDC-TR-78-4 AFATL-TR-77-110 2 GOVT ACCESSION NO.	3 RECIPIENT'S CATALOG NUMBER
4 TITLE (and Subtitle) RESULTS OF A WIND TUNNEL AND FLIGHT TEST PROGRAM TO DEVELOP A MAXIMUM VOLUME BOMB (MVB) CONFIGURATION FOR MULTIPLE CARRIAGE AND SEPARATION FROM TACTICAL AIRCRAFT AT MACH NUMBERS FROM 0.50 TO 1.10	5 TYPE OF REPORT & PERIOD COVERED Final Report-February 4, 1975 - May 21, 1976 6 PERFORMING ORG REPORT NUMBER
7 AUTHOR(s) David W. Hill, Jr., ARO, Inc.	8 CONTRACT OR GRANT NUMBER(s)
9 PERFORMING ORGANIZATION NAME AND ADDRESS Arnold Engineering Development Center/DO Air Force Systems Command Arnold Air Force Station, Tennessee 37389	10 PROGRAM ELEMENT PROJECT TASK AREA & WORK UNIT NUMBERS Program Element 62602F Project 2567, Task 02
11 CONTROLLING OFFICE NAME AND ADDRESS Air Force Armament Laboratory/DLJC Eglin AFB, Florida 32542	12 REPORT DATE May 1978 13 NUMBER OF PAGES 173
14 MONITORING AGENCY NAME & ADDRESS (if different from Controlling Office)	15 SECURITY CLASS (of this report) UNCLASSIFIED 15a DECLASSIFICATION DOWNGRADING SCHEDULE N/A

16 DISTRIBUTION STATEMENT (of this Report)

Approved for public release; distribution unlimited.

17 DISTRIBUTION STATEMENT (of the abstract entered in Block 20, if different from Report)

18 SUPPLEMENTARY NOTES

Available in DDC

19 KEY WORDS (Continue on reverse side if necessary and identify by block number)

wind tunnel tests	separation	static stability
flight testing	Mach numbers	dynamics
maximum volume bomb (MVB)	F-4C aircraft	stability
carriages	A-7D aircraft	

20 ABSTRACT (Continue on reverse side if necessary and identify by block number)

Wind tunnel tests, supported by flight test data, were conducted in order to determine separation characteristics of a 16-in.-diam maximum volume bomb (MVB) from the inboard-pylon triple ejection rack (TER) on the F-4C aircraft. The wind tunnel tests were conducted in the Aerodynamic Wind Tunnels (1T) and (4T) of the Propulsion Wind Tunnel Facility (PWT) to obtain static and dynamic stability data on the store in the free stream, and

DD FORM 1 JAN 73 1473 EDITION OF 1 NOV 65 IS OBSOLETE

20. ABSTRACT (Continued)

captive trajectory data on the store when released from the F-4C and A-7D aircraft. The fins of the MVB were canted from 0 to -12 deg, with and without fin tabs, to assess their effectiveness in reducing the severe nose-down pitch motion encountered during separation at high subsonic Mach numbers. The tests were conducted at Mach numbers from 0.50 to 1.10 at simulated pressure altitudes of 5,000 and 20,000 ft. The wind tunnel tests indicated, at all Mach numbers, that the nose-down pitch motion of the store was significantly reduced by canting the fins. However, the flight tests at Mach number 0.90 indicated that the severe nose-down pitch motion continued even with the canted fins. The in-flight film data showed that collision occurred between the MVB tail-fin tabs and the fins of the adjacent stores. This "hang-up" of the tail fins resulted in a pivotal, or constrained, motion up to -40 deg pitch angle.

PREFACE

The work reported herein was conducted by the Arnold Engineering Development Center (AEDC), Air Force Systems Command (AFSC), at the request of the Air Force Armament Laboratory (AFATL/DLJC), AFSC, under Program Element 62602F, Project 2567, Task 02. The AFATL project monitor was Maj. R. Van Putte. The results were obtained by ARO, Inc., AEDC Division (a Sverdrup Corporation Company), operating contractor for the AEDC, AFSC, Arnold Air Force Station, Tennessee. The tests were conducted under ARO Project No. P41C-79A. Data reduction was completed in January 1977, and the manuscript was submitted for publication on December 21, 1977.

CONTENTS

Page

1.0 INTRODUCTION 9
2.0 APPARATUS
2.1 Test Facility 10
2.2 Test Articles 11
2.3 Instrumentation 12
3.0 TEST DESCRIPTION
3.1 Test Conditions 13
3.2 Dynamic Stability Data Acquisition 13
3.3 Static Stability Data Acquisition 13
3.4 Trajectory Data Acquisition 13
3.5 Corrections 14
3.6 Precision of Data 14
4.0 RESULTS AND DISCUSSION
4.1 Static Stability Data 15
4.2 Aerodynamic Data in the F-4C Aircraft Flow Field 17
4.3 Separation Trajectories from the F-4C Aircraft 17
4.4 Separation Trajectories from the A-7D Aircraft 18
4.5 Wind Tunnel and Flight Test Separation Trajectories from the F-4C Aircraft 18
4.6 Dynamic Stability Data 21
5.0 SUMMARY OF RESULTS 22
REFERENCES 23

ILLUSTRATIONS

Figure

1. Typical Store Separation Installation and a Block Diagram of the Computer Control Loop 25
2. Tunnel 4T Test Section Showing Aircraft Model Locations 26
3. Tunnel Test Section and Installation Details of the 0.25-Scale MVB Model 28
4. Tunnel 1T Dynamic Damping Rig Showing Installation of 0.075-Scale MVB 29
5. Aircraft Models 30
6. Details of the Aircraft Pylons 32
7. Details and Dimensions of the Aircraft TER Models 34

Figure | Page

8. Details and Dimensions of the A-7D MER Model 36
9. Details and Dimensions of the F-4C Outboard 370-gal Fuel Tank Model 37
10. Details and Dimensions of the 0.05-Scale MVB Model 38
11. Tunnel 4T Installation Photograph of F-4C Aircraft, MVB, and CTS 39
12. Details and Dimensions of the 0.25-Scale MVB Model 40
13. Tunnel 4T Installation Photograph of 0.25-Scale MVB Model 42
14. Tunnel 1T Installation Photograph of 0.075-Scale MVB Model with Interchangeable Tails 43
15. Installation Photograph of Full-Scale MVB on TER and F-4C Aircraft 44
16. MER and TER Store Stations and Orientations 46
17. Comparison of Wind Tunnel 0.25-Scale MVB Static Stability Data with Predicted Data of CAMS 47
18. Effects of Fuze, Tabs, and Fins on the 0.25-Scale MVB Static Stability 51
19. Effects of Fuze and Tabs on the MVB Static Stability, Fins Canted 55
20. Effects of Model Scale on the Static Stability of the MVB, Fins Canted 59
21. Effects of Reynolds Number on the MVB Static Stability 62
22. Aerodynamic Characteristics of the MVB in the F-4C Flow Field, Fins Uncanted 66
23. Aerodynamic Characteristics of the MVB in the F-4C Flow Field, Fins Canted 69
24. Variation of the Aerodynamic Coefficients of the MVB with Fin Cant Angle, Two Fins Canted 73
25. Variation of the Aerodynamic Coefficients of the MVB with Fin Cant Angle, Four Fins Canted 74
26. Wind Tunnel Separation Trajectories of the MVB from the No. 1 TER Station of the F-4C Aircraft, Four Fins Canted 75
27. Wind Tunnel Separation Trajectories of the MVB from the No. 1 TER Station of the F-4C Aircraft, Two Fins Canted 83

Figure | Page

28. Wind Tunnel Separation Trajectories of the MVB from the No. 2 TER Station of the F-4C Aircraft. Two Fins Canted 91
29. Wind Tunnel Separation Trajectories of the MVB from the No. 3 TER Station of the F-4C Aircraft, Two Fins Canted 95
30. Wind Tunnel Separation Trajectories of the MVB with Simulation of Fins Returned from -12 to 0 deg during the Trajectory 99
31. Illustration of MVB Trajectories with Simulation of Fins Returned from -12 to 0 deg Cant 103
32. Wind Tunnel Separation Trajectories of the MVB from the A7-D Aircraft at M_∞ = 0.90 105
33. Wind Tunnel Captive Trajectory and Flight Test Separation Trajectories of the MVB with Uncanted Fins, M_∞ = 0.50 115
34. Illustration of Wind Tunnel Captive Trajectory and Flight Test Separation Trajectories of the MVB with Uncanted Fins, M_∞ = 0.50 119
35. Release Sequence of the MVB with Uncanted Fins, No Tabs, M_∞ = 0.50 120
36. Wind Tunnel Captive Trajectory and Flight Test Separation Trajectories of the MVB with Uncanted Fins, M_∞ = 0.70 121
37. Illustration of Wind Tunnel Captive Trajectory and Flight Test Separation Trajectories of the MVB with Uncanted Fins, M_∞ = 0.70 123
38. Wind Tunnel Captive Trajectory and Flight Test Separation Trajectories of the MVB with Canted Fins, M_∞ = 0.70 124
39. Illustration of Wind Tunnel Captive Trajectory and Flight Test Separation Trajectories of the MVB with Canted Fins, M_∞ = 0.70 126
40. Release Sequence of the MVB at M_∞ = 0.70 127
41. Wind Tunnel Captive Trajectory and Flight Test Separation Trajectories of the MVB with Uncanted Fins, M_∞ = 0.90 128

Figure — Page

42. Illustration of Wind Tunnel Captive Trajectory and Flight Test Separation Trajectories of the MVB with Uncanted Fins, M_∞ = 0.90 130
43. Wind Tunnel Captive Trajectory and Flight Test Separation Trajectories of the MVB with Canted Fins, M_∞ = 0.90 131
44. Illustration of Wind Tunnel Captive Trajectory and Flight Test Separation Trajectories of the MVB with Canted Fins, M_∞ = 0.90 133
45. Wind Tunnel Captive Trajectory and Flight Test Separation Trajectories of the MVB with Canted Fins and Tabs. M_∞ = 0.90 134
46. Illustration of Wind Tunnel Captive Trajectory and Flight Test Separation Trajectories of the MVB with Canted Fins and Tabs, M_∞ = 0.90 136
47. Release Sequence of the MVB at M_∞ = 0.90 137
48. Wind Tunnel Captive Trajectory and Flight Test Separation Trajectories of the MVB with Uncanted Fins, No. 1 TER Station, M_∞ = 1.02 138
49. Illustration of Wind Tunnel Captive Trajectory and Flight Test Separation Trajectories of the MVB with Uncanted Fins, No. 1 TER Station, M_∞= 1.02 140
50. Wind Tunnel Captive Trajectory and Flight Test Separation Trajectories of the MVB with Uncanted Fins, No. 2 TER Station, M_∞= 1.02 141
51. Release Sequence of the MVB with Uncanted Fins, No Tabs, M_∞ = 1.02 143
52. Effects of Angle of Attack on the Pitch-Damping Derivative of the MVB 144

TABLES

1. Full-Scale Store Parameters 146
2. Identification of Captive Trajectory Test Configurations and Test Conditions for F-4C Aircraft 147
3. Identification of Captive Trajectory Test Configurations with Test Conditions for A-7D Aircraft 153

TABLES (Continued)

Page

4. Identification of Static Stability Test Conditions for the 0.05-Scale MVB Model 158
5. Identification of Static Stability Test Conditions for the 0.25-Scale MVB Model 161
6. Dynamic Stability Test Configurations and Test Conditions for the 0.075-Scale MVB Model 168
7. Typical Uncertainties for Force and Moment Coefficient Data and Trajectory Data 169

NOMENCLATURE 170

1.0 INTRODUCTION

Store separation problems have been encountered during release of large diameter stores from the triple ejection rack (TER) on the inboard pylon of the F-4C aircraft. The maximum store diameter is limited to approximately 16 in. for multiple carriage on the TER. The most rapid nose-down pitch motion occurs for release from the bottom station of the TER at Mach numbers greater than 0.70. The excessive nose-down pitch is undesirable, and in some cases unacceptable, from the standpoint of aircraft safety and munition delivery. Previous wind tunnel tests have shown that there is a large pressure buildup in the nose cavity region of the cluster of three stores. and an upwash flow field near the store afterbody. The resulting curvilinear flow field over the store is somewhat decreased as the store diameter is decreased from 16 to 12 in. In fact, 12-in.-diam stores have been successfully released (Ref. 1) up to Mach number 1.20. However, the purpose of carrying 16-in.-diam stores is to provide maximum payload for the aircraft. As a result of the stores being closely clustered, there is minimal space for providing a large fin area to increase the static stability of the store. Some 16-in.-diam weapons contain "pop-out" fins for deployment after the store is released, but the increased static margin is to little avail as the store nose-down angular acceleration is too great to be overcome. There has been one wind tunnel test in which the TER geometry was modified to allow better flow characteristics around the adjacent stores. but these modifications did not show much improvement on the separation trajectories.

The Air Force Armament Laboratory (AFATL) sponsored a program for the aerodynamic design of a 16-in.-diam store that would separate from the TER station without severe nose-down pitch motion. The store would generally be used for a munition dispenser. The design requirements for the store were to be the following:

Aircraft release Mach number	0.90
Aircraft release altitude	5,000 ft
Store length (including fuze)	92 in.
Store diameter	16 in.
Maximum fin span	22 in.
Hemispherical nose radius	8 in.
Store weight	800 lb
Moment of inertia	65 slug-ft^2
Center-of-gravity location from nose (without fuze)	36.5 in.

These dimensions were selected to provide maximum payload when installed on a TER. Henceforth in this report, the store designed to these criteria will be referred to as the maximum volume bomb (MVB).

After review of past wind tunnel data, it appeared that successful release over the complete speed range would require the imposition of a compensating nose-up moment on the store during the initial release motion. The amount of the required moment varied directly with the magnitude of the offending aerodynamic moment. It was thus concluded that the best approach would be to use aerodynamic means to provide the compensating forces. The solution suggested by the present evaluation was to utilize the tail fins (needed anyway for basic aerodynamic stability) to generate the necessary loads. The tail fins would be rotated (canted) to a leading-edge-down attitude while the store is carried on the rack and during the initial release period. When the store has moved a short distance away from the rock (approximately one body diameter), the fins would be returned by a lanyard to the normal symmetric position. Wind tunnel and flight tests were conducted to determine if this technique were feasible.

The wind tunnel tests were conducted in the Aerodynamic Wind Tunnel (4T) (Tunnel 4T) of the Propulsion Wind Tunnel Facility (PWT). The aerodynamic loads test, dynamic stability test, and captive trajectory tests covered a Mach number range from 0.50 to 1.10. The simulated flight altitude for the captive trajectory tests was 5,000 ft. The flight tests were conducted at Eglin AFB and covered a Mach number range from 0.50 to 1.02, with a release altitude of 5,000 ft.

2.0 APPARATUS

2.1 TEST FACILITY

Tunnel 4T is a closed-loop, continuous flow, variable density tunnel in which the Mach number can be varied from 0.10 to 1.30. At all Mach numbers, the stagnation pressure can be varied from 300 to 3,700 psfa. The test section is 4 ft square and 12.5 ft long with perforated, variable porosity (0.5- to 10-percent open) walls. It is completely enclosed in a plenum chamber from which the air can be evacuated, allowing part of the tunnel airflow to be removed through the perforated walls of the test section. A more thorough description of the tunnel is given in Ref. 2.

The Aerodynamic Wind Tunnel (1T) (Tunnel 1T) of PWT is a continuous flow wind tunnel capable of being operated at Mach numbers from 0.20 to 1.50 utilizing variable nozzle contours above M_∞ = 1.00. The tunnel is operated at a stilling chamber total pressure of approximately 2.850 psfa. The test section is 1 ft square and 3.13 ft long

with six-percent-open area, inclined, perforated walls. A more thorough description of the tunnel is given in Ref. 2.

For store separation testing in Tunnel 4T, two separate and independent support systems were used to support the models. The aircraft model was inverted in the test section and supported by an offset sting attached to the main pitch sector. The store model was supported by the captive trajectory support (CTS) which extends down from the tunnel top wall and provides store movement (six degrees of freedom) independent of the aircraft model. An isometric drawing of a typical store separation installation is shown in Fig. 1.

Also shown in Fig. 1 is a block diagram of the computer control loop used during captive trajectory testing. The analog system and the digital computer work as an integrated unit and, utilizing required input information, control the store movement during a trajectory. Store positioning is accomplished by use of six individual d-c electric motors. Maximum translational travel of the CTS is ±15 in. from the tunnel centerline in the lateral and vertical directions and 36 in. in the axial direction. Maximum angular displacements are ±45 deg in pitch and yaw and ±360 deg in roll. A schematic showing the test section details of the models in the tunnel is shown in Fig. 2.

For static force testing in Tunnel 4T, the model support system consisted of a pitch sector strut and sting attachment which had a pitch capability of -6 to 26 deg with respect to the tunnel centerline and a roll capability of -180 to 180 deg with respect to the sting centerline. A schematic of the test section showing the location of the models is presented in Fig. 3.

For dynamic testing in Tunnel 1T, the model support system consisted of a sting attached to a free-oscillation mechanism mounted on top of the test section. The model was mounted on a circular strut perpendicular to the model longitudinal axis and through the center of gravity. The pitch capability of the mechanism was -90 to 90 deg with respect to the tunnel centerline. A schematic of the mechanism and location of the model is shown in Fig. 4.

2.2 TEST ARTICLES

For CTS testing, the test articles were 0.05-scale models of the MVB and the A-7D and F-4C aircraft. Because of interference with the CTS sting, the horizontal stabilizers of both aircraft models were removed for these tests. Dimensional sketches of the F-4C and A-7D aircraft models are shown in Fig. 5. Details and dimensions of the pylon, TER, MER, and 370-gal fuel tank models are shown in Figs. 6 through 9. Details and

dimensions of the 0.05-scale MVB model used for trajectory testing are shown in Fig. 10. The 5- and 8-in. hinge lines are noted in the figure. For the 5-in. hinge line, the four tail-fin root chords were contoured to fit the boattail (no gap), whereas with the 8-in. hinge line the tail-fin root chord was straight and the fin was mounted directly (gap) to the boattail body by means of the hinge. Figure 11 is a photograph showing the 0.05-scale MVB installed on the CTS sting and the installation of the F-4C aircraft.

Details and dimensions of the 0.25-scale MVB model used for static stability testing are shown in Fig. 12. The tail fins were mounted at the 5-in. hinge line, and interchangeable fins were provided so that varying gap configurations could be simulated. Figure 13 is a photograph showing the 0.25-scale MVB installation.

Figure 14 is a photograph showing the 0.075-scale MVB model installed for dynamic stability testing in Tunnel 1T, along with the various interchangeable afterbody sections. Figure 15 is a photograph showing the full-scale MVB installed on the TER of the F-4C aircraft.

2.3 INSTRUMENTATION

For CTS testing, a 0.3-in.-diam, six-component, internal strain-gage balance was used to obtain the force and moment data on the MVB model. The F-4C and A-7D aircraft angle of attack was set using a gravimetric angular position indicator located in the nose of each aircraft model. Translational and angular positions of the store model were obtained from the CTS analog inputs. The pylons and racks were instrumented with touch wires to indicate when the MVB model was in its carriage position. The system was also electrically connected to automatically stop the CTS and main pitch sector movements if the store or CTS rig contacted the aircraft model, sting, or the test section walls.

For static stability testing, a 0.8-in.-diam, six-component balance was used to measure the MVB aerodynamic loads.

The dynamic stability tests used the free-oscillation technique, and the model position was measured with a strain-gaged beam. A signal proportional to model oscillation amplitude was conditioned and recorded on an oscillograph, on a damping system that instantaneously records cycles to decay to one-half amplitude, and on magnetic tape for offline data reduction. Model angle of attack was measured with a linear potentiometer which was mounted between the inner and outer shells of the test mechanism. All of the online signals were input into a digital computer for reduction to aerodynamic coefficients.

3.0 TEST DESCRIPTION

3.1 TEST CONDITIONS

Separation trajectory data were obtained at Mach numbers from 0.50 to 1.10. Tunnel dynamic pressure ranged from 200 psf at M_∞ = 0.50 to 1,200 psf at M_∞ = 1.10, and tunnel stagnation temperature was maintained near 90 °F.

Tunnel conditions were held constant at the desired Mach number and stagnation pressure while data for trajectory, static stability, and dynamic stability were obtained. The trajectories were terminated when the store or sting contacted the aircraft model or a CTS limit was reached. The static stability data acquisition was terminated when the desired angle-of-attack range was obtained. The dynamic stability data acquisition was terminated when sufficient model oscillation frequency data were obtained. Full-scale store parameters of the MVB used in the wind tunnel trajectories are listed in Table 1. Configurations and test conditions are listed in Tables 2 through 6.

3.2 DYNAMIC STABILITY TEST DATA ACQUISITION

The model was initially deflected to 4 deg and then released. During the decay period, data were recorded on a damping meter and a magnetic tape system. An oscillograph was used to monitor the balance system. Data points at a given test condition were continued until repeatability was observed.

3.3 STATIC STABILITY DATA ACQUISITION

After the desired test conditions were established in the tunnel, control of the MVB model support was switched to the automatic model attitude positioning system (AMAPS). The AMAPS is a computer-controlled system which automatically steps the model through a preprogrammed sequence of model attitudes and takes data at each set position. Model pitch and roll angles were used by the AMAPS to generate combinations of angle of attack and sideslip. Model parameters used in the reduction of force and moment data to aerodynamic coefficients are presented in Table 1.

3.4 TRAJECTORY DATA ACQUISITION

To obtain a trajectory, test conditions were established in the tunnel and the aircraft model was positioned at the desired angle of attack. The store model was then oriented to a position corresponding to the store carriage location. After the store was set at the desired initial position, operational control of the CTS was switched to the digital computer which controlled the store movement during the trajectory through commands

to the CTS analog system (see block diagram, Fig. 1). Data from the wind tunnel, consisting of measured model forces and moments, wind tunnel operating conditions, and CTS rig positions were input to the digital computer for use in the full-scale trajectory calculations.

The digital computer was programmed to solve the six-degree-of-freedom equations to calculate the angular and linear displacements of the store relative to the aircraft pylon. In general, the program involved using the last two successive measured values of each static aerodynamic coefficient to predict the magnitude of the coefficients over the next time interval of the trajectory. These predicted values were used to calculate the new position and attitude of the store at the end of the time interval. The CTS was then commanded to move the store model to this new position, and the aerodynamic loads were measured. If these new measurements agreed with the predicted values, the process was continued over another time interval of the same magnitude. If the measured and predicted values did not agree within the desired precision, the calculation was repeated over a time interval one-half the previous value. This process was repeated until a complete trajectory had been obtained.

In applying the wind tunnel data to the calculations of the full-scale store trajectories, the measured forces and moments were reduced to coefficient form and then applied with proper full-scale store dimensions and flight dynamic pressure. Dynamic pressure was calculated using a flight velocity equal to the free-stream velocity component plus the components of store velocity relative to the aircraft, and a density corresponding to the simulated altitude.

The initial portion of each launch trajectory incorporated simulated ejector forces in addition to the measured aerodynamic forces acting on the store. The ejector force was considered to act perpendicular to the rack or pylon mounting surface. The locations of the applied ejector forces and other full-scale store parameters used in the trajectory calculations are listed in Table 1.

3.5 CORRECTIONS

Balance, sting, and support deflections caused by the aerodynamic loads on the models were accounted for in the data reduction program to calculate the true model angles. Corrections were also made for model weight tares to calculate the net aerodynamic forces on the store model.

3.6 PRECISION OF DATA

Accuracy of the data presented was affected by such quantities as uncertainties in setting tunnel conditions, sensitivity of the balance, and, in separation testing, the CTS

rig positions. Typical uncertainties in the data for both the static stability and trajectory tests are presented in Table 7. The values presented are for the sets of conditions that produced the largest uncertainties and were determined for a confidence level of 95 percent. The estimated uncertainties in Mach number and angle-of-attack setting are ±0.005 and ±0.1, respectively.

4.0 RESULTS AND DISCUSSION

Wind tunnel and flight test trajectory data were obtained on the MVB for determining the feasibility of canting the tail fins and thus reducing the large nose-down pitch motion during separation from the TER at the design Mach number of 0.90. To verify that the aerodynamic data obtained during a trajectory with the 0.05-scale MVB model were representative of the full-scale MVB, the following data were obtained:

1. Both the 0.05- and 0.25-scale models were tested in the free stream to assess the effects of model scale, Reynolds number, and location of the fin hinge line on the static stability of the MVB.

2. Free-stream dynamic stability data were obtained with 0.075-scale MVB models. These values of pitch-damping derivatives were used in the wind tunnel trajectory simulations.

Separation trajectory data were also obtained from the A-7D aircraft to assess the separation characteristics of the MVB from aircraft other than the F-4C.

4.1 STATIC STABILITY DATA

Static stability data for the MVB are presented in Figs. 17 through 21. Plots of C_N versus α_s and C_m are presented for Mach numbers 0.50, 0.70, 0.90, and 1.10. Included in the figures are effects of model size (0.05- and 0.25-scale) and Reynolds number on the static stability of the MVB. Typical stability data are presented for fin roll angles of zero and 45 deg. The roll angle of zero deg represents the fin orientation for the MVB in the No. 1 TER position. A complete listing of the configurations and test conditions for both the 0.05- and 0.25-scale static stability data is given in Tables 4 and 5. Figure 17 presents the static stability data for the 0.25-scale MVB for fin cant angles of zero deg and fin roll orientation of 45 deg. A comparison of values predicted by the CAMS computer program (Ref. 3) with the experimental data is shown for each Mach number. The fin planform was chosen so as to give the best static margin over the Mach number range. Since the fin span of the MVB was limited (22 in.) by the small interstore clearance on the TER, the tail-fin planform was varied analytically to find the optimum static margin. The resultant tip chord length was found to be 9 in. (full scale), and this selection was verified later by

Gomillion (Ref. 4) in a wind tunnel test program. Figure 17 shows good agreement between predicted and 0.25-scale experimental data for Mach numbers 0.50, 0.70, and 0.90. For Mach number 1.10, the wind tunnel and predicted static stability data are significantly different. This disagreement may be a result of the limited experimental data in the CAMS program for that Mach number.

The 0.25-scale MVB static stability data for various tail-fin and nose configurations are presented in Fig. 18. The fin gap, or air gap, simulates the gap between fin and body which results from canting the fin.

Allee (Ref. 5) has shown that the addition of tabs to the base of the fins would increase the static stability significantly. The tabs are attached to the tail-fin trailing edge rather than the fin tip chord in order to maintain clearance between stores in the clustered configuration on the TER. The tab geometry selected for the MVB was based on the data in Ref. 5, and is shown in Fig. 12b. Figure 18 shows the static stability data with and without fins, with and without fin tabs, and with and without the nose fuze. For all Mach numbers, the MVB is neutrally stable without tabs and stable with tabs. The addition of the nose fuze decreases the stability slightly. The neutral point location, X_{NP}, represents the most aft location of the center of gravity to produce neutral static stability and is evaluated at the trim condition. The data in Fig. 19 show the effect of fin tabs, FMU-56 fuze, and location of the fin hinge line on the static stability of the MVB with two fins canted. In general, the addition of the fin tabs increases the static stability and results in trim angles of 15, 10, and 6 deg for Mach numbers 0.50, 0.70, and 0.90, respectively. The corresponding trim angles were 20, 20, and 22 deg for the fins without tabs. At Mach number 1.10, a trim condition was not achieved.

The effect of geometric scaling (ability to reproduce full-scale MVB geometry) on the static stability of the MVB is shown in Fig. 20. The 0.05-scale model data show a slightly decreased static stability for large negative angles of attack. The normal-force coefficient was unaffected by the scaling. Data are presented for Mach numbers 0.70 and 0.90 for different hinge line positions for the 0.05-scale models. The effect of shifting the hinge line forward was to reduce the static stability of the MVB. The normal-force coefficient again was unaffected.

The effects of model scale and Reynolds number variation on the static stability of the MVB are shown in Fig. 21. For Mach numbers 0.50 to 1.10, decreasing the Reynolds number decreased the static stability of the MVB only slightly. The normal-force coefficient was insensitive to Reynolds number variation.

4.2 AERODYNAMIC DATA IN THE F-4C AIRCRAFT FLOW FIELD

Figures 22 and 23 present the aerodynamic coefficient data for the MVB at various distances from TER station No. 1 in the aerodynamic interference flow field of the F-4C aircraft. The data are presented for uncanted fins with and without tabs (Fig. 22) and for two or four fins canted (Fig. 23). For the MVB model with canted fins, aerodynamic coefficients are presented for hinge line positions of 5 and 8 in. (full scale). The data in Fig. 22 and 23 show that increasing Mach number from 0.50 to 1.10 results in an increase in the depth of the interference flow field from approximately 2 to 5 ft. A comparison of Figs. 22 and 23 illustrates the effectiveness of the control fins in reducing the nose-down pitching moment (negative). The fin tabs and hinge line position had small effects on C_N and C_m, as illustrated in Figs. 25b and c. Figures 24 and 25 present MVB static aerodynamic coefficients as a function of fin cant angle for the 2- and 4-fin canted configurations at Mach numbers 0.50 to 1.10 in the No. 1 TER carriage position. The four-fins-canted configuration is more effective than the two-fins-canted configuration in reducing the nose-down pitching moment, whereas canting either two or four fins has a small effect on the axial-force coefficient.

4.3 SEPARATION TRAJECTORIES FROM THE F-4C AIRCRAFT

Figures 26 through 30 present the separation trajectories of the 0.05-scale MVB from the No. 1 TER position of the F-4C aircraft. The data are presented for Mach numbers 0.50 to 1.10. Data showing the linear displacements of the store relative to the carriage position and angular displacements relative to the attitude at carriage are presented as functions of full-scale trajectory time. In addition, angular displacements are plotted versus translational displacements with collision boundaries superimposed. The full-scale store parameters used in the trajectory calculations are listed in Table 1.

Figure 26 presents separation trajectories of the MVB from the No. 1 TER position with fin cant angles of 0, -3, -6, -9, and -12 deg. The data for zero deg cant angle demonstrates the increasing nose-down pitch motion with increasing Mach number. The resulting motion caused a tail-fin collision or sting collision at Mach numbers 0.70, 0.90, and 1.10. The effect of increasing the cant angle was to reduce the nose-down pitch motion. A fin cant angle of -12 deg produced trajectories that would allow separation at the higher Mach numbers. However, at Mach number 0.70 (Fig. 26b), the nose-up pitch motion resulted in collision of the MVB with the adjacent stores on the TER. The large nose-up motion may cause the MVB to collide later on with the aircraft. To reduce this nose-up motion at the lower Mach numbers, the MVB with two fins canted and with fin tabs was tested. The purpose of the tabs was to increase the static margin of the MVB and produce a lower trim angle.

Separation trajectory data are presented in Fig. 27 for the 0.05-scale MVB from the No. 1 TER position with two fins canted and with tabs. At the lower Mach numbers, 0.50 and 0.70, the nose-up motion is significantly reduced when compared to the four-fin cant. At Mach number 0.9 (Fig. 27c), the MVB store separated without colliding, but at Mach number 1.10 the tail collided with the adjacent store on the TER. The two-fin, -12 deg cant with tabs was chosen as the tail configuration which best satisfied the design requirements.

Trajectories of the MVB with two fins canted when separated from the No. 2 and 3 TER stations, respectively, are presented in Figs. 28 and 29. For Mach numbers of 0.50 to 0.90, the store separated with acceptable pitch and yaw oscillations (no collision) for the two-fin cant. At Mach number 1.10, for separation trajectories with the two-fin cant, the MVB appears not to recover in yaw motion.

Figure 30 presents separation trajectories of the MVB with simulation of fins returned from -12 to 0 deg. The lanyard length which would activate a mechanism and return the fins to zero cant angle was chosen to be 1.5 ft to provide the best separation characteristics. Figure 31 presents an illustration of this type of trajectory at Mach number 0.50.

4.4 SEPARATION TRAJECTORIES FROM THE A-7D AIRCRAFT

Separation trajectories of the MVB from the pylon, TER, and MER on the A-7D aircraft with various tail-fin configurations at Mach number 0.90 are presented in Fig. 32. Only selected data for the design release Mach number 0.90 are presented. Table 3 presents the other conditions tested. Table 1 presents the full-scale store parameters used in the trajectory calculations.

The trajectories for TER stations 1 and 2 and MER station 1 were abbreviated because of aircraft model dynamics creating store-to-aircraft collisions. In general, the MVB with canted tail fins and tabs exhibits better separation characteristics (less pitch and yaw motion) than the MVB without tabs.

4.5 WIND TUNNEL AND FLIGHT TEST SEPARATION TRAJECTORIES FROM THE F-4C AIRCRAFT

Comparisons of wind tunnel and flight test separation trajectory data of the MVB from the TER on the F-4C aircraft are presented in Figs. 33 through 51. The flight tests and wind tunnel tests were conducted with the MVB fins uncanted and canted. The canted fins remained in the deflected position throughout the trajectories to simulate the "fail-safe" mode. This mode ensures safe separation in the event of failure of the

mechanism for returning the fins to the zero deg cant position after release. The MVB was released at Mach numbers 0.50, 0.70, 0.90, and 1.02. The Mach number of 1.02 was the maximum which the F-4C could attain at 5,000-ft altitude. The flight test conditions are reported in Ref. 6. The Mach number was recorded from the Machmeter, the altitude from the altimeter, and the angle of attack was computed from the aircraft gross weight and Mach number.

Photographic data were obtained by a motion-picture camera located on the bottom of the aircraft fuselage. A chase aircraft obtained additional motion-picture data during release. The photographic data were reduced to trajectory data (angles and displacements as functions of time) at the Air Force Armament Laboratory, Eglin AFB, Florida.

The comparison of wind tunnel and flight test data at Mach number 0.50 is presented in Fig. 33. The pitch angular motion of the MVB agrees reasonably well, but yaw angle and vertical displacement do not. The wind tunnel trajectory data (Fig. 33a) show that changes in Mach number of ±0.02 from 0.50 have an insignificant effect on the MVB trajectory.

The effect of aircraft angle of attack on the wind tunnel separation trajectories of the MVB is shown in Fig. 33c. The effect of angle of attack is appreciable on the pitch and yaw motion of the MVB but insignificant on the displacements.

A pictorial illustration of the wind tunnel and flight test trajectories of the MVB with uncanted fins at $M_\infty = 0.50$ is shown in Fig. 34. Figure 35 presents a photographic sequence of the flight test trajectory taken from the chase aircraft camera data.

The wind tunnel and flight test trajectory data for the MVB with uncanted fins at Mach number 0.70 is presented in Fig. 36. The angular and translational displacements show large discrepancies between wind tunnel and flight test. The wind tunnel data show that the pitch motion does not recover, whereas the flight trajectory data indicate recovery in pitch motion at approximately 19 deg. The effect of a small variation in Mach number on the wind tunnel trajectories was small. A pictorial illustration of the wind tunnel and flight test trajectories of the MVB with uncanted fins at Mach number 0.70 is shown in Fig. 37.

The wind tunnel and flight test trajectories of the MVB with two fins canted at -12 deg at Mach number 0.70 are presented in Fig. 38. The comparison between the wind tunnel and flight test trajectories shows fair agreement. The effect of varying Mach number on the wind tunnel trajectories is insignificant. Canting the fins seems to be very effective in reducing the nose-down pitch motion in the flight test trajectory. A pictorial

illustration of the wind tunnel and flight test trajectories for the MVB with two fins canted at Mach number 0.70 is presented in Fig. 39. The illustration shows sufficient clearance as a result of the nose-up pitch motion. Figure 40 shows time sequence photographs from the chase aircraft of the separation trajectories of the MVB with and without fins canted at Mach number 0.70. The photographs clearly illustrate the effect of fin cant on the separation trajectories. The MVB with canted fins exhibits a large nose-up motion because of nonrestoring pitching-moment coefficients at positive angles of attack, and an increase in the magnitude of the coefficients at angles of attack above 20 deg (Fig. 20b).

The separation trajectories of the MVB without fins canted at Mach number 0.90 are presented in Fig. 41. The wind tunnel trajectory data are presented for pivotal motion up to -40 deg and for free motion. The pivotal motion constrains the tail of the store at a fixed point of rotation to simulate the collision between the tail and adjacent stores. The vertical translational displacement, Z_P, and pitch angular displacement show some disagreements between wind tunnel and flight data when plotted versus time. However, the pitch variation with displacement (Fig. 41b) shows reasonable agreement. The free-release wind tunnel trajectory had to be initiated at a vertical displacement Z_P, equivalent to 0.35 ft to eliminate collision of the tail with the adjacent stores on the TER. A pictorial illustration of the MVB separation with uncanted fins for wind tunnel and flight test at Mach number 0.90 is shown in Fig. 42. It can be seen that for both wind tunnel and flight test the rotation occurred at the tail of the MVB.

The MVB separation trajectories with two fins canted at -12 deg at Mach number 0.90 for the wind tunnel and flight test is shown in Fig. 43. Presented are two wind tunnel trajectories, one initiated at carriage position and the other at Z_P = 0.35 ft. It can be seen that the trajectory initiated at Z_P = 0.35 ft is significantly different from the trajectory initiated at the carriage position (Z_P = 0). Also presented are two repeat flight test trajectories of the MVB. Although the trends of the repeat trajectories are the same, the angular displacements, $\Delta\theta$ and $\Delta\psi$, show differences at any particular trajectory time of the same magnitude as the differences between wind tunnel and flight data (Fig. 43a). A pictorial illustration of the MVB trajectories with two fins canted at Mach number 0.90 is shown in Fig. 44.

The separation trajectories of the MVB with fins canted and with tabs at Mach number 0.90 are presented in Fig. 45. The tabs were installed to increase the static stability of the MVB and thus produce a recovery of the nose-down pitch motion. The wind tunnel data are presented for free release and simulated pivotal releases with θ_R = -10, -20, and -40 deg. The pivotal release trajectories were obtained because the flight test onboard motion-picture data indicated collision and "hanging-up" of the tabs on the tail

fin with the adjacent store fin tabs, thus creating a constrained motion or pivotal release up to -40 deg. The wind tunnel data showed that with constrained motion for -20 deg or greater, the MVB will not recover in pitch motion.

The wind tunnel trajectory data show the same trends as the flight test data except for the yaw angular displacement, $\Delta\psi$. In Fig. 45b, the constrained motion with θ_R = -40 deg shows good agreement with the flight test trajectory. This good agreement implies that tail collision, and thus constrained motion, did occur in flight, and probably explains why the wind tunnel free-release and flight test data did not agree. A pictorial illustration of the wind tunnel free-release and flight test trajectories of the MVB with canted fins and tabs is presented in Fig. 45. A sequence of flight test photographic data for the MVB with (a) uncanted fins without tabs, (b) canted fins without tabs, and (c) canted fins with tabs is presented in Fig. 47.

The wind tunnel and flight test trajectory data for the MVB from TER station No. 1 with uncanted fins and without tabs at Mach number 1.02 are shown in Fig. 48. Wind tunnel trajectory data are presented for free release and simulated constrained motions (θ_R = -40). Wind tunnel trajectory data for aircraft angles of attack of zero and 1 deg are also presented. The wind tunnel data show that the MVB trajectory is insensitive to aircraft angle of attack. The MVB pitch motion for the free-release condition is greater than for the constrained motion simulation. The flight test and wind tunnel trajectory data show reasonable agreement when compared on the basis of displacements (Fig. 48b). A pictorial illustration of the wind tunnel and flight test trajectories with fins uncanted and without tabs for Mach number 1.02 is presented in Fig. 49. The figure (flight test) illustrates the upward vertical displacement of the tail fins on separation, thus producing a possible collision with adjacent store tail fins.

The separation trajectory data of the MVB (fins uncanted, without tabs) from TER station No. 2 at Mach numbers 1.00, 1.02, and 1.04 are presented in Fig. 50. The wind tunnel trajectory data show that the motion of the MVB is only slightly sensitive to Mach number variations. The flight test trajectory data agreed with wind tunnel trajectory data when compared on the basis of displacements (Fig. 50b).

The photographic sequences of trajectory data for the MVB released from the TER No. 1 and 2 stations at Mach number 1.02 are shown in Fig. 51.

4.6 DYNAMIC STABILITY DATA

The variation in pitch-damping ($C_{m_q} + C_{m_{\dot{\alpha}}}$) coefficient with angle of attack is shown in Fig. 52 for the 0.075-scale model of the MVB with and without tabs. Presented are the pitch-damping data for Mach numbers 0.50, 0.70, 0.90, and 1.10. Generally, the

pitch-damping coefficient increased in magnitude with Mach number for angles of attack near zero. The effects of canting the MVB fins and adding fin tabs on the pitch damping were not appreciable for angles of attack near zero. Conditions of pitch-damping instability occurred at higher angles of attack at Mach numbers 0.50, 0.70, and 1.10 with and without tabs. Figure 52b shows one case of instability in pitch damping for an angle of attack of 10 deg at Mach number 1.10 for the MVB with all fins canted -12 deg. Values of pitch-damping coefficient predicted by the method of Marshall and Summers (Ref. 7) show reasonable agreement with the experimental data for all Mach numbers. The predicted values were calculated on the assumption that the pitch-damping coefficients are not highly sensitive to Mach number or angle-of-attack variations. Average values of the pitch-damping coefficients for angles of attack between ±20 deg were used as constant inputs for the computation of the wind tunnel trajectories.

5.0 SUMMARY OF RESULTS

Dynamic stability, static stability and captive trajectory wind tunnel data. along with flight test trajectory data, were obtained on the MVB with and without fins canted, and with and without tabs, at Mach numbers 0.50 to 1.10. The wind tunnel trajectory data were obtained for release from all TER and MER stations on the A-7D and F-4C aircraft. Flight test data were obtained only with the F-4C aircraft. Based on the test results, the following comments can be made:

1. Flight test data indicated that the use of a two-tail-fin cant is not a feasible technique for alleviating the excessive pitch down of large diameter stores when released from TER station No. 1 at Mach number 0.90.

2. Comparisons of wind tunnel trajectory data with flight test trajectory data for the MVB with and without fins canted and without fin tabs showed generally good agreement.

3. The wind tunnel and flight test trajectories for the MVB with canted fins and tabs, from TER station No. 1, at Mach number 0.90, could only be made to agree when using constrained motion in the wind tunnel data, simulating contact and restraint between the fins of the released store and the adjacent stores on the TER.

4. The wind tunnel trajectory test data showed that the MVB released at Mach number 1.10 from TER station No. 1 with fins canted and with fin tabs showed no improvement on release as compared to the uncanted fins.

5. The wind tunnel trajectory test data indicated the MVB with canted and uncanted fins and with fin tabs could be separated from TER station No. 2 and 3 for Mach numbers 0.50 to 1.10.

REFERENCES

1. Holmberg, John L. "Tradeoffs Among Weapon Aerodynamic Stability, Trajectory Perturbations, and F-4 Aircraft Performance." AFATL-TR-73-47, February 1973.

2. Test Facilities Handbook (Tenth Edition). "Propulsion Wind Tunnel Facility, Vol. 4." Arnold Engineering Development Center, May 1974.

3. Tipping, Derrick, et al. "Computer-Aided Missile Synthesis (CAMS)." OR 12,034, June 1972.

4. Gomillion, G. R. "Aerodynamic Load Characteristics of Six 0.05-Scale Stores in the Flow Field of an F-4C Aircraft at Mach Numbers 0.5 to 1.1" AEDC-TR-76-45 (ADA029144), August 1976.

5. Allee, E. G., Jr. "Static Stability and Separation Characteristics of the CBU-24 Dispenser Fitted with Various-Tail-Fin Configurations at Mach Numbers from 0.5 to 1.10." AEDC-TR-70-37 (AD865412), February 1970.

6. Kratzert, Keith A. "Improved Cluster Munition Evaluation." ADTC-TR-76-61, August 1976.

7. Marshall, J. C. and Summers, W. E. "An Analysis of the Relative Importance of Parameters Required for the Simulation of Store Separation Trajectories." Aircraft/Stores Compatibility Symposium Proceedings, Dayton, Ohio, September 1971, AFFDL-TR-72-67.

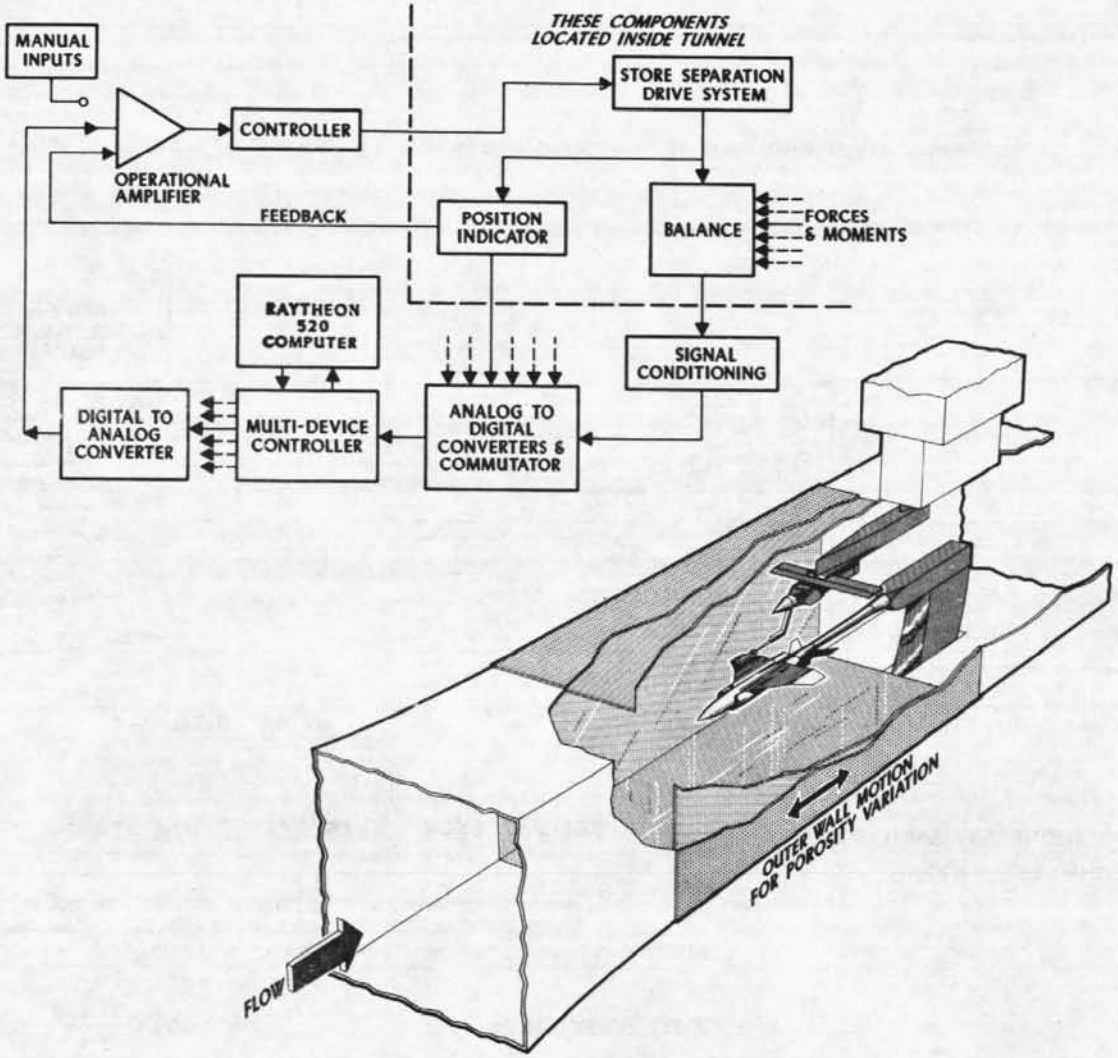

Figure 1. Typical store separation installation and a block diagram of the computer control loop.

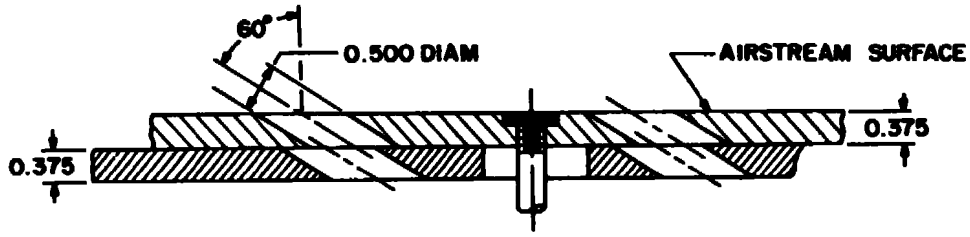

TYPICAL PERFORATED WALL CROSS SECTION

DIMENSIONS AND TUNNEL STATIONS IN INCHES

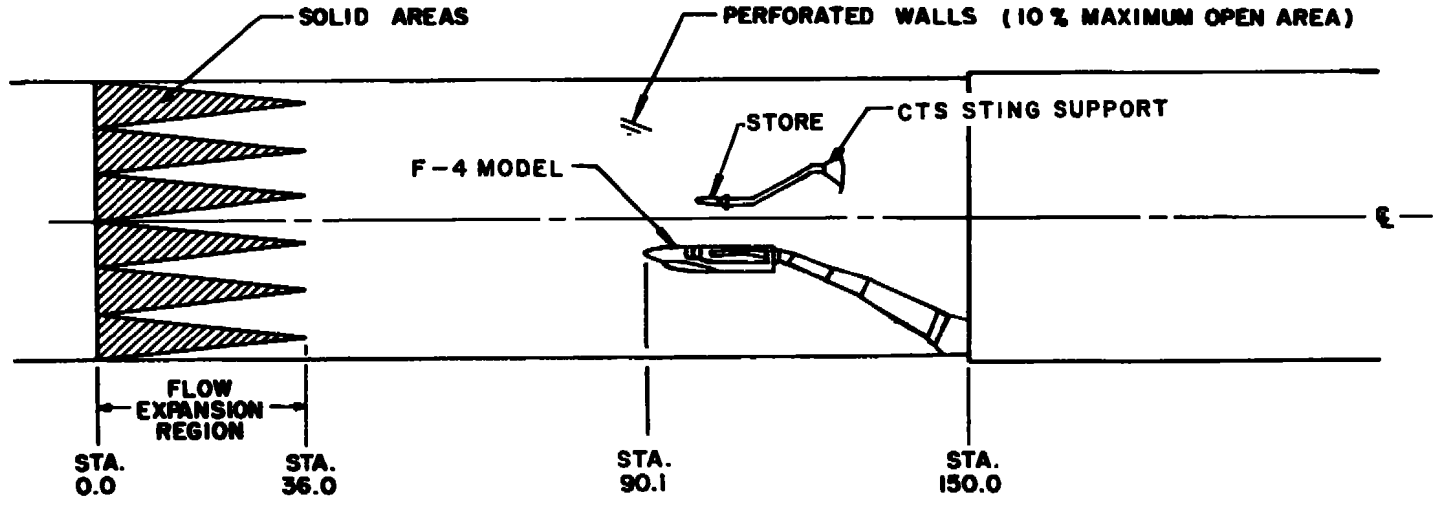

a. F-4C

Figure 2. Tunnel 4T test section showing aircraft model locations.

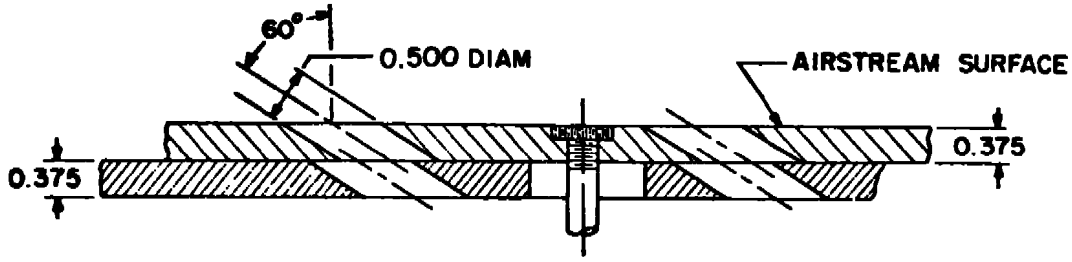

TYPICAL PERFORATED WALL CROSS SECTION

DIMENSIONS AND TUNNEL STATIONS IN INCHES

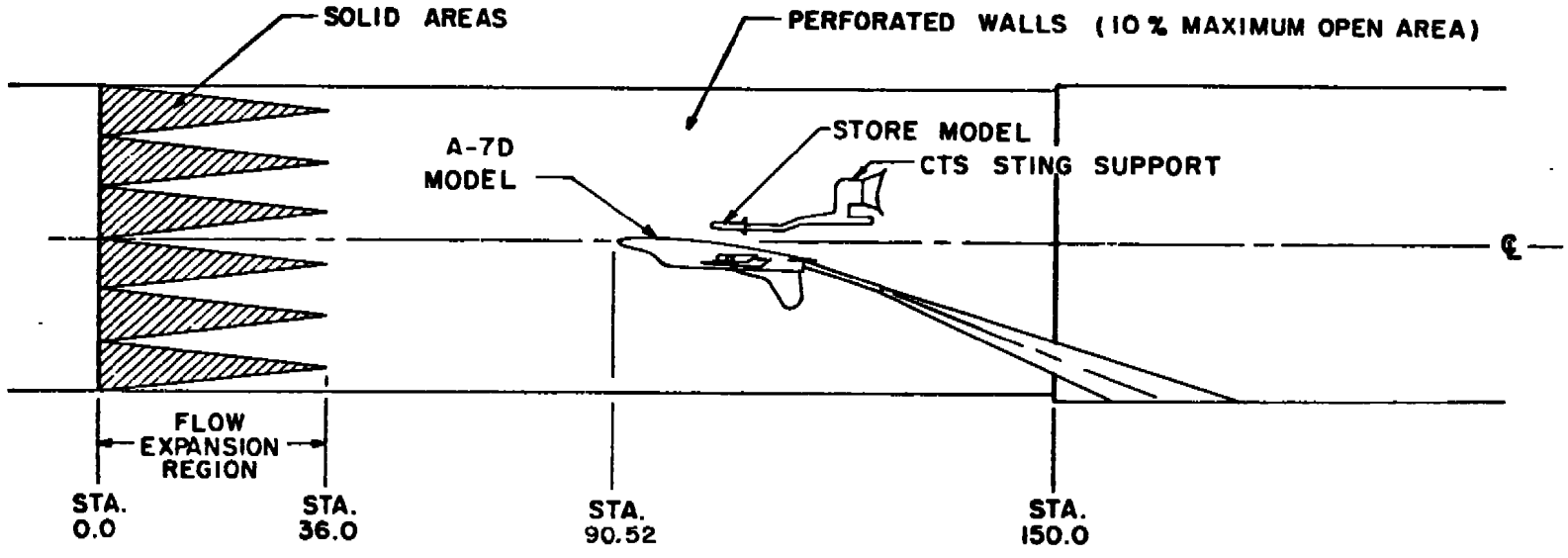

b. A-7D

Figure 2. Concluded.

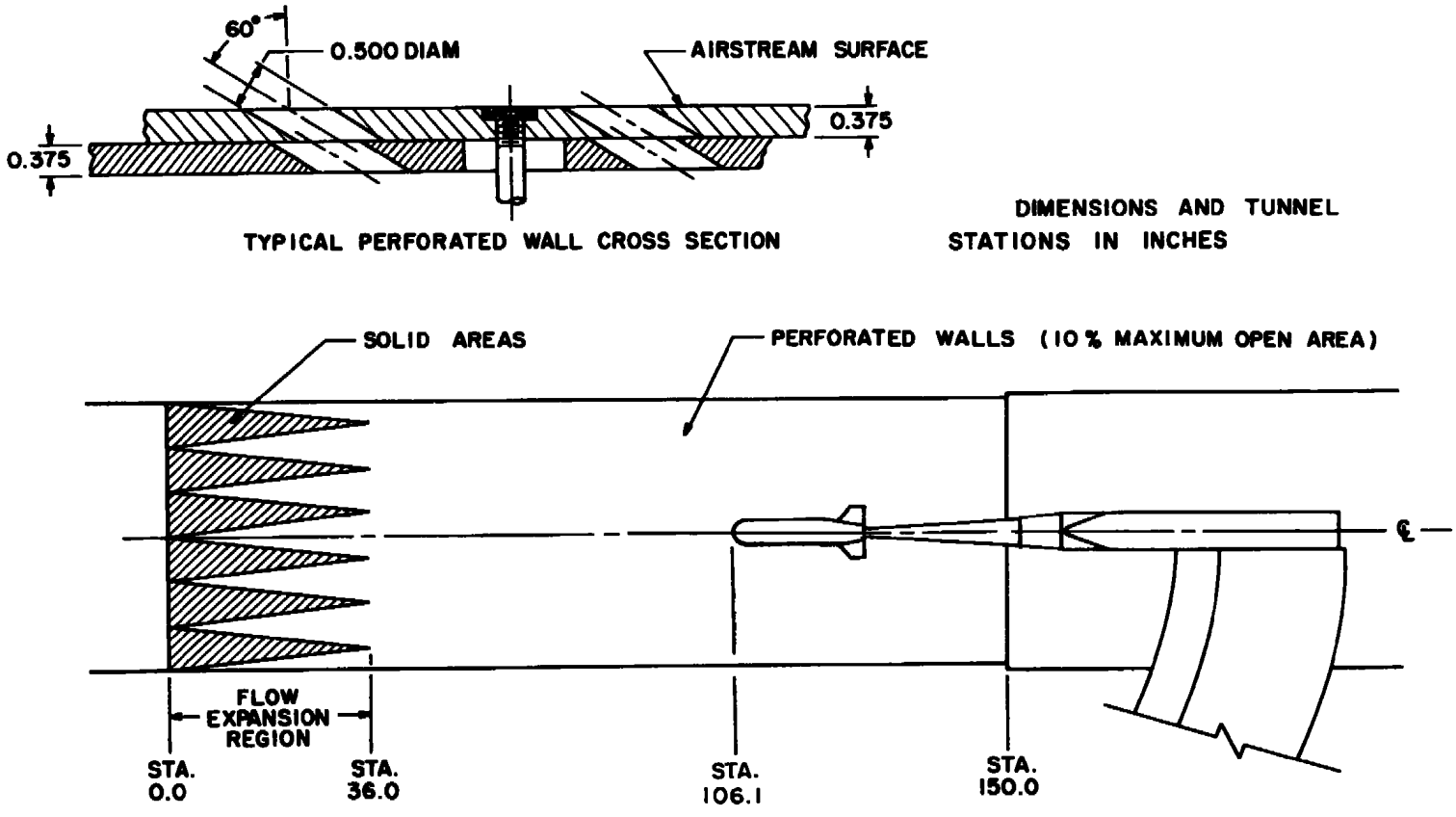

Figure 3. Tunnel test section and installation details of the 0.25-scale MVB model.

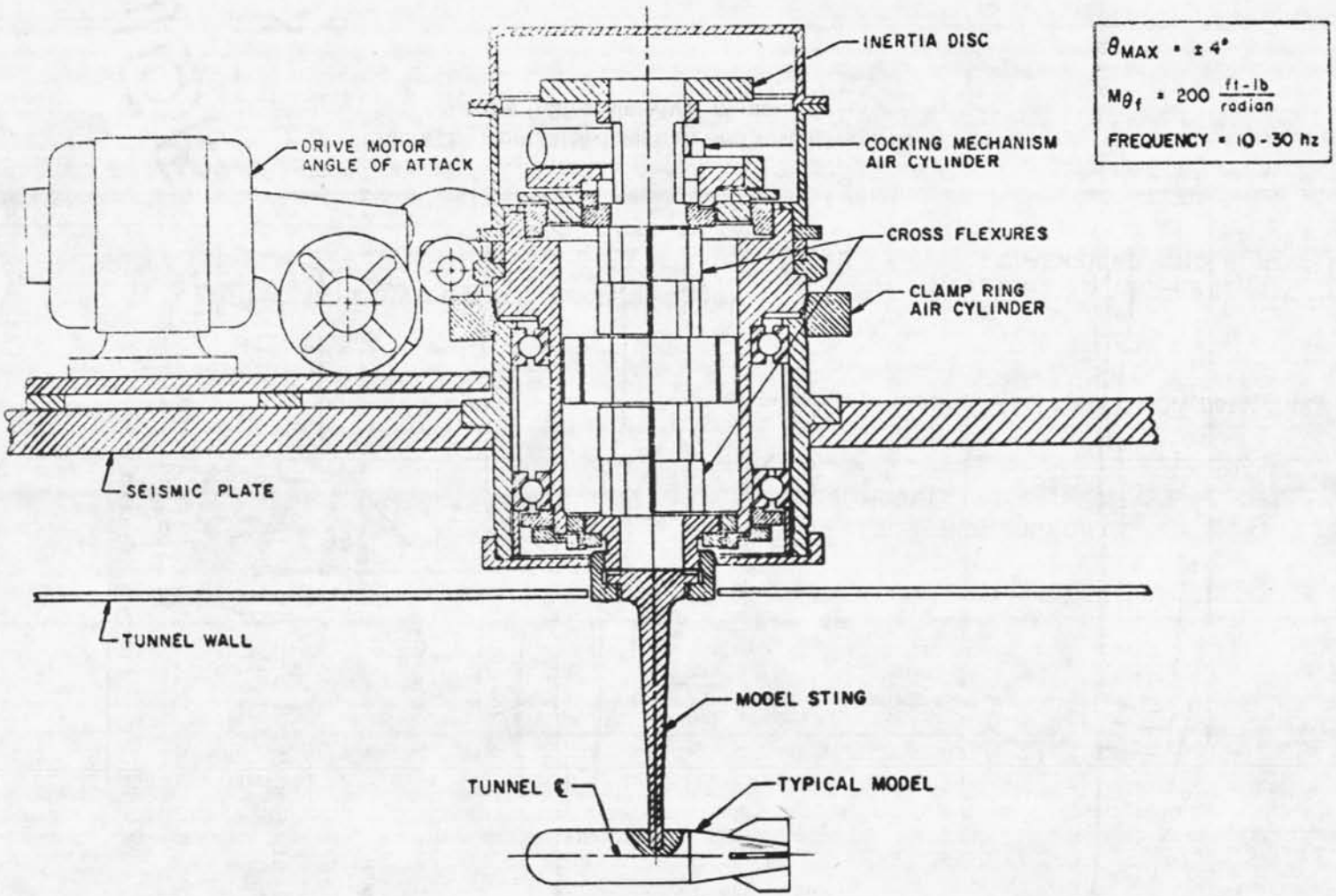

Figure 4. Tunnel 1T dynamic damping rig showing installation of 0.075-scale MVB.

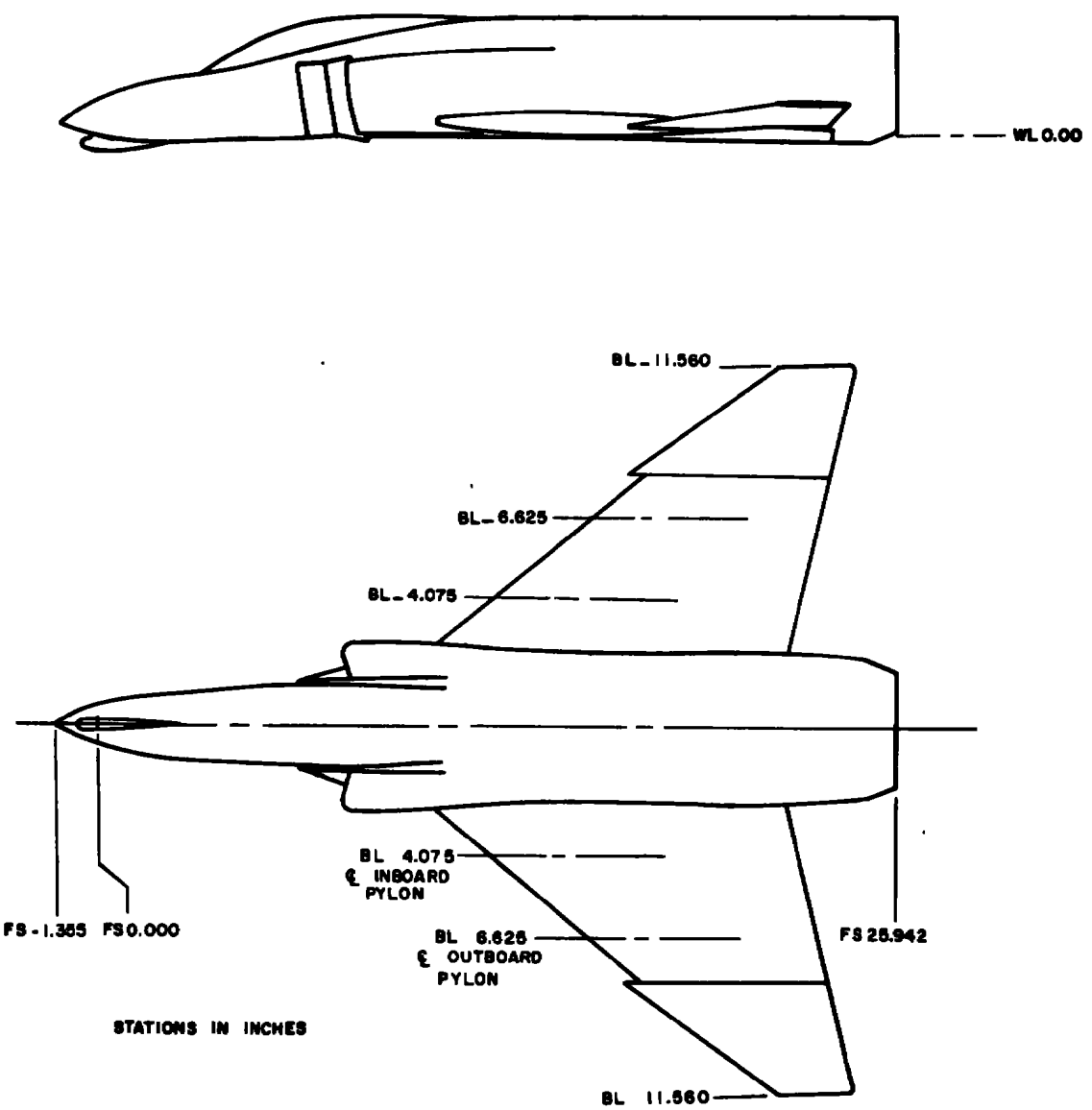

a. F-4C

Figure 5. Aircraft models.

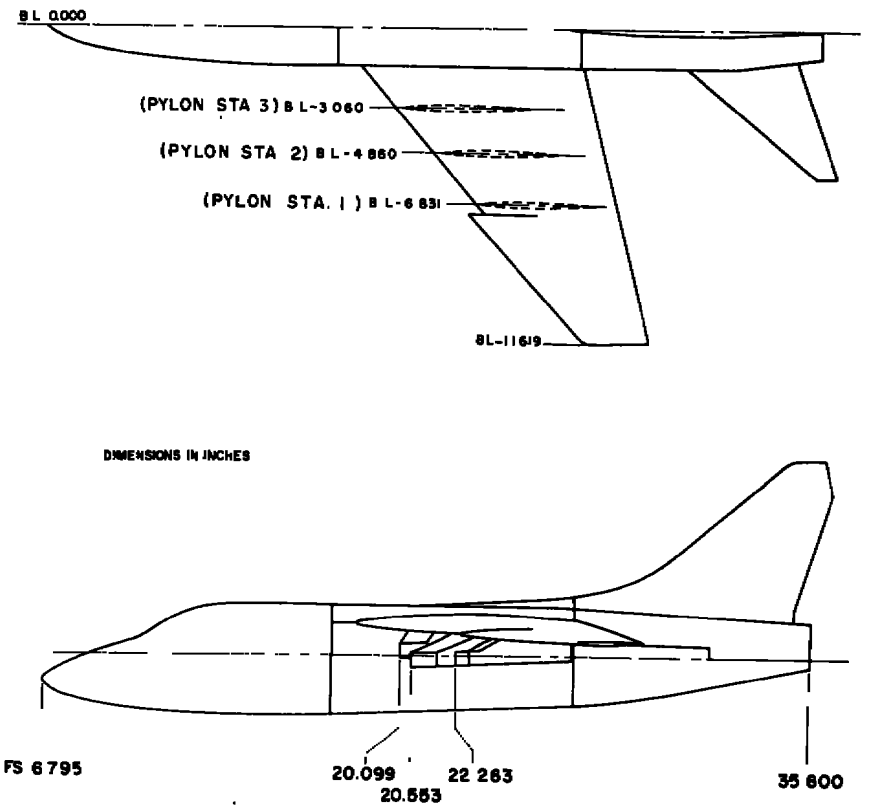

b. A-7D

Figure 5. Concluded.

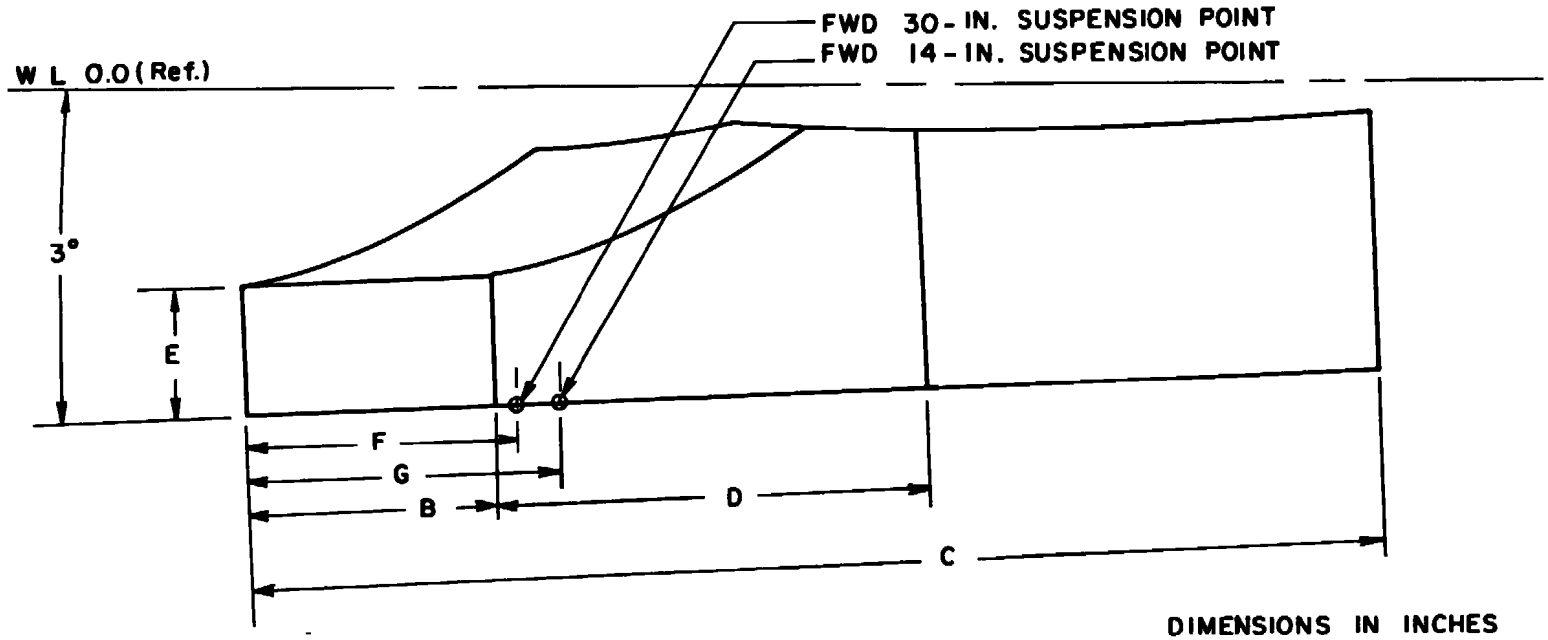

	INBOARD	CENTER	OUTBOARD
B	1.030	1.030	0.515
C	4.580	4.850	4.437
D	1.630	1.905	2.008
E	0.575	0.575	0.513
F	0.950	0.950	0.750
G	1.350	1.350	1.150

a. A-7D

Figure 6. Details of the aircraft pylons.

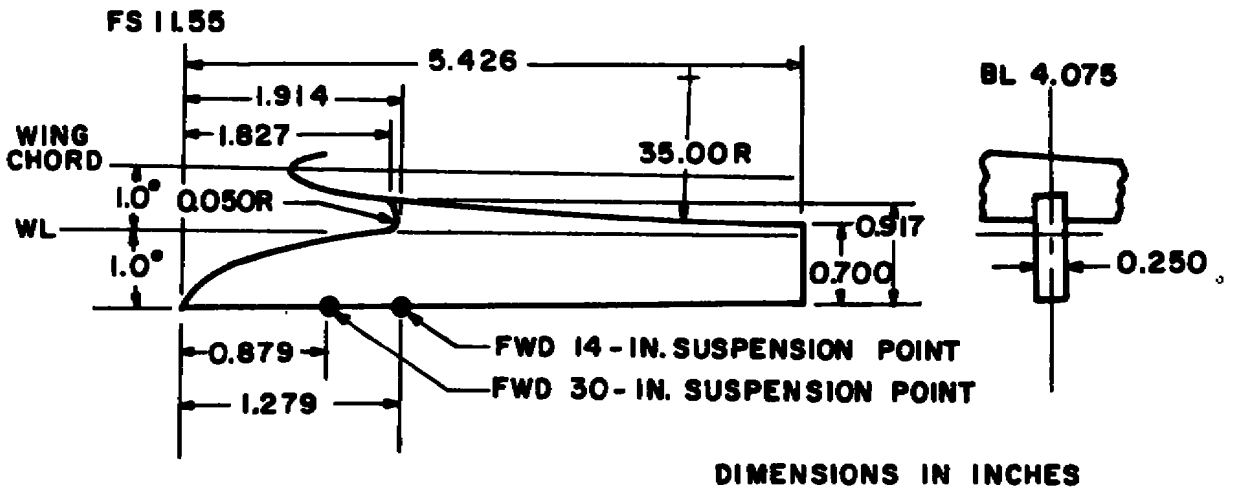

b. F-4C
Figure 6. Concluded.

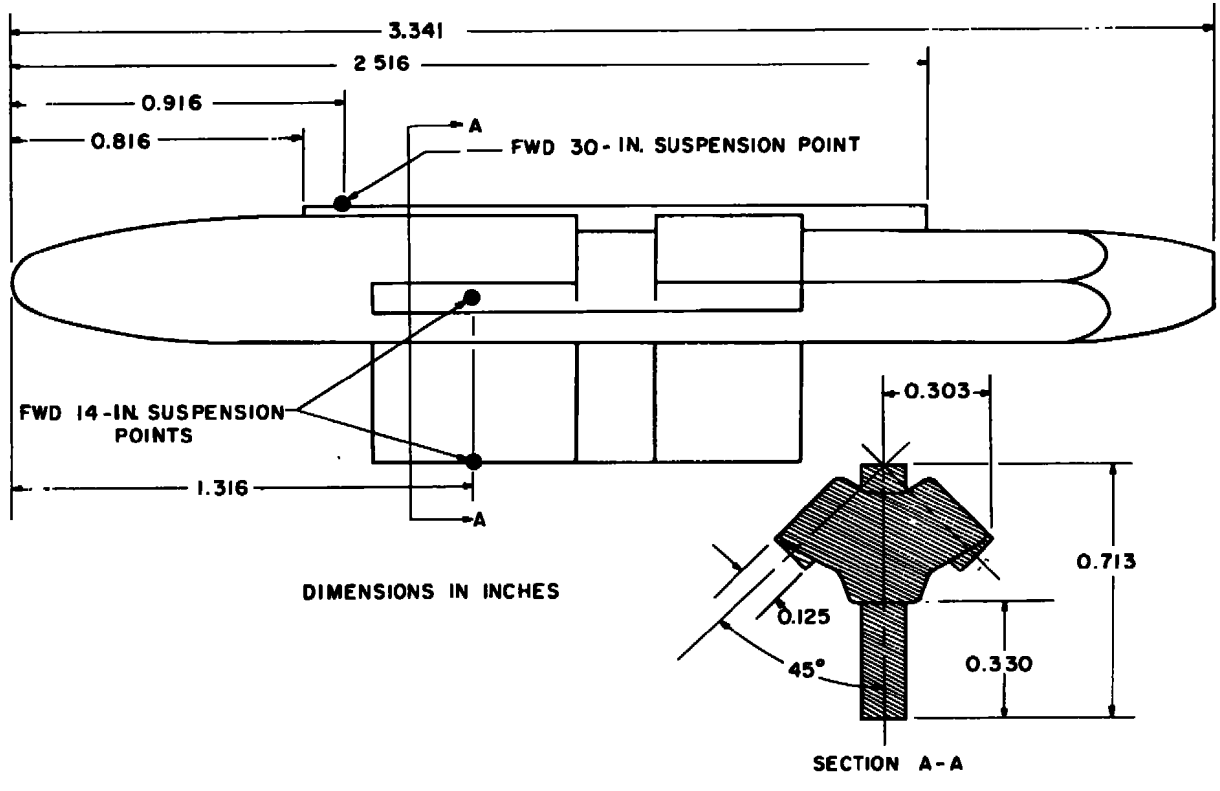

a. F-4C

Figure 7. Details and dimensions of the aircraft TER models.

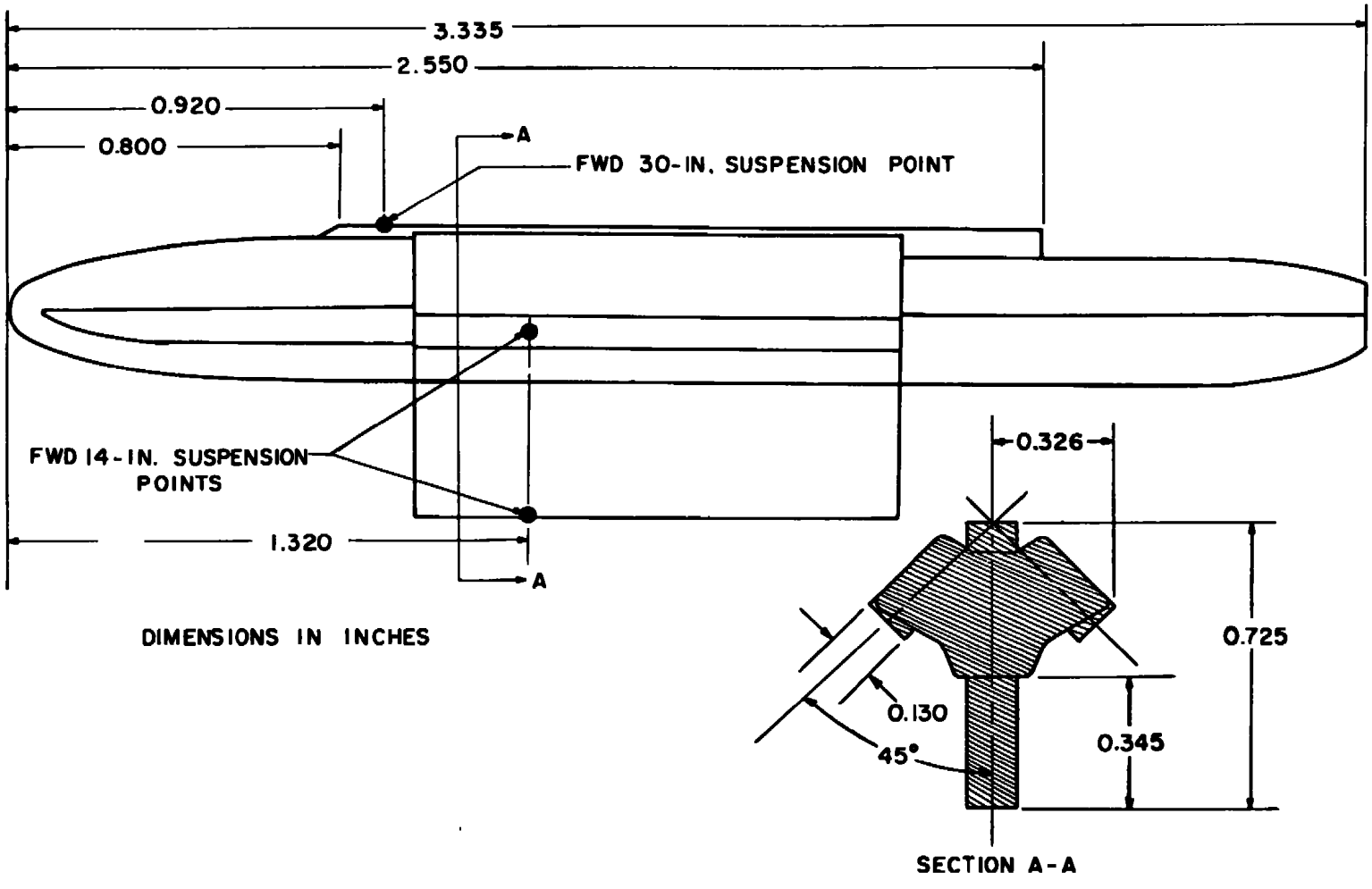

b. A-7D

Figure 7. Concluded.

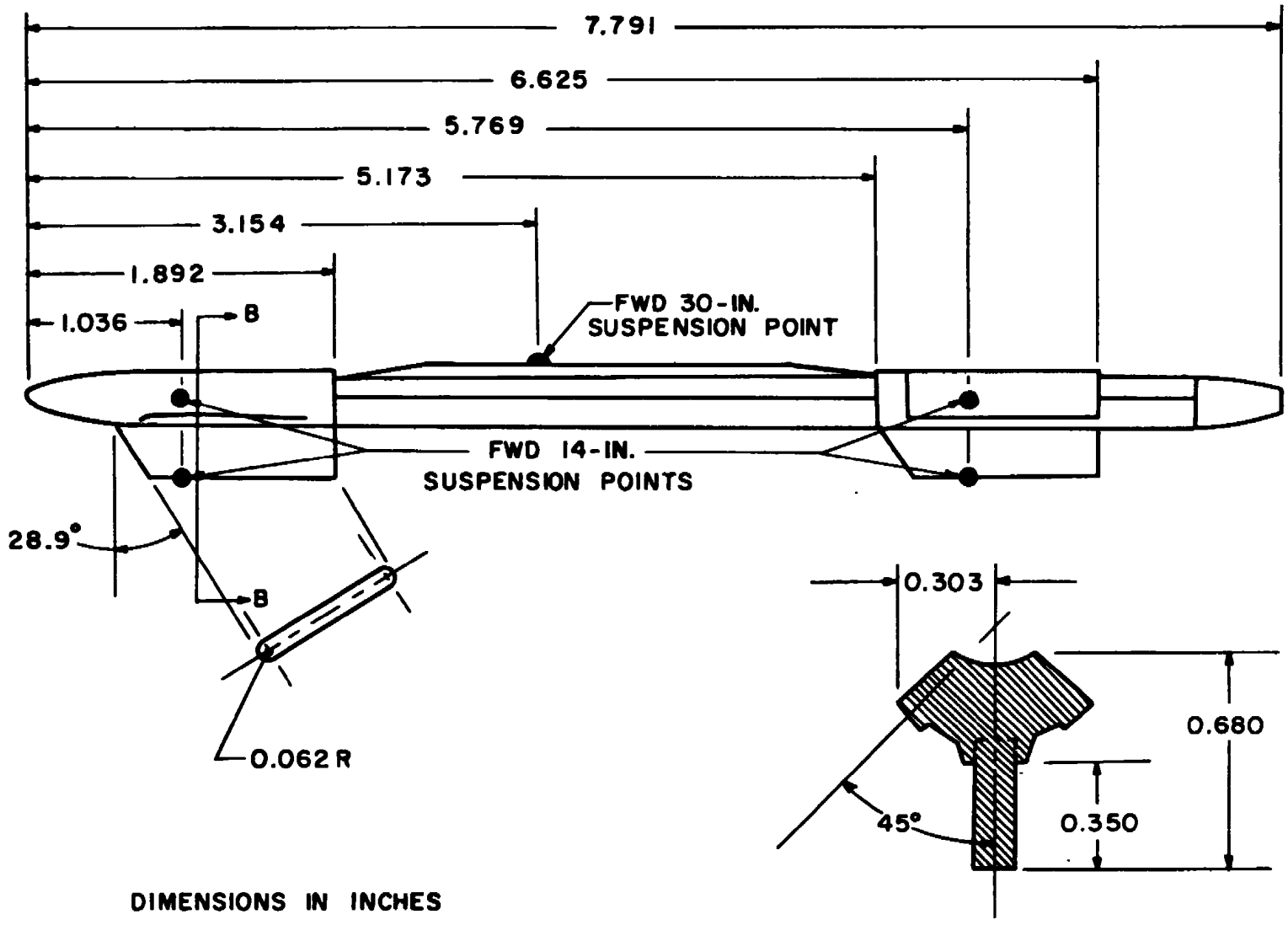

Figure 8. Details and dimensions of the A-7D MER model.

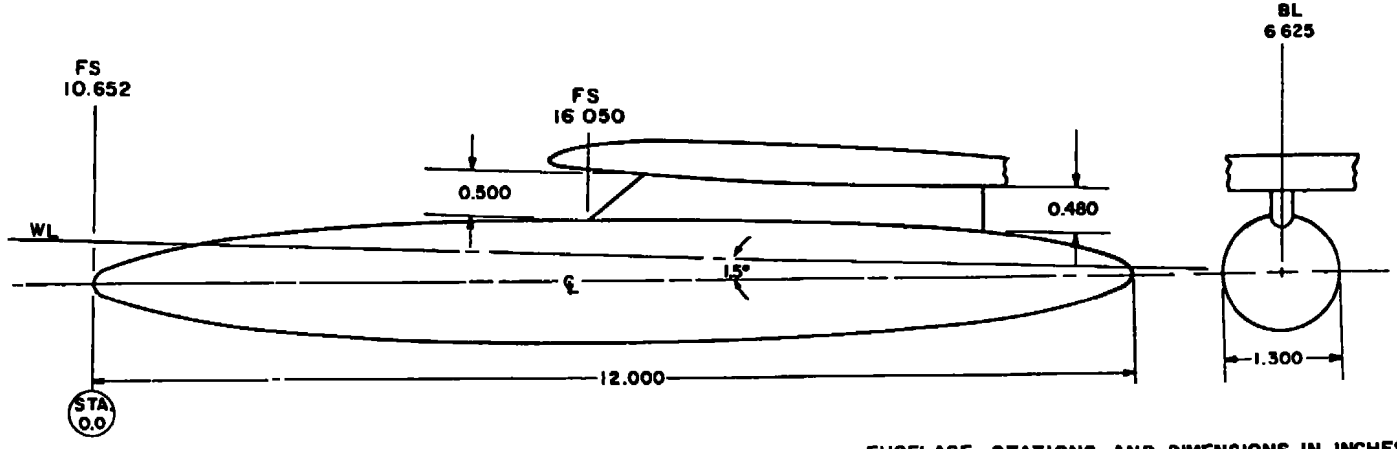

FUSELAGE STATIONS AND DIMENSIONS IN INCHES

BODY CONTOUR, TYPICAL BOTH ENDS

STATION	BODY DIAM	STATION	BODY DIAM
0 000	0 000	2 500	1.116
0 025	0 100	2 750	1 156
0.050	0 144	3 000	1 190
0 150	0 258	3 250	1 218
0 250	0 340	3 500	1 242
0 500	0 498	3 750	1 260
0 750	0 622	4 000	1 274
1 000	0 724	4 250	1 286
1 250	0 812	4 500	1 294
1 500	0 890	4 750	1 298
1 750	0 958	5 000	1 300
2 000	1 016	6 000	1 300
2 250	1 070		

Figure 9. Details and dimensions of the F-4C outboard 370-gal fuel tank model.

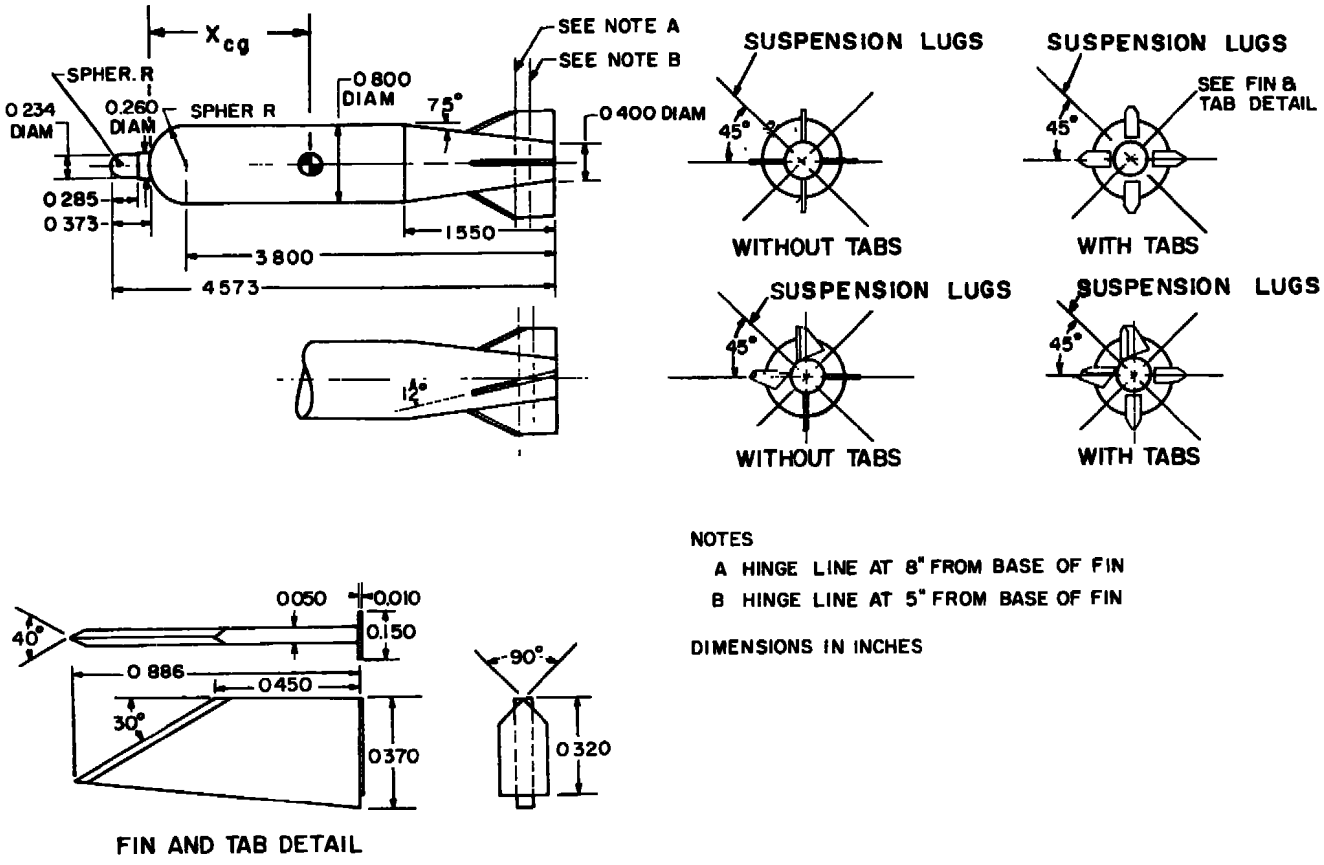

Figure 10. Details and dimensions of the 0.05-scale MVB model.

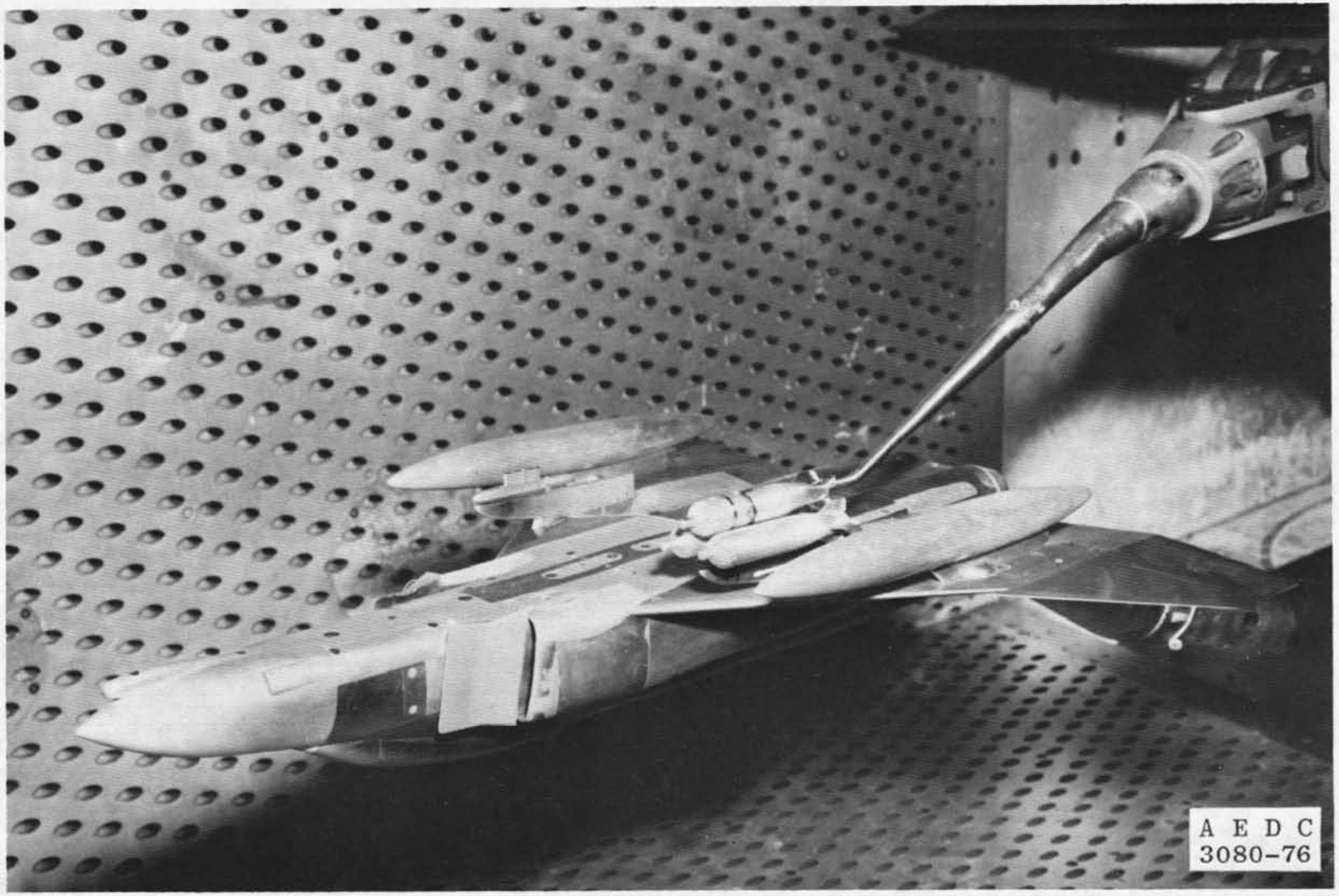

Figure 11. Tunnel 4T installation photograph of F-4C aircraft, MVB, and CTS.

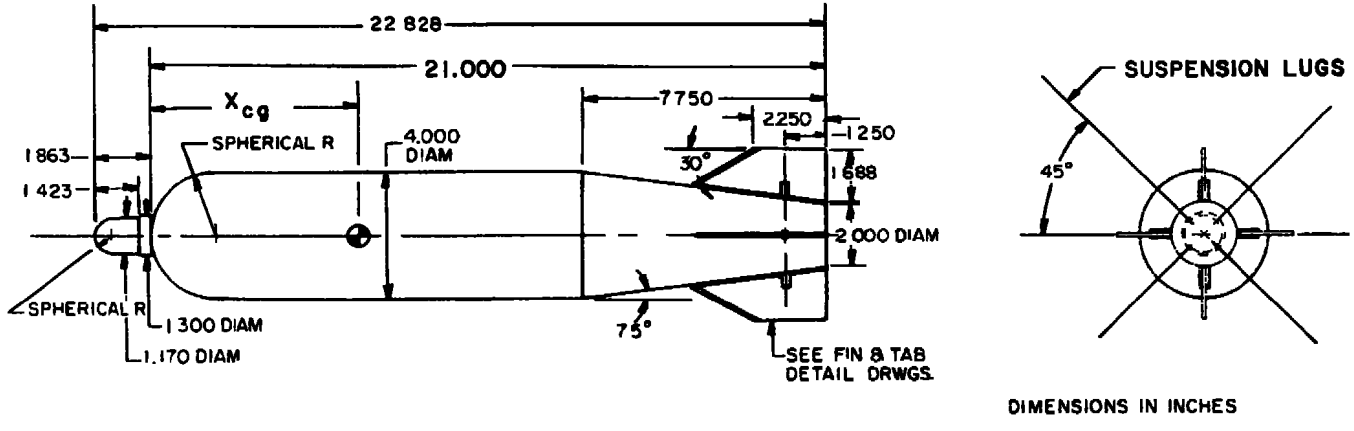

a. Details and dimensions of body and fins

Figure 12. Details and dimensions of the 0.25-scale MVB model.

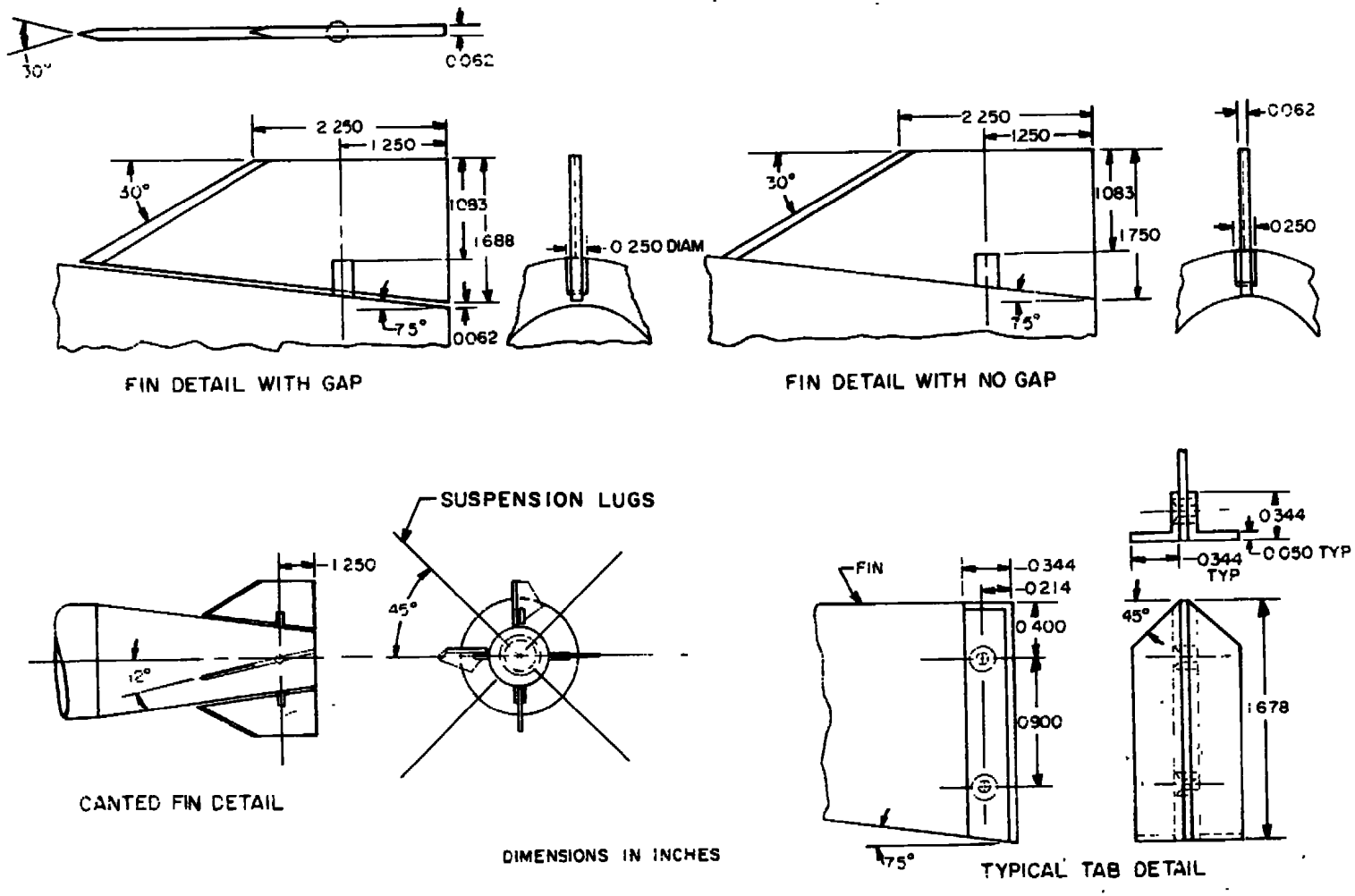

b. Details and dimensions of fins
Figure 12. Concluded.

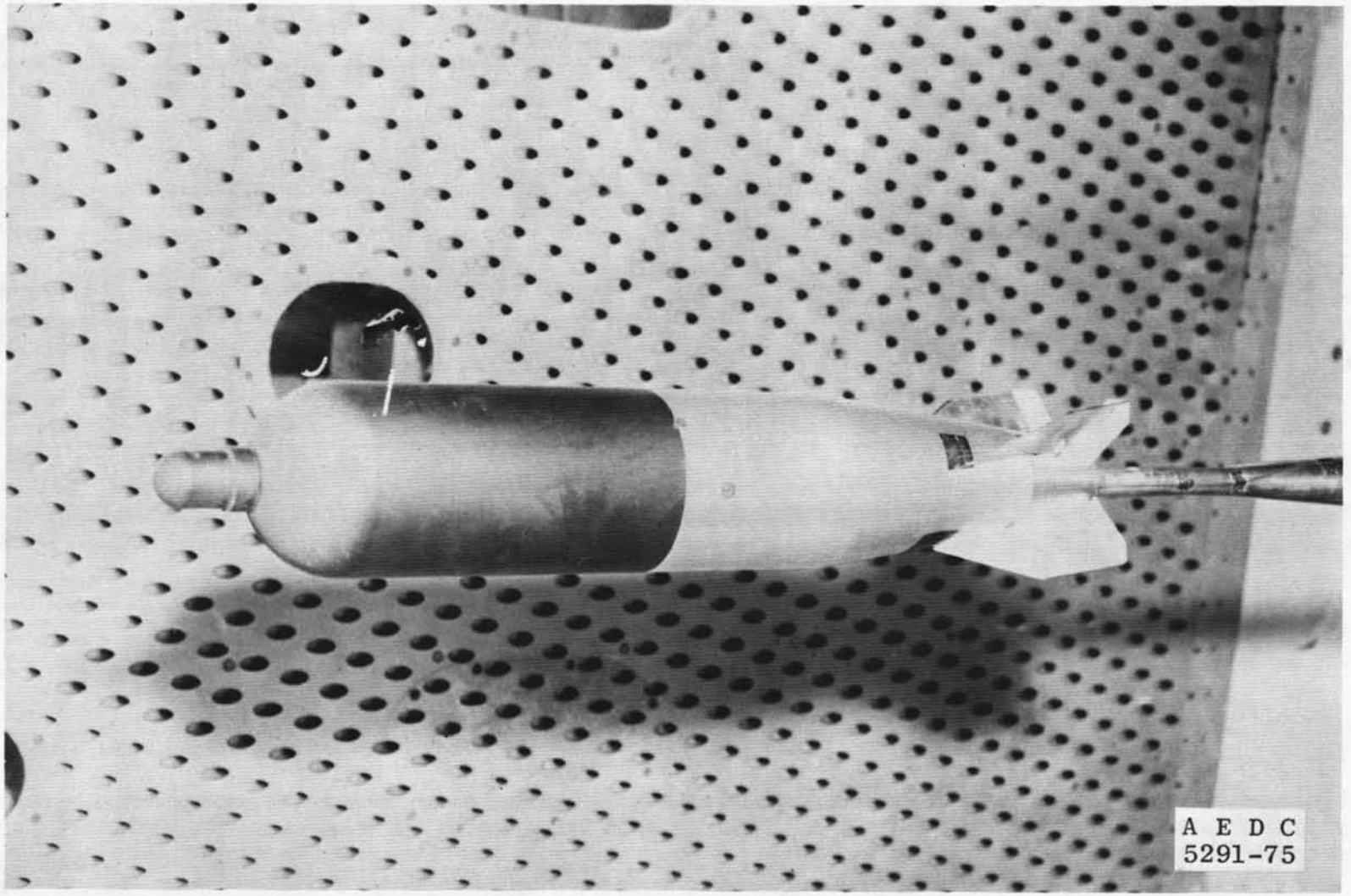

Figure 13. Tunnel 4T installetion photograph of 0.25-scale MVB model.

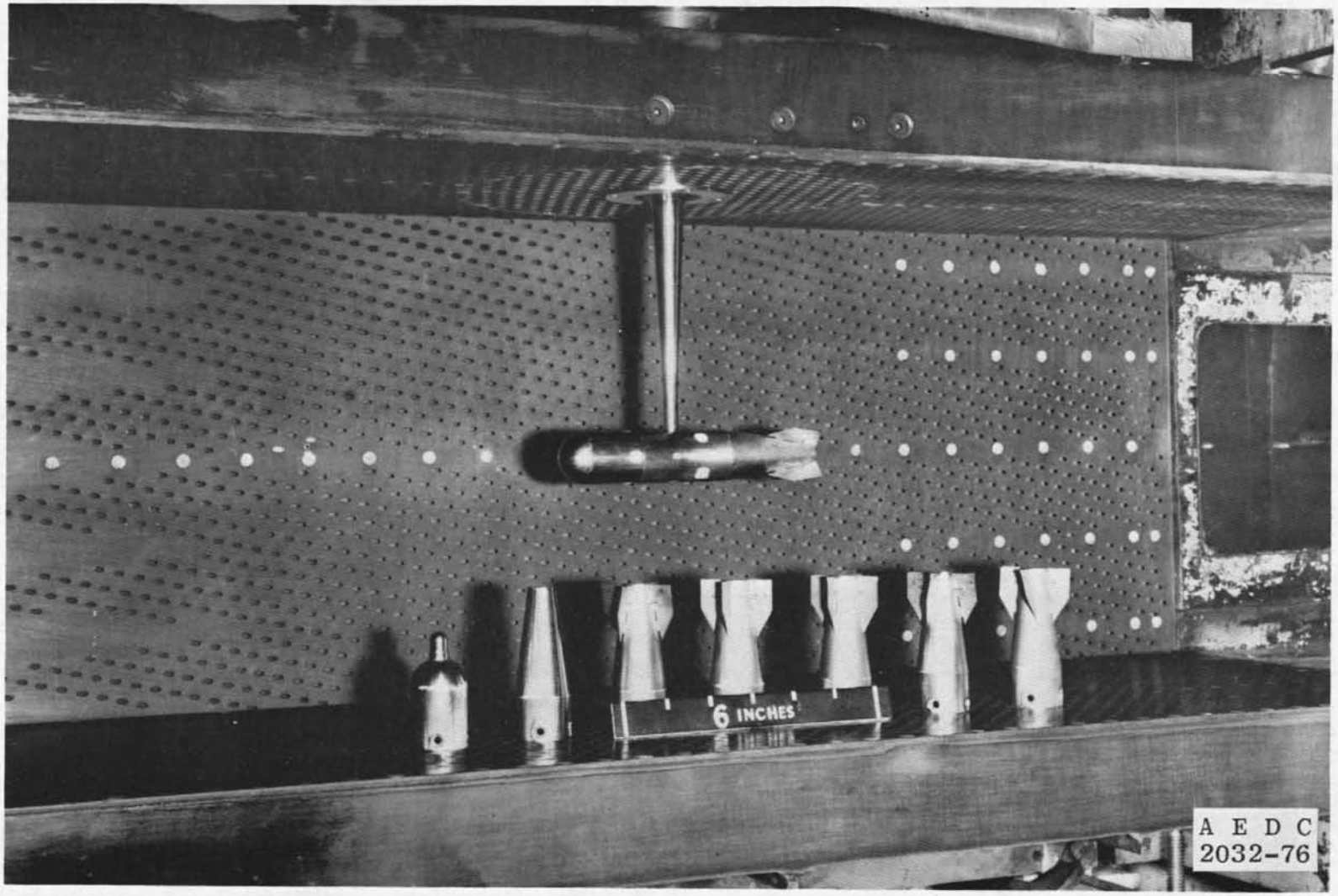

Figure 14. Tunnel 1T installation photograph of 0.075-scale MVB model with interchangeable tails.

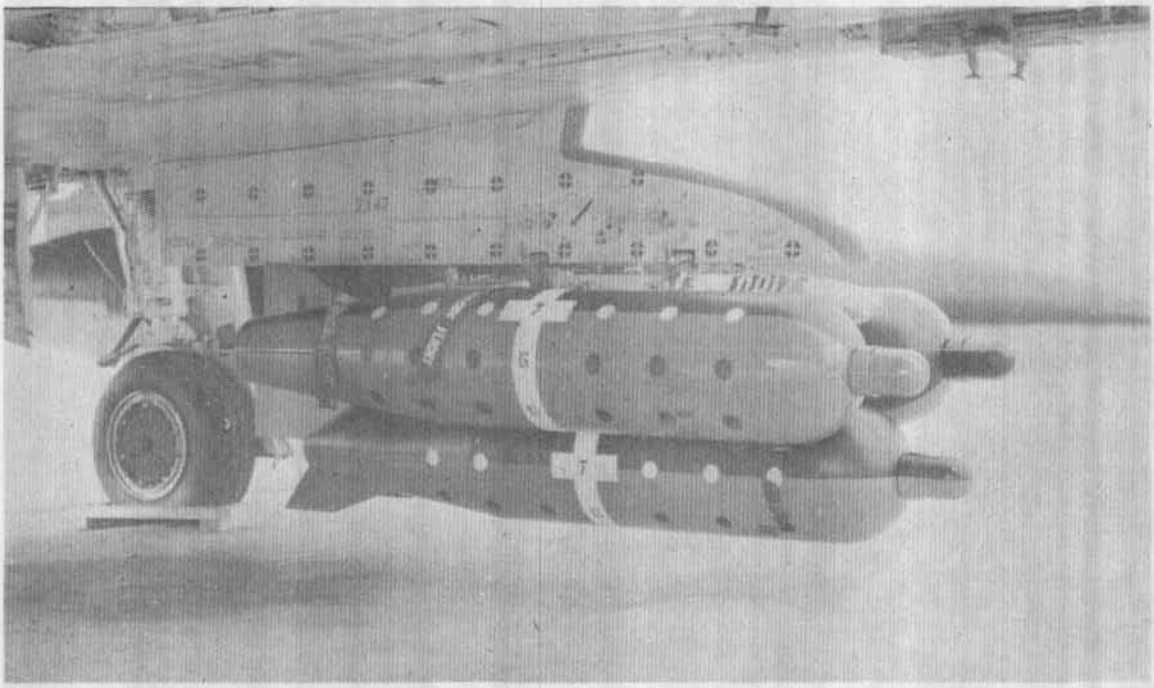

a. Side view

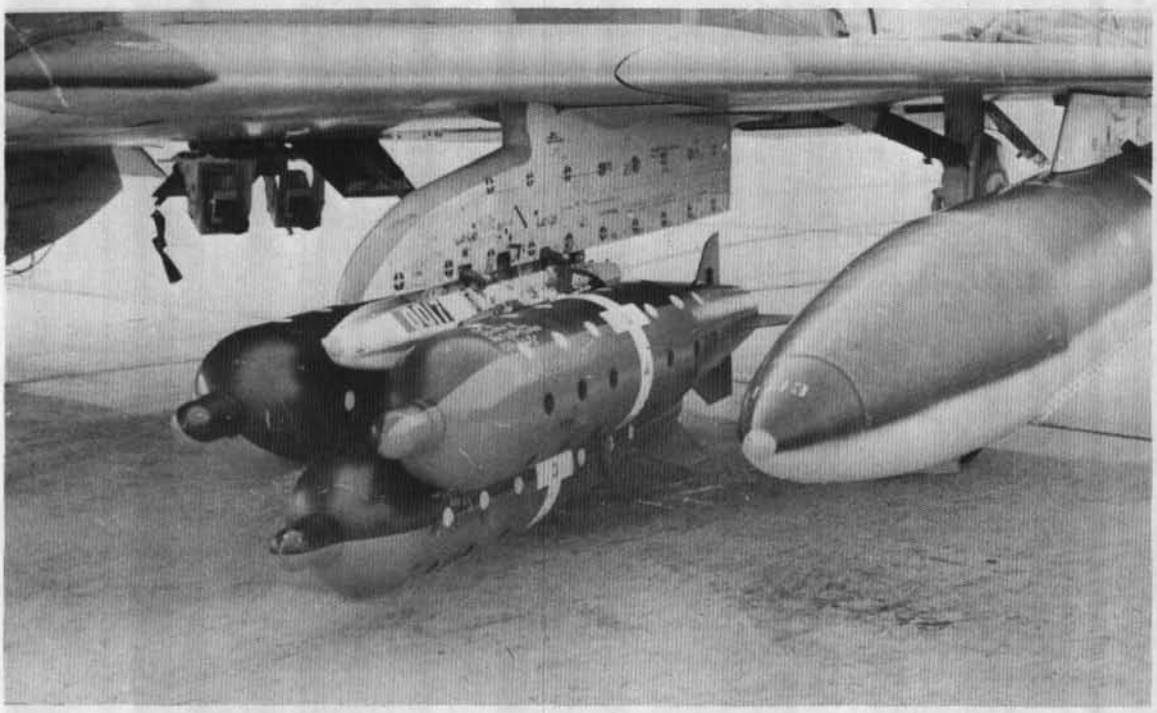

b. Front view

Figure 15. Installation photograph of full-scale MVB on TER and F-4C aircraft.

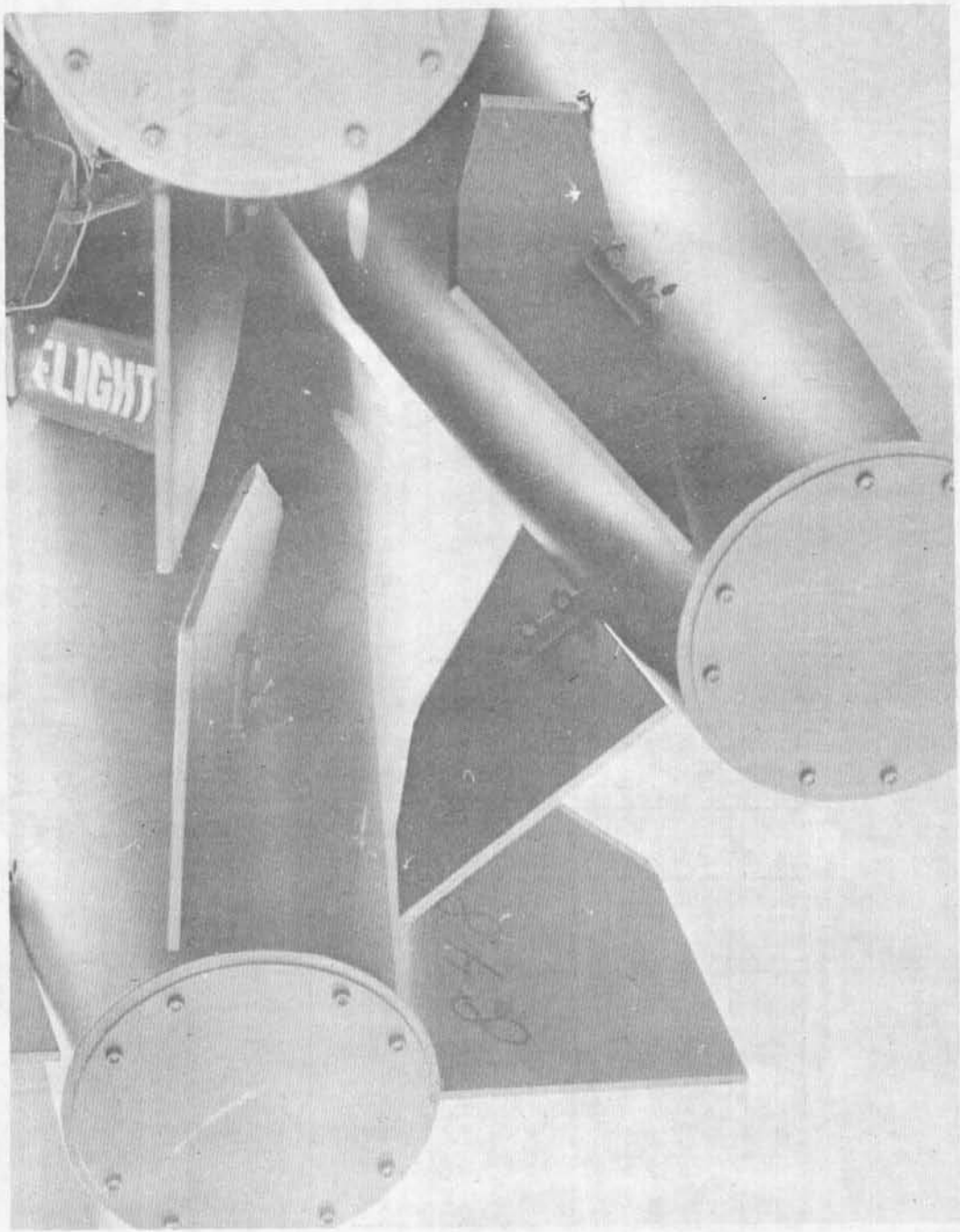

c. Aft view
Figure 15. Concluded.

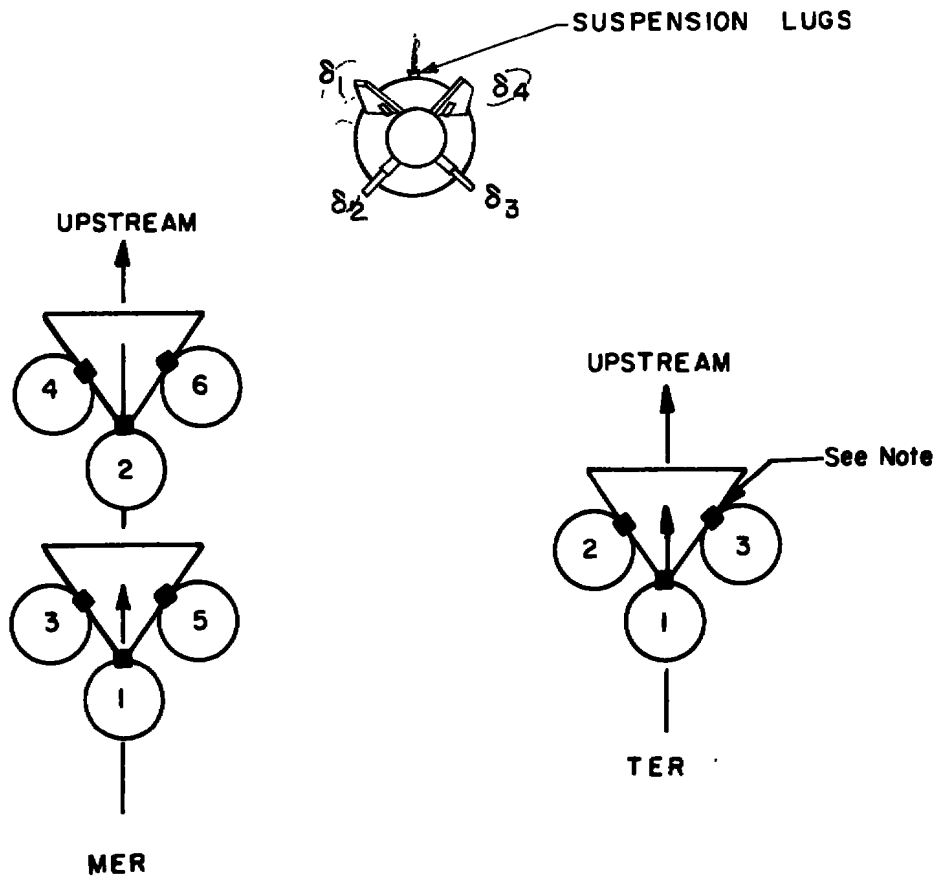

NOTE: The square indicates the orientation of the suspension lugs

TYPE RACK	STATION	ROLL ORIENTATION, deg
MER	1	0
	2	0
	3	45
	4	45
	5	-45
	6	-45
TER	1	0
	2	45
	3	-45

Figure 16. MER and TER store stations and orientations.

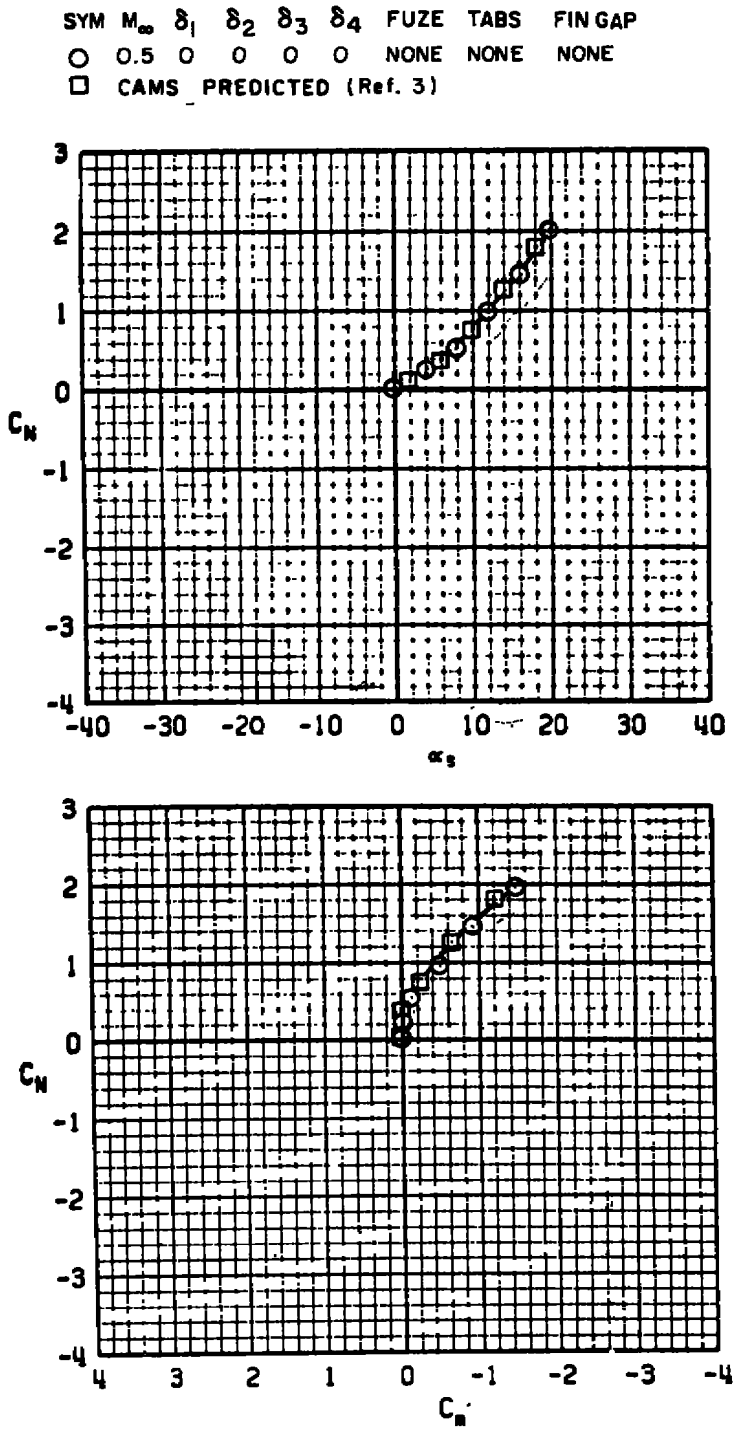

a. $M_\infty = 0.50$

Figure 17. Comparison of wind tunnel 0.25-scale MVB static stability data with predicted data of CAMS.

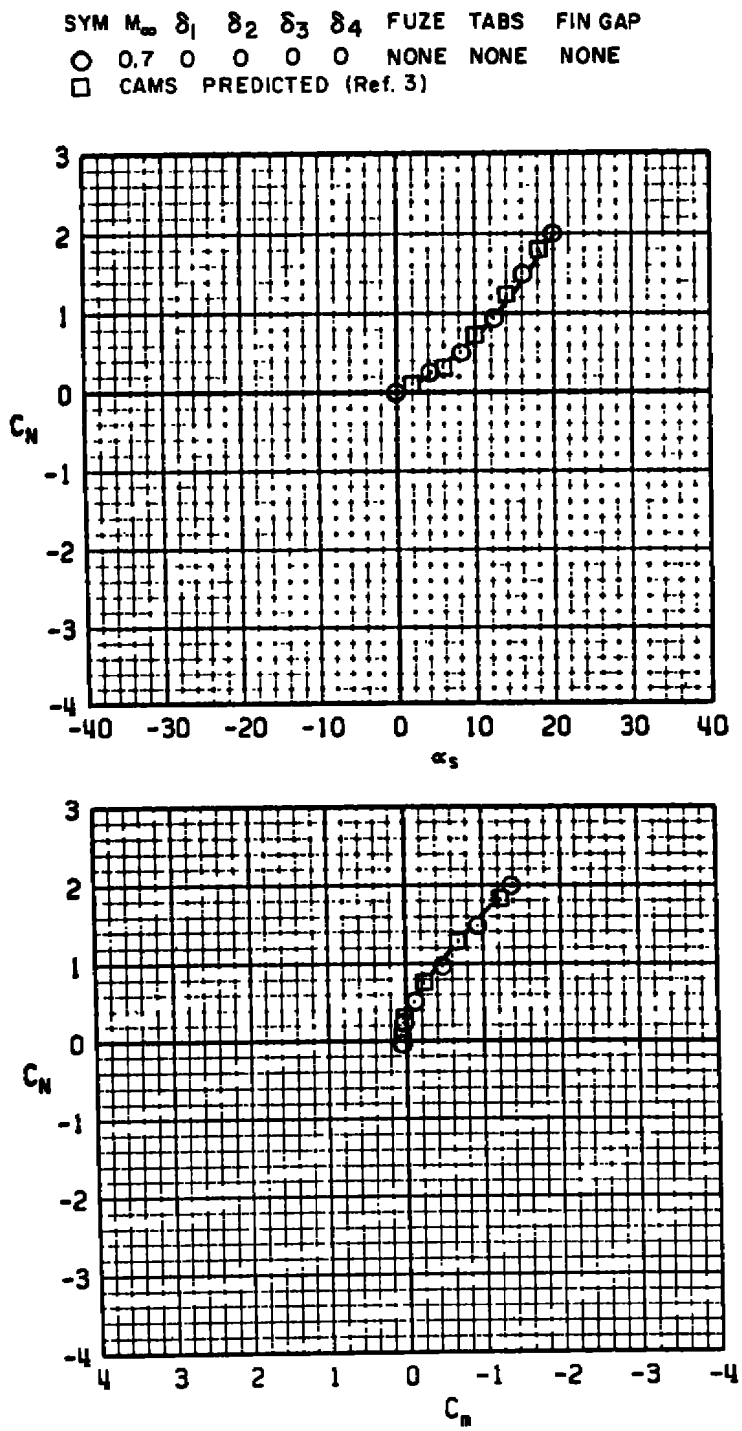

b. $M_\infty = 0.70$

Figure 17. Continued.

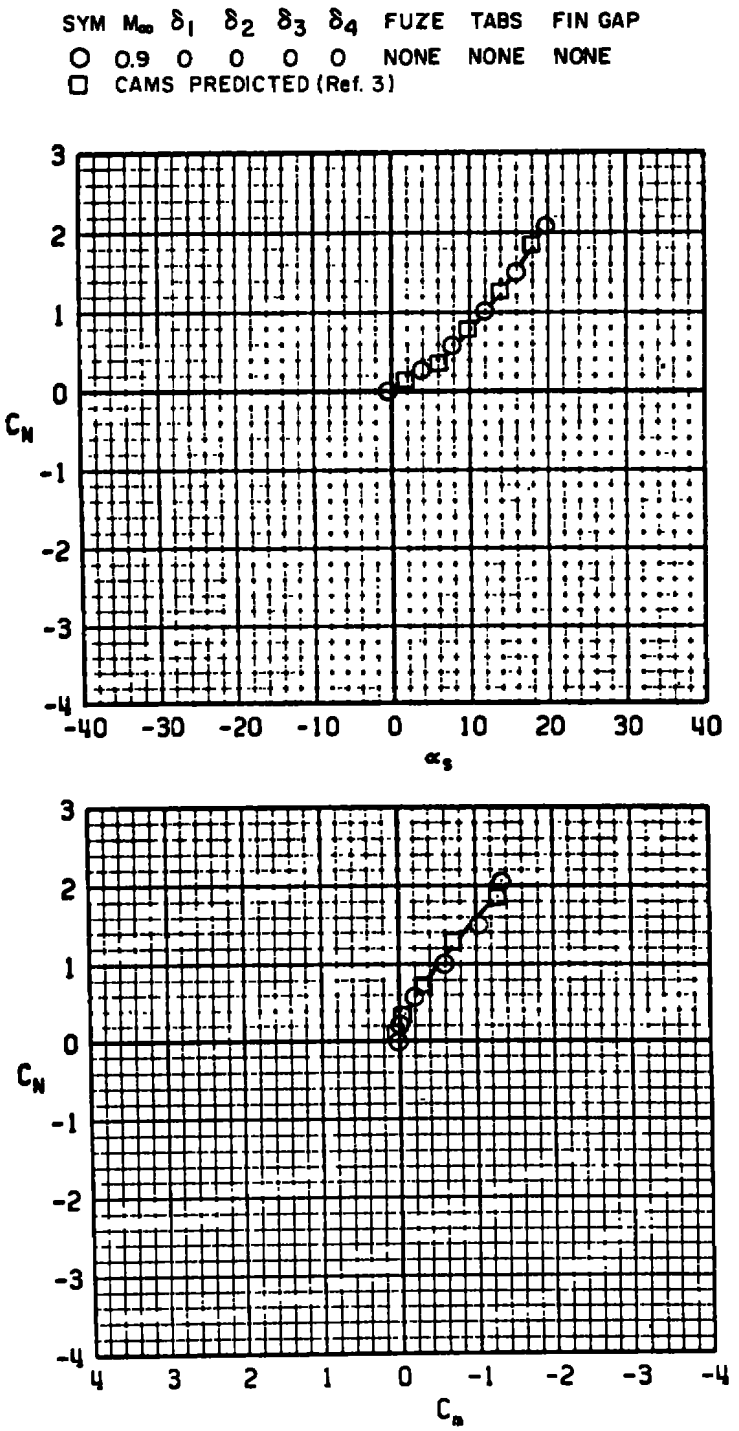

c. $M_\infty = 0.90$

Figure 17. Continued.

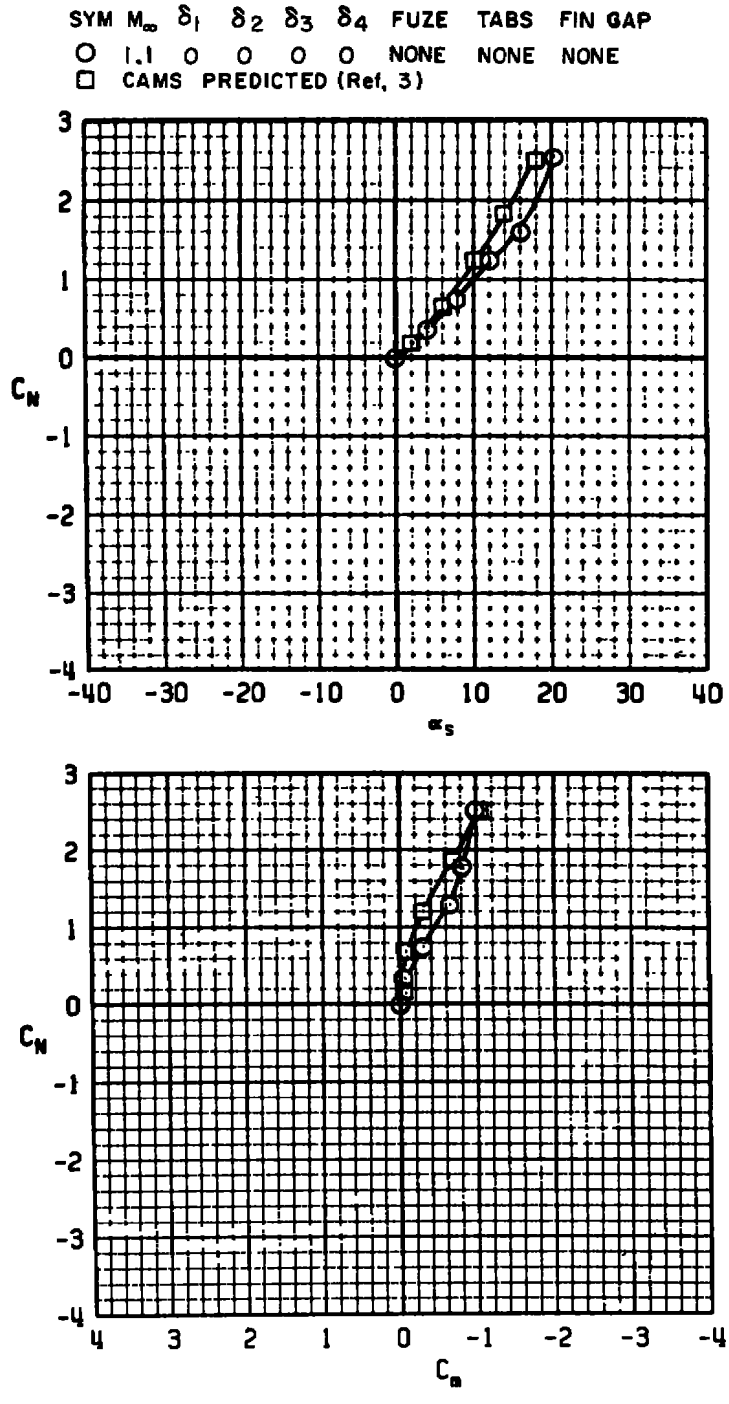

d. $M_\infty = 1.10$

Figure 17. Concluded.

SYM	M_∞	δ_1	δ_2	δ_3	δ_4	FUZE	TABS	FIN GAP	X_{NP}
⊙	0.5	0	0	0	0	NONE	NONE	NO FINS	-60.69
⊡	0.5	0	0	0	0	NONE	NONE	YES	35.36
△	0.5	0	0	0	0	NONE	YES	YES	46.75
◇	0.5	0	0	0	0	FMU-56	YES	YES	45.88

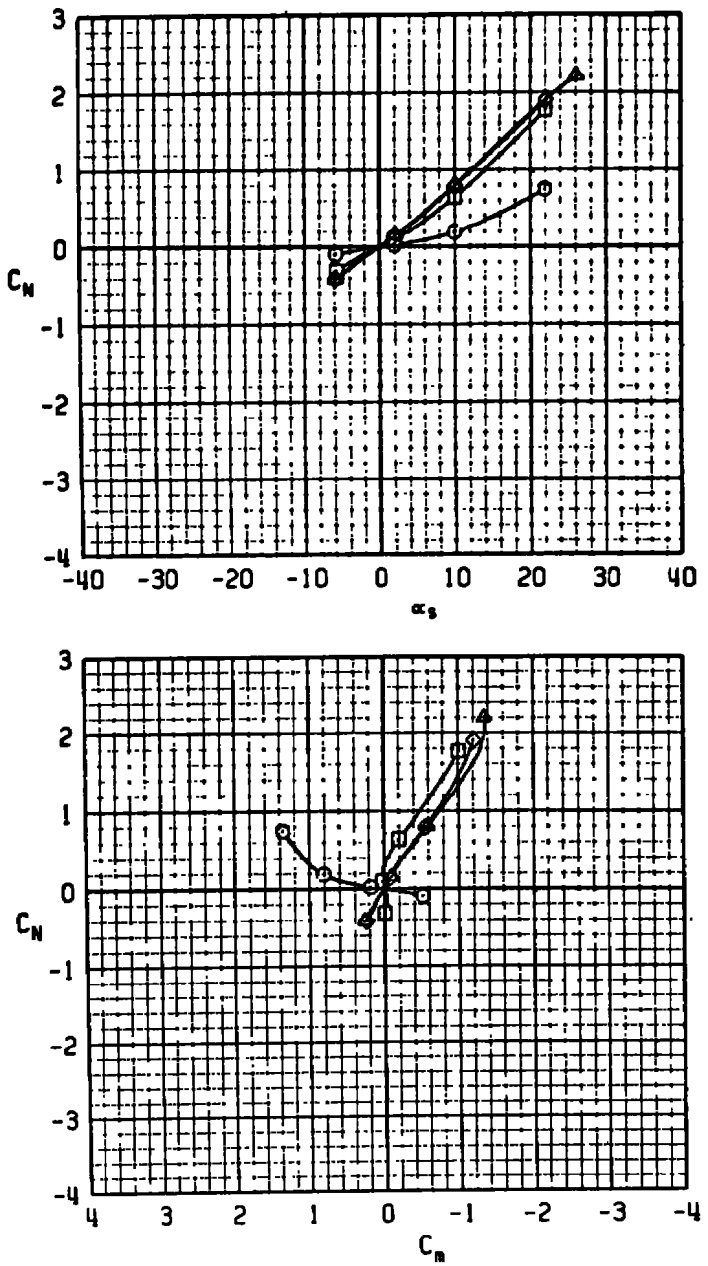

a. $M_\infty = 0.50$

Figure 18. Effects of fuze, tabs, and fins on the 0.25-scale MVB static stability.

SYM	M_∞	δ_1	δ_2	δ_3	δ_4	FUZE	TABS	FIN GAP	X_{NP}
⊙	0.7	0	0	0	0	NONE	NONE	NO FINS	-63.36
⊡	0.7	0	0	0	0	NONE	NONE	YES	32.096
△	0.7	0	0	0	0	NONE	YES	YES	47.36
◇	0.7	0	0	0	0	FMU-56	YES	YES	45.98

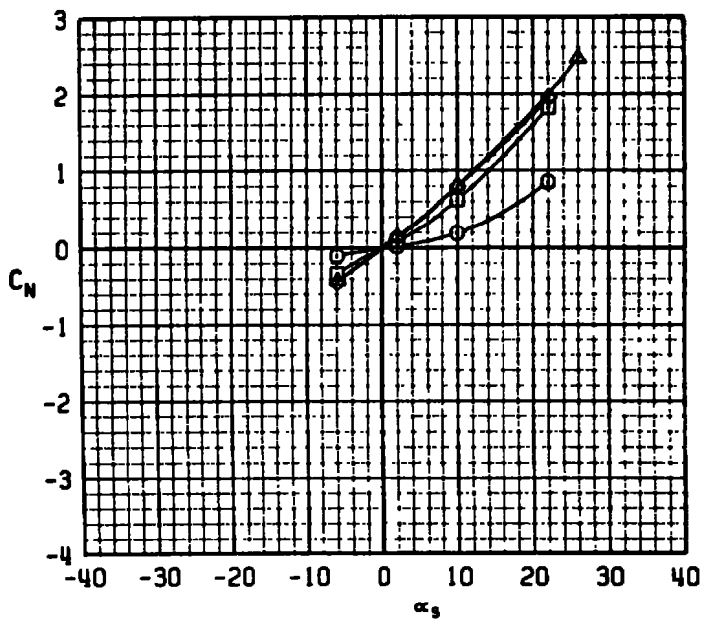

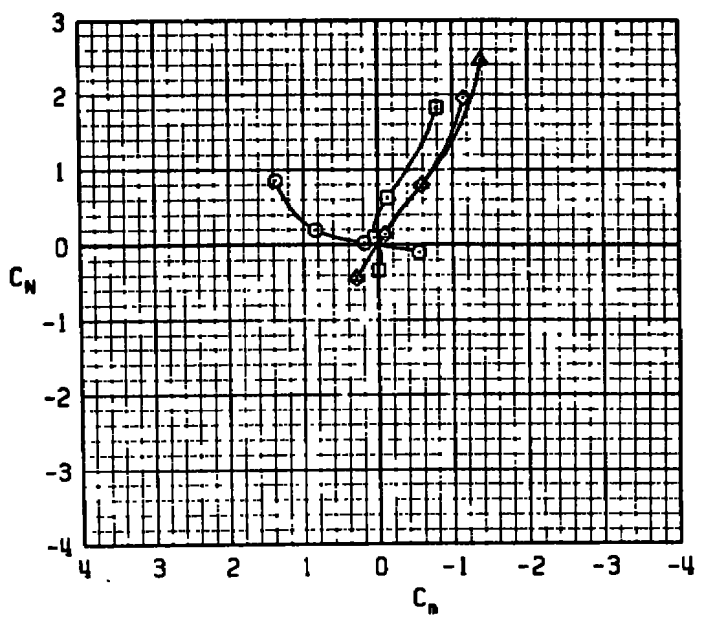

b. $M_\infty = 0.70$

Figure 18. Continued.

SYM	M_∞	δ_1	δ_2	δ_3	δ_4	FUZE	TABS	FIN GAP	X_{NP}
⊙	0.9	0	0	0	0	NONE	NONE	NO FINS	-28.72
⊡	0.9	0	0	0	0	NONE	NONE	YES	35.04
△	0.9	0	0	0	0	NONE	YES	YES	52.59
◇	0.9	0	0	0	0	FMU-56	YES	YES	47.34

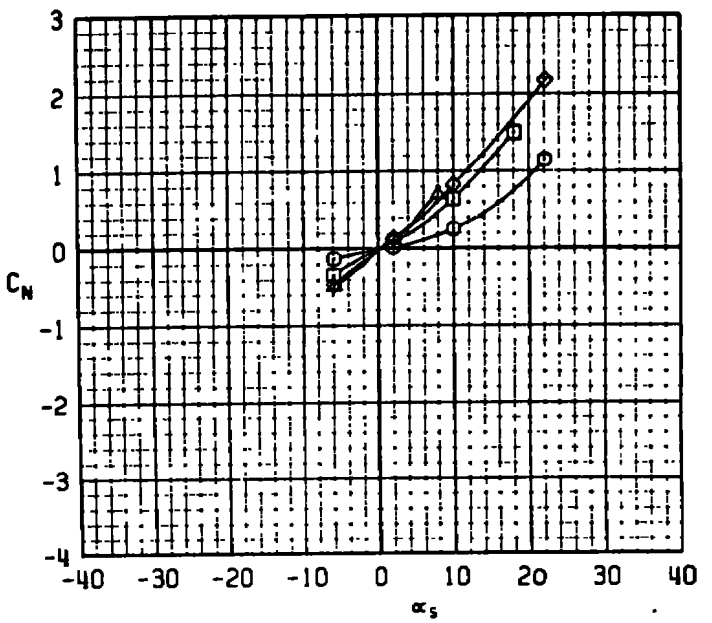

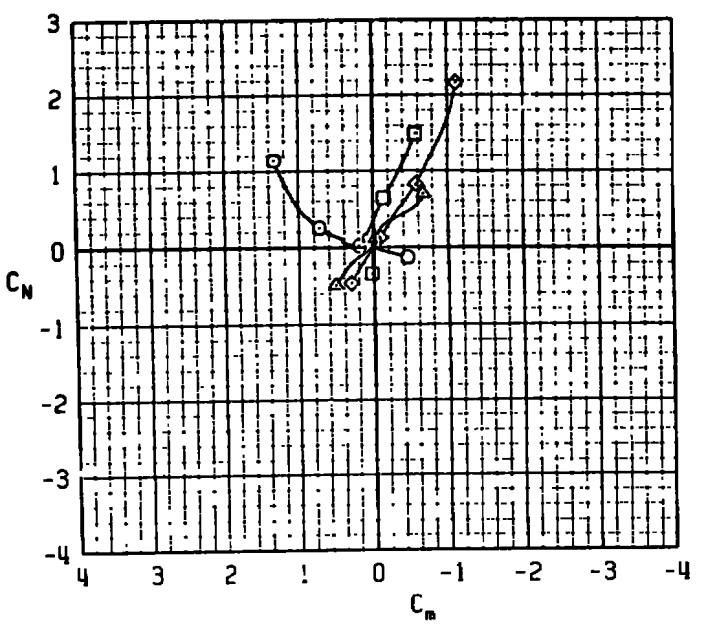

c. $M_\infty = 0.90$

Figure 18. Continued.

SYM	M_∞	δ_1	δ_2	δ_3	δ_4	FUZE	TABS	FIN GAP	X_{NP}
⊙	1.1	0	0	0	0	NONE	NONE	NO FINS	-54.03
⊡	1.1	0	0	0	0	NONE	NONE	YES	31.36
△	1.1	0	0	0	0	NONE	YES	YES	45.47
◇	1.1	0	0	0	0	FMU-56	YES	YES	44.27

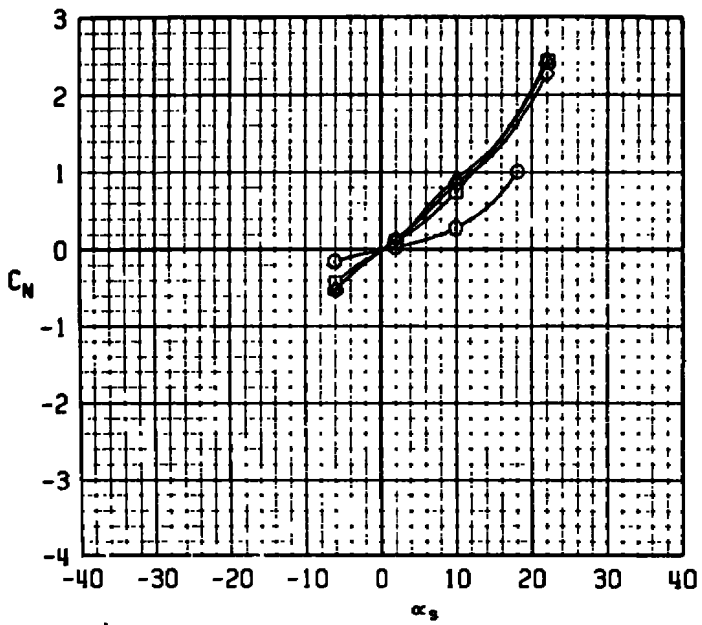

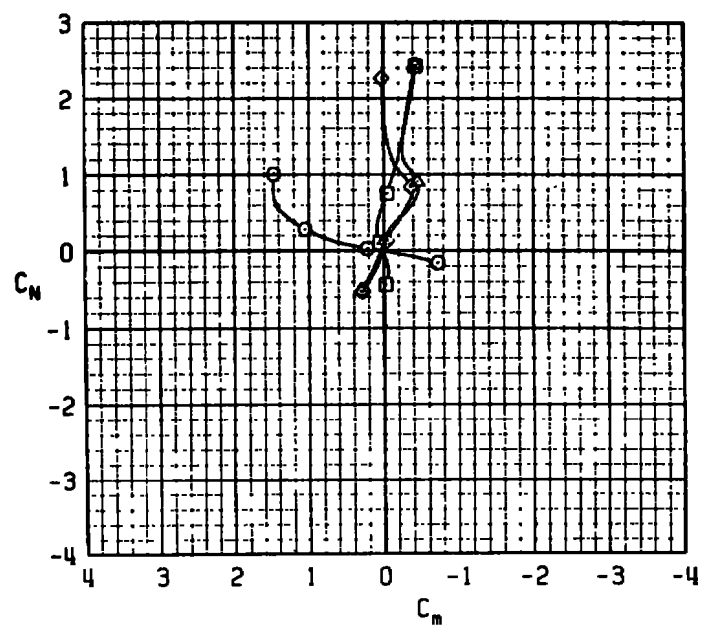

d. $M_\infty = 1.10$

Figure 18. Concluded.

SYM	M_∞	δ_1	δ_2	δ_3	δ_4	FUZE	TABS	FIN GAP
□	0.5	-12	0	0	-12	NONE	NONE	YES
△	0.5	-12	0	0	-12	NONE	YES	YES
◇	0.5	-12	0	0	-12	FMU-56	YES	YES

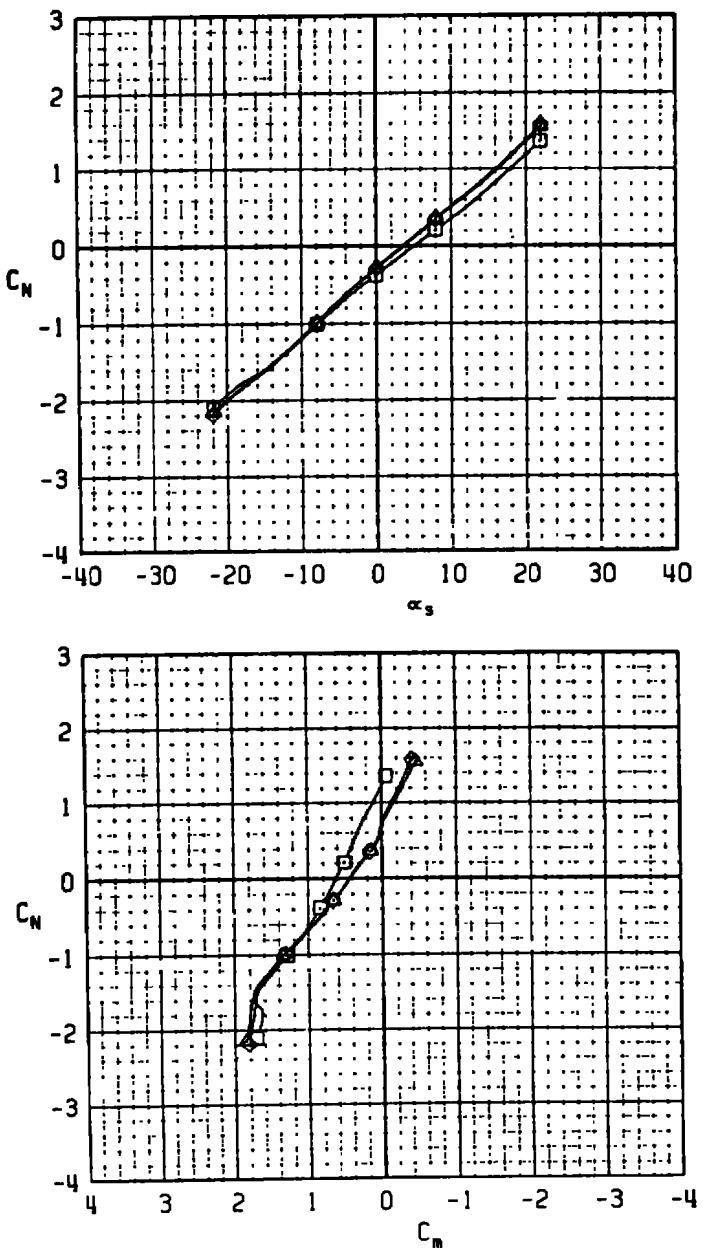

a. $M_\infty = 0.50$

Figure 19. Effects of fuze and tabs on the MVB static stability, fins canted.

SYM	M_∞	δ_1	δ_2	δ_3	δ_4	FUZE	TABS	FIN GAP
⊡	0.7	-12	0	0	-12	NONE	NONE	YES
◇	0.7	-12	0	0	-12	FMU-56	YES	YES

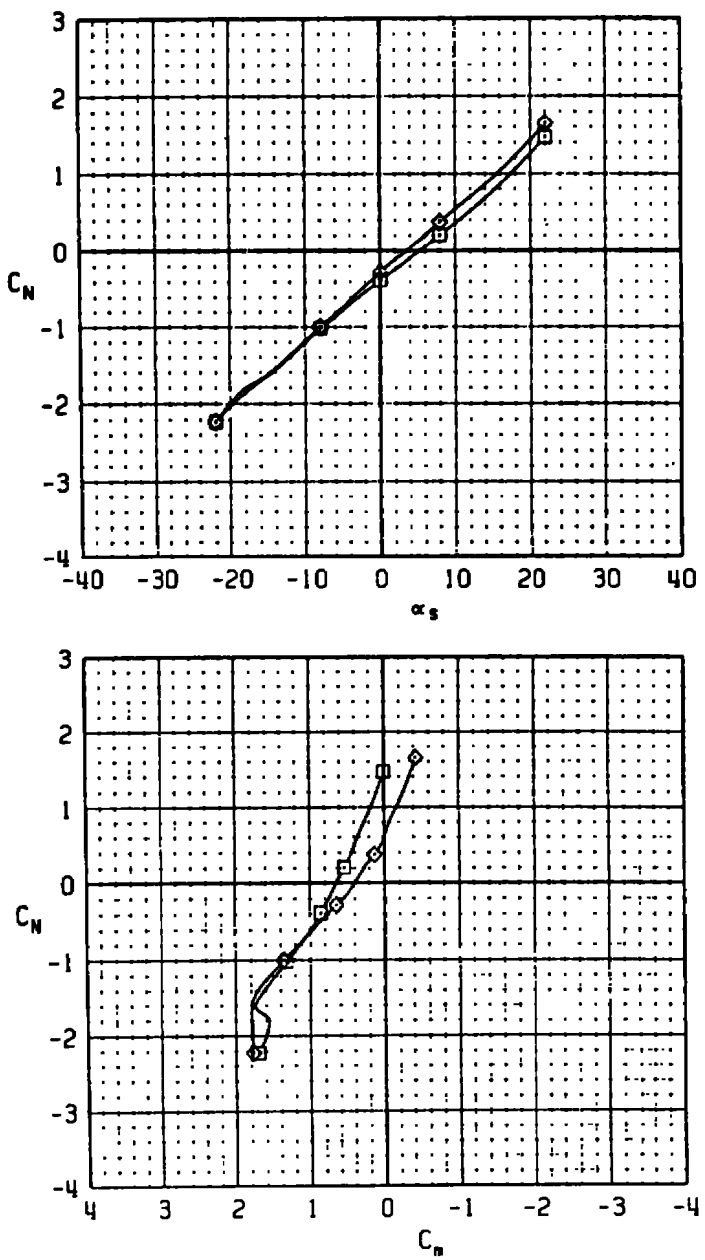

b. $M_\infty = 0.70$

Figure 19. Continued.

SYM	M_∞	δ_1	δ_2	δ_3	δ_4	FUZE	TABS	FIN GAP	H.L.
⊡	0.9	-12	0	0	-12	NONE	NONE	YES	5
△	0.9	-12	0	0	-12	NONE	YES	YES	5
◇	0.9	-12	0	0	-12	FMU-56	YES	YES	5
⊙	0.9	-12	0	0	-12	FMU-56	YES	YES	8

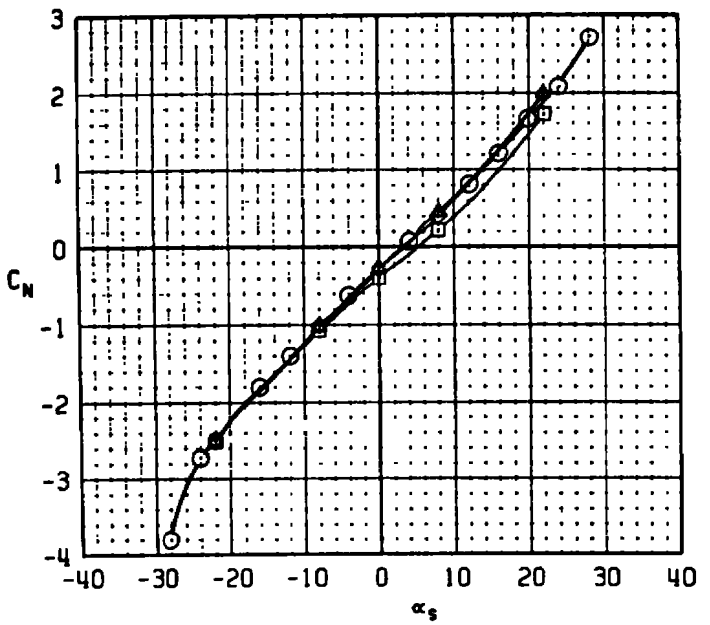

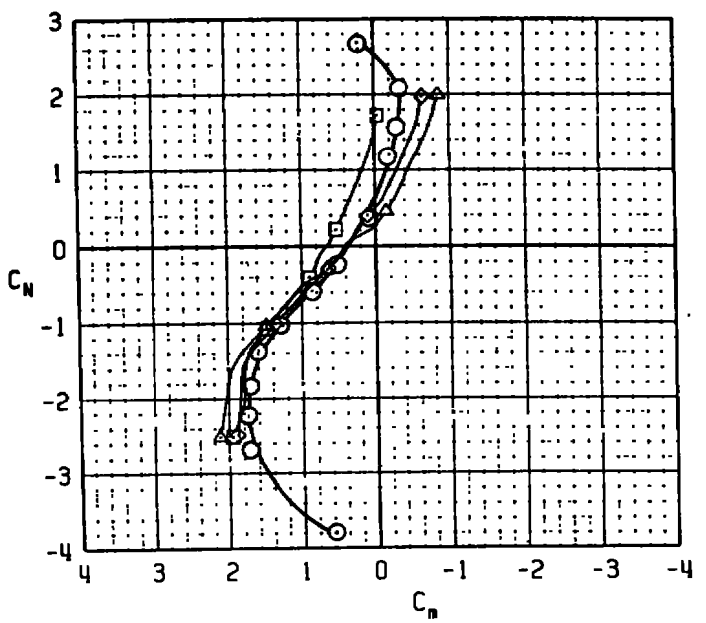

c. $M_\infty = 0.90$

Figure 19. Continued.

SYM	M_∞	δ_1	δ_2	δ_3	δ_4	FUZE	TABS	FIN GAP
⊡	1.1	-12	0	0	-12	NONE	NONE	YES
▲	1.1	-12	0	0	-12	NONE	YES	YES
◈	1.1	-12	0	0	-12	FMU-56	YES	YES

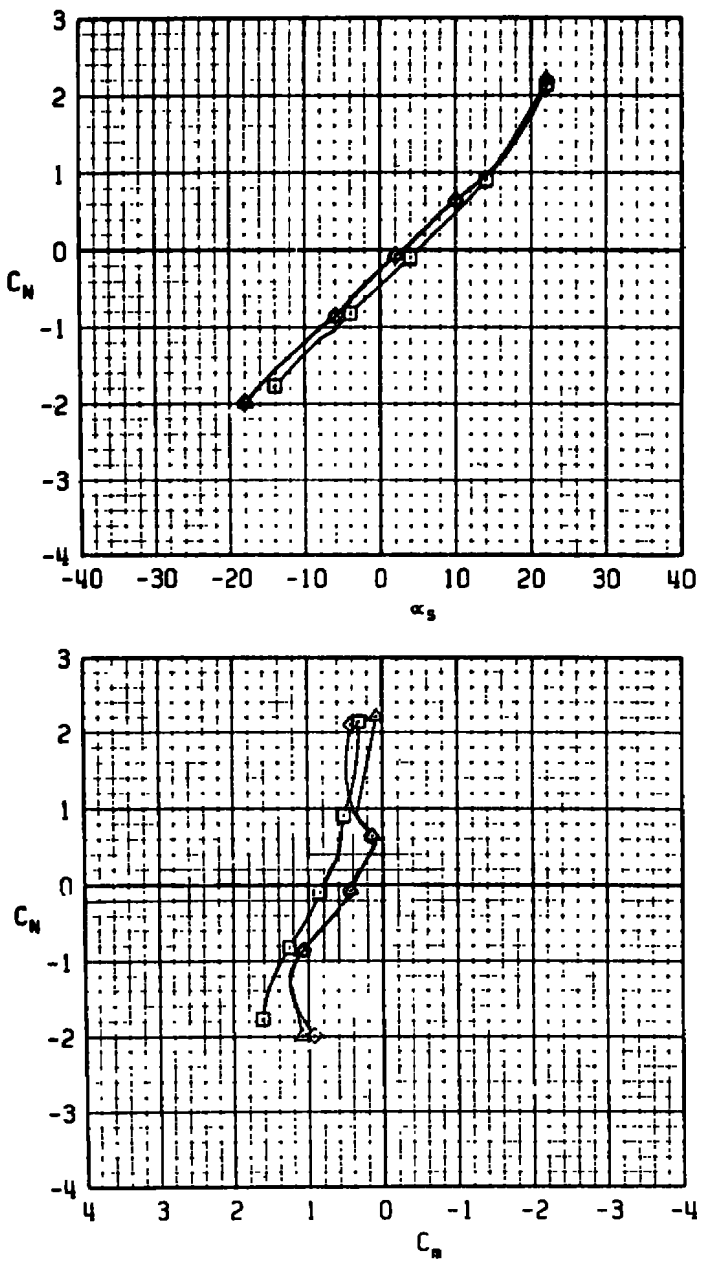

d. $M_\infty = 1.10$

Figure 19. Concluded.

SYM	M_∞	δ_1	δ_2	δ_3	δ_4	FUZE	TABS	FIN GAP	SCALE
△	0.5	-12	0	0	-12	FMU-56	NONE	YES	0.25
◇	0.5	-12	0	0	-12	NONE	NONE	NONE	0 05

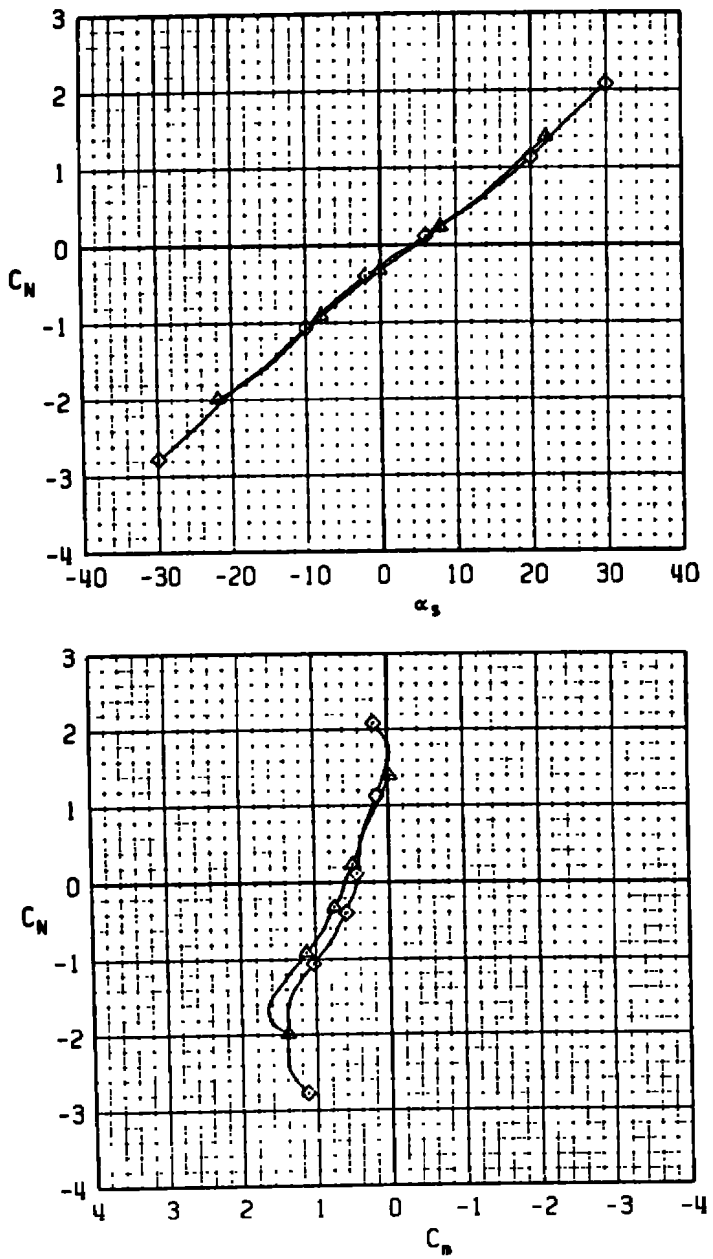

a. $M_\infty = 0.50$

Figure 20. Effects of model scale on the static stability of the MVB, fins canted.

SYM	M_∞	δ_1	δ_2	δ_3	δ_4	FUZE	TABS	FIN GAP	H.L.	SCALE
△	0.7	-12	0	0	-12	FMU-56	NONE	YES	5	0.25
◇	0.7	-12	0	0	-12	NONE	NONE	NONE	5	0.05
⊙	0.7	-12	0	0	-12	FMU-56	NONE	YES	8	0.05

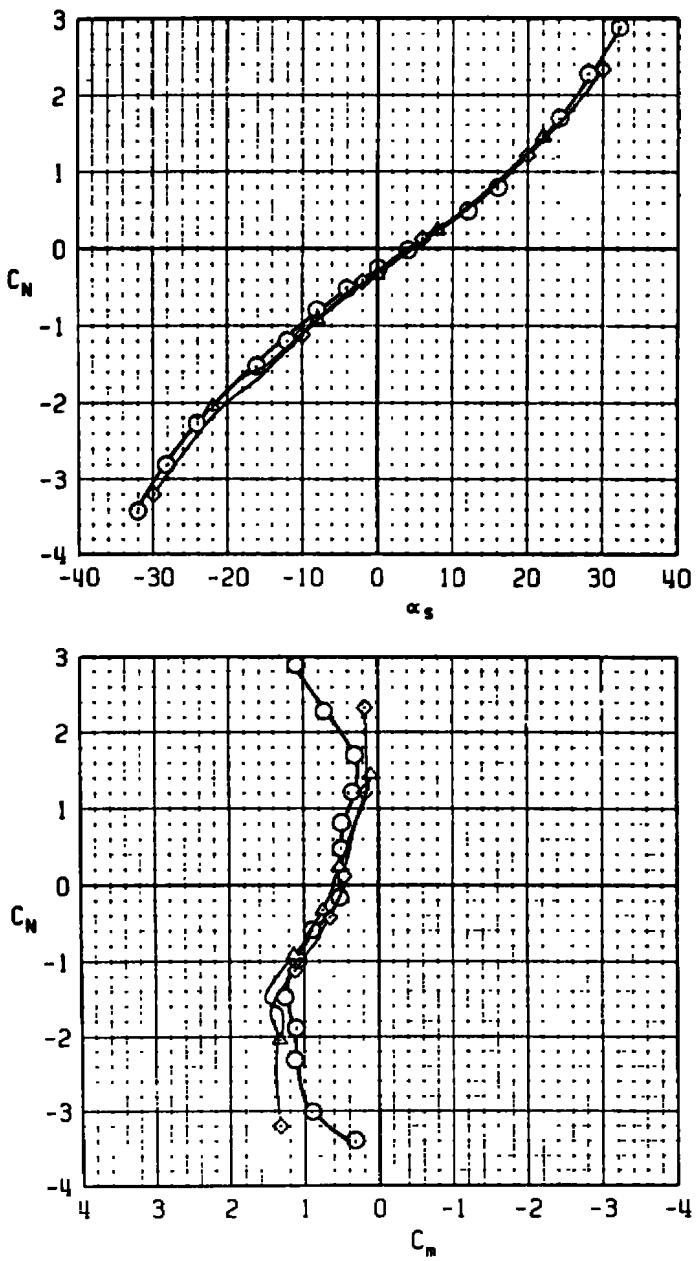

b. $M_\infty = 0.70$

Figure 20. Continued.

SYM	M_∞	δ_1	δ_2	δ_3	δ_4	FUZE	TABS	FIN GAP	H.L.	SCALE
△	0.9	-12	0	0	-12	FMU-56	NONE	YES	5	0.25
◇	0.9	-12	0	0	-12	NONE	NONE	NONE	5	0.05
○	0.9	-12	0	0	-12	FMU-56	NONE	YES	8	0.05

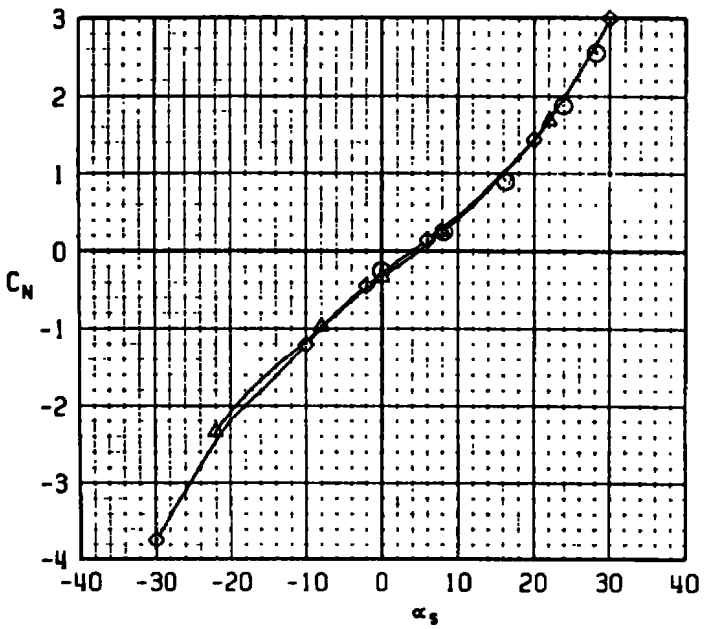

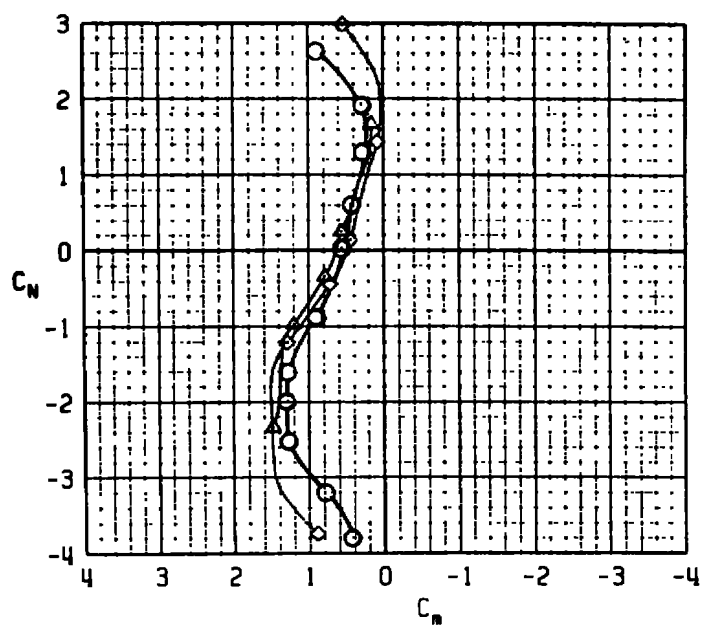

c. $M_\infty = 0.90$

Figure 20. Concluded.

SYM	M_∞	δ_1	δ_2	δ_3	δ_4	FUZE	TABS	FIN GAP	$Re_d \times 10^{-5}$	X_{NP}	SCALE
⊡	0.5	0	0	0	0	NONE	NONE	NONE	10.80	39.33	0.25
△	0.5	0	0	0	0	NONE	NONE	NONE	1.87	38.40	0.25
⊙	0.5	0	0	0	0	NONE	NONE	NONE	1.81	38.20	0.05

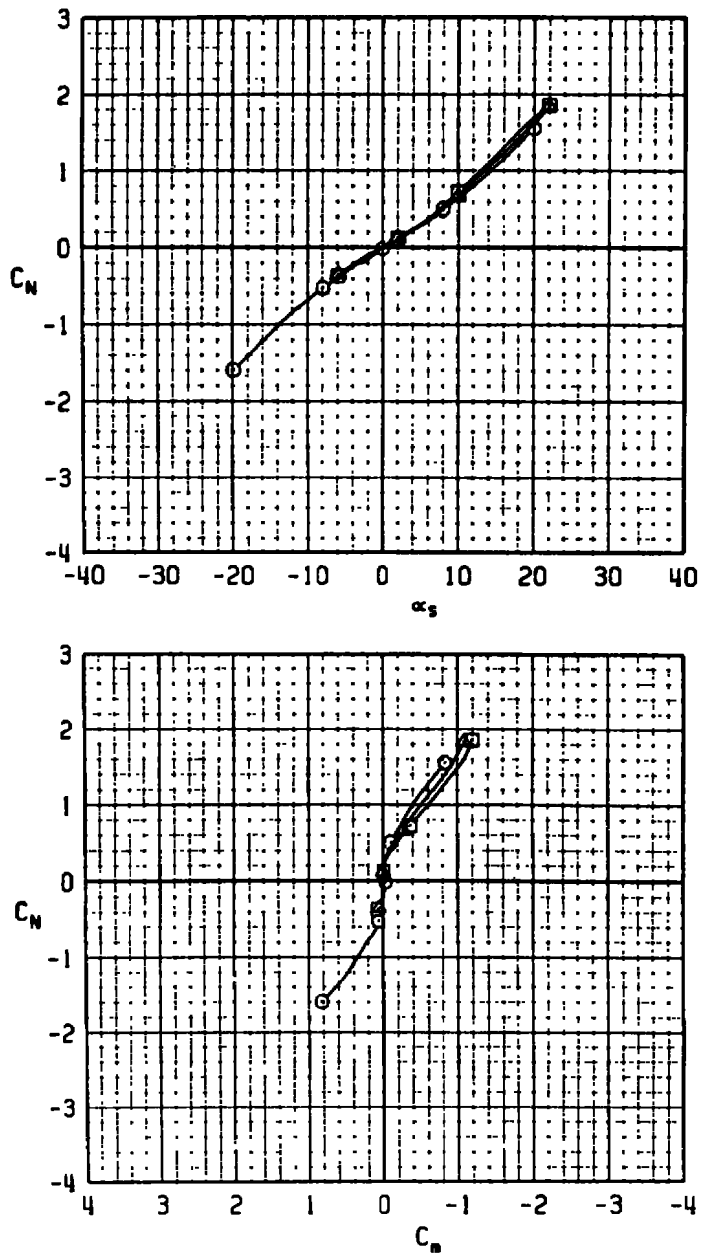

a. $M_\infty = 0.50$

Figure 21. Effects of Reynolds number on the MVB static stability.

SYM	M_∞	δ_1	δ_2	δ_3	δ_4	FUZE	TABS	FIN GAP	$Re_d \times 10^{-5}$	X_{NP}	SCALE
⊡	0.7	0	0	0	0	NONE	NONE	NONE	8.03	37.57	0.25
△	0.7	0	0	0	0	NONE	NONE	NONE	1.82	37.10	0.25
⊙	0.7	0	0	0	0	NONE	NONE	NONE	1.38	37.00	0.05

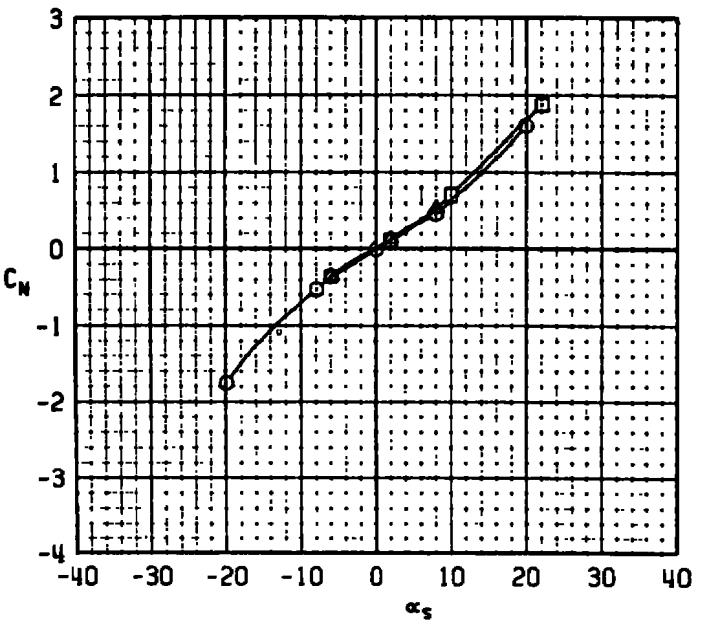

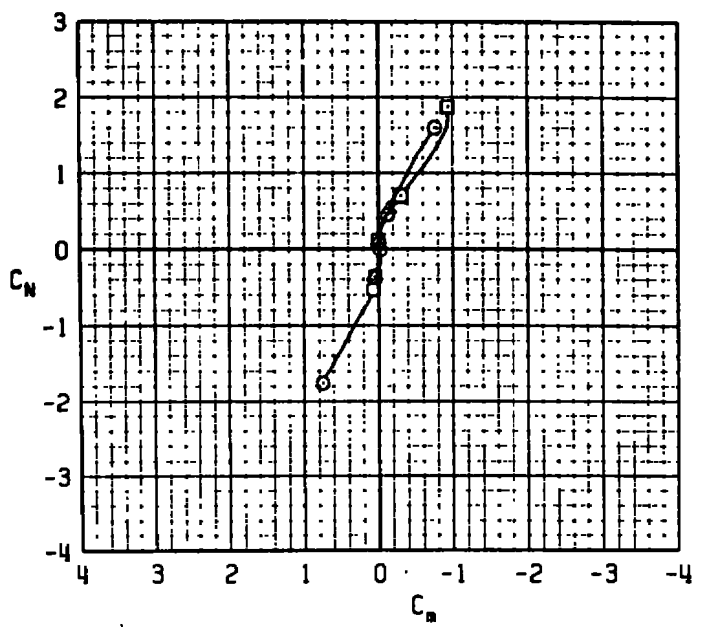

b. $M_\infty = 0.70$

Figure 21. Continued.

SYM	M_∞	δ_1	δ_2	δ_3	δ_4	FUZE	TABS	FIN GAP	$Re_d \times 10^{-5}$	X_{NP}	SCALE
⊡	0.9	0	0	0	0	NONE	NONE	NONE	6.62	39.68	0.25
△	0.9	0	0	0	0	NONE	NONE	NONE	1.48	38.96	0.25
⊙	0.9	0	0	0	0	NONE	NONE	NONE	1.58	38.86	0.05

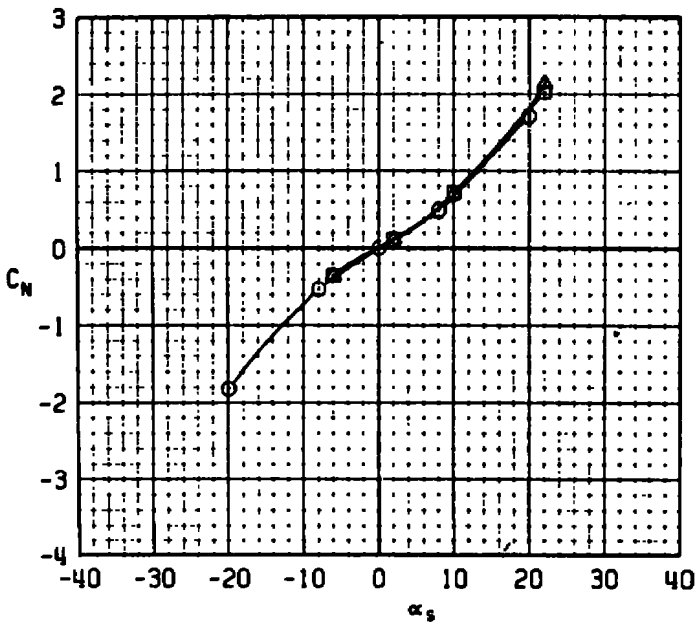

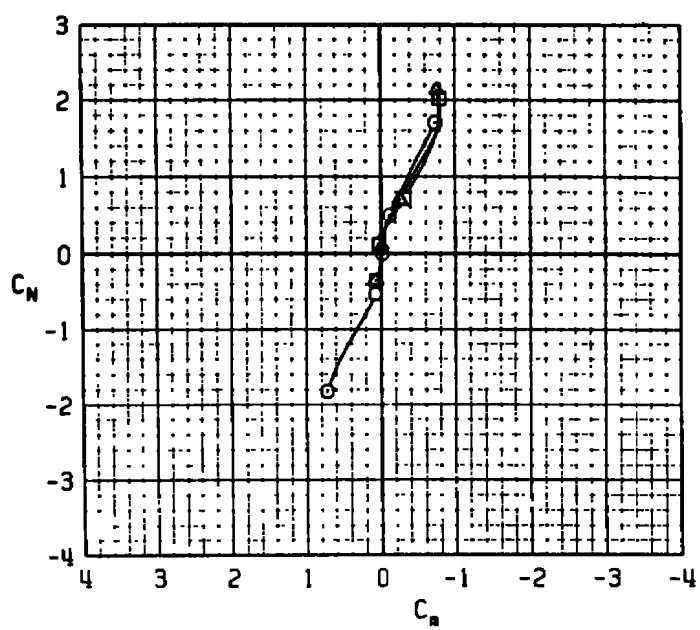

c. $M_\infty = 0.90$

Figure 21. Continued.

SYM	M_∞	δ_1	δ_2	δ_3	δ_4	FUZE	TABS	FIN GAP	$Re_d \times 10^{-5}$	X_{NP}	SCALE
⊡	1.1	0	0	0	0	NONE	NONE	NONE	6.31	35.66	0.25
⊙	1.1	0	0	0	0	NONE	NONE	NONE	1.65	35.00	0.05

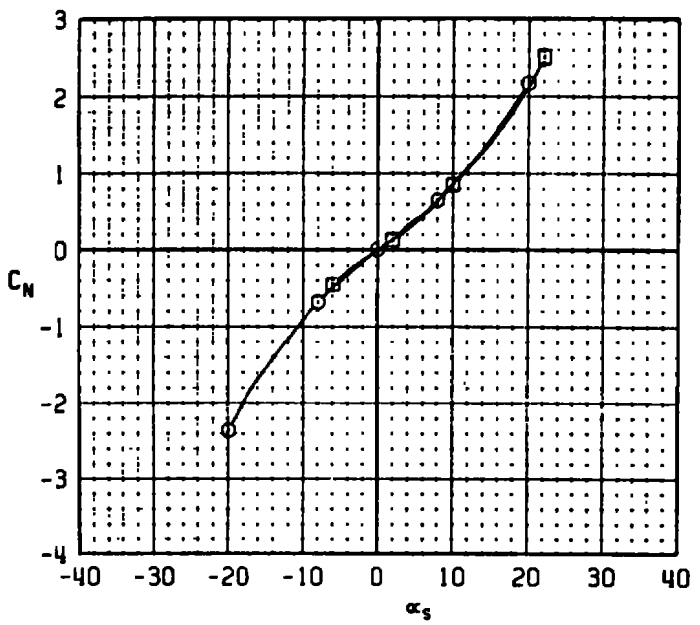

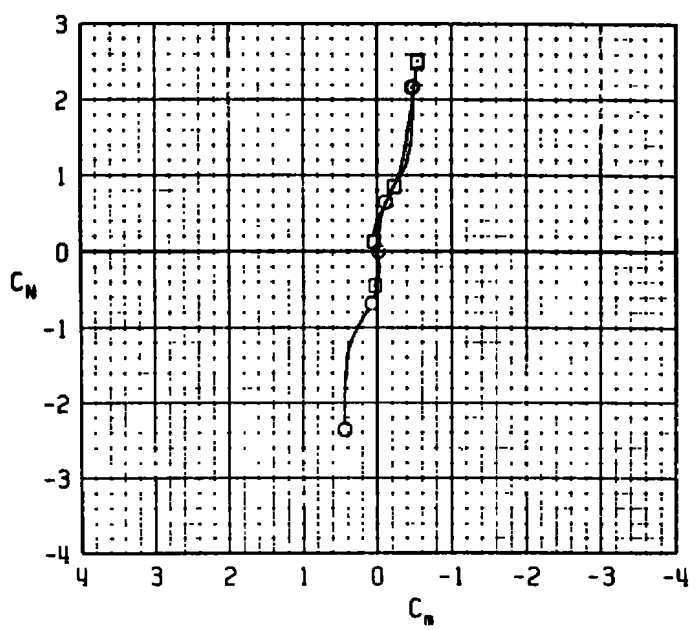

d. $M_\infty = 1.10$

Figure 21. Concluded.

SYM	M_∞	α	δ_1	δ_2	δ_3	δ_4	FUZE	TABS	FIN GAP	H.L.
○	0.5	4	0	0	0	0	NONE	NONE	NONE	5
□	0.5	4	0	0	0	0	NONE	YES	NONE	5

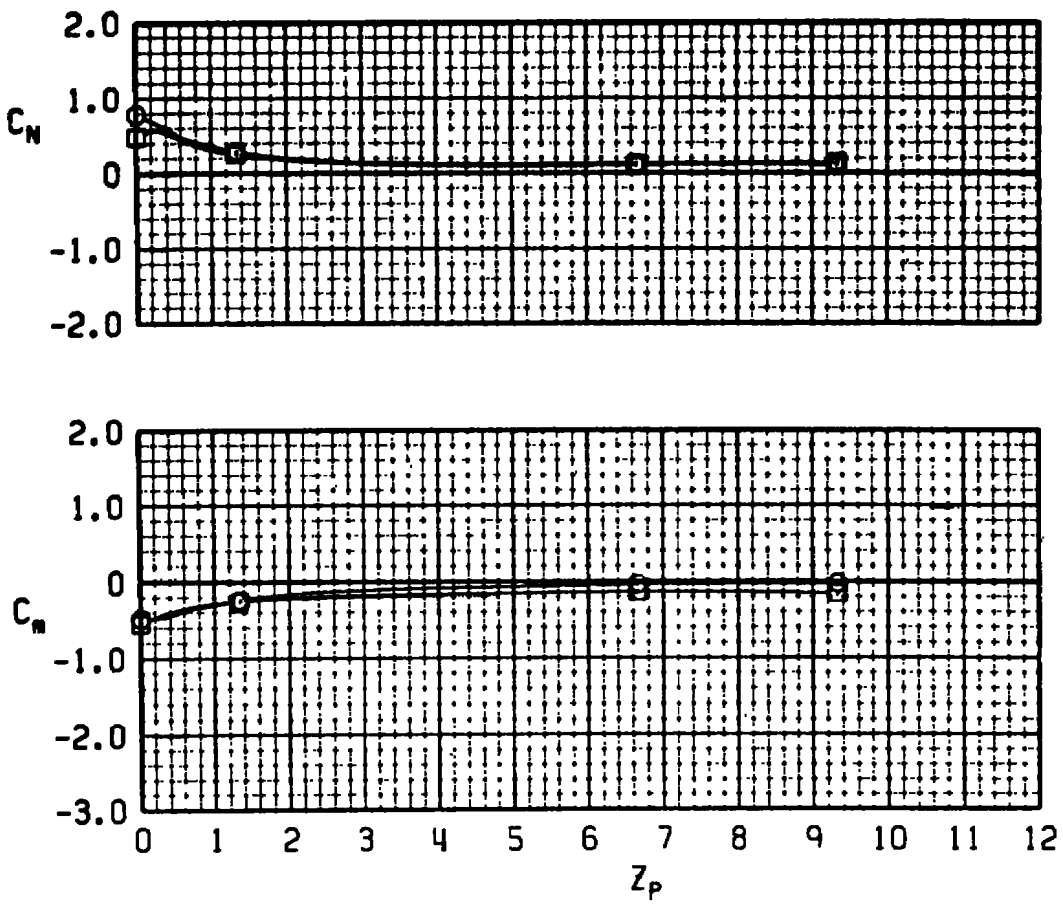

a. $M_\infty = 0.50$

Figure 22. Aerodynamic characteristics of the MVB in the F-4C flow field, fins uncanted.

SYM	M_∞	α	δ_1	δ_2	δ_3	δ_4	FUZE	TABS	FIN GAP	H.L.
○	0.9	0	0	0	0	0	NONE	NONE	NONE	5
□	0.9	0	0	0	0	0	NONE	YES	NONE	5

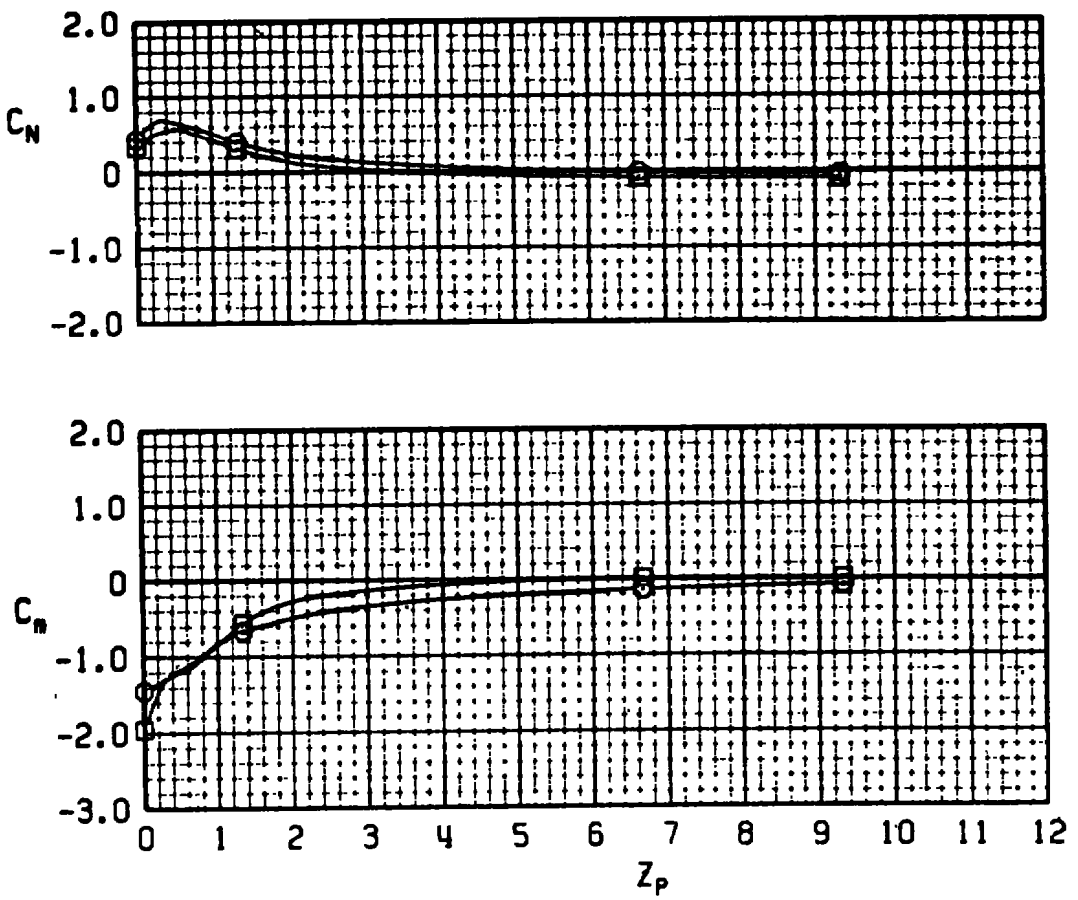

b. $M_\infty = 0.90$
Figure 22. Continued.

SYM	M_∞	α	δ_1	δ_2	δ_3	δ_4	FUZE	TABS	FIN GAP	H.L.
○	1.1	0	0	0	0	0	NONE	NONE	NONE	5
□	1.1	0	0	0	0	0	NONE	YES	NONE	5

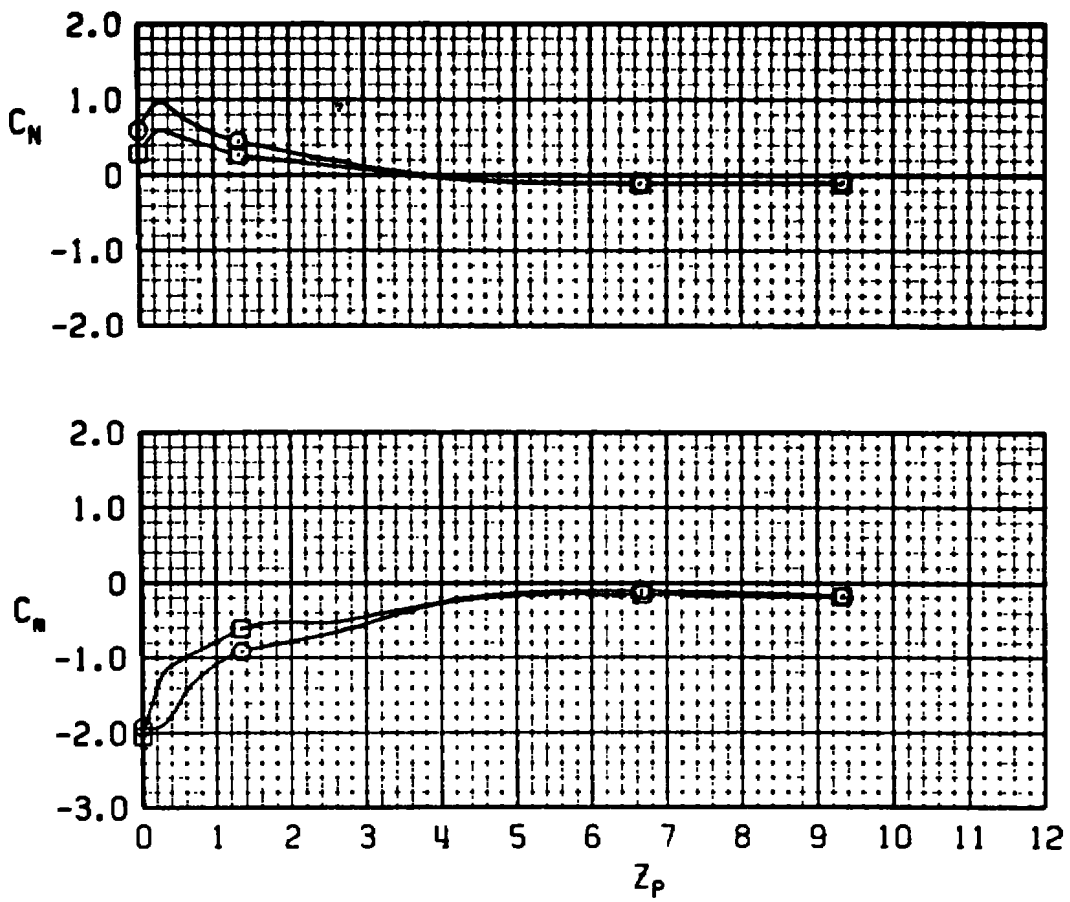

c. $M_\infty = 1.10$

Figure 22. Concluded.

SYM	M_∞	α	δ_1	δ_2	δ_3	δ_4	FUZE	TABS	FIN GAP	H.L.
○	0.5	4	-12	-12	-12	-12	NONE	NONE	NONE	5
□	0.5	4	-12	-12	-12	-12	NONE	YES	NONE	5

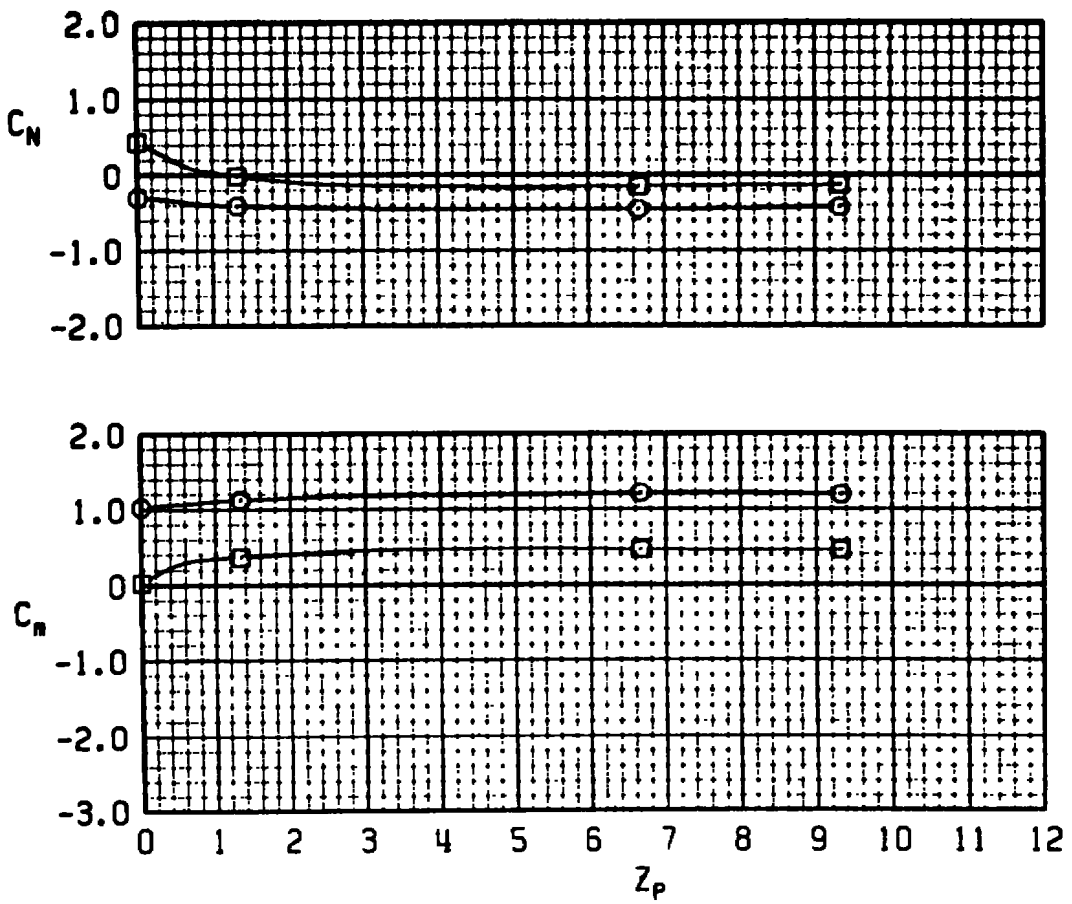

a. $M_\infty = 0.50$

Figure 23. Aerodynamic characteristics of the MVB in the F-4C flow field, fins canted.

SYM	M_∞	α	δ_1	δ_2	δ_3	δ_4	FUZE	TABS	FIN GAP	H.L.
○	0.7	2	-12	-12	-12	-12	NONE	NONE	NONE	5
□	0.7	2	-12	0	0	-12	NONE	YES	NONE	5
△	0.7	2	-12	0	0	-12	YES	NONE	NONE	8

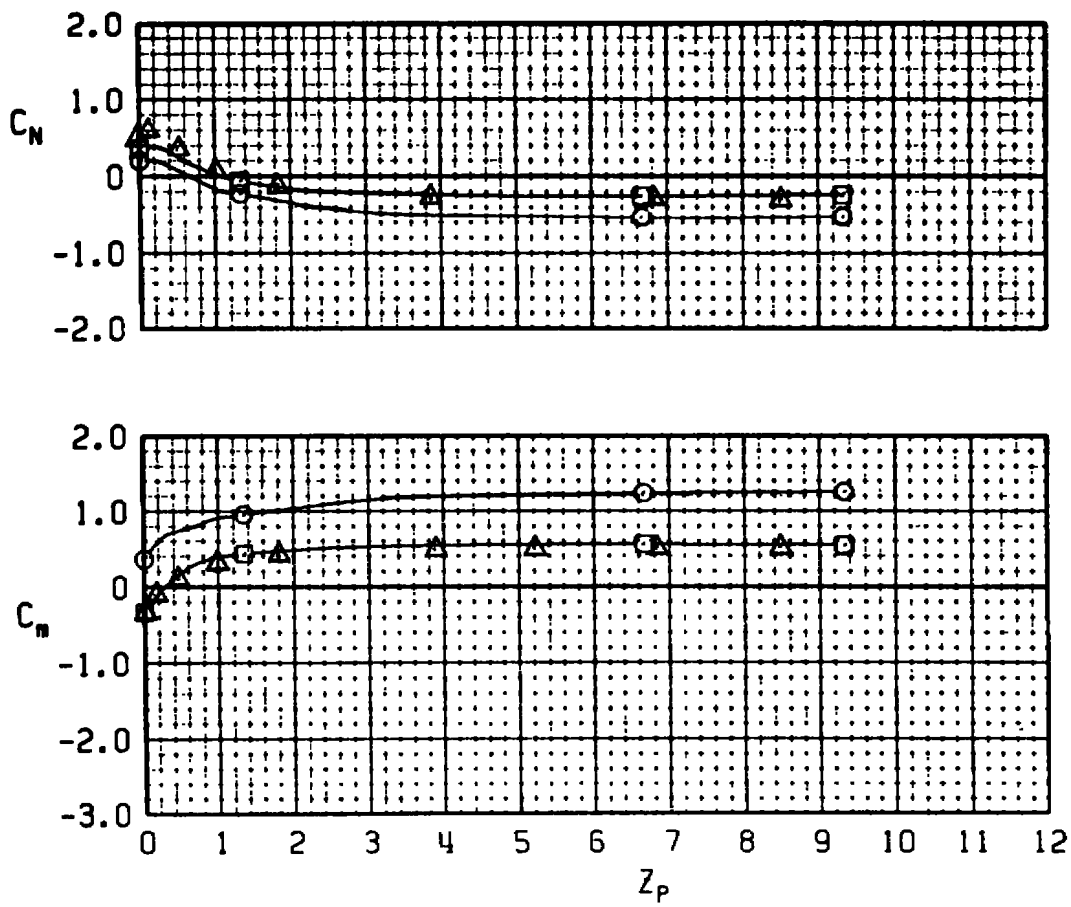

b. M_∞ = 0.70
Figure 23. Continued.

SYM	M_∞	α	δ_1	δ_2	δ_3	δ_4	FUZE	TABS	FIN GAP	H.L.
○	0.9	0	-12	-12	-12	-12	NONE	NONE	NONE	5
□	0.9	0	-12	0	0	-12	NONE	YES	NONE	5
△	0.9	0	-12	0	0	-12	YES	YES	YES	8
◇	0.9	0	-12	0	0	-12	YES	NONE	YES	8

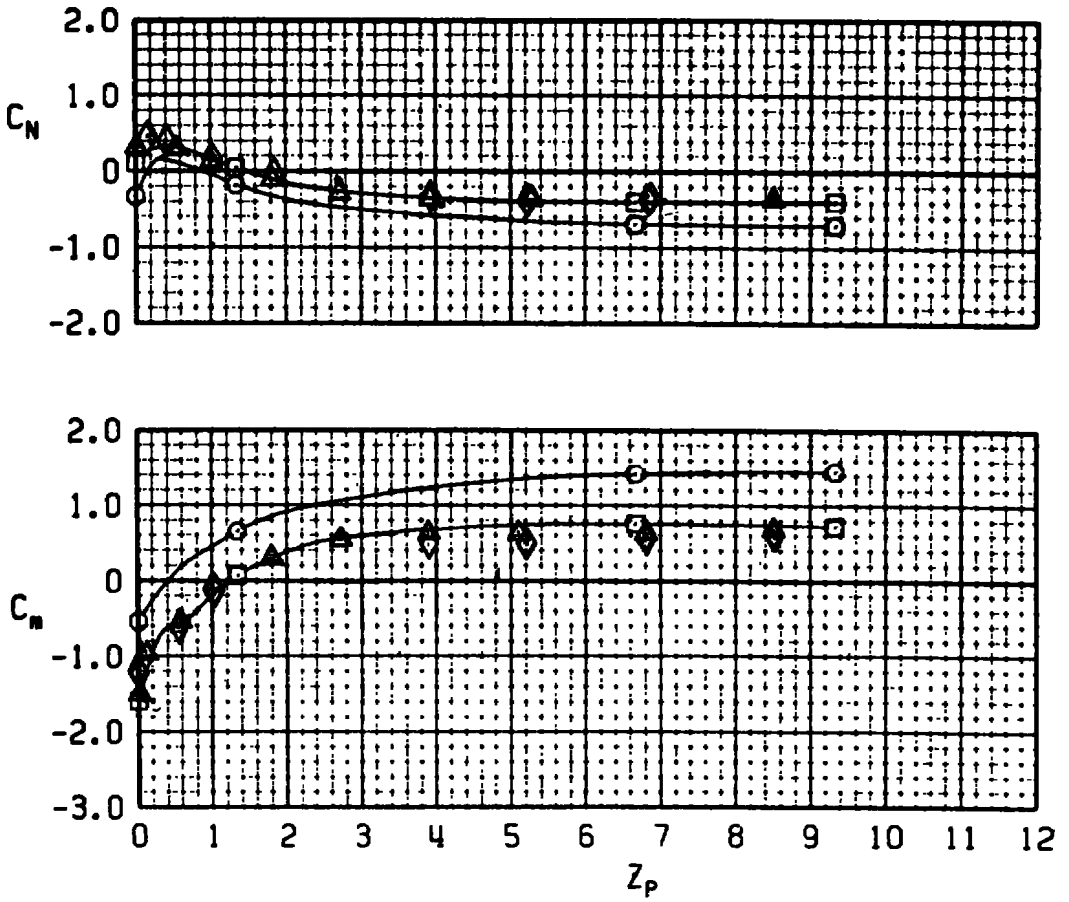

c. $M_\infty = 0.90$

Figure 23. Continued.

SYM	M_∞	α	δ_1	δ_2	δ_3	δ_4	FUZE	TABS	FIN GAP	H.L.
○	1.1	0	-12	-12	-12	-12	NONE	NONE	NONE	5
□	1.1	0	-12	0	0	-12	NONE	YES	NONE	5

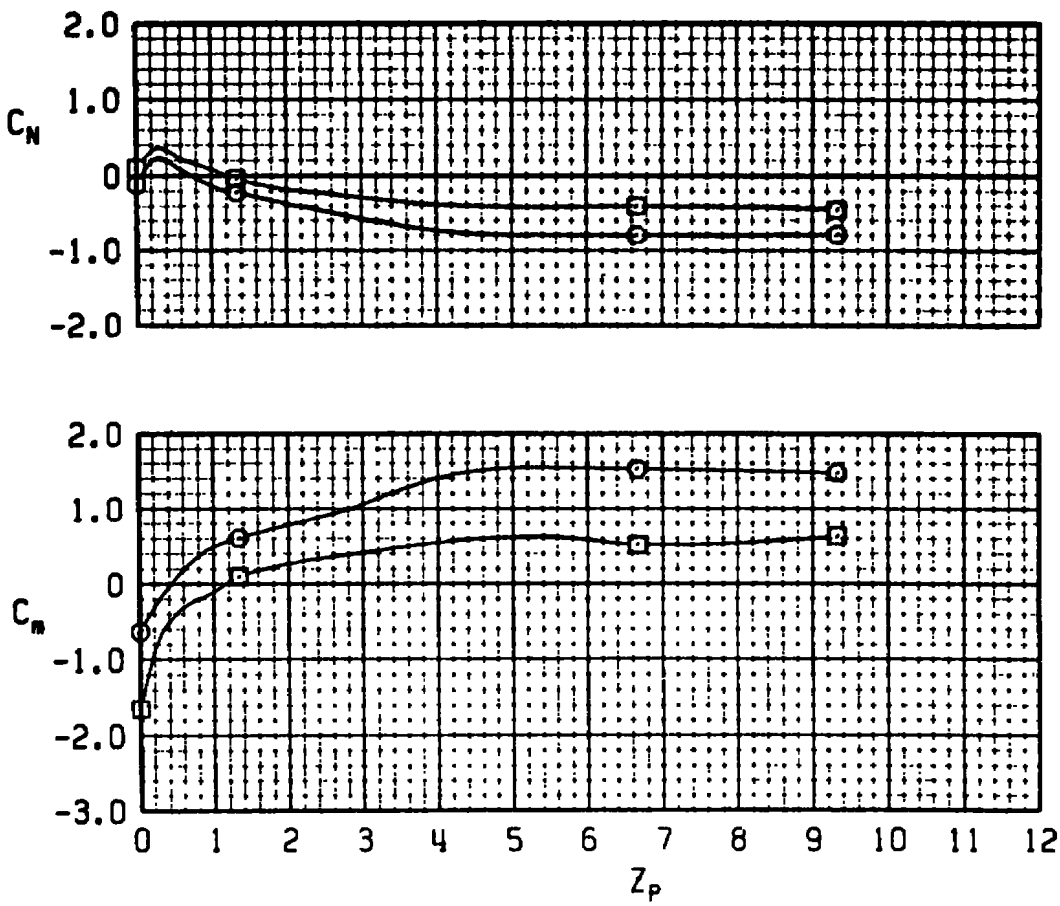

d. $M_\infty = 1.10$

Figure 23. Concluded.

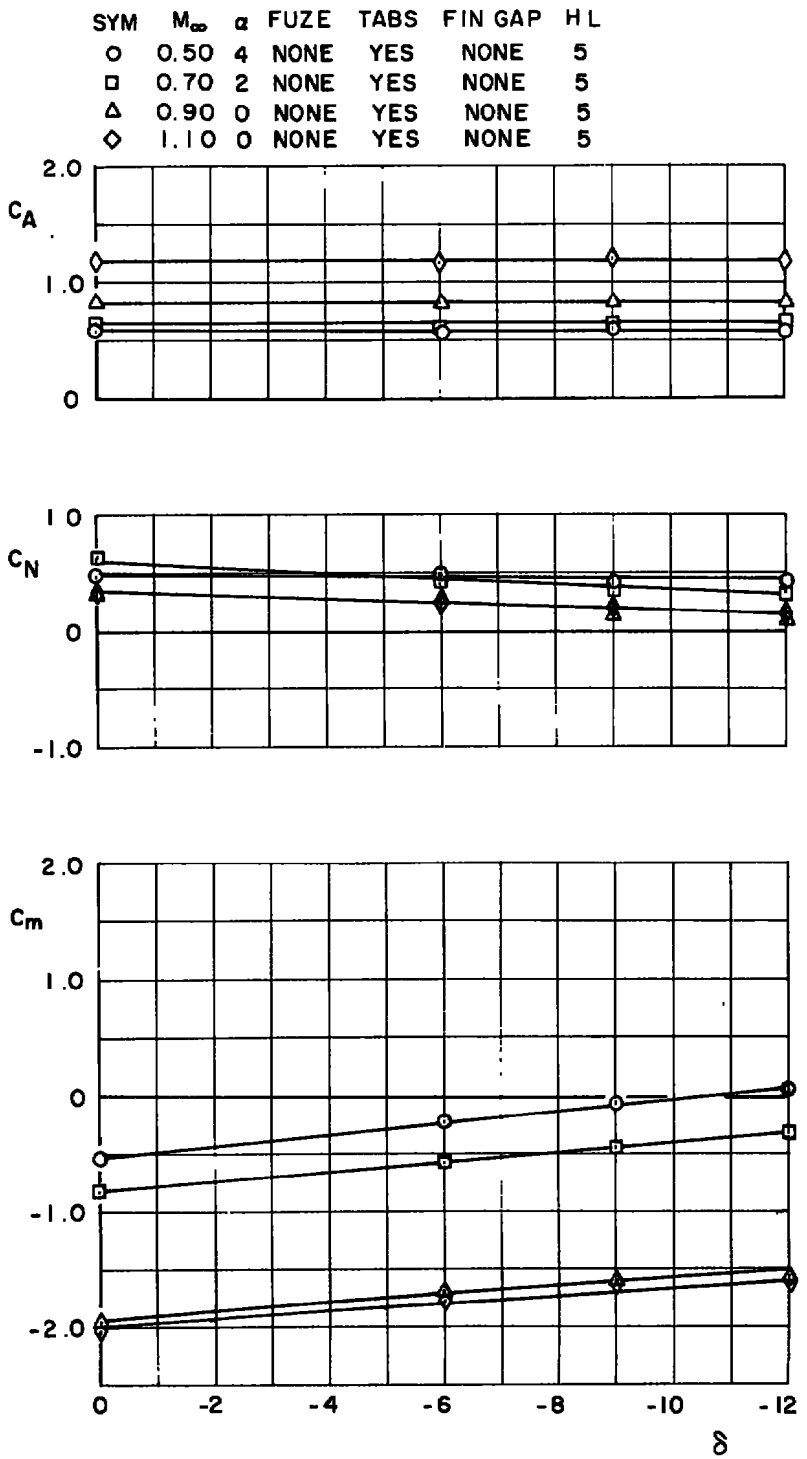

Figure 24. Variation of the aerodynamic coefficients of the MVB with fin cant angle, two fins canted.

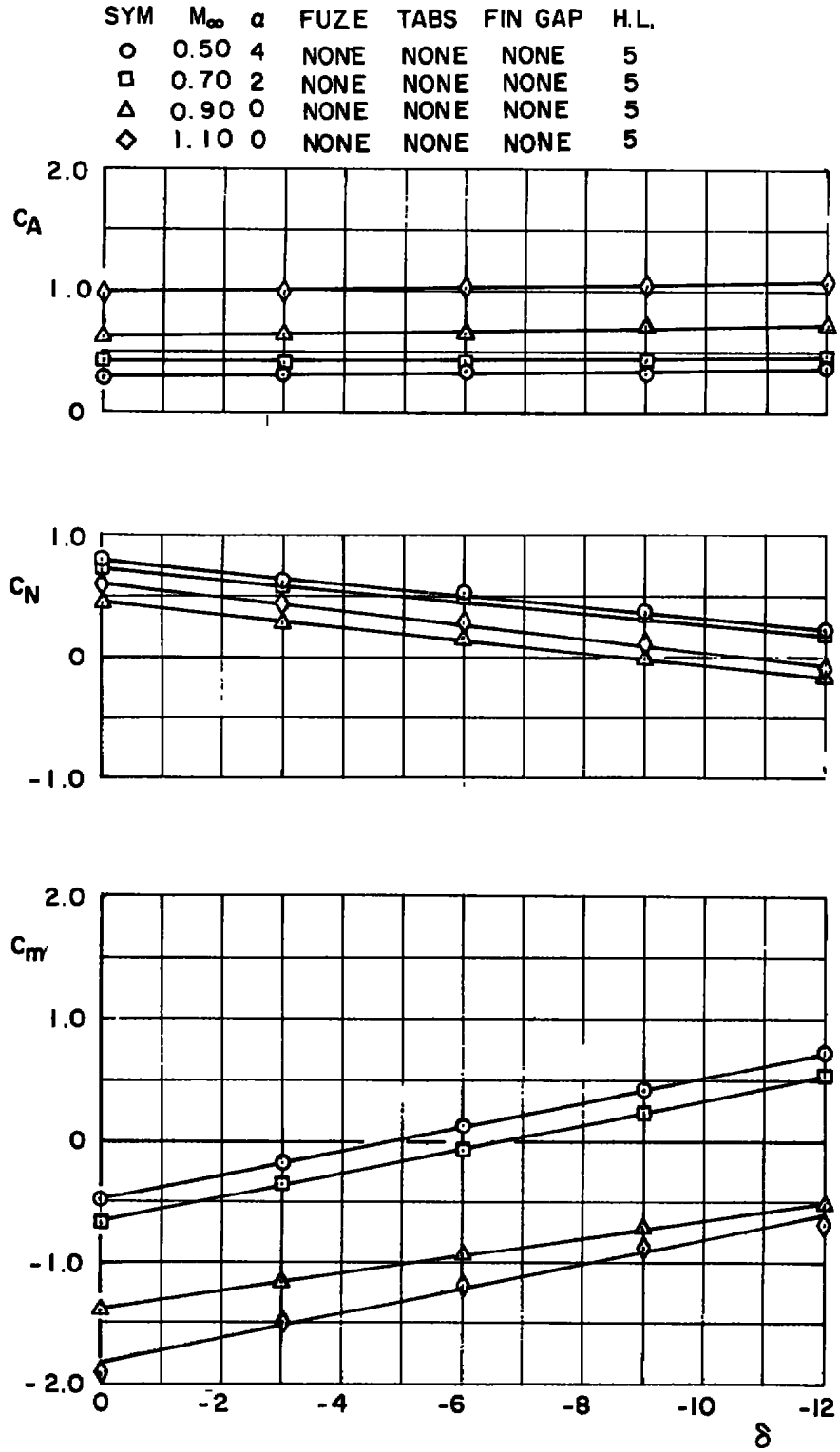

Figure 25. Variation of the aerodynamic coefficients of the MVB with fin cant angle, four fins canted.

SYM	M_∞	α	TABS	δ_1	δ_2	δ_3	δ_4	TER	CONF	AIR.
⊙	0.5	4	NONE	0	0	0	0	1	1	F-4
⊡	0.5	4	NONE	-3	-3	-3	-3	1	2	F-4
△	0.5	4	NONE	-6	-6	-6	-6	1	3	F-4
▽	0.5	4	NONE	-9	-9	-9	-9	1	4	F-4
◇	0.5	4	NONE	-12	-12	-12	-12	1	5	F-4

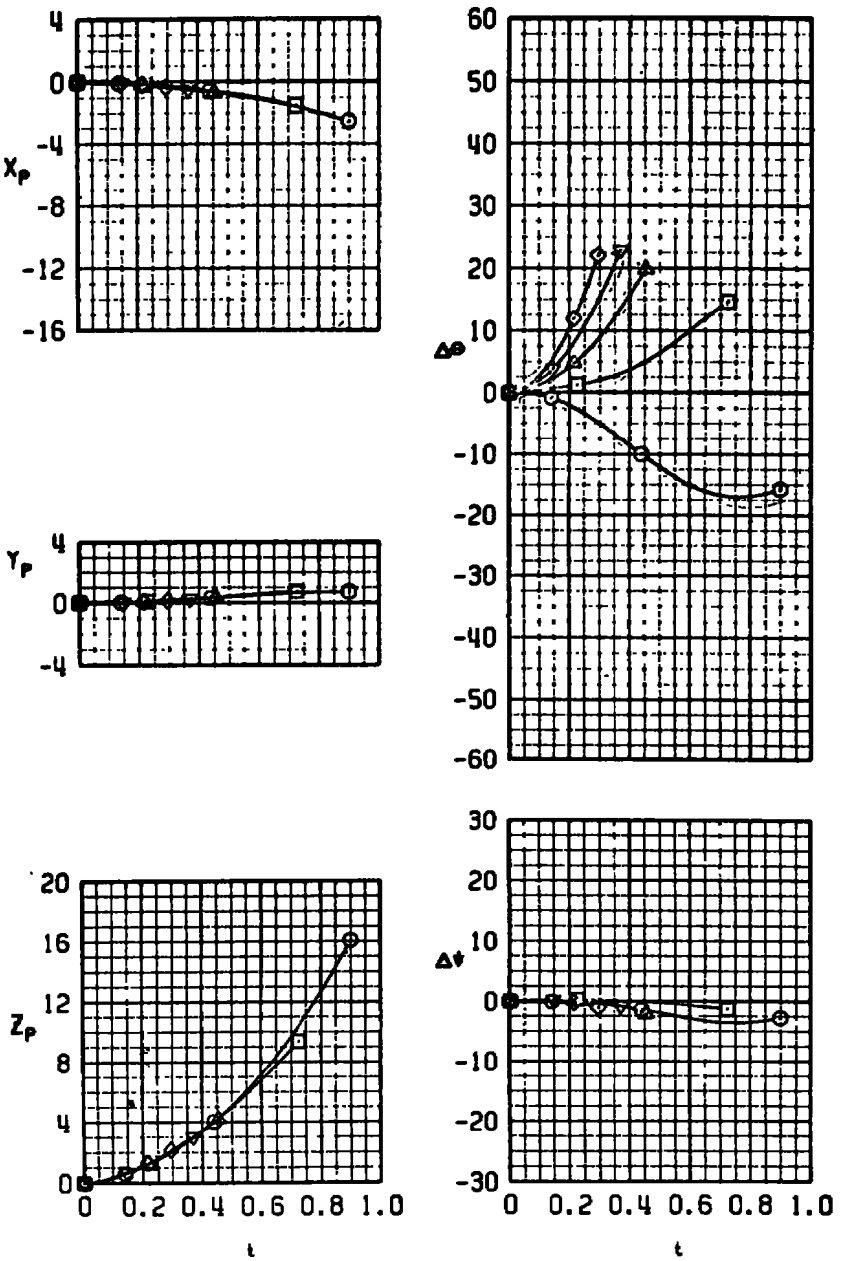

a. $M_\infty = 0.50$

Figure 26. Wind tunnel separation trajectories of the MVB from the No. 1 TER station of the F-4C aircraft, four fins canted.

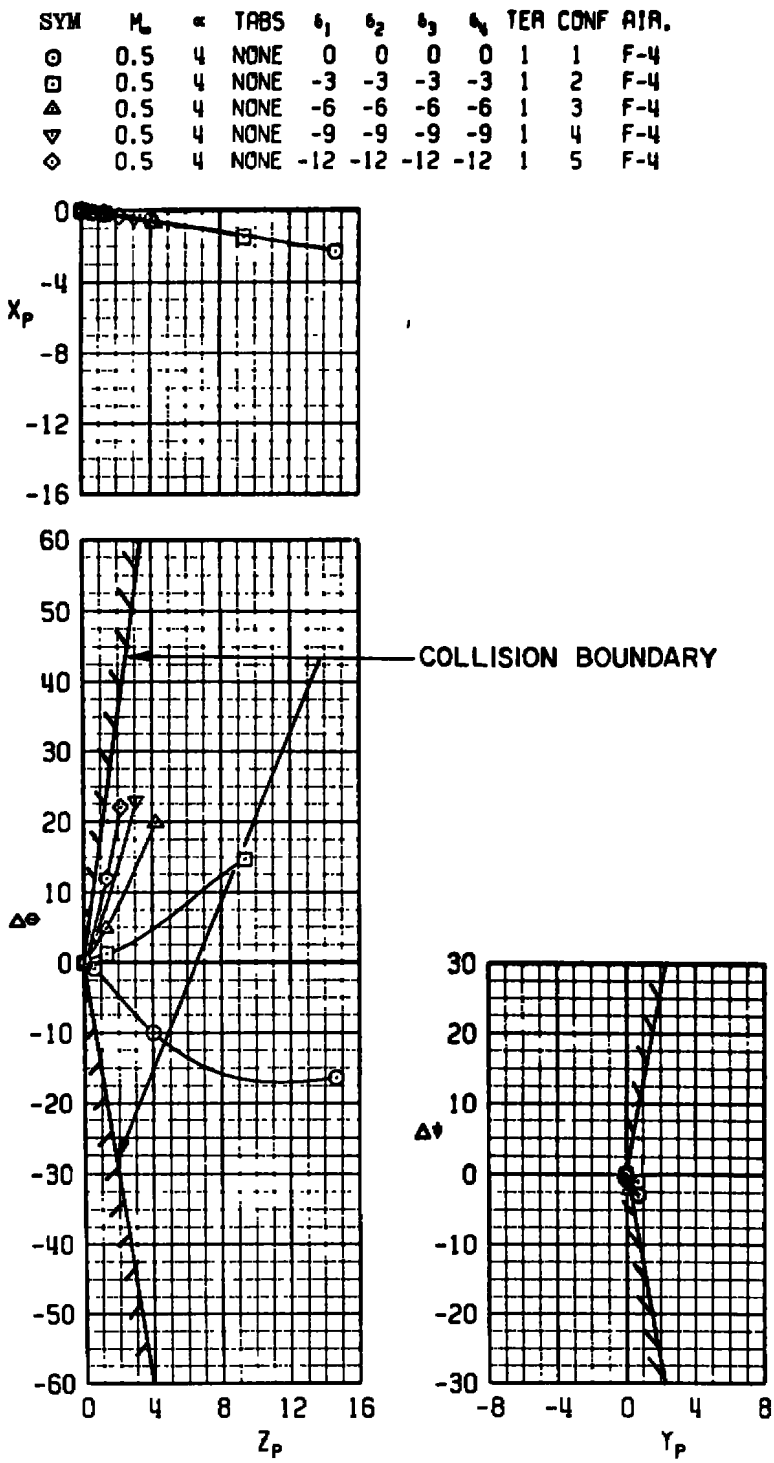

a. Concluded

Figure 26. Continued.

SYM	M_∞	α	TABS	δ_1	δ_2	δ_3	δ_4	TER	CONF	AIR.
⊙	0.7	2	NONE	0	0	0	0	1	1	F-4
⊡	0.7	2	NONE	-3	-3	-3	-3	1	2	F-4
△	0.7	2	NONE	-6	-6	-6	-6	1	3	F-4
▽	0.7	2	NONE	-9	-9	-9	-9	1	4	F-4
◇	0.7	2	NONE	-12	-12	-12	-12	1	5	F-4

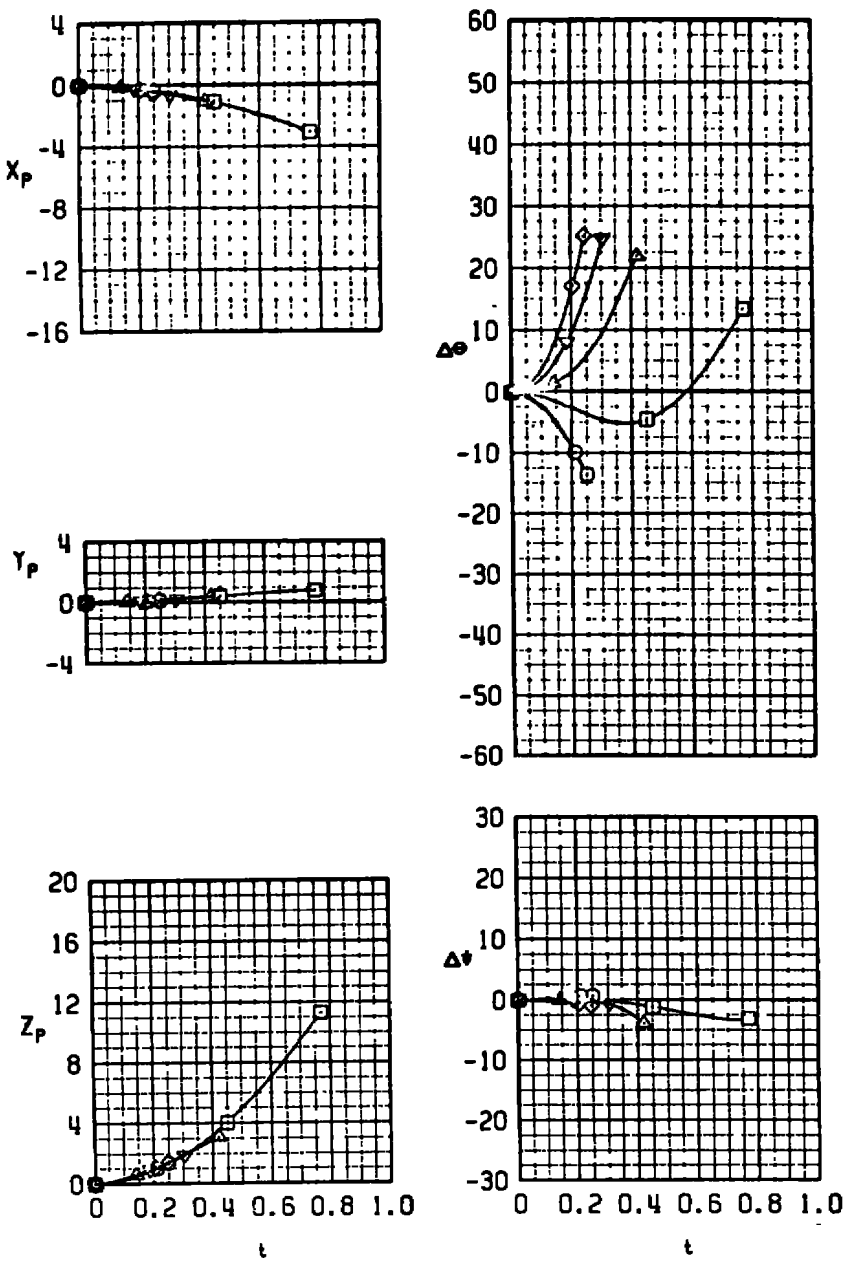

b. $M_\infty = 0.70$

Figure 26. Continued.

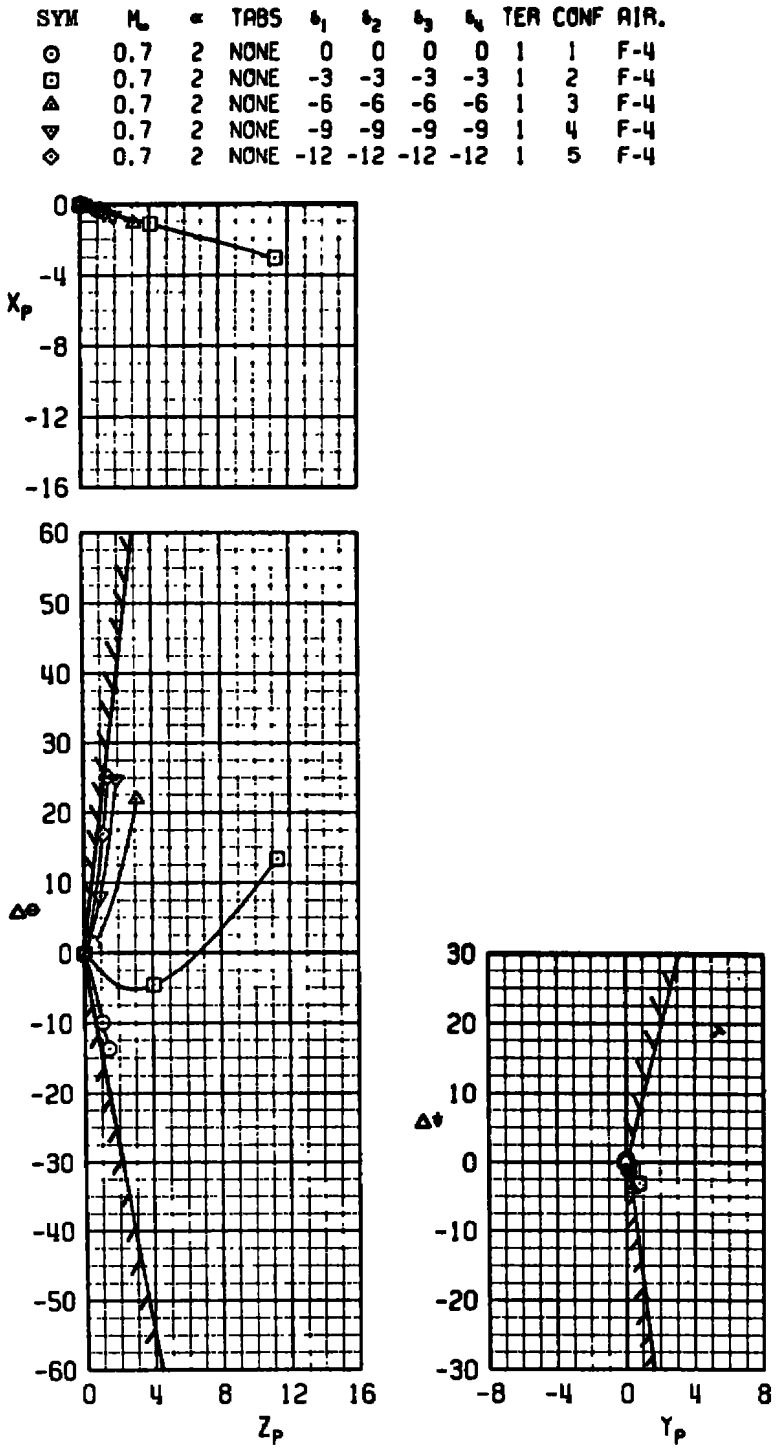

b. Concluded
Figure 26. Continued.

SYM	M_∞	α	TABS	δ_1	δ_2	δ_3	δ_4	TER	CONF	AIR.
⊙	0.9	0	NONE	0	0	0	0	1	1	F-4
⊡	0.9	0	NONE	-3	-3	-3	-3	1	2	F-4
△	0.9	0	NONE	-6	-6	-6	-6	1	3	F-4
▽	0.9	0	NONE	-9	-9	-9	-9	1	4	F-4
◇	0.9	0	NONE	-12	-12	-12	-12	1	5	F-4

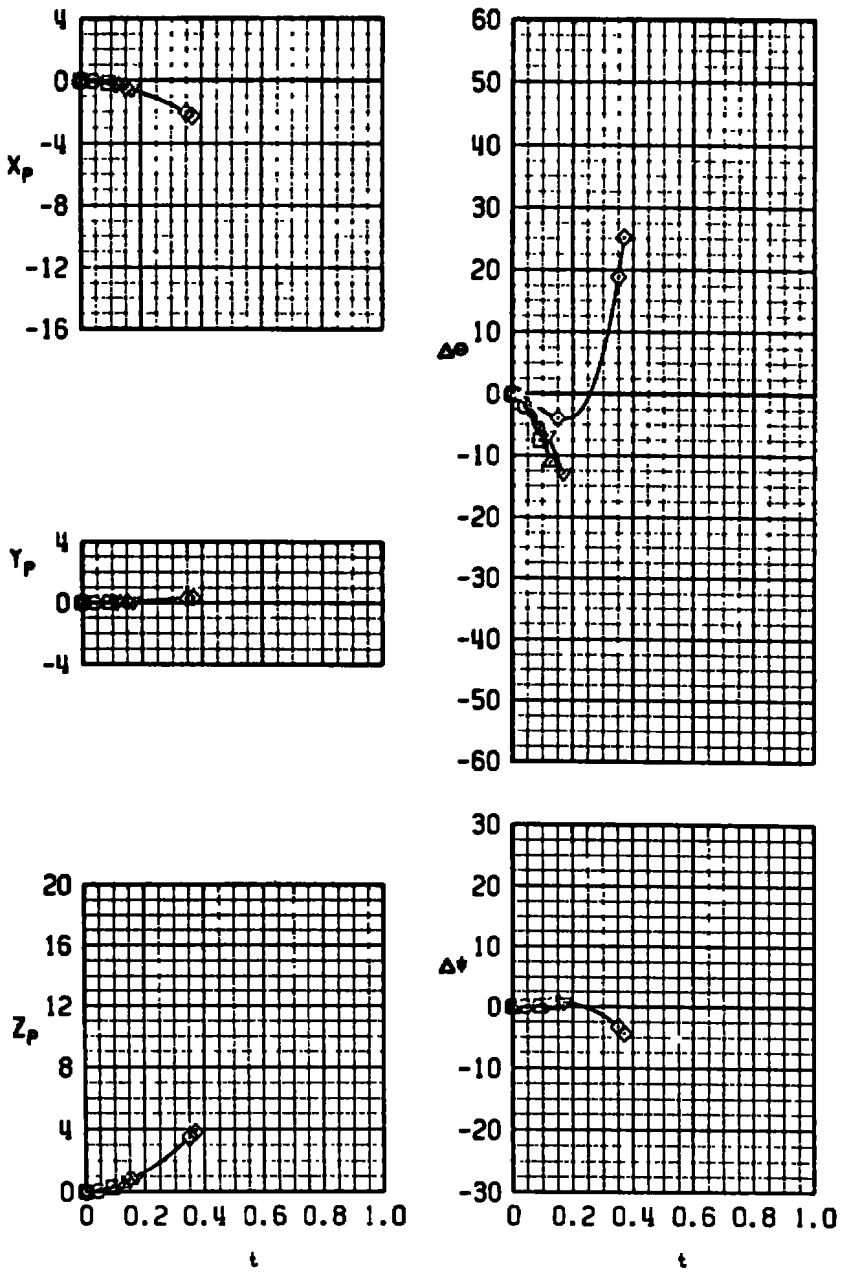

c. $M_\infty = 0.90$

Figure 26. Continued.

SYM	M_∞	α	TABS	δ_1	δ_2	δ_3	δ_4	TER	CONF	AIR.
⊙	0.9	0	NONE	0	0	0	0	1	1	F-4
⊡	0.9	0	NONE	-3	-3	-3	-3	1	2	F-4
△	0.9	0	NONE	-6	-6	-6	-6	1	3	F-4
▽	0.9	0	NONE	-9	-9	-9	-9	1	4	F-4
◇	0.9	0	NONE	-12	-12	-12	-12	1	5	F-4

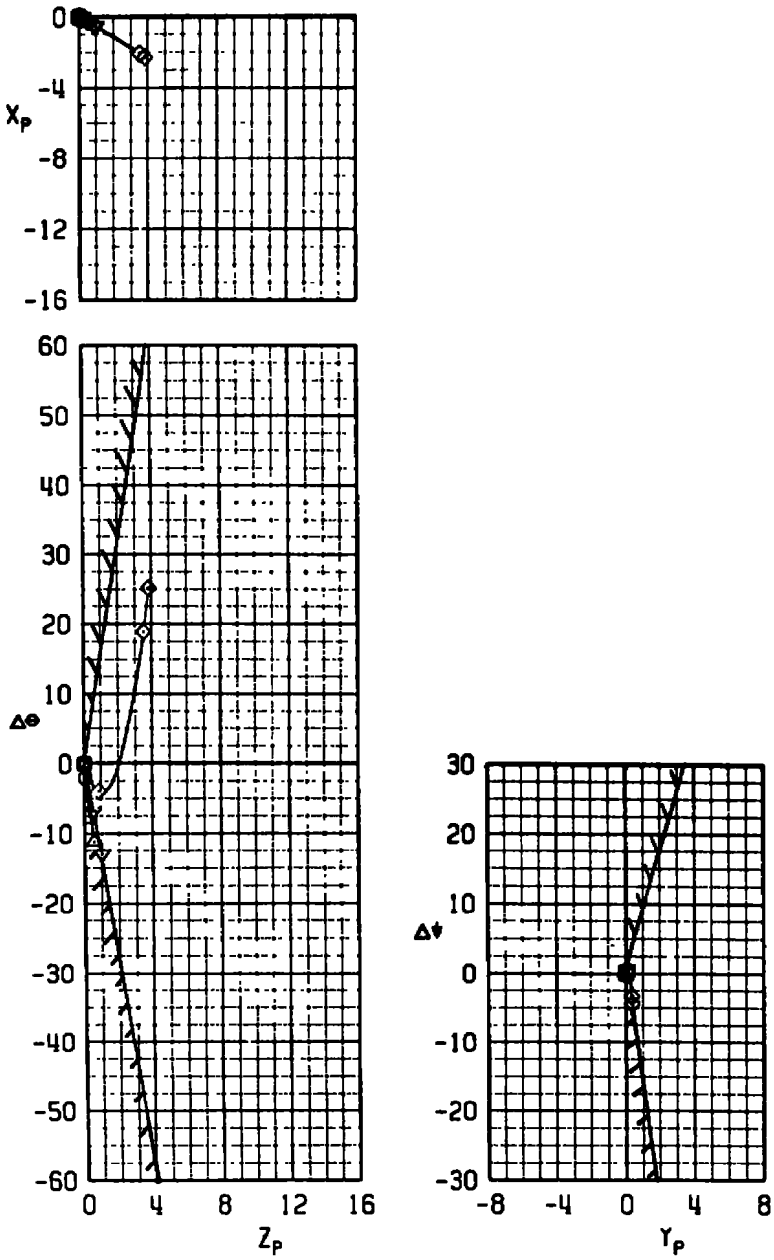

c. Concluded
Figure 26. Continued.

SYM	M_∞	α	TABS	δ_1	δ_2	δ_3	δ_4	TER	CONF	AIR.
⊙	1.1	0	NONE	0	0	0	0	1	1	F-4
⊡	1.1	0	NONE	-3	-3	-3	-3	1	2	F-4
△	1.1	0	NONE	-6	-6	-6	-6	1	3	F-4
▽	1.1	0	NONE	-9	-9	-9	-9	1	4	F-4
◇	1.1	0	NONE	-12	-12	-12	-12	1	5	F-4

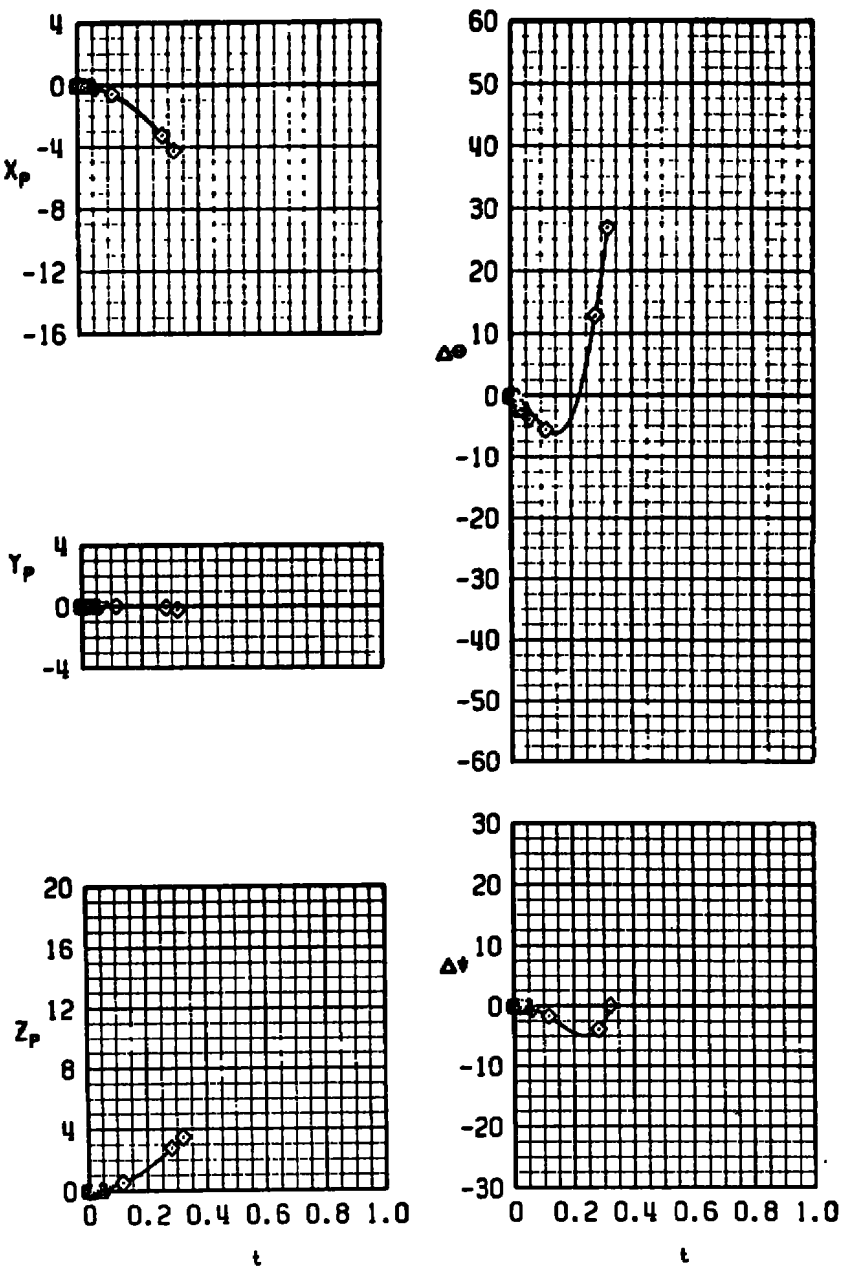

d. $M_\infty = 1.10$

Figure 26. Continued.

SYM	M_∞	α	TABS	δ_1	δ_2	δ_3	δ_4	TER	CONF	AIR.
⊙	1.1	0	NONE	0	0	0	0	1	1	F-4
⊡	1.1	0	NONE	-3	-3	-3	-3	1	2	F-4
△	1.1	0	NONE	-6	-6	-6	-6	1	3	F-4
▽	1.1	0	NONE	-9	-9	-9	-9	1	4	F-4
◇	1.1	0	NONE	-12	-12	-12	-12	1	5	F-4

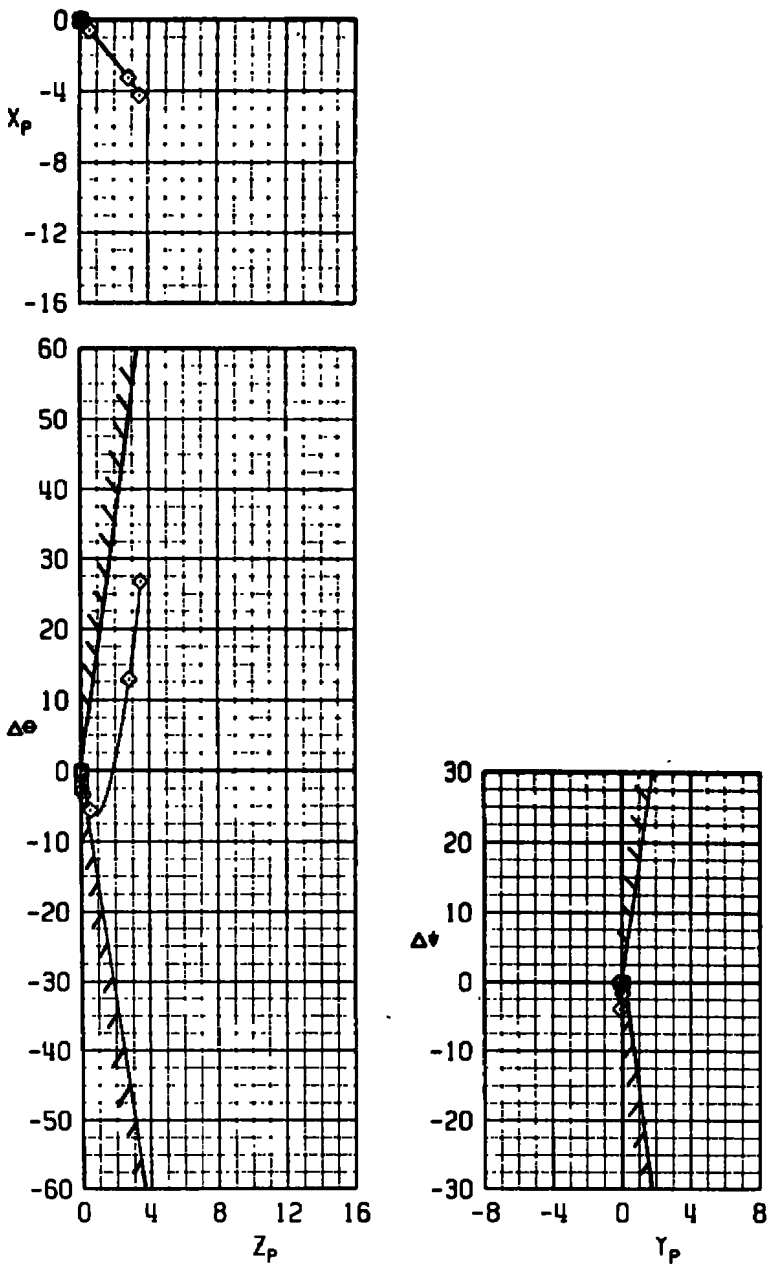

d. Concluded

Figure 26. Concluded.

SYM	M_∞	α	TABS	δ_1	δ_2	δ_3	δ_4	TER	CONF	AIR.
⊙	0.5	4	YES	0	0	0	0	1	10	F-4
△	0.5	4	YES	-6	0	0	-6	1	11	F-4
▽	0.5	4	YES	-9	0	0	-9	1	12	F-4
◇	0.5	4	YES	-12	0	0	-12	1	14	F-4

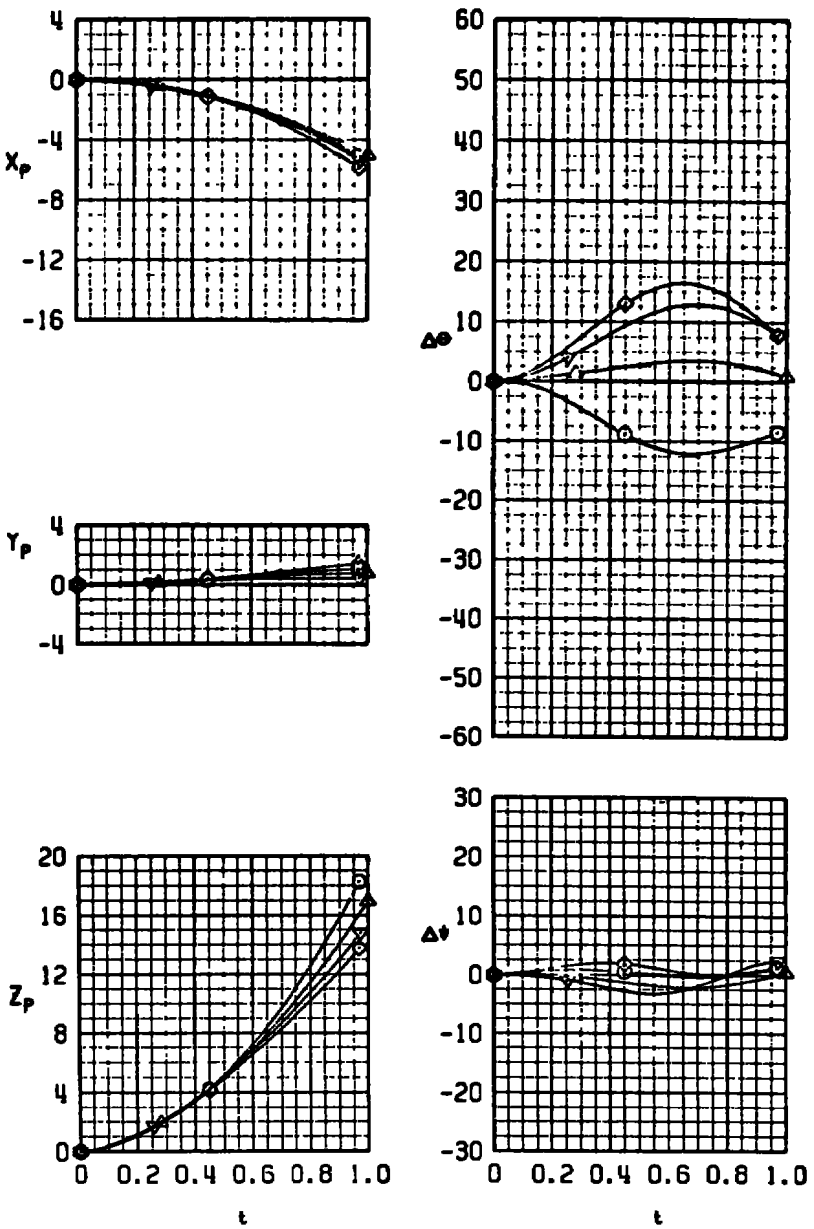

a. $M_\infty = 0.50$

Figure 27. Wind tunnel separation trajectories of the MVB from the No. 1 TER station of the F-4C aircraft, two fins canted.

SYM	M_∞	α	TABS	δ_1	δ_2	δ_3	δ_4	TER	CONF	AIR.
⊙	0.5	4	YES	0	0	0	0	1	10	F-4
△	0.5	4	YES	-6	0	0	-6	1	11	F-4
▽	0.5	4	YES	-9	0	0	-9	1	12	F-4
◇	0.5	4	YES	-12	0	0	-12	1	14	F-4

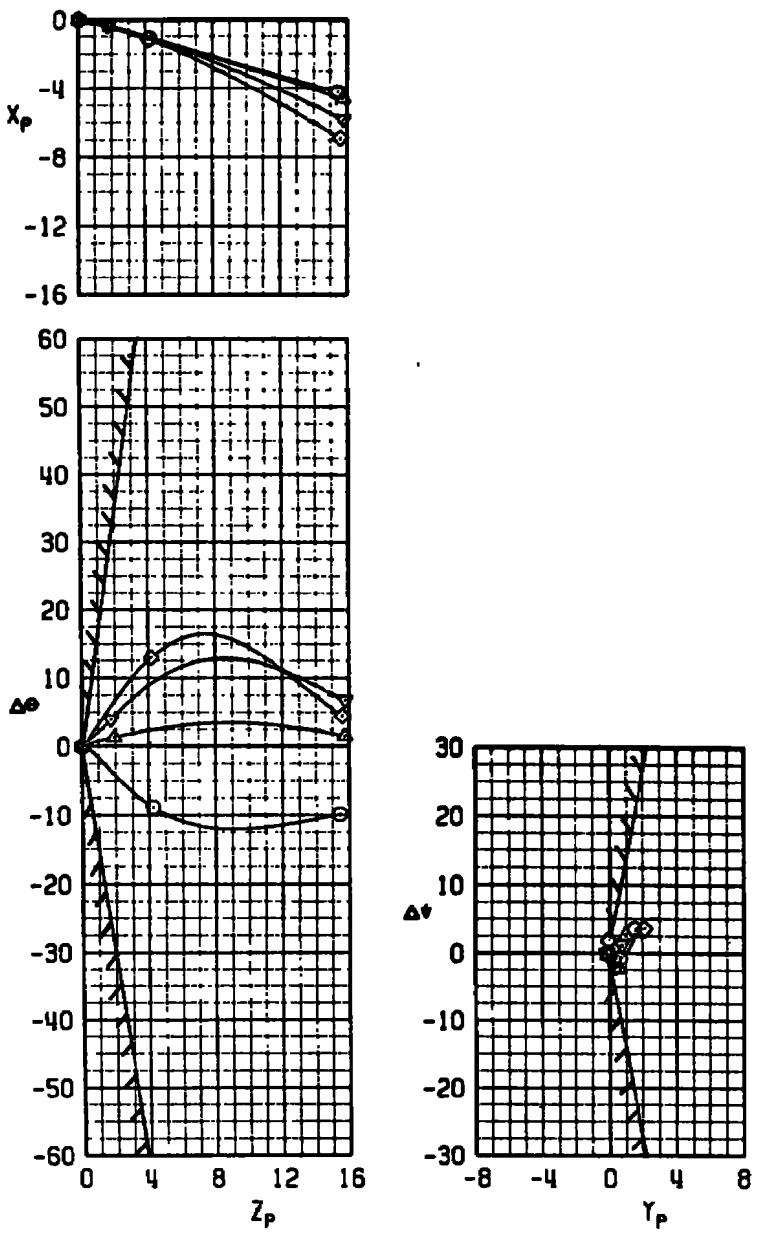

a. Concluded

Figure 27. Continued.

SYM	M_∞	α	TABS	δ_1	δ_2	δ_3	δ_4	TER	CONF	AIR.
⊙	0.7	2	YES	0	0	0	0	1	10	F-4
△	0.7	2	YES	-6	0	0	-6	1	11	F-4
▽	0.7	2	YES	-9	0	0	-9	1	12	F-4
◇	0.7	2	YES	-12	0	0	-12	1	14	F-4

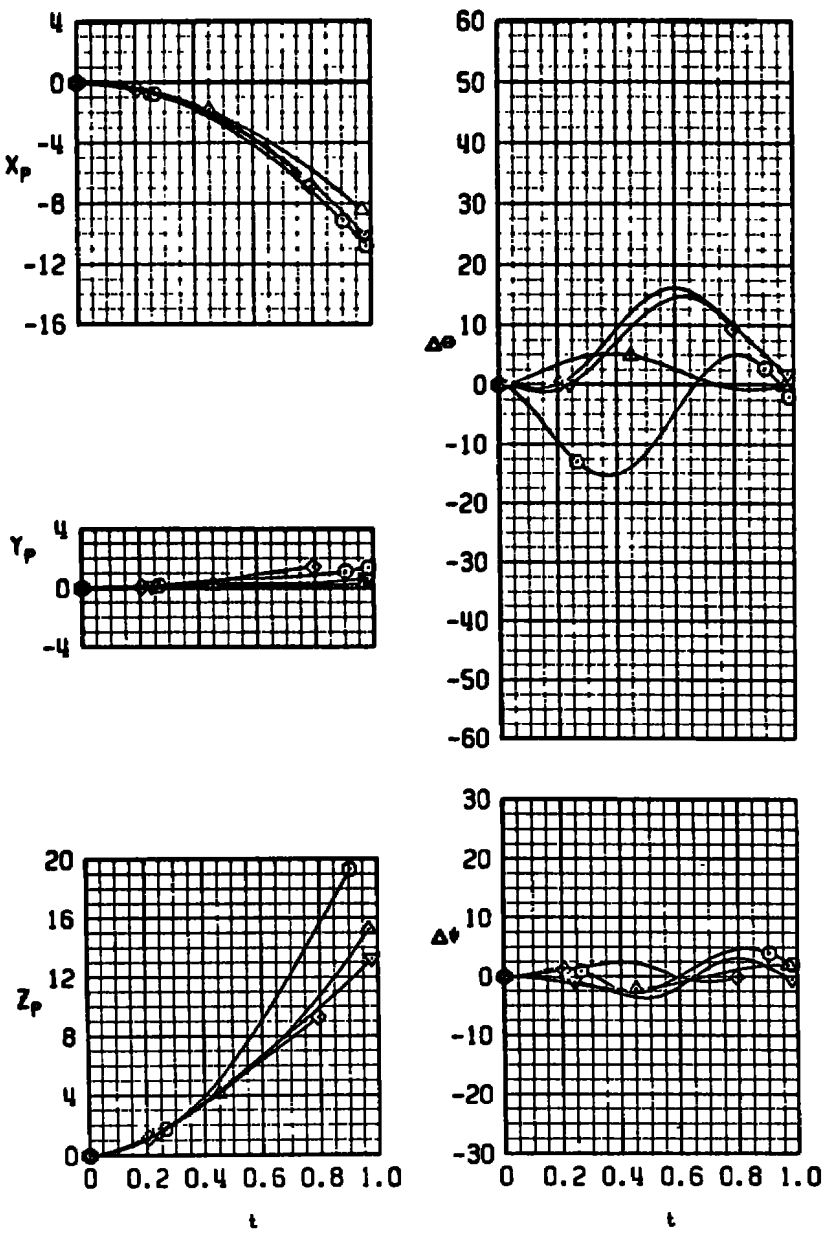

b. $M_\infty = 0.70$

Figure 27. Continued.

SYM	M_∞	α	TABS	δ_1	δ_2	δ_3	δ_4	TER	CONF	AIR.
⊙	0.7	2	YES	0	0	0	0	1	10	F-4
△	0.7	2	YES	-6	0	0	-6	1	11	F-4
▽	0.7	2	YES	-9	0	0	-9	1	12	F-4
◇	0.7	2	YES	-12	0	0	-12	1	14	F-4

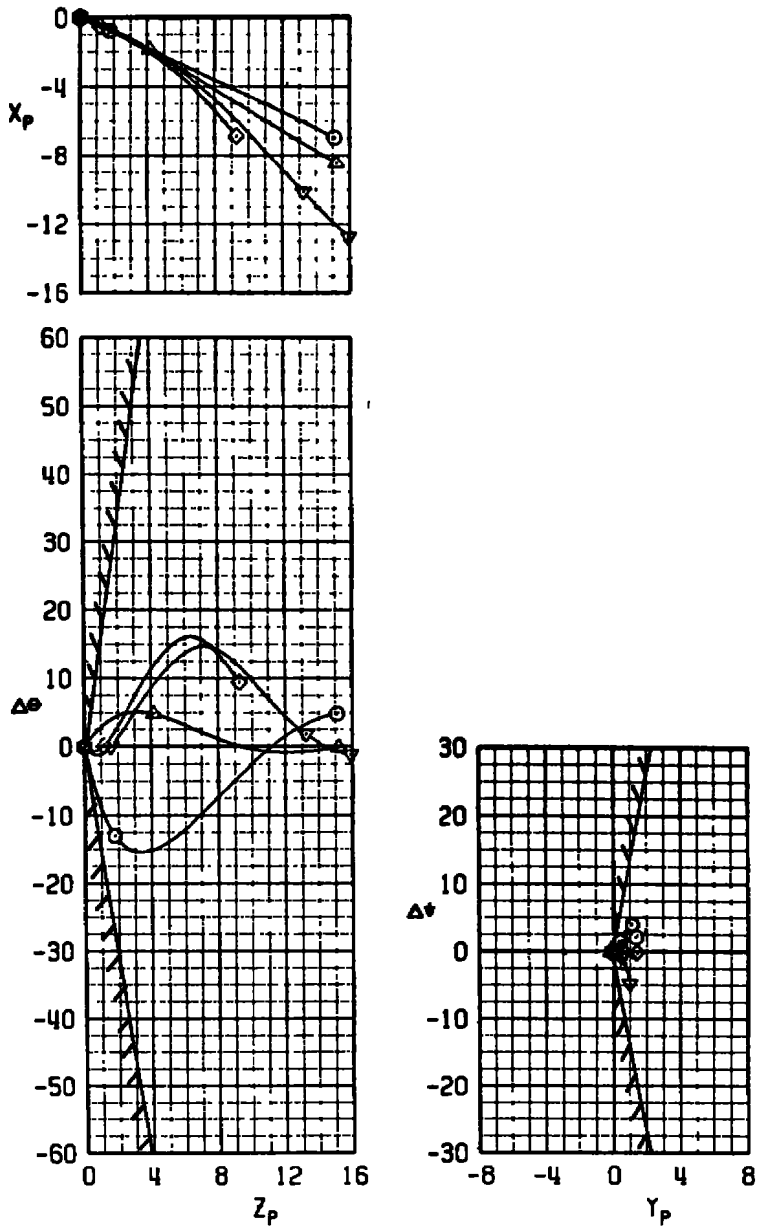

b. Concluded
Figure 27. Continued.

SYM	M_∞	α	TABS	δ_1	δ_2	δ_3	δ_4	TER	CONF	AIR.
⊙	0.9	0	YES	0	0	0	0	1	10	F-4
△	0.9	0	YES	-6	0	0	-6	1	11	F-4
▽	0.9	0	YES	-9	0	0	-9	1	12	F-4
◇	0.9	0	YES	-12	0	0	-12	1	14	F-4

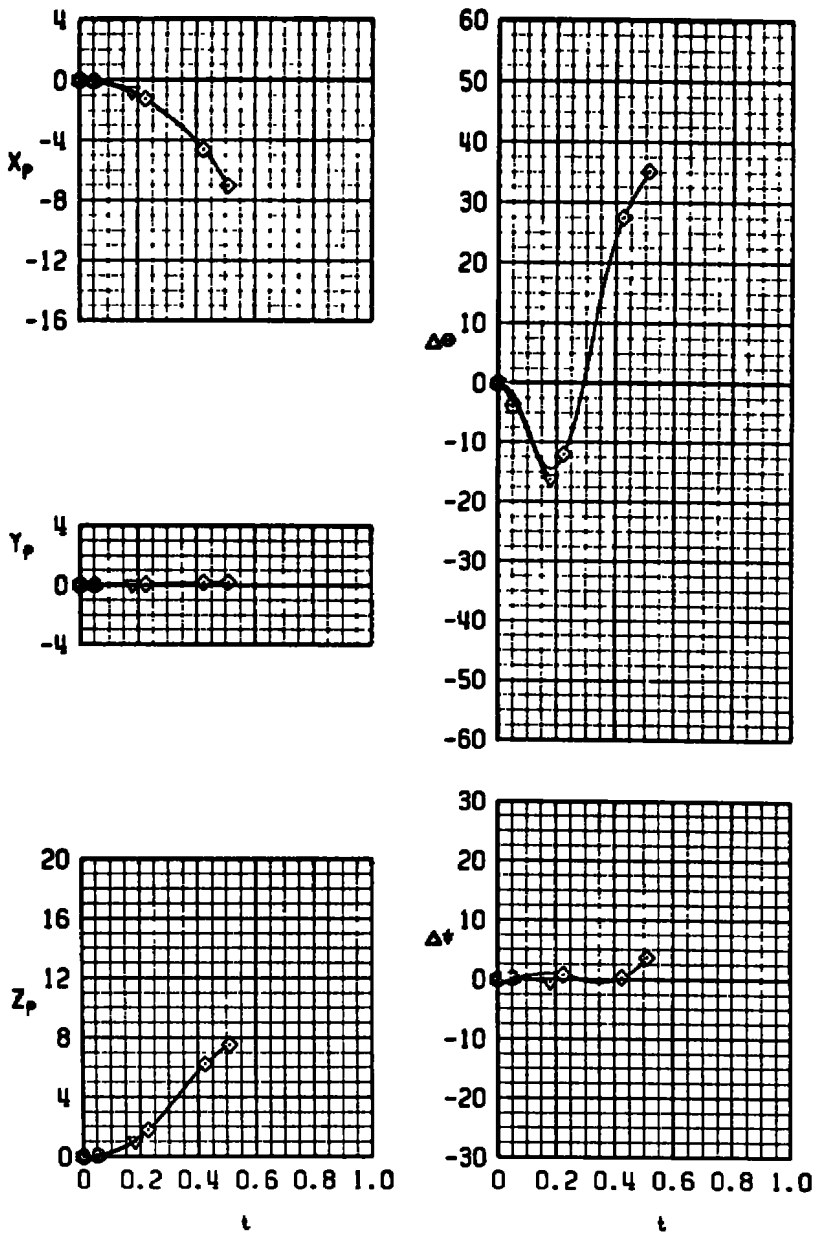

c. $M_\infty = 0.90$

Figure 27. Continued.

SYM	M_∞	α	TABS	δ_1	δ_2	δ_3	δ_4	TER	CONF	AIR.
⊙	0.9	0	YES	0	0	0	0	1	10	F-4
△	0.9	0	YES	-6	0	0	-6	1	11	F-4
▽	0.9	0	YES	-9	0	0	-9	1	12	F-4
◇	0.9	0	YES	-12	0	0	-12	1	14	F-4

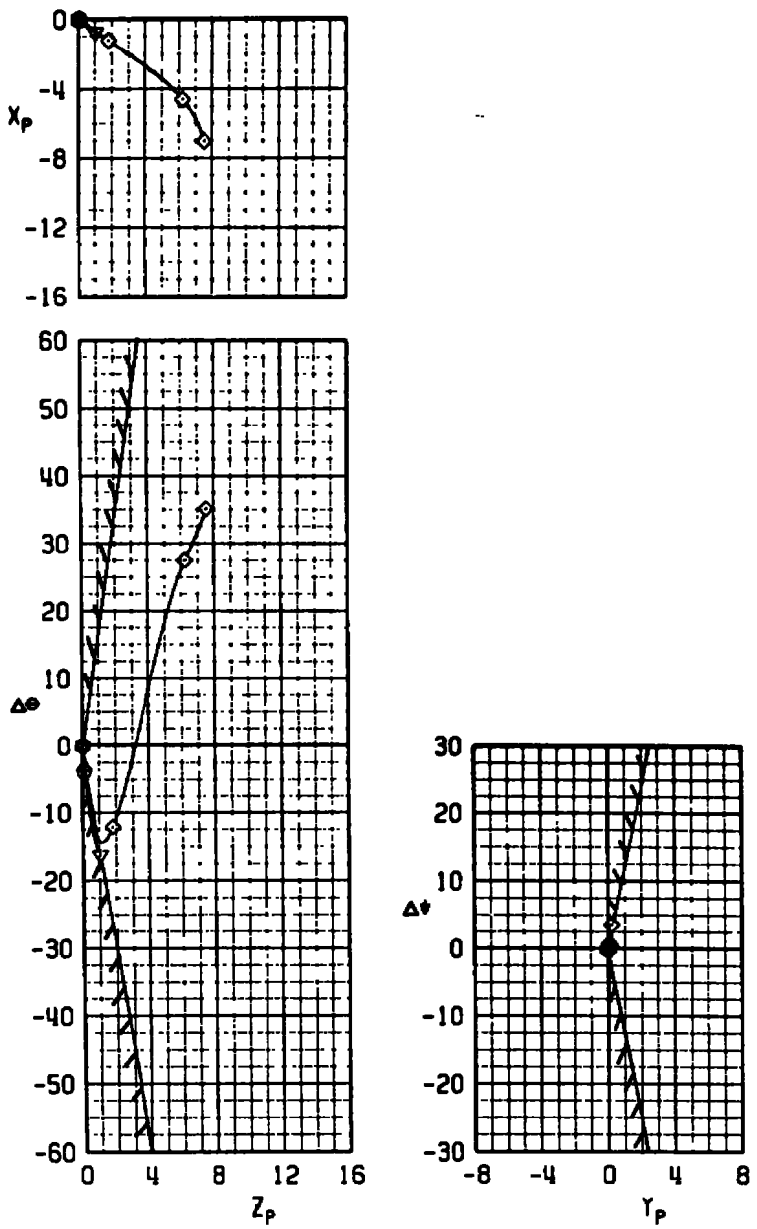

c. Concluded

Figure 27. Continued.

SYM	M_∞	α	TABS	δ_1	δ_2	δ_3	δ_4	TER	CONF	AIR.
⊙	1.1	0	YES	0	0	0	0	1	10	F-4
△	1.1	0	YES	-6	0	0	-6	1	11	F-4
▽	1.1	0	YES	-9	0	0	-9	1	12	F-4
◇	1.1	0	YES	-12	0	0	-12	1	14	F-4

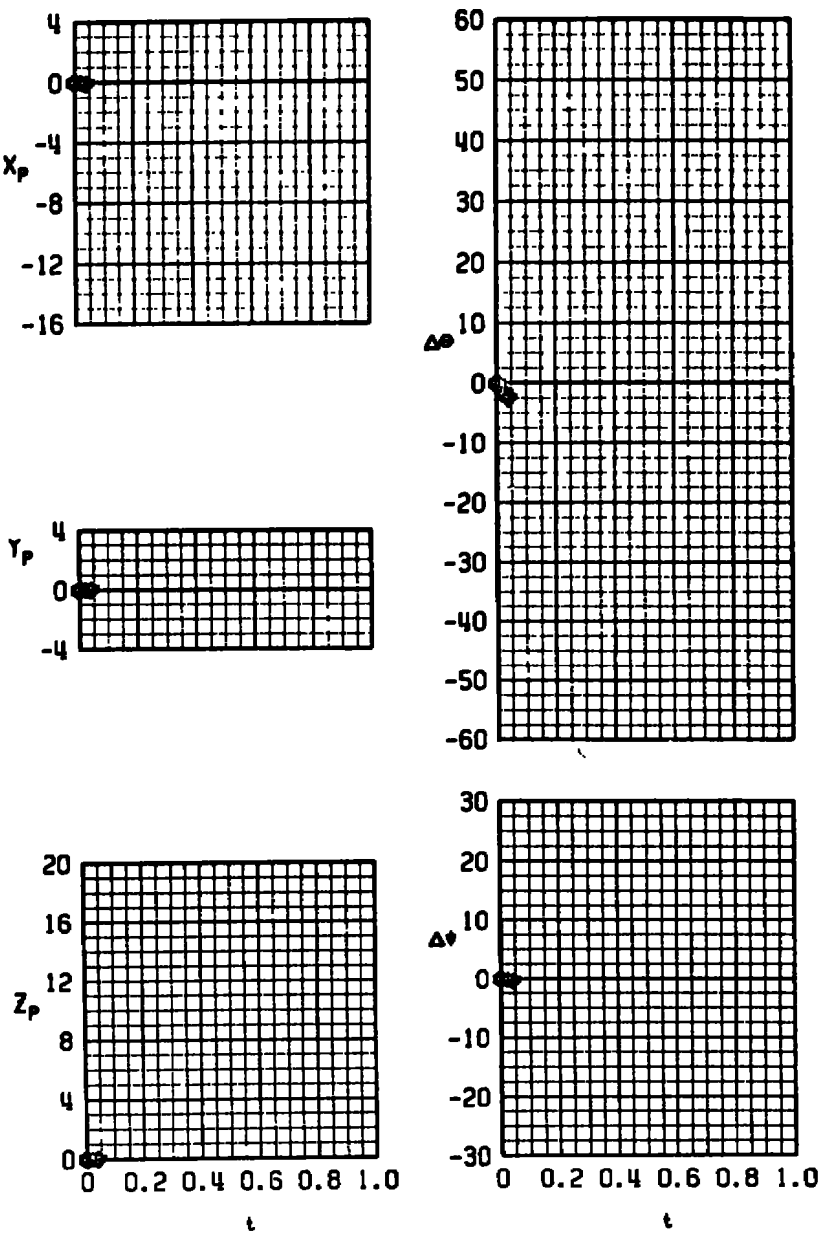

d. $M_\infty = 1.10$

Figure 27. Continued.

SYM	M_∞	α	TABS	δ_1	δ_2	δ_3	δ_4	TER	CONF	AIR.
⊙	1.1	0	YES	0	0	0	0	1	10	F-4
△	1.1	0	YES	-6	0	0	-6	1	11	F-4
▽	1.1	0	YES	-9	0	0	-9	1	12	F-4
◇	1.1	0	YES	-12	0	0	-12	1	14	F-4

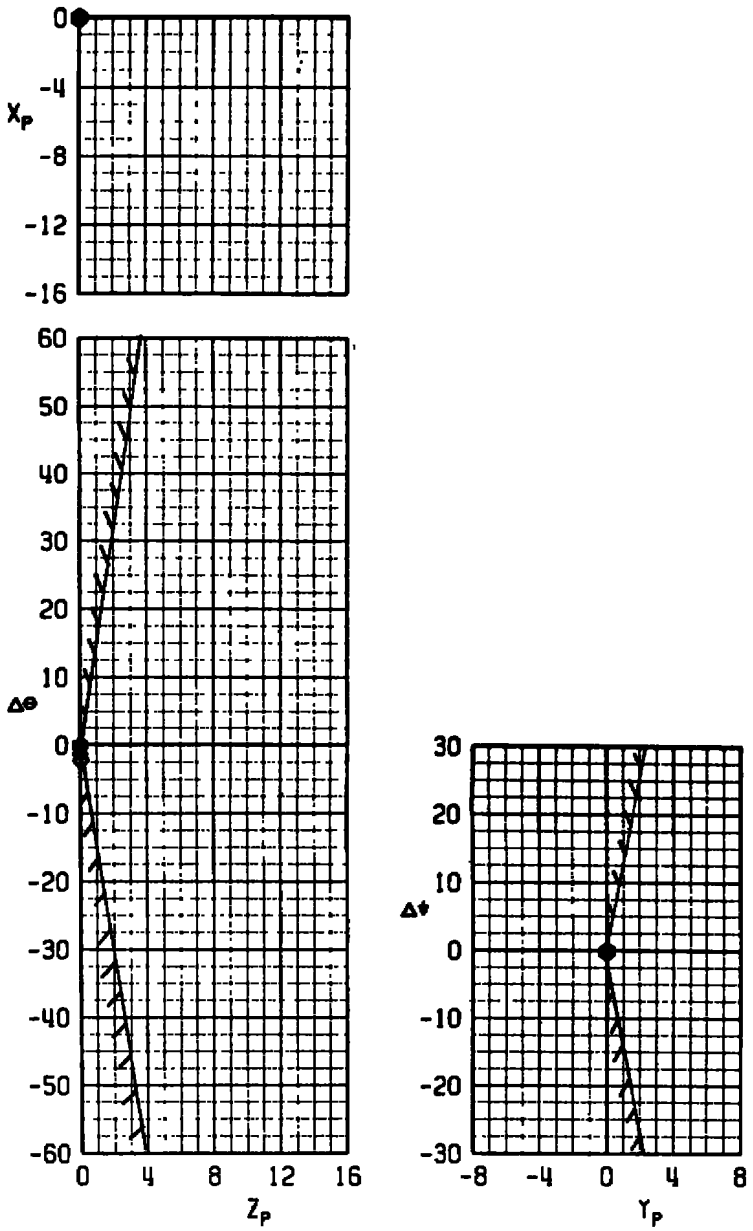

d. Concluded
Figure 27. Concluded.

SYM	M_∞	α	TABS	δ_1	δ_2	δ_3	δ_4	TER	CONF	AIR.
▽	0.5	4	YES	-9	0	0	-9	2	3	F-4
◇	0.5	4	YES	-12	0	0	-12	2	4	F-4

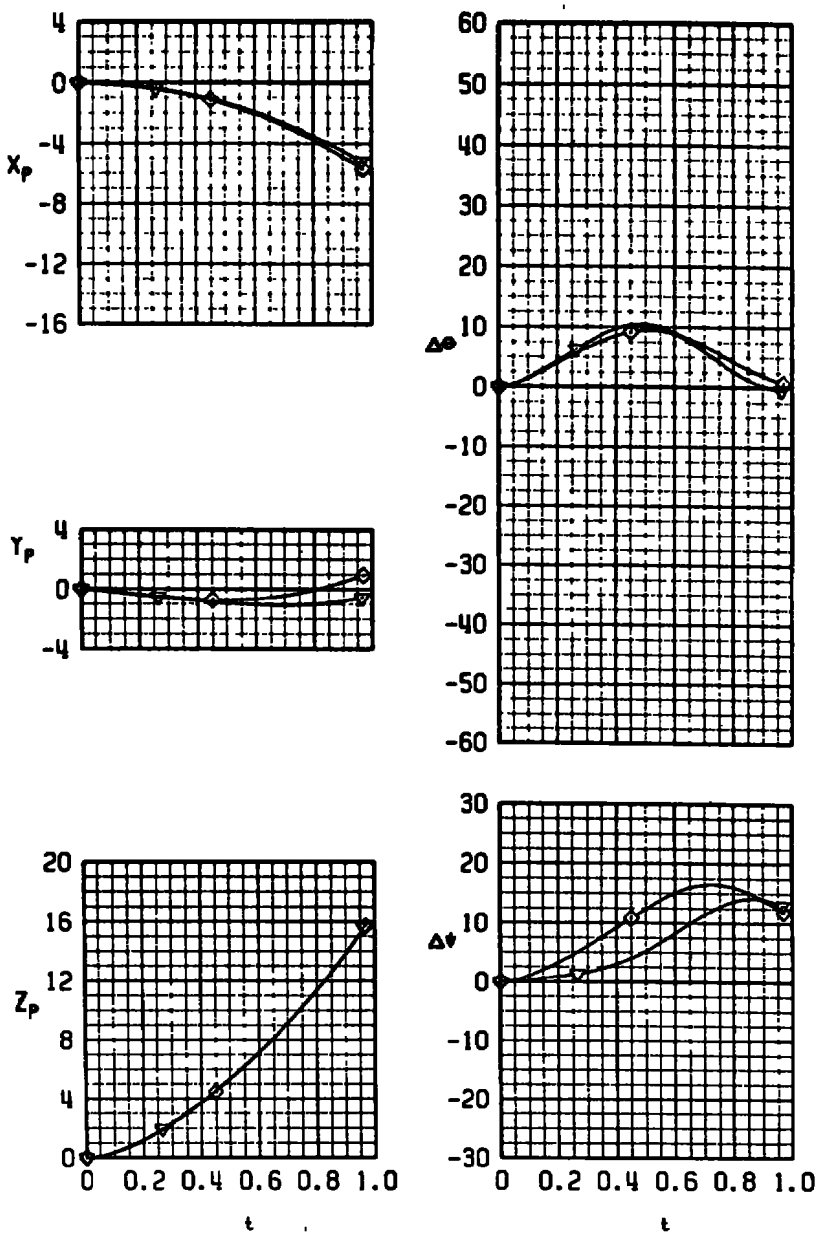

a. $M_\infty = 0.50$

Figure 28. Wind tunnel separation trajectories of the MVB from the No. 2 TER station of the F-4C aircraft, two fins canted.

SYM	M_∞	α	TABS	δ_1	δ_2	δ_3	δ_4	TER	CONF	AIR.
▽	0.7	2	YES	-9	0	0	-9	2	3	F-4
◇	0.7	2	YES	-12	0	0	-12	2	4	F-4

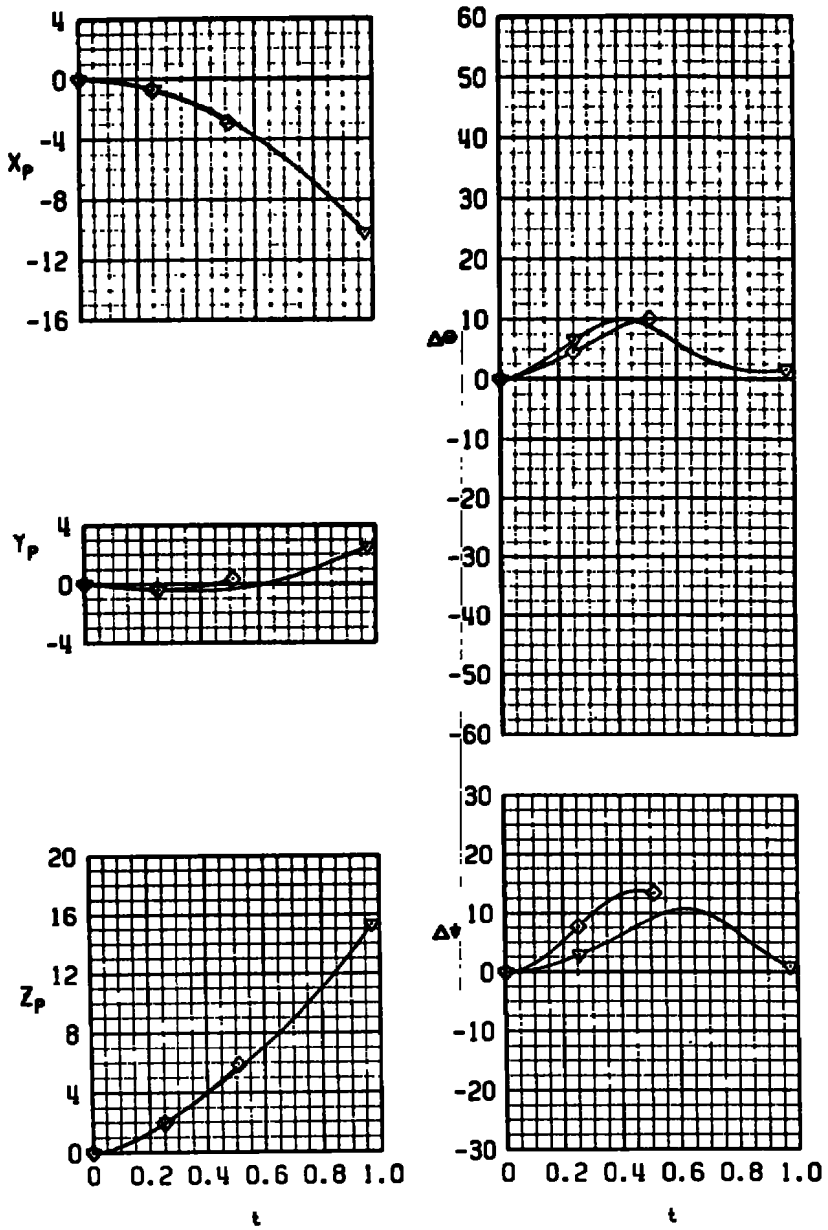

a. Concluded

Figure 28. Continued.

SYM	M_∞	α	TABS	δ_1	δ_2	δ_3	δ_4	TER	CONF	AIR.
▽	0.9	0	YES	-9	0	0	-9	2	3	F-4
◇	0.9	0	YES	-12	0	0	-12	2	4	F-4

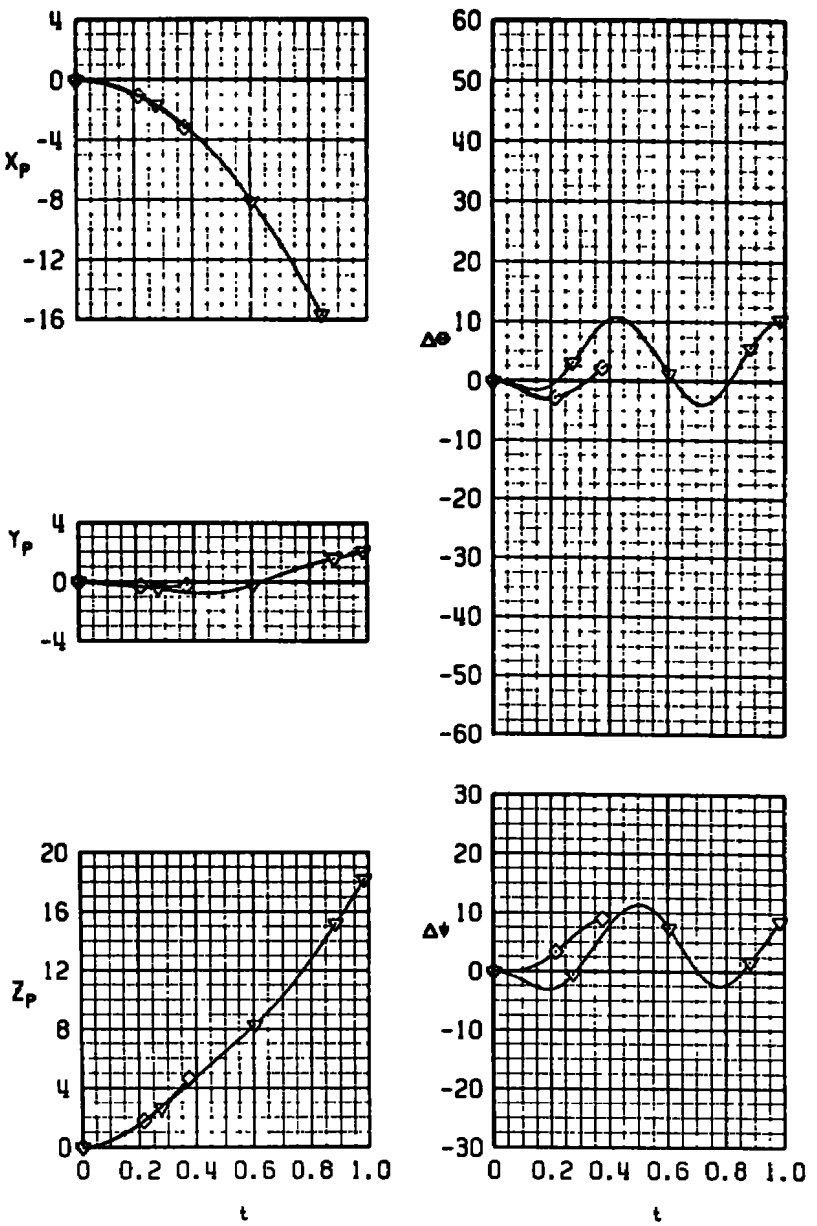

b. $M_\infty = 0.90$

Figure 28. Continued.

SYM	M_∞	α	TABS	δ_1	δ_2	δ_3	δ_4	TER	CONF	AIR.
▽	1.1	0	YES	-9	0	0	-9	2	3	F-4
◇	1.1	0	YES	-12	0	0	-12	2	4	F-4

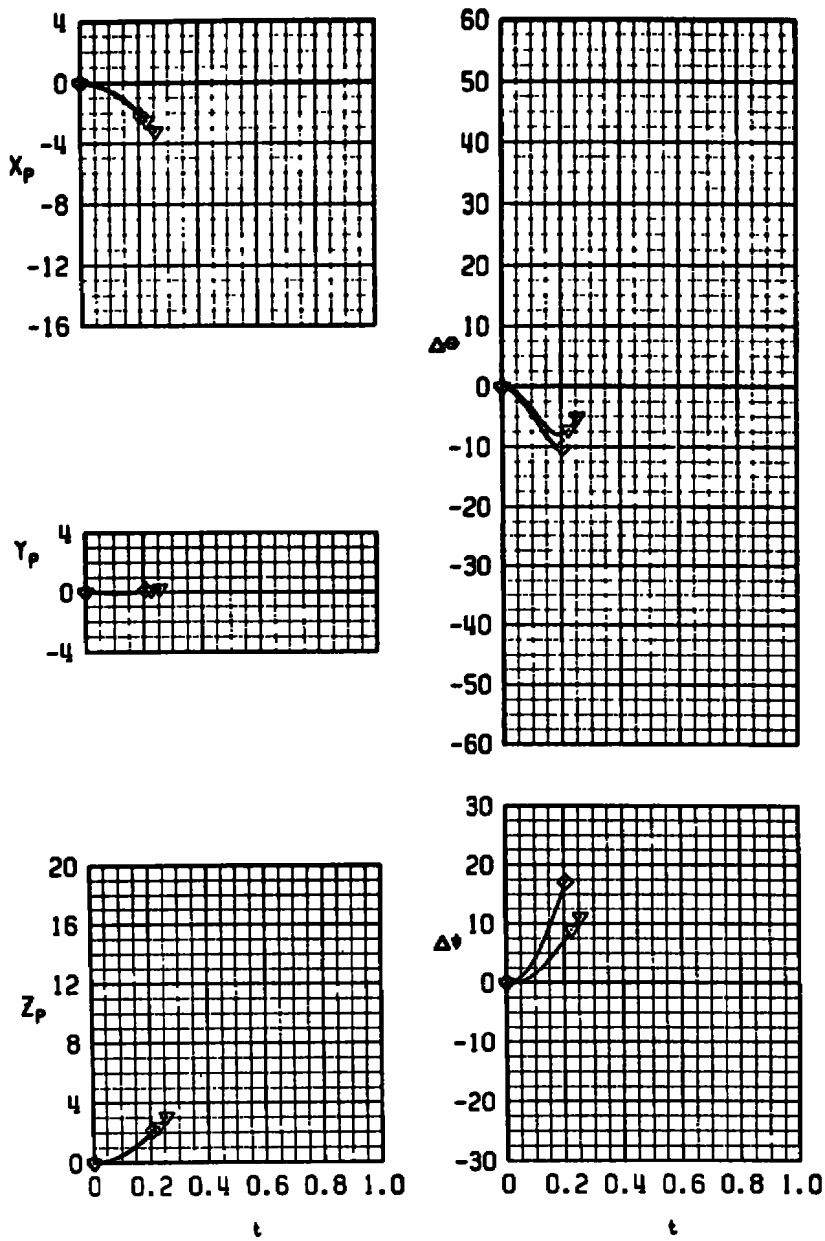

b. Concluded

Figure 28. Concluded.

SYM	M_∞	α	TABS	δ_1	δ_2	δ_3	δ_4	TER	CONF	AIR.
▽	0.5	4	YES	-9	0	0	-9	3	3	F-4
◇	0.5	4	YES	-12	0	0	-12	3	4	F-4

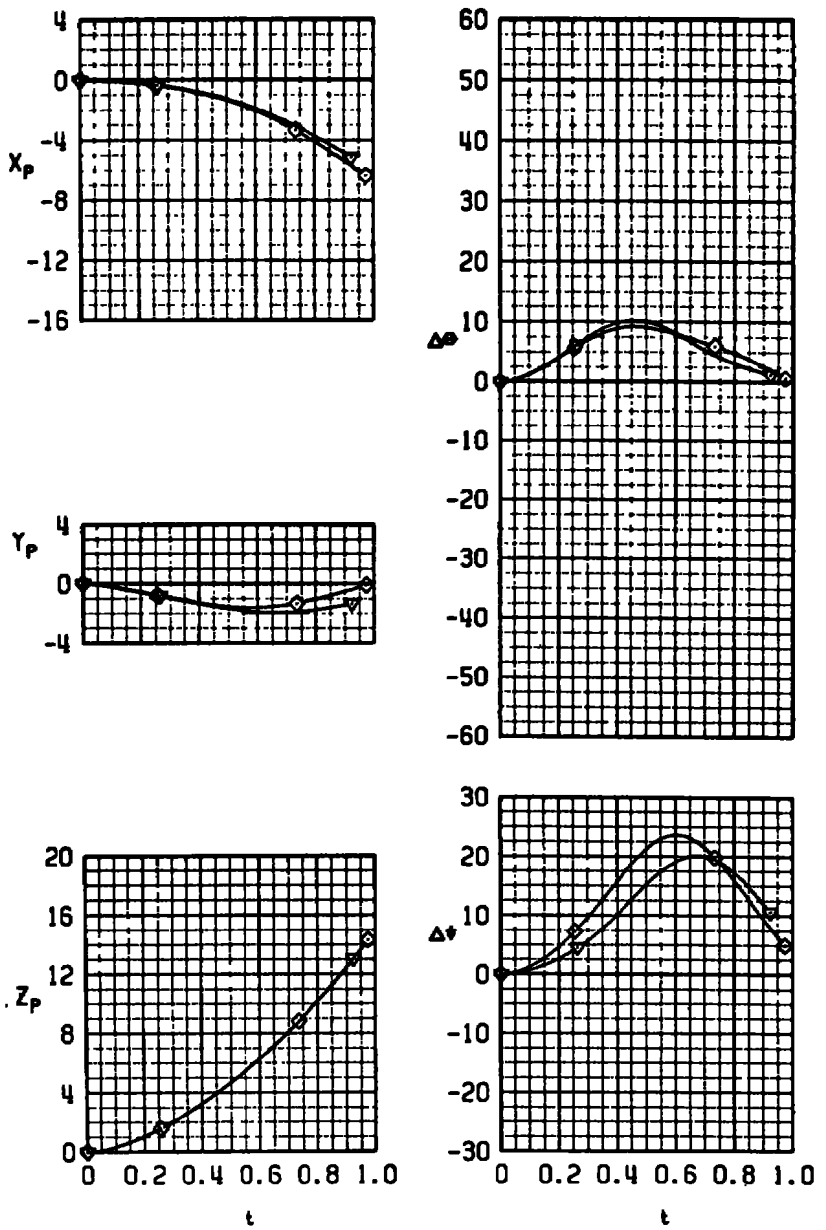

a. $M_\infty = 0.50$

Figure 29. Wind tunnel separation trajectories of the MVB from the No. 3 TER station of the F-4C aircraft, two fins canted.

SYM	M_∞	α	TABS	δ_1	δ_2	δ_3	δ_4	TER	CONF	AIR.
▽	0.7	2	YES	-9	0	0	-9	3	3	F-4
◇	0.7	2	YES	-12	0	0	-12	3	4	F-4

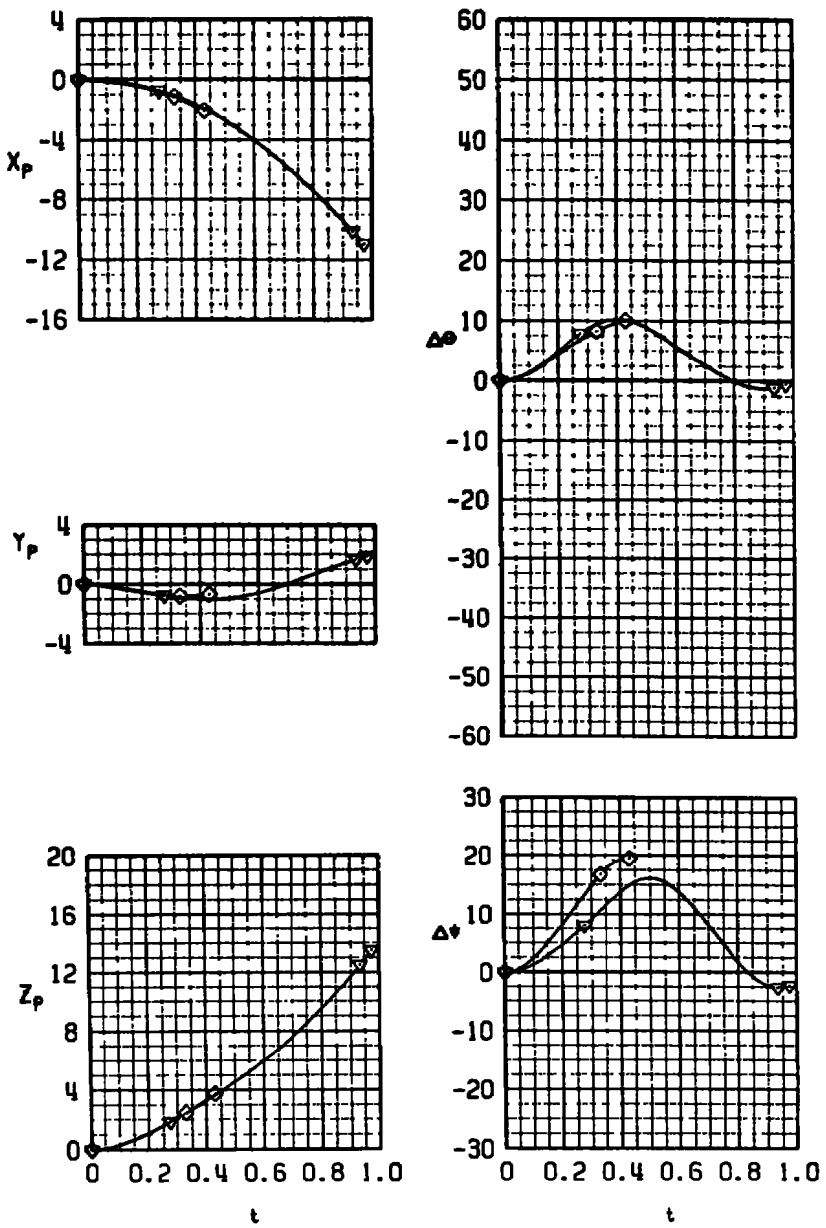

b. $M_\infty = 0.70$

Figure 29. Continued.

SYM	M_∞	α	TABS	δ_1	δ_2	δ_3	δ_4	TER	CONF	AIR.
▽	0.9	0	YES	-9	0	0	-9	3	3	F-4
◇	0.9	0	YES	-12	0	0	-12	3	4	F-4

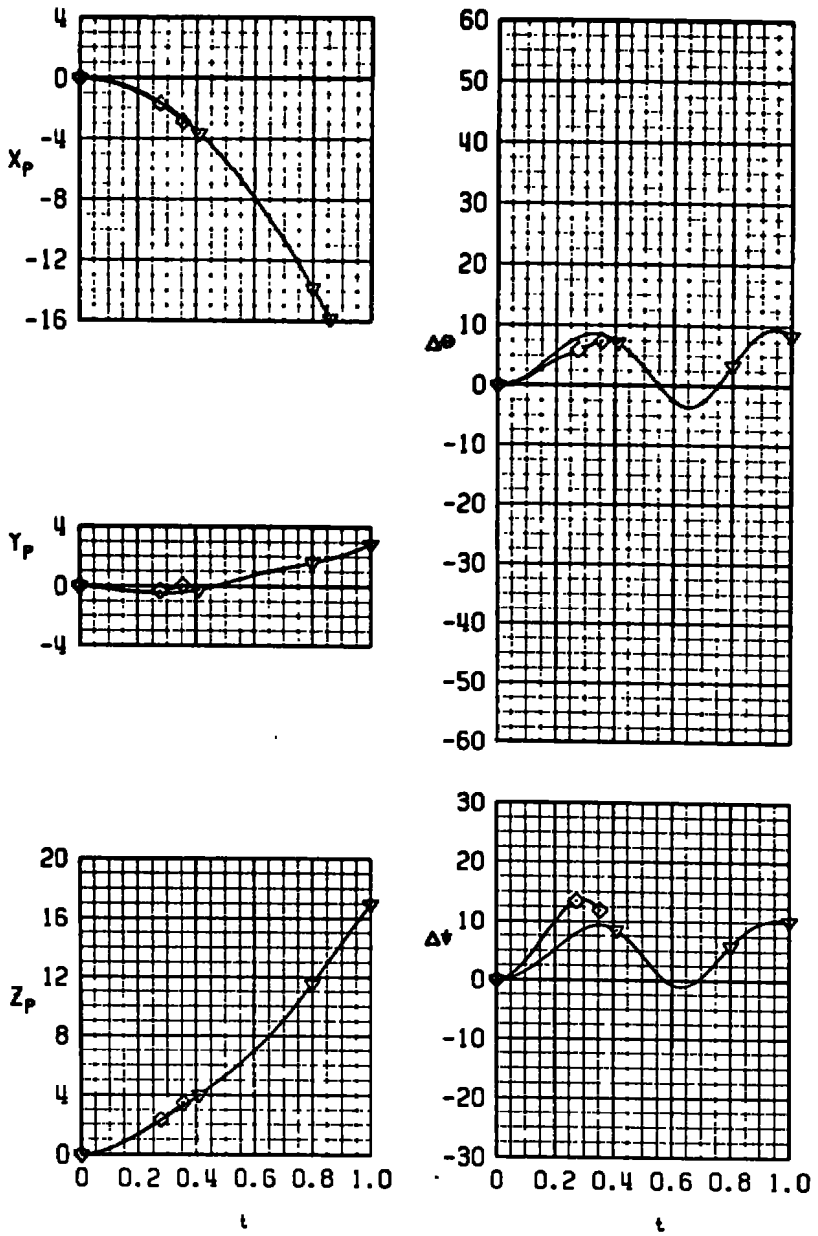

c. $M_\infty = 0.90$
Figure 29. Continued.

SYM	M_∞	α	TABS	δ_1	δ_2	δ_3	δ_4	TER	CONF	AIR.
▽	1.1	0	YES	-9	0	0	-9	3	3	F-4
◇	1.1	0	YES	-12	0	0	-12	3	4	F-4

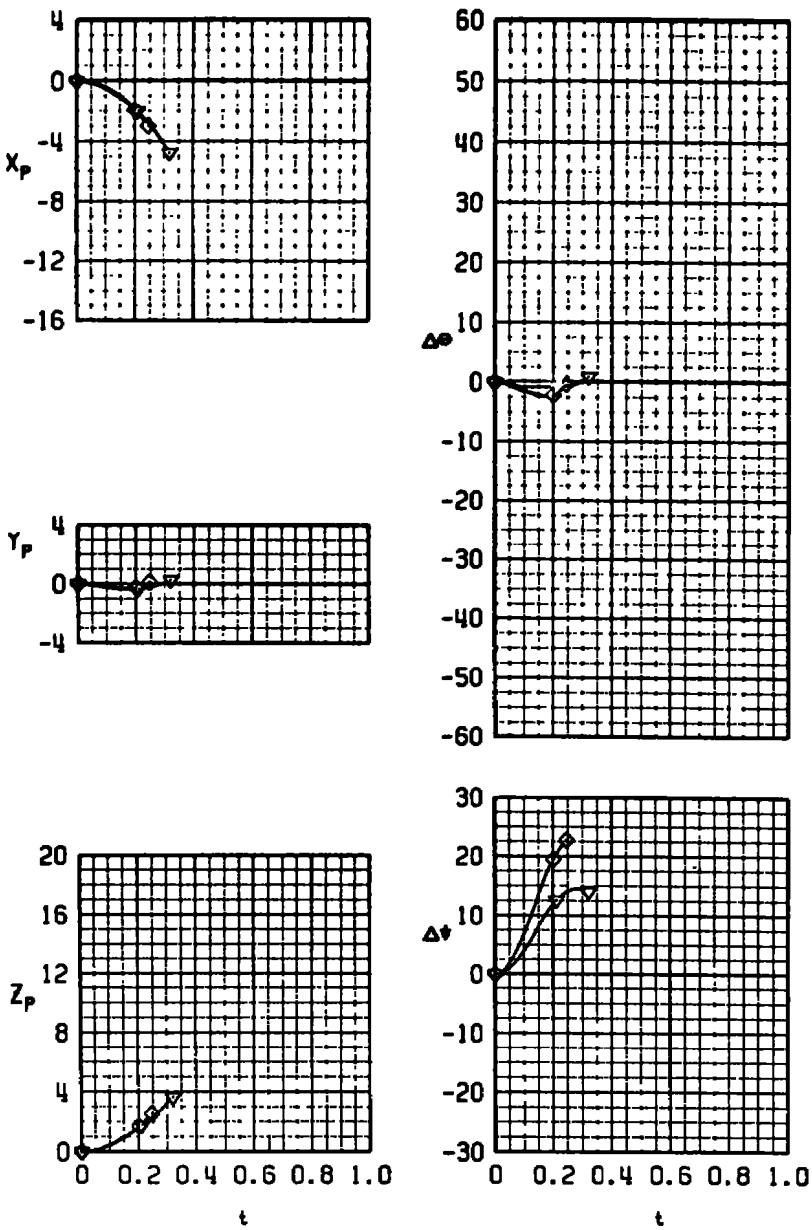

d. $M_\infty = 1.10$

Figure 29. Concluded.

SYM	M_∞	α	TABS	δ_1	δ_2	δ_3	δ_4	TER CONF AIR.
⊙	0.5	4	NONE	-12	-12	-12	-12	1 5/5A F-4
⊡	0.5	4	YES	-12	0	0	-12	1 14/14A F-4

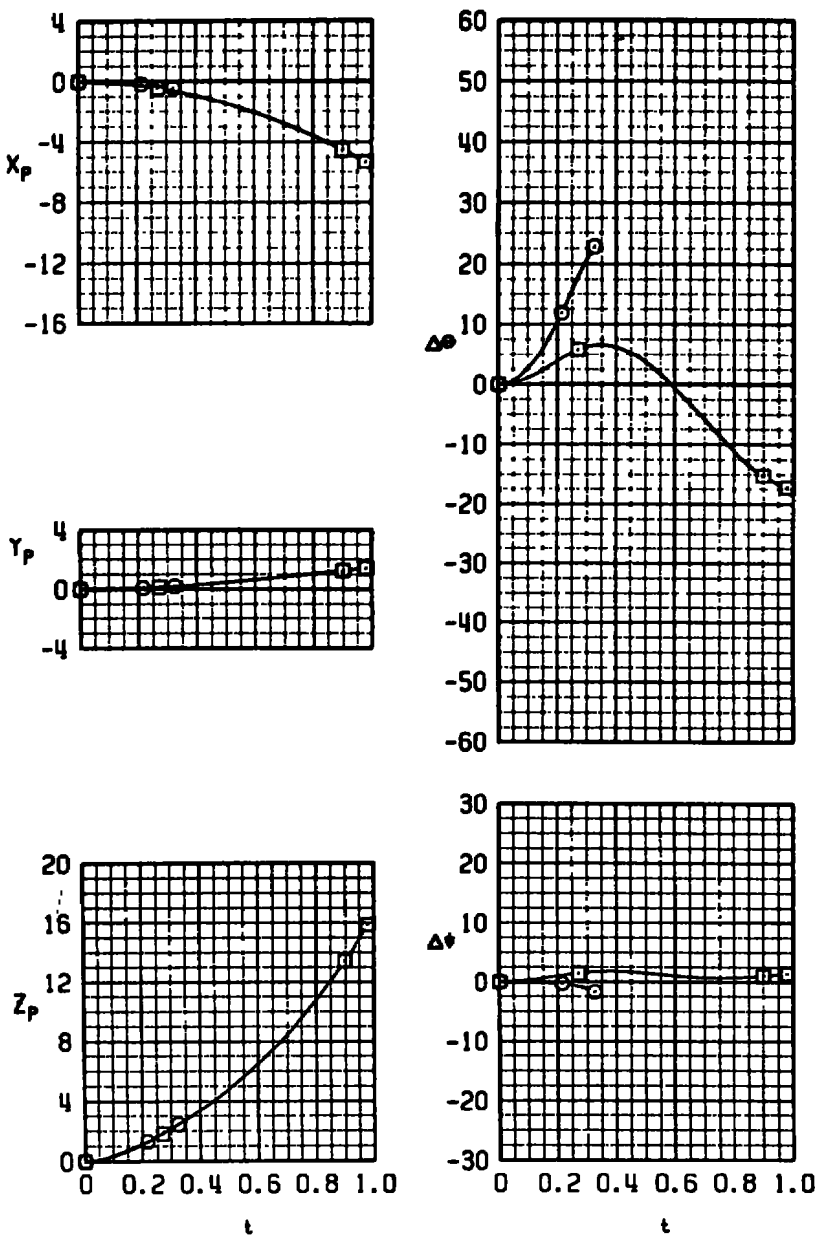

a. $M_\infty = 0.50$

Figure 30. Wind tunnel separation trajectories of the MVB with simulation of fins returned from -12 to 0 deg during the trajectory.

SYM	M_∞	α	TABS	δ_1	δ_2	δ_3	δ_4	TER	CONF	AIR.
⊡	0.7	2	YES	-12	0	0	-12	1	14/14A	F-4

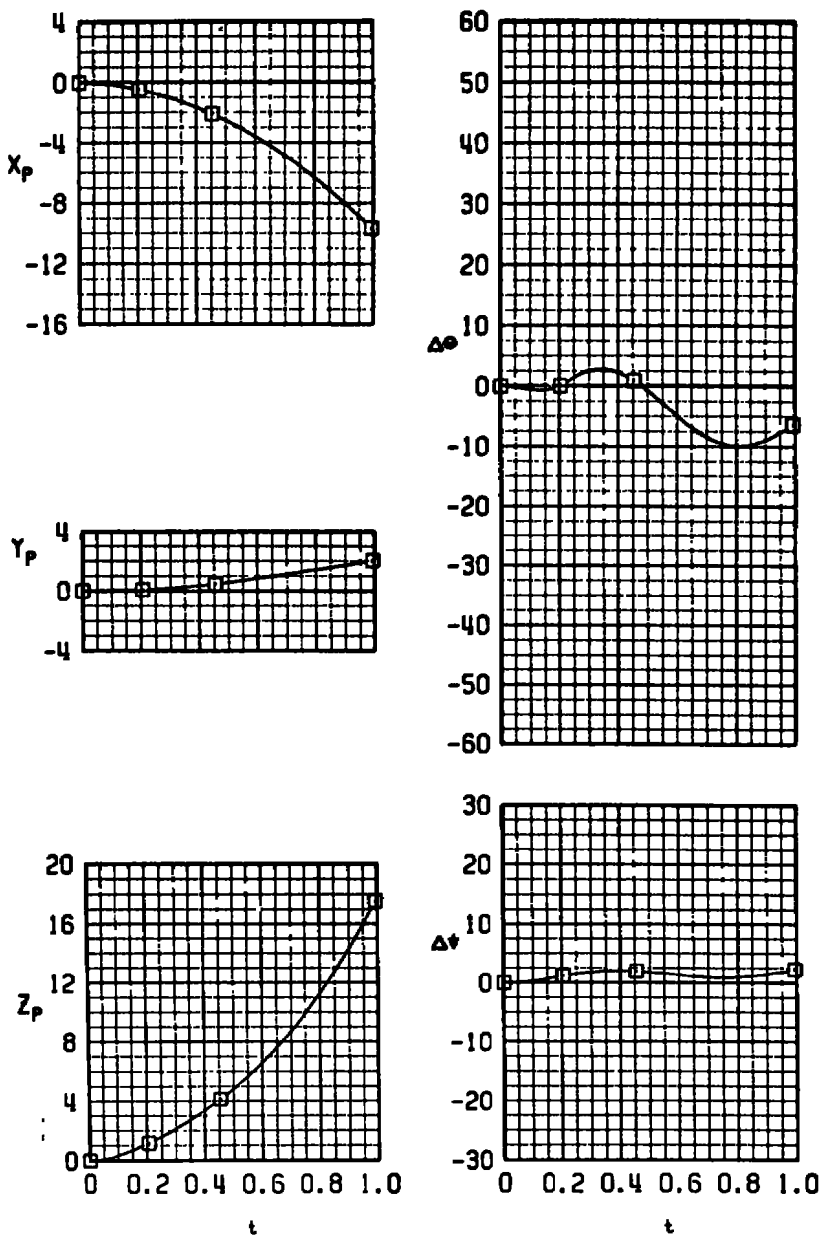

b. $M_\infty = 0.70$

Figure 30. Continued.

SYM	M_∞	α	TABS	δ_1	δ_2	δ_3	δ_4	TER CONF AIR.
⊙	0.9	0	NONE	-12	-12	-12	-12	1 5/5A F-4
⊡	0.9	0	YES	-12	0	0	-12	1 14/14A F-4

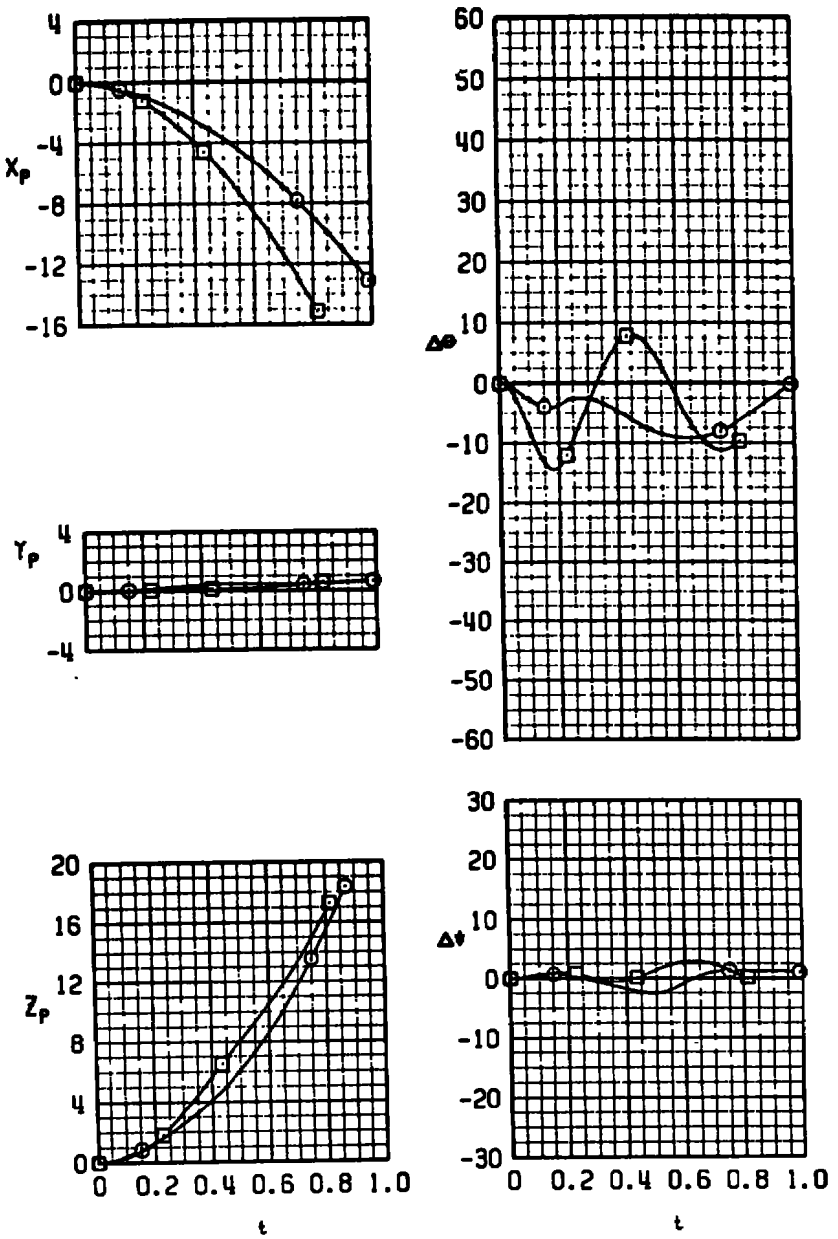

c. $M_\infty = 0.90$

Figure 30. Continued.

SYM	M_∞	α	TABS	δ_1	δ_2	δ_3	δ_4	TER CONF	AIR.
⊙	1.1	0	NONE	-12	-12	-12	-12	1	5/5A F-4

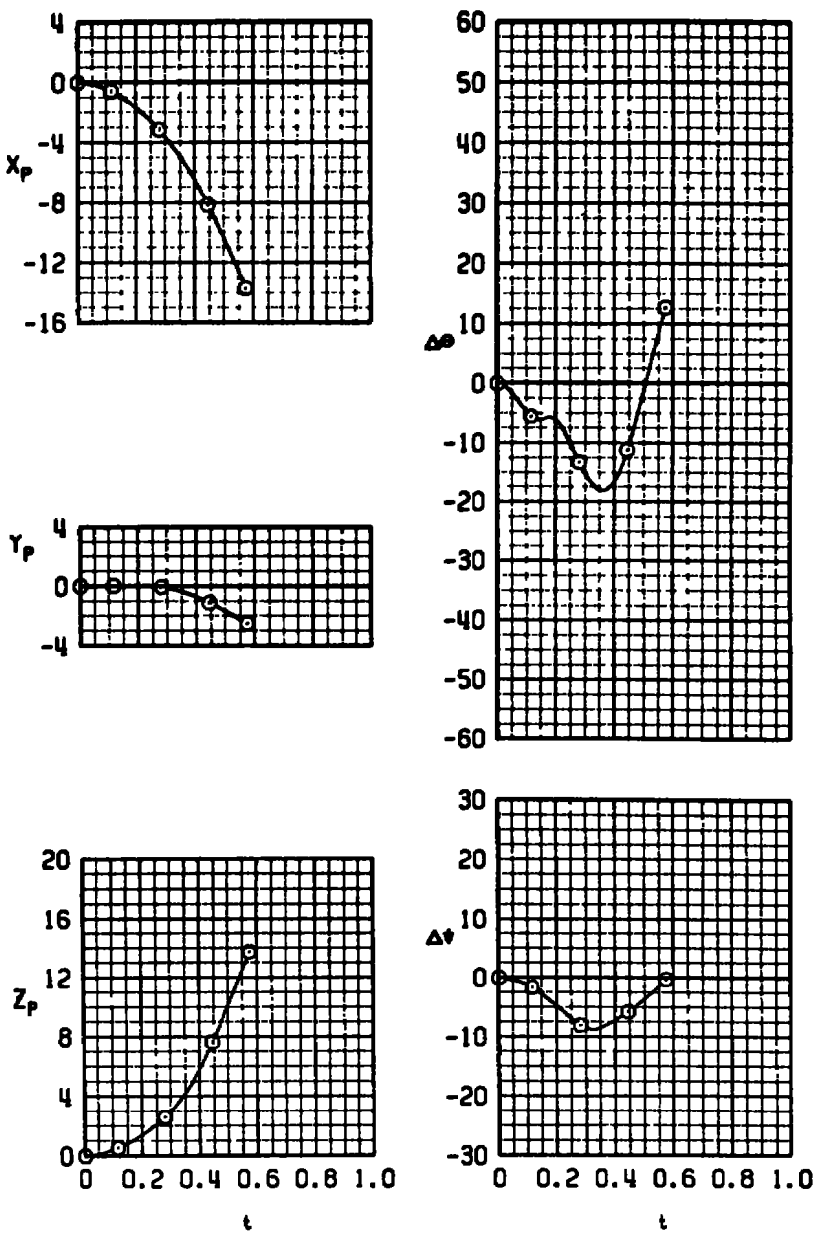

d. $M_\infty = 1.10$

Figure 30. Concluded.

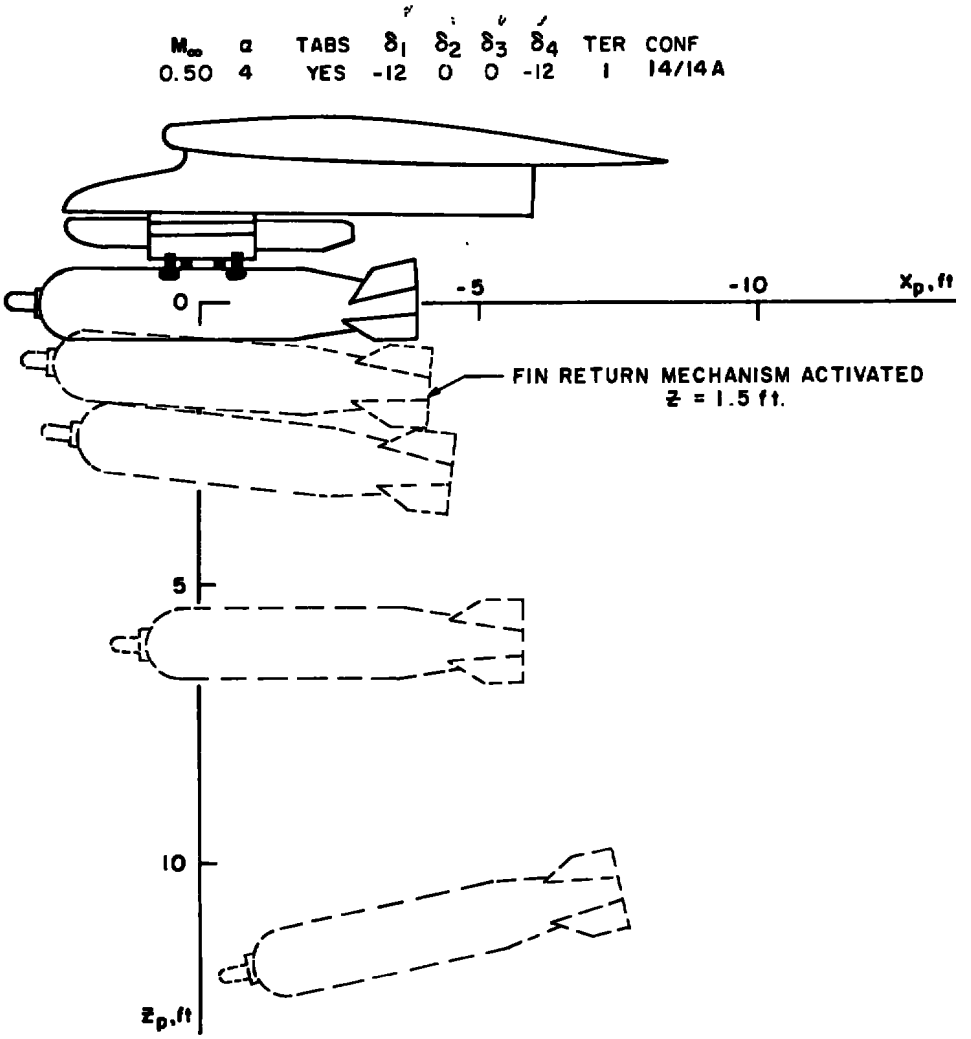

a. $M_\infty = 0.50$

Figure 31. Illustration of MVB trajectories with simulation of fins returned from -12 to 0 deg cant.

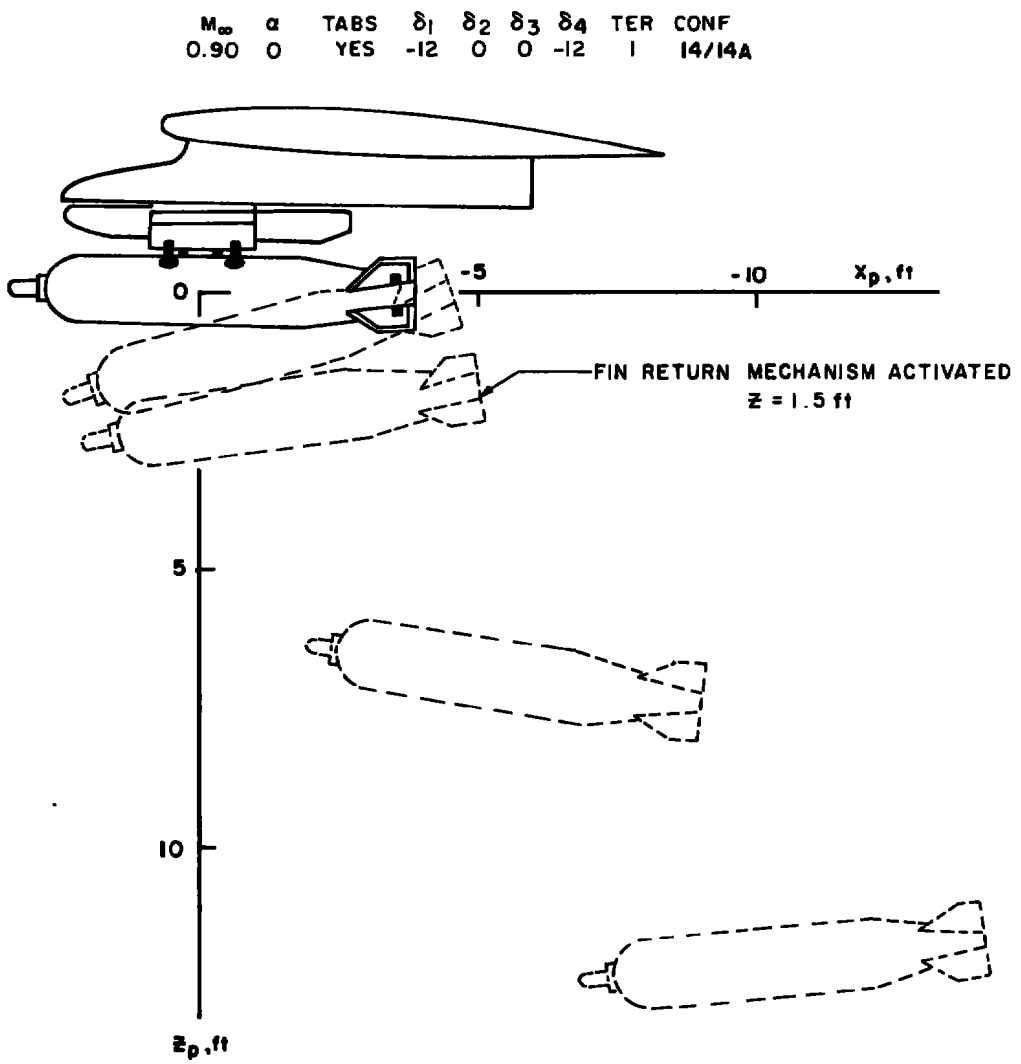

b. $M_\infty = 0.90$

Figure 31. Concluded.

SYM	M_∞	α	TABS	δ_1	δ_2	δ_3	δ_4	TER	CONF	AIR.
⊙	0.9	2	NONE	-12	0	0	-12	1	37	A-7D
△	0.9	2	YES	-12	0	0	-12	1	38	A-7D
▽	0.9	2	NONE	0	0	0	0	1	39	A-7D

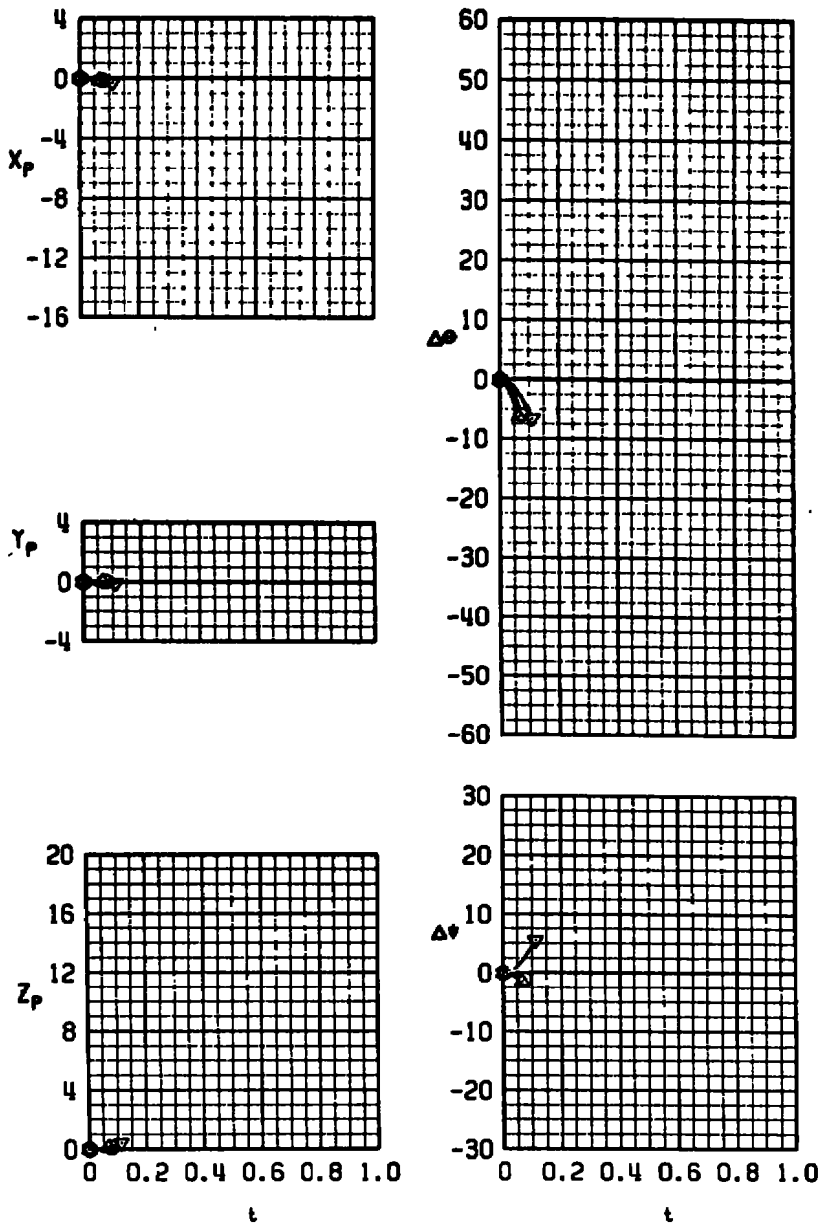

a. TER station No. 1

Figure 32. Wind tunnel separation trajectories of the MVB from the A7-D aircraft at M_∞ = 0.90.

SYM	M_∞	α	TABS	δ_1	δ_2	δ_3	δ_4	TER	CONF	AIR.
⊙	0.9	2	NONE	-12	0	0	-12	2	40	A-70
△	0.9	2	YES	-12	0	0	-12	2	41	A-70
▽	0.9	2	NONE	0	0	0	0	2	42	A-70

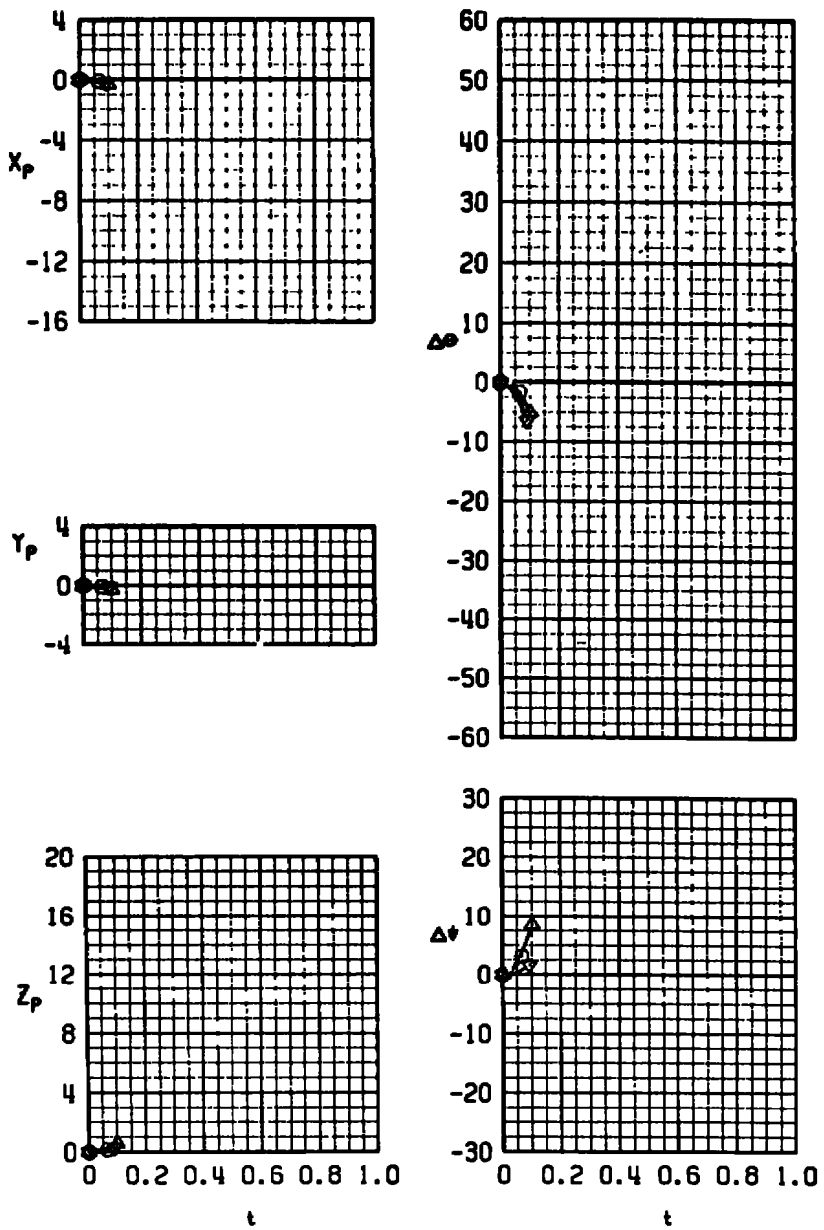

b. TER station No. 2
Figure 32. Continued.

SYM	M_∞	α	TABS	δ_1	δ_2	δ_3	δ_4	TER	CONF	AIR.
⊙	0.9	2	NONE	-12	0	0	-12	3	43	A-7D
⊡	0.9	2	NONE	-12	0	0	-12	3	43	A-7D
△	0.9	2	YES	-12	0	0	-12	3	44	A-7D
▽	0.9	2	NONE	0	0	0	0	3	45	A-7D

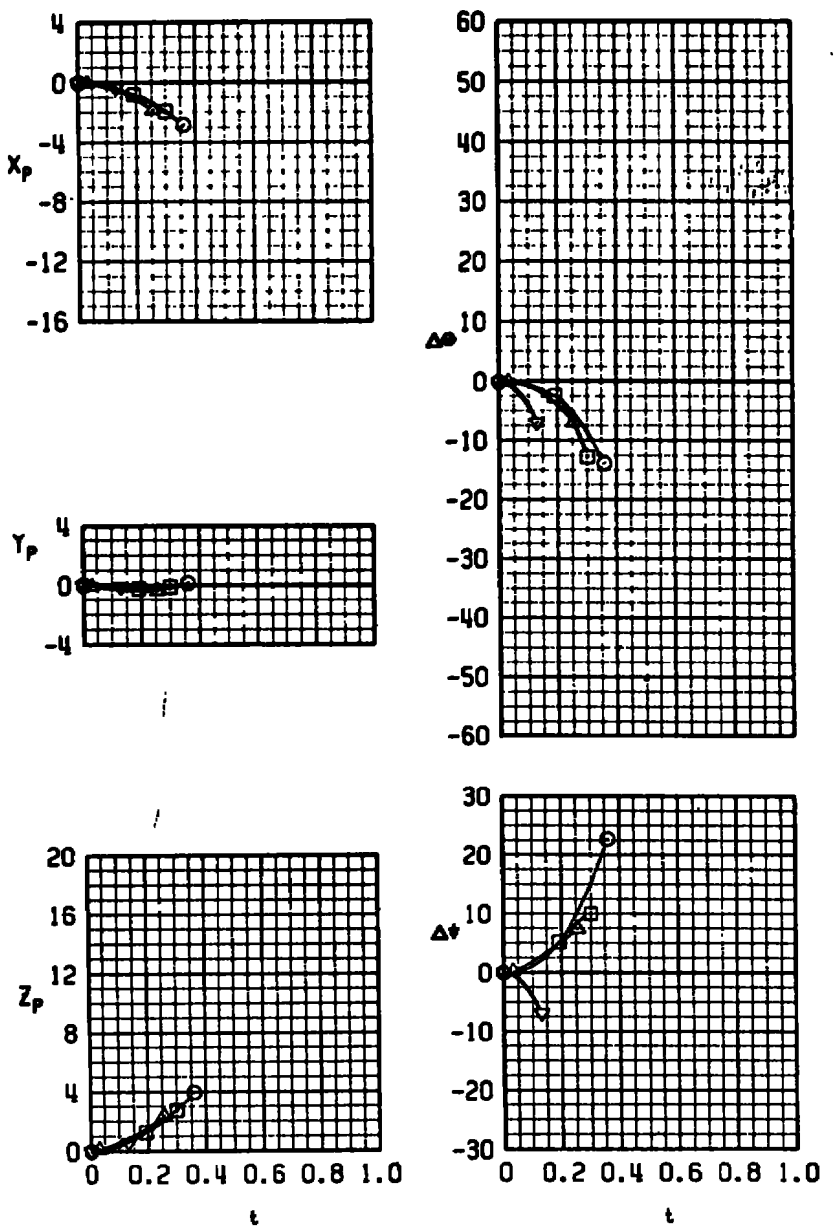

c. TER station No. 3
Figure 32. Continued.

SYM	M_∞	α	TABS	δ_1	δ_2	δ_3	δ_4	PYLON	CONF	AIR.
⊙	0.9	2	NONE	-12	0	0	-12	6	23	A-70
△	0.9	2	YES	-12	0	0	-12	6	24	A-70

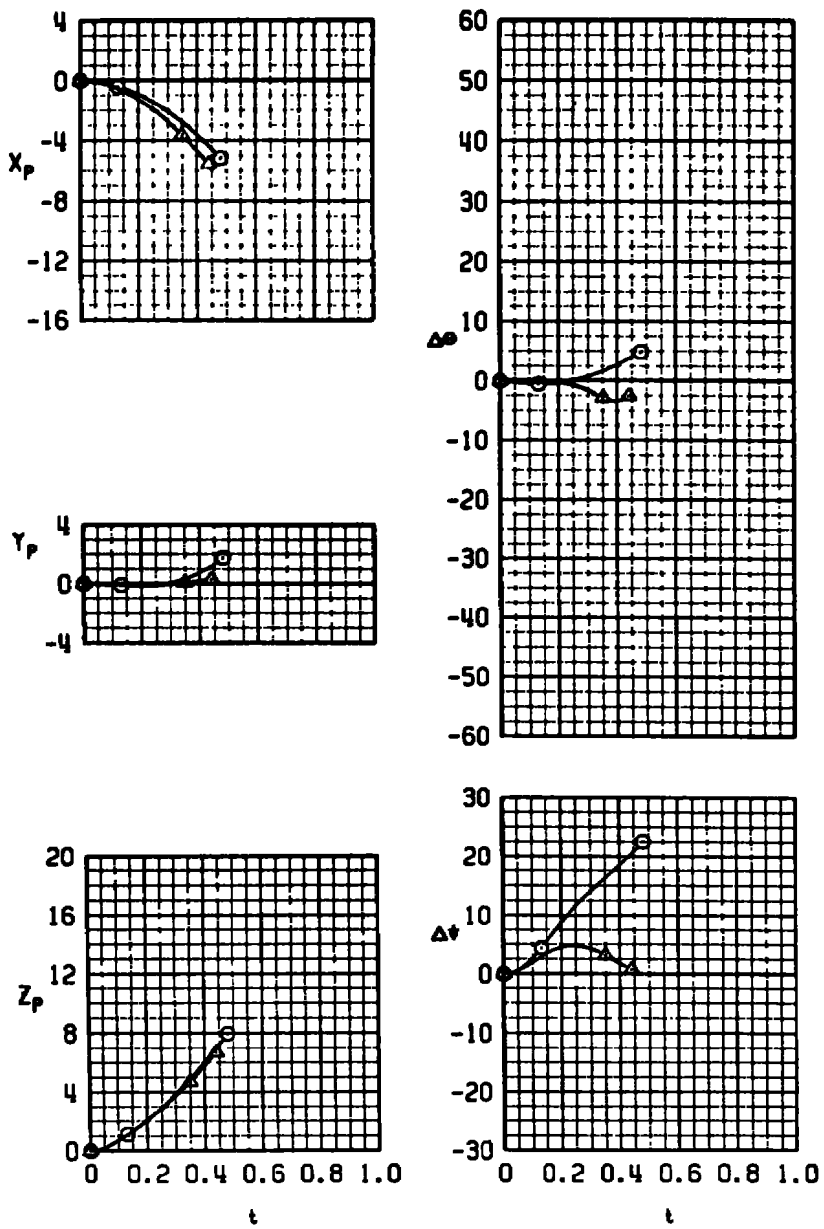

d. Pylon station No. 6
Figure 32. Continued.

SYM	M_∞	α	TABS	δ_1	δ_2	δ_3	δ_4	MER	CONF	AIR.
⊙	0.9	2	NONE	-12	0	0	-12	1	25	A-70

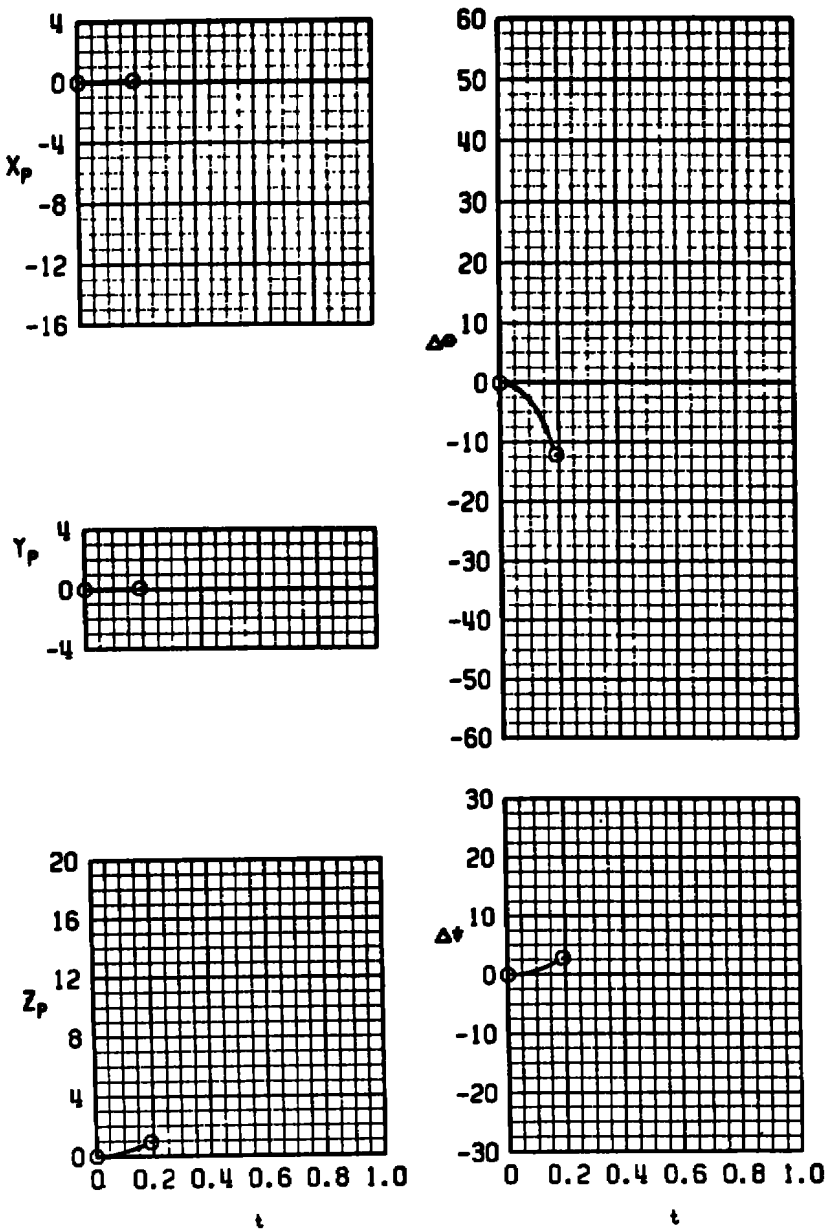

e. MER station No. 1
Figure 32. Continued.

SYM	M_∞	α	TABS	δ_1	δ_2	δ_3	δ_4	MER	CONF	AIR.
⊙	0.9	2	NONE	-12	0	0	-12	2	27	A-70
△	0.9	2	YES	-12	0	0	-12	2	28	A-70

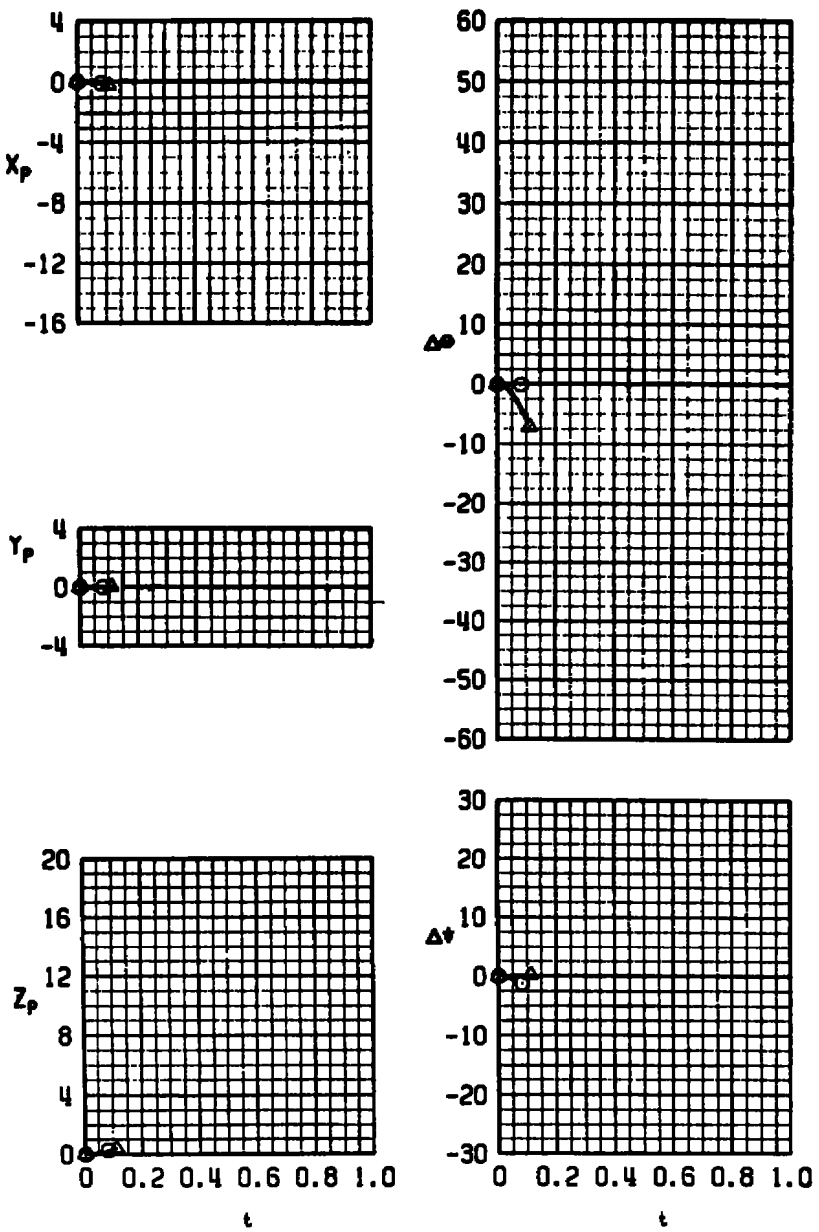

f. MER station No. 2
Figure 32. Continued.

SYM	M_∞	α	TABS	δ_1	δ_2	δ_3	δ_4	MER	CONF	AIR.
⊙	0.9	2	NONE	-12	0	0	-12	3	30	A-70

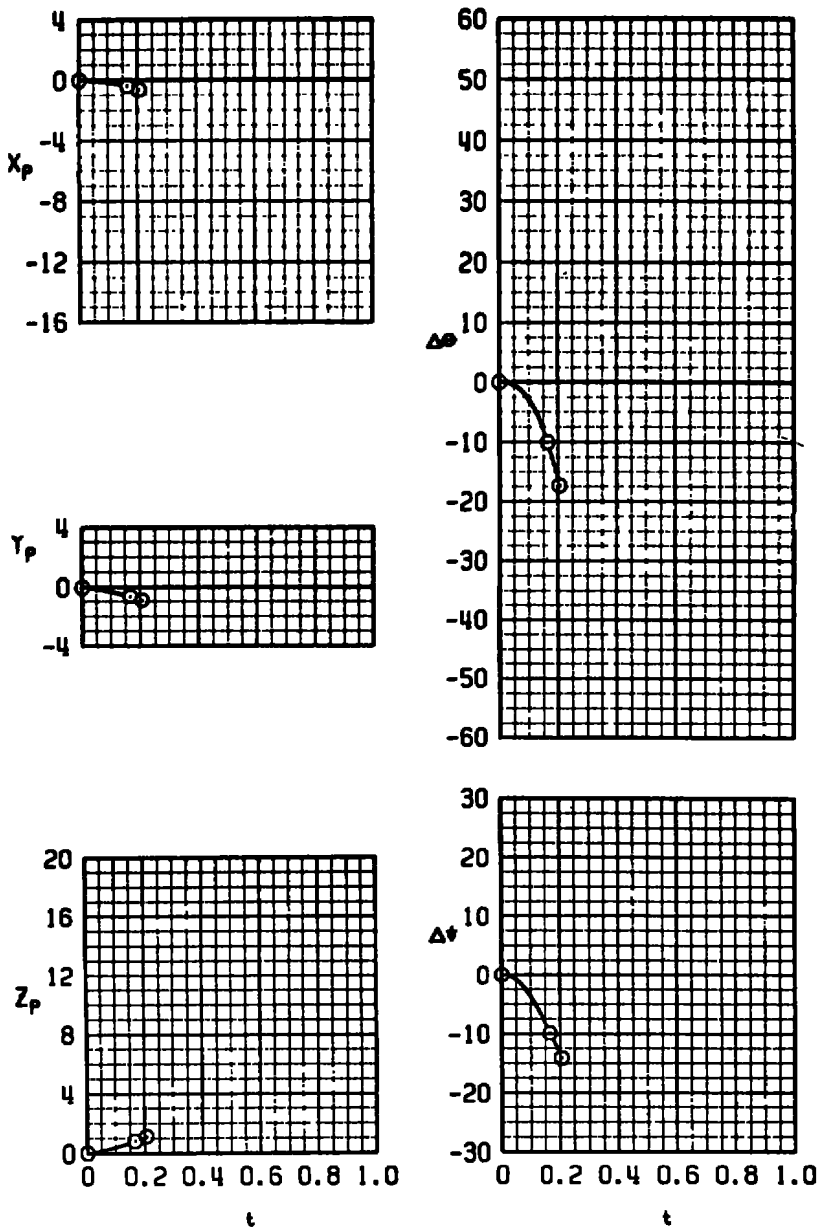

g. MER station No. 3

Figure 32. Continued.

SYM	M_∞	α	TABS	δ_1	δ_2	δ_3	δ_4	MER	CONF	AIR.
⊙	0.9	2	NONE	-12	0	0	-12	4	31	A-70
△	0.9	2	YES	-12	0	0	-12	4	32	A-70

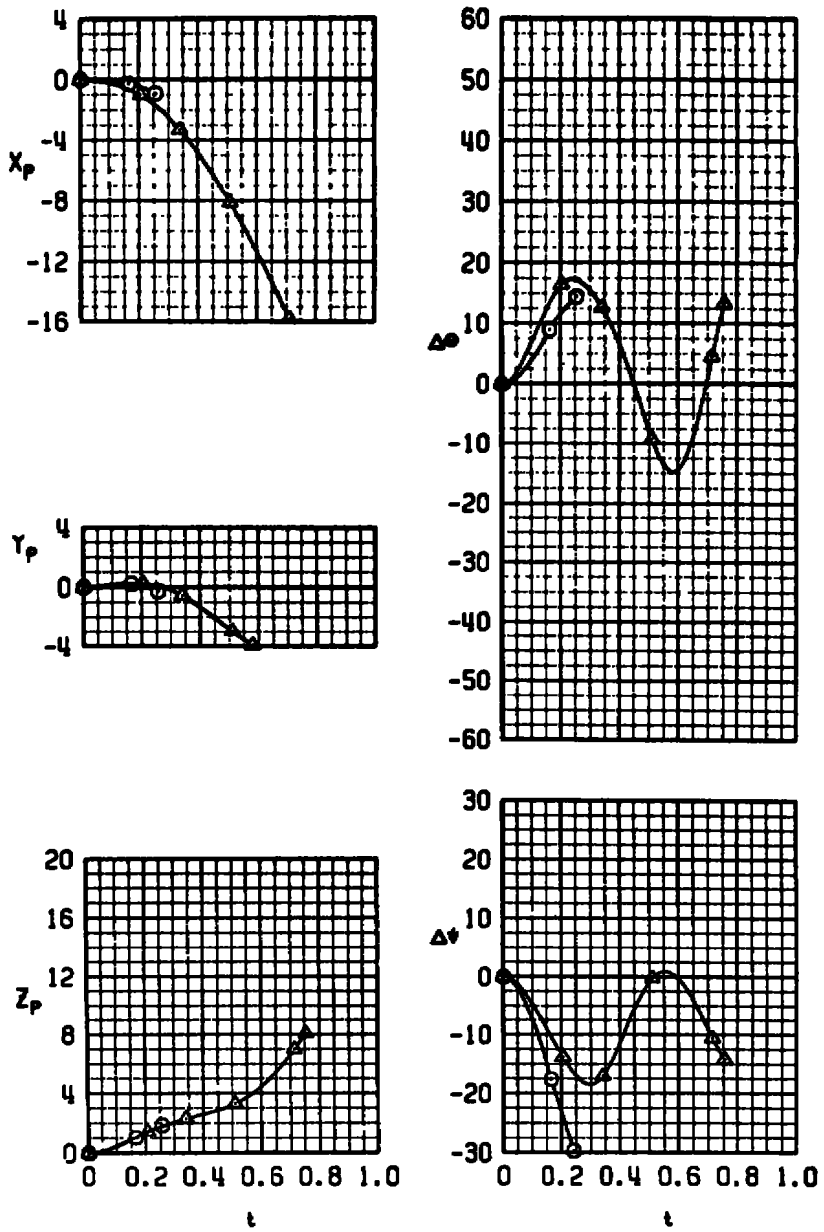

h. MER station No. 4
Figure 32. Continued.

SYM	M_∞	α	TABS	δ_1	δ_2	δ_3	δ_4	MER	CONF	AIR.
⊙	0.9	2	NONE	-12	0	0	-12	5	31	A-70
△	0.9	2	YES	-12	0	0	-12	5	34	A-70

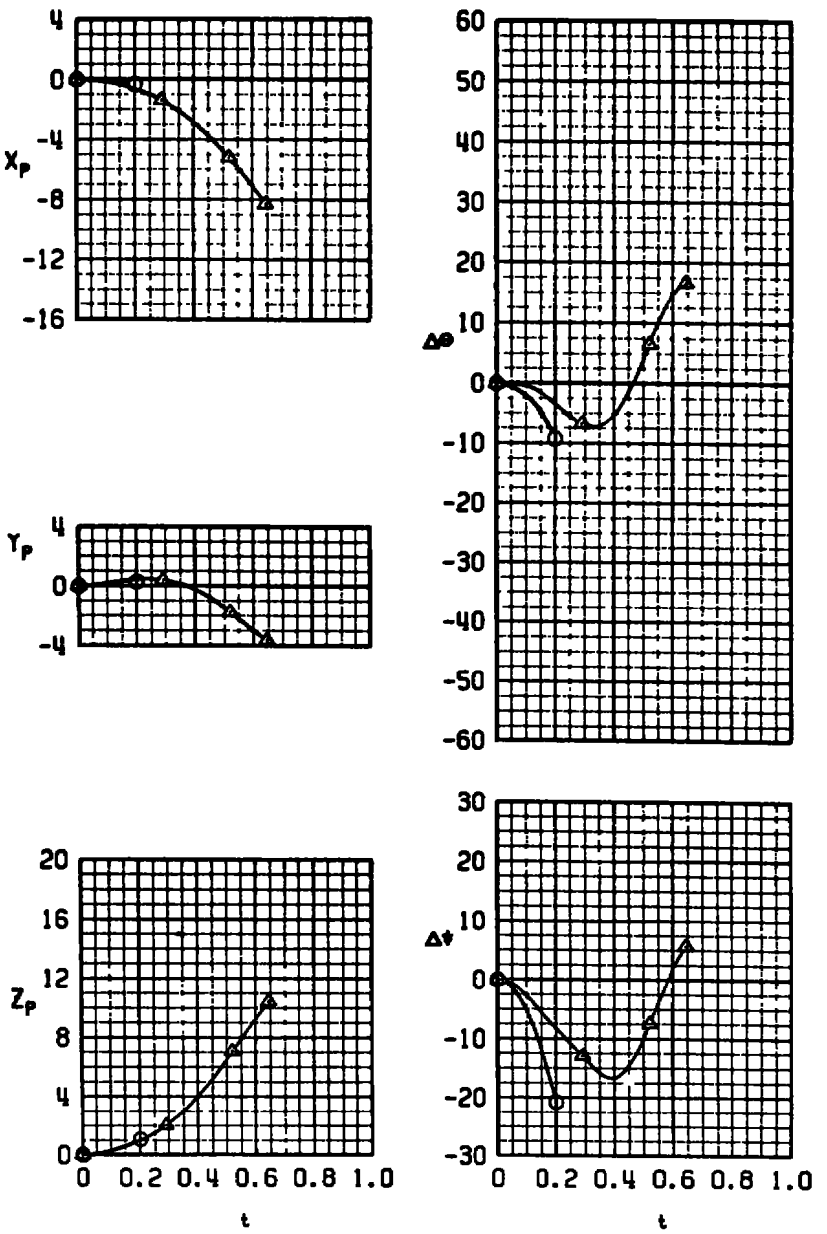

i. MER station No. 5
Figure 32. Continued.

SYM	M_∞	α	TABS	δ_1	δ_2	δ_3	δ_4	MER	CONF	AIR.
⊙	0.9	2	NONE	-12	0	0	-12	6	35	A-7D
△	0.9	2	YES	-12	0	0	-12	6	36	A-7D

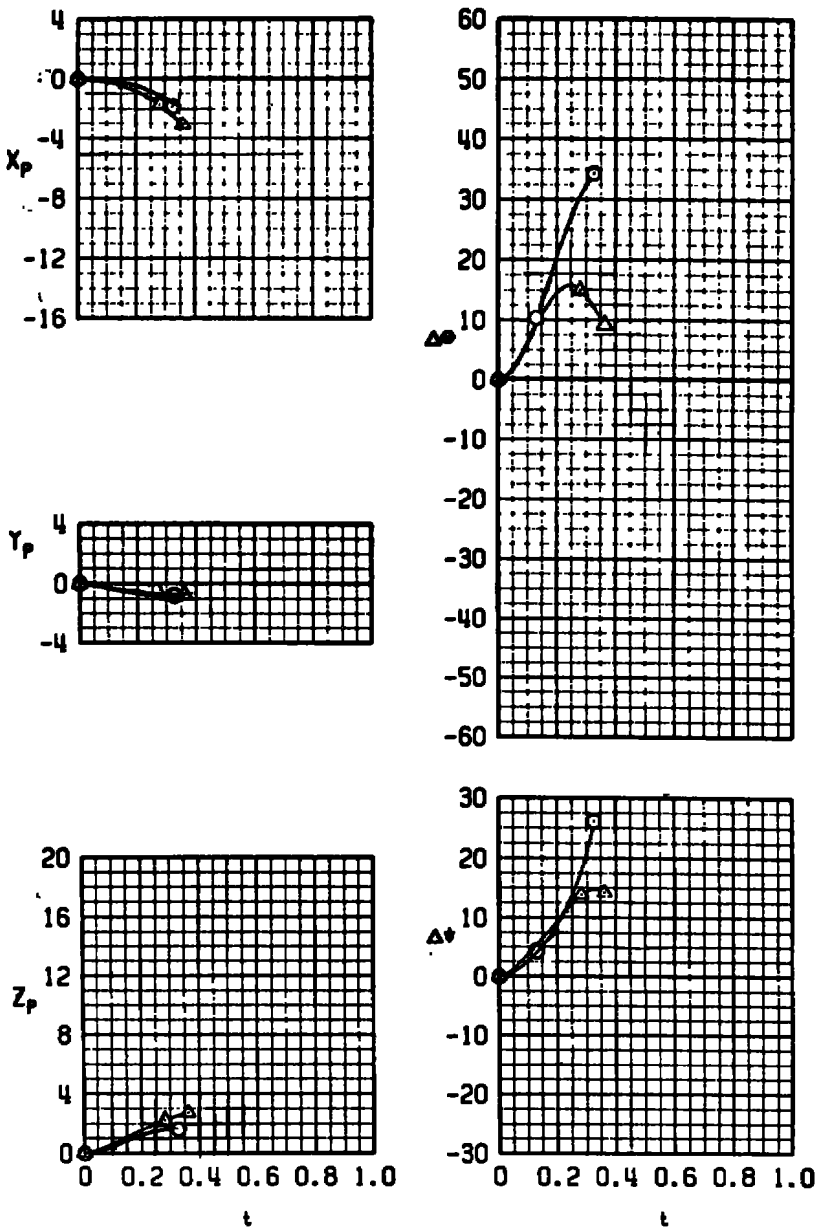

j. MER station No. 6
Figure 32. Concluded.

SYM	M_∞	α	TABS	δ_1	δ_2	δ_3	δ_4	TER	CONF	AIR.	z_0
⊙	0.48	4	NONE	0	0	0	0	1	15	F-4	0.01
⊡	0.50	4	NONE	0	0	0	0	1	15	F-4	0.01
△	0.52	4	NONE	0	0	0	0	1	15	F-4	0.01
■	0.50	4	NONE	0	0	0	0	1	15	FLIGHT TEST	

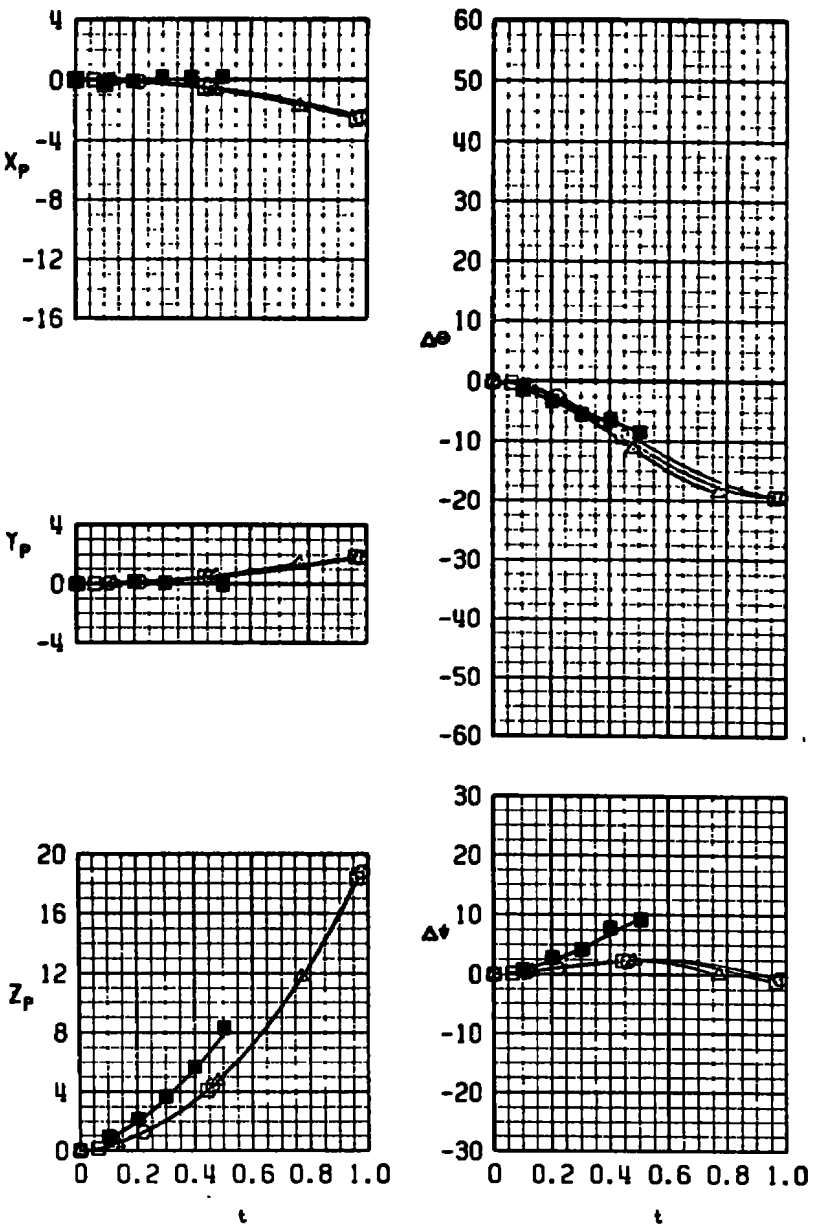

a. Time

Figure 33. Wind tunnel captive trajectory and flight test separation trajectories of the MVB with uncanted fins, M_∞ = 0.50.

SYM	M_∞	α	TABS	δ_1	δ_2	δ_3	δ_4	TER	CONF	AIR.	Z_0
⊙	0.48	4	NONE	0	0	0	0	1	15	F-4	0.01
⊡	0.50	4	NONE	0	0	0	0	1	15	F-4	0.01
△	0.52	4	NONE	0	0	0	0	1	15	F-4	0.01
■	0.50	4	NONE	0	0	0	0	1	15	FLIGHT TEST	

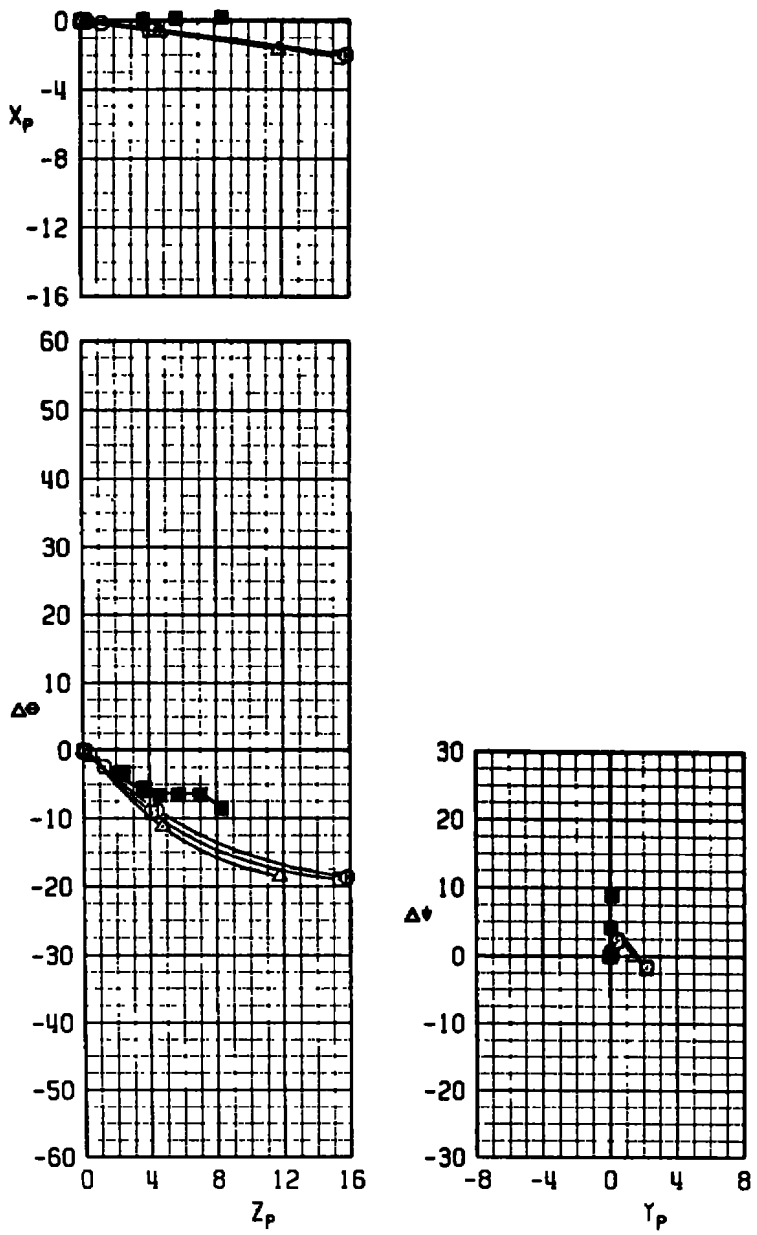

b. Displacement

Figure 33. Continued.

SYM	M_∞	α	TABS	δ_1	δ_2	δ_3	δ_4	TER	CONF	AIR.	z_0
⊙	0.50	3°	NONE	0	0	0	0	1	15	F-4	0.03
⊡	0.50	4°	NONE	0	0	0	0	1	15	F-4	0.01
■	0.50	4°	NONE	0	0	0	0	1	15	FLIGHT TEST	

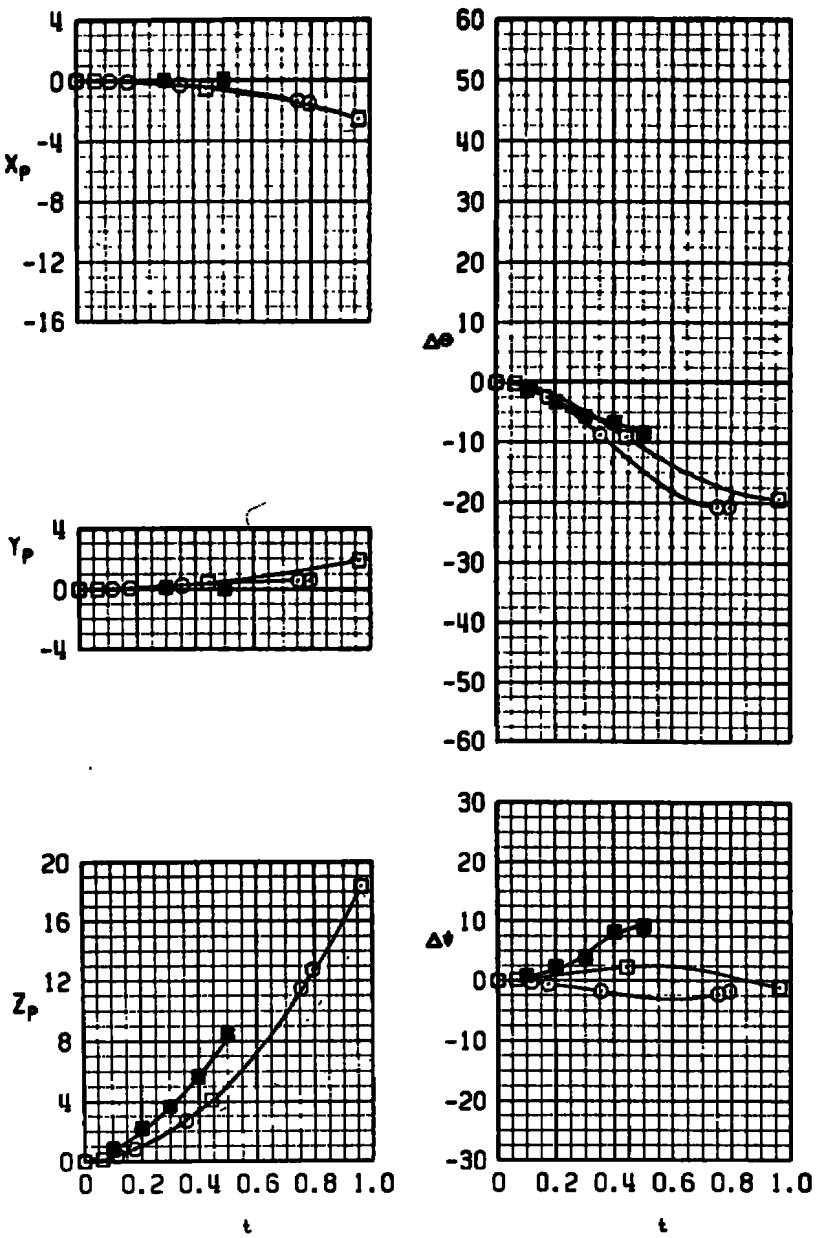

c. Time

Figure 33. Continued.

SYM	M_∞	α	TABS	δ_1	δ_2	δ_3	δ_4	TER	CONF	AIR.	Z_0
⊙	0.50	3	NONE	0	0	0	0	I	15	F-4	0.03
⊡	0.50	4	NONE	0	0	0	0	I	15	F-4	0.01
■	0.50	4	NONE	0	0	0	0	I	15	FLIGHT TEST	

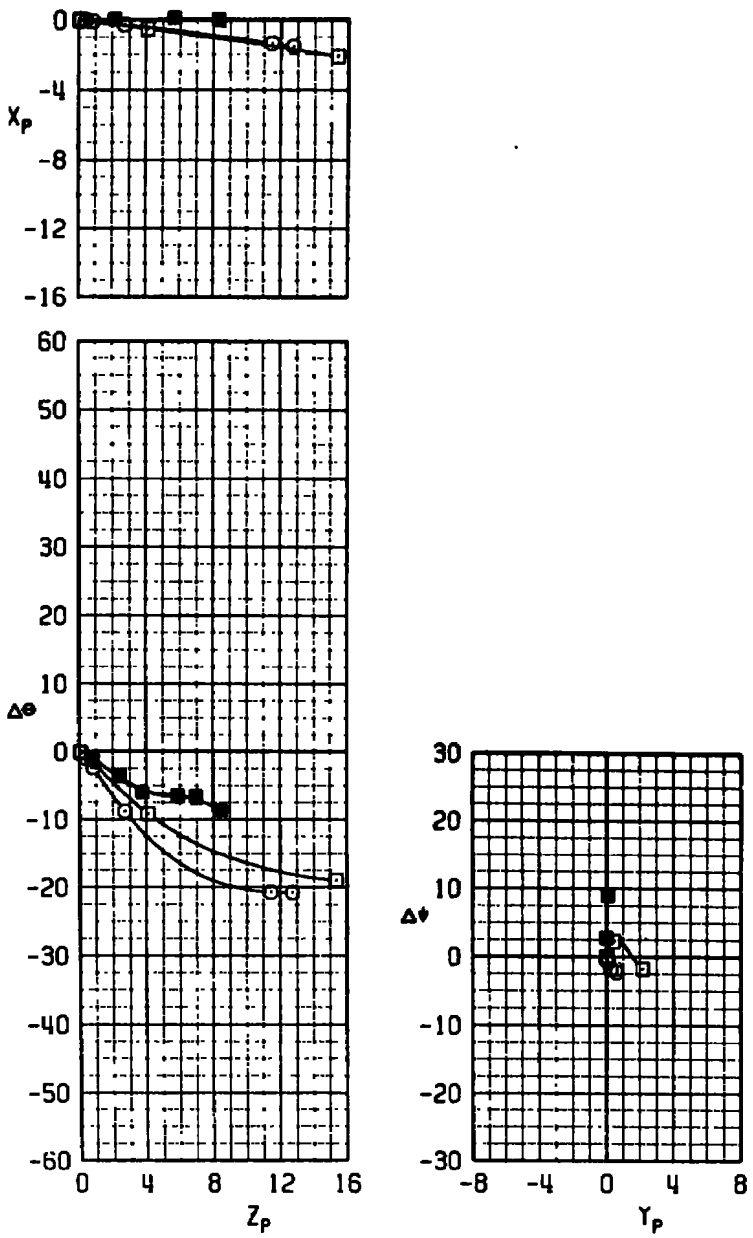

d. Dispalcement

Figure 33. Concluded.

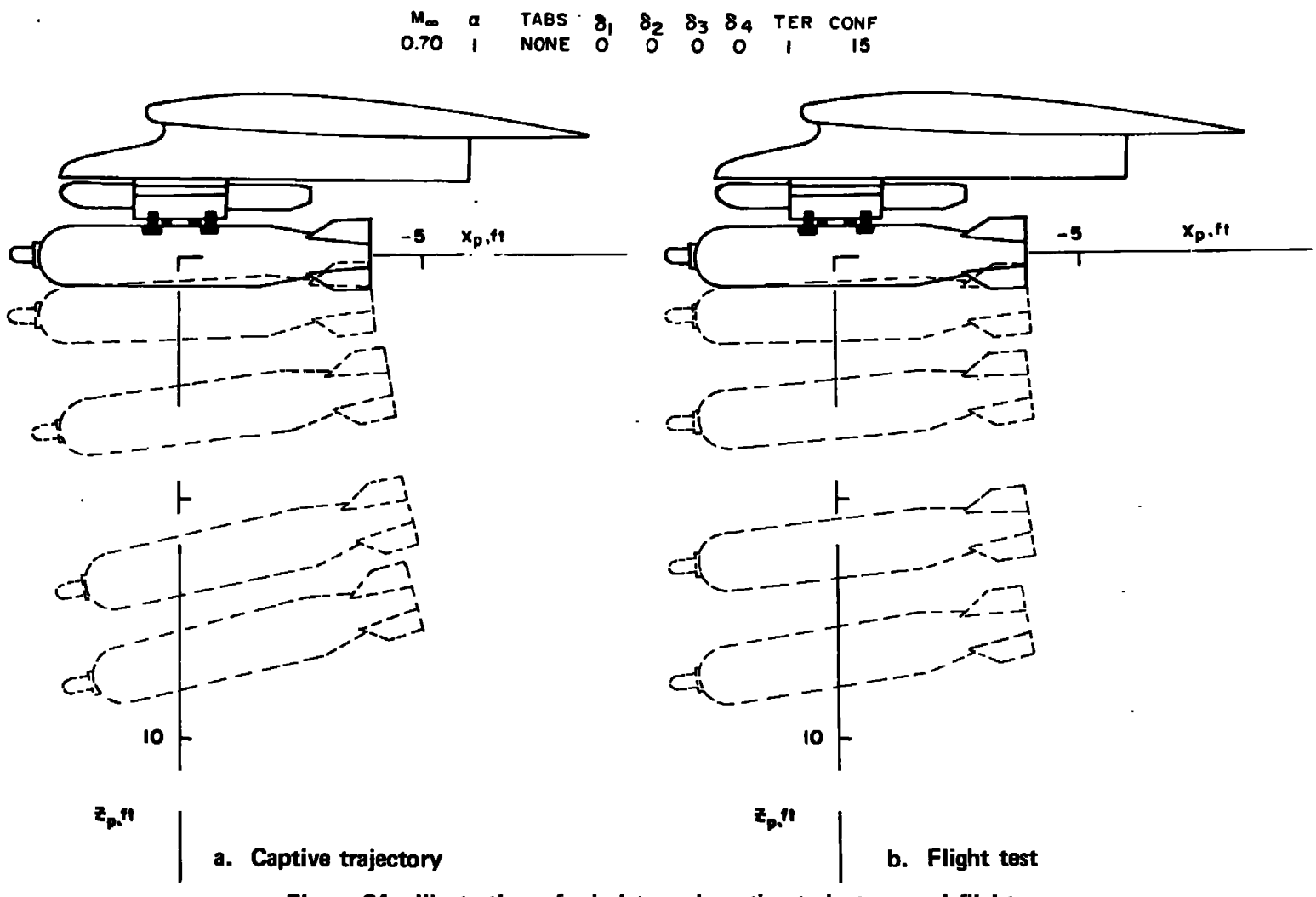

Figure 34. Illustration of wind tunnel captive trajectory and flight test separation trajectories of the MVB with uncanted fins, M_∞ = 0.50.

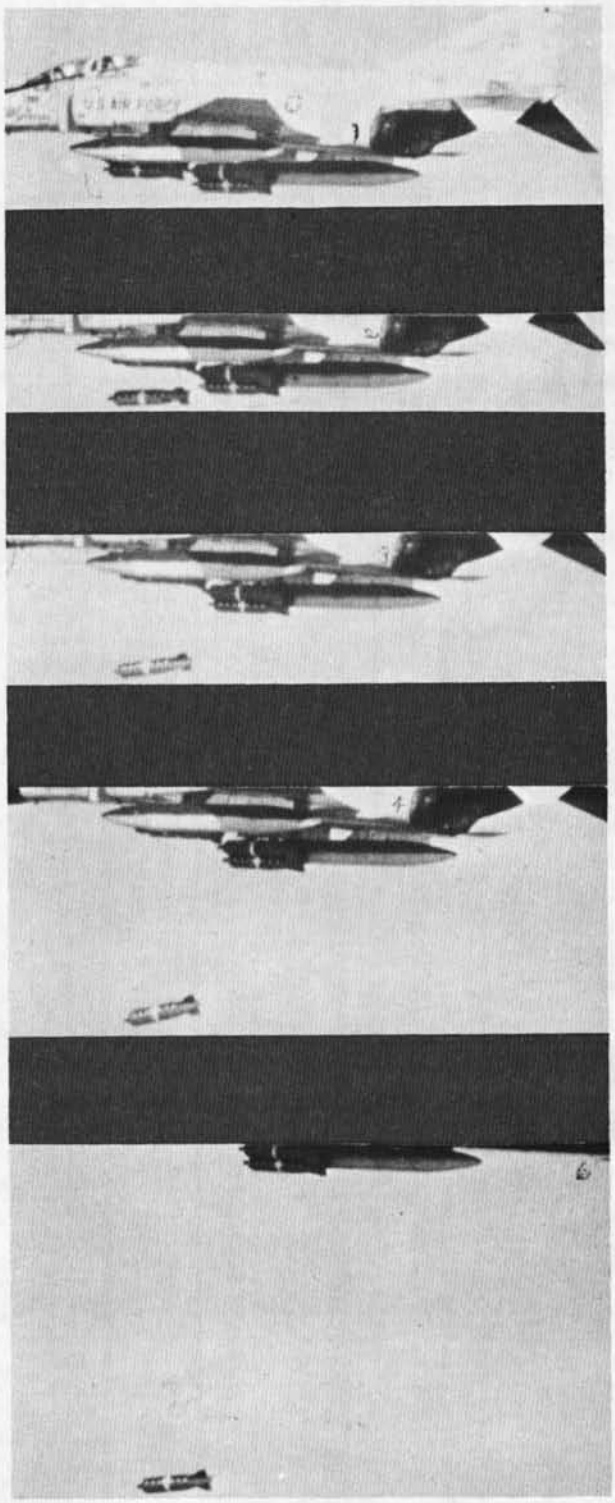

Figure 35. Release sequence of the MVB with uncanted fins, no tabs, M_∞ = 0.50.

SYM	M_∞	α	TABS	δ_1	δ_2	δ_3	δ_4	TER	CONF	AIR.	z_0
⊡	0.70	1	NONE	0	0	0	0	1	15	F-4	0.03
△	0.72	2	NONE	0	0	0	0	1	15	F-4	0.01
■	0.70	1	NONE	0	0	0	0	1	15	FLIGHT TEST	

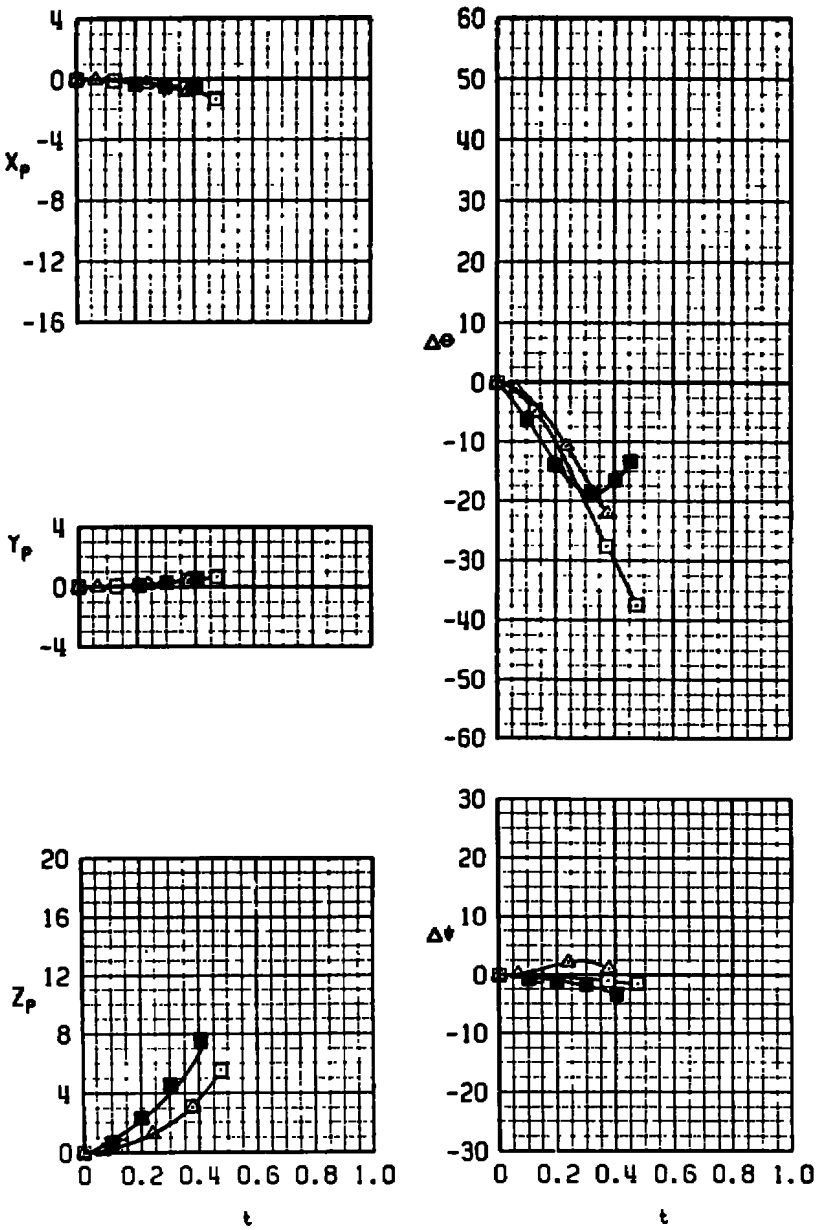

a. Time

Figure 36. Wind tunnel captive trajectory and flight test separation trajectories of the MVB with uncanted fins, M_∞ = 0.70.

SYM	M_∞	α	TABS	δ_1	δ_2	δ_3	δ_4	TER	CONF	AIR.	z_o
⊡	0.70	1	NONE	0	0	0	0	1	15	F-4	0.03
△	0.72	2	NONE	0	0	0	0	1	15	F-4	0.01
■	0.70	1	NONE	0	0	0	0	1	15	FLIGHT TEST	

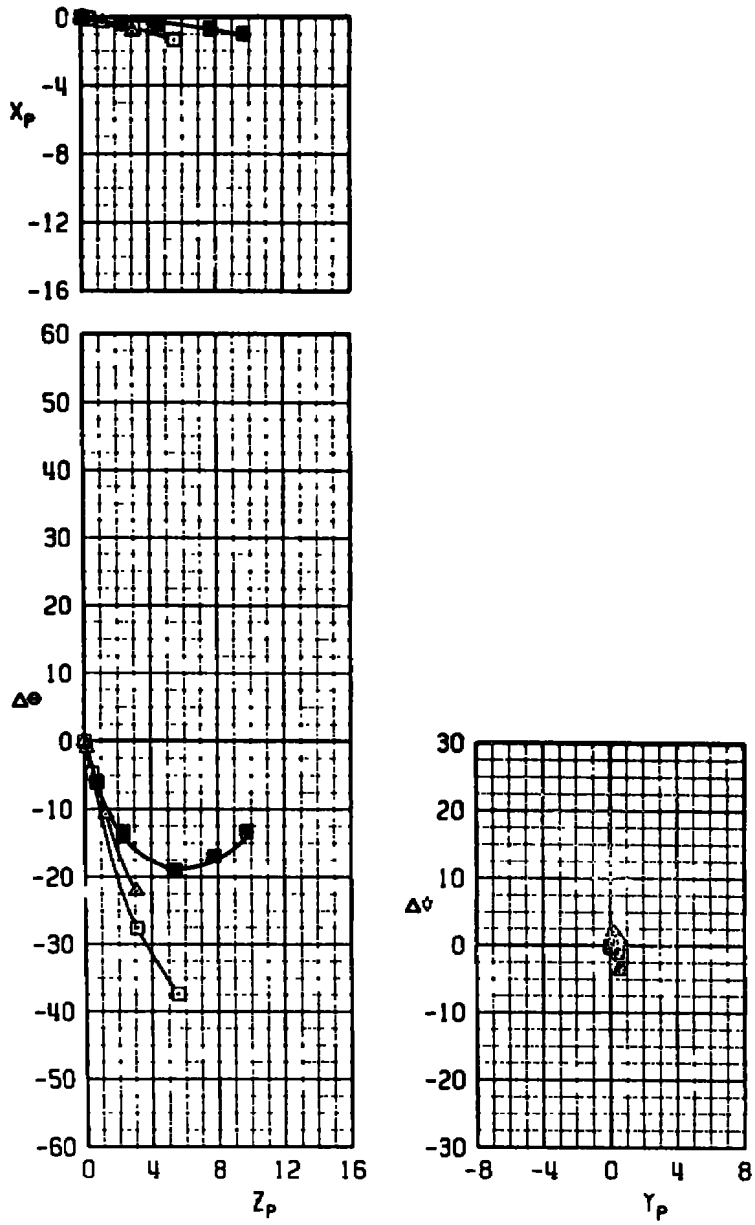

b. Displacement

Figure 36. Concluded.

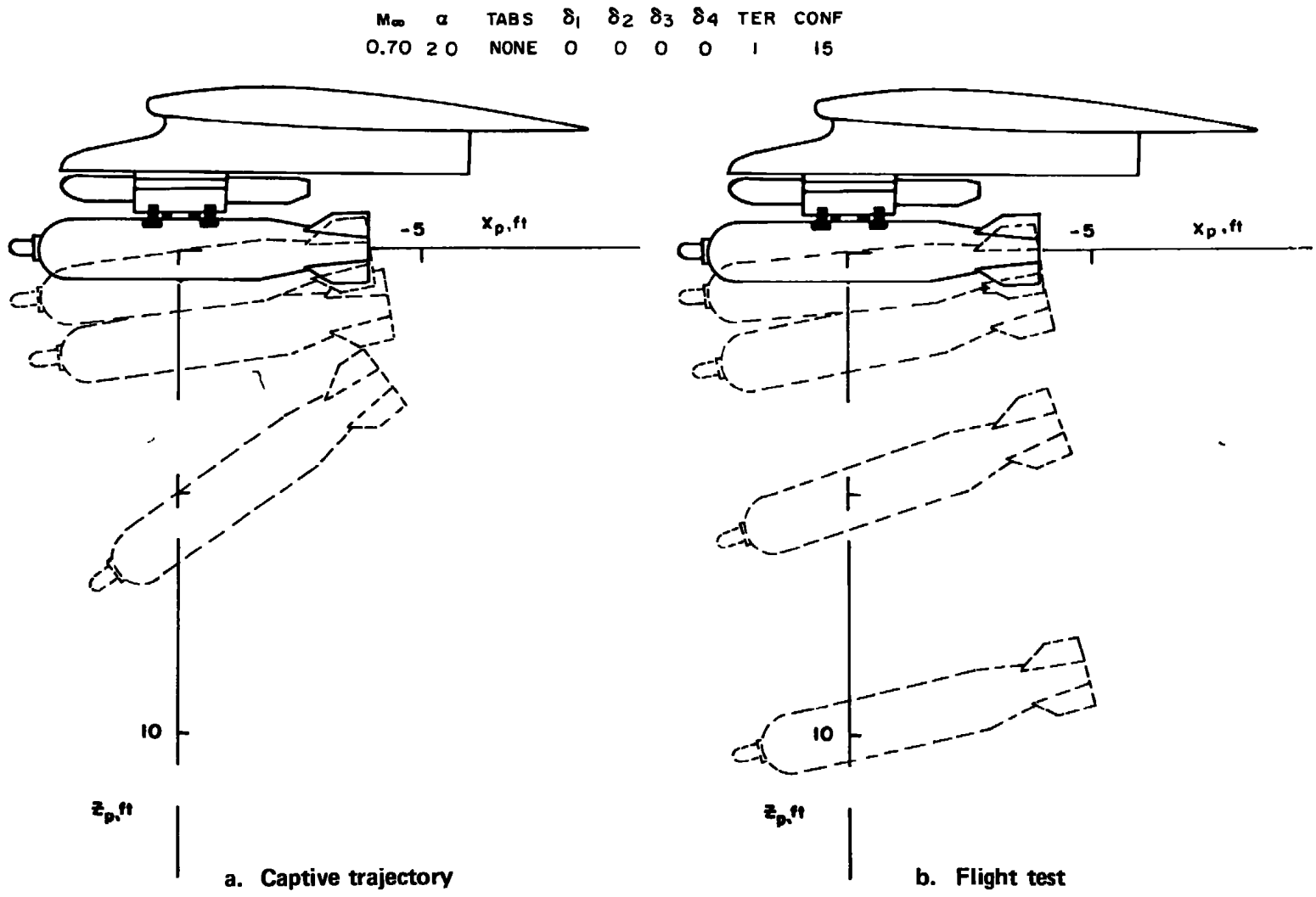

Figure 37. Illustration of wind tunnel captive trajectory and flight test separation trajectories of the MVB with uncanted fins, M_∞ = 0.70.

SYM	M_∞	α	TABS	δ_1	δ_2	δ_3	δ_4	TER	CONF	AIR.	z_0	$\Delta\theta_R$
⊙	0.68	1	NONE	-12	0	0	-12	1	17	F-4	0.03	0
⊡	0.70	1	NONE	-12	0	0	-12	1	17	F-4	0.03	0
△	0.72	1	NONE	-12	0	0	-12	1	17	F-4	0.03	0
■	0.70	1	NONE	-12	0	0	-12	1	17	FLIGHT TEST		

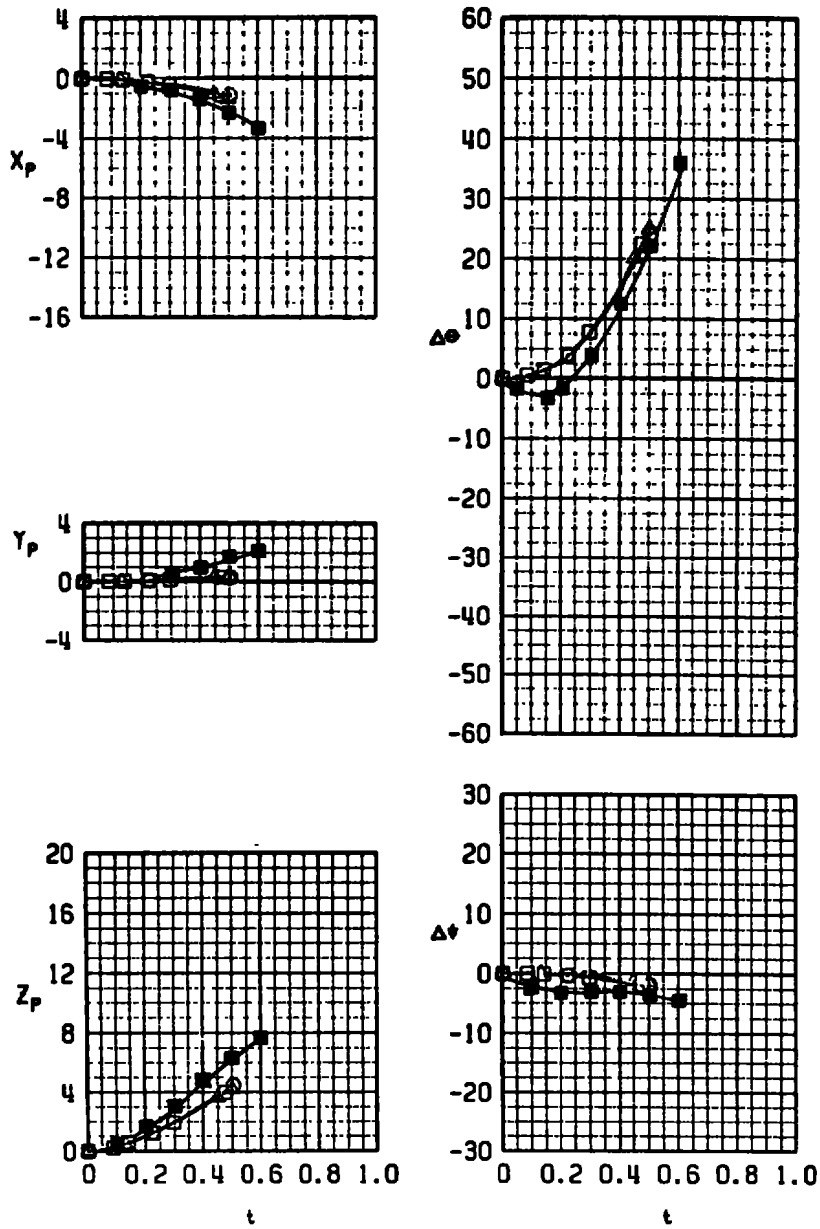

a. Time

Figure 38. Wind tunnel captive trajectory and flight test separation trajectories of the MVB with canted fins, M_∞ = 0.70.

SYM	M_∞	α	TABS	δ_1	δ_2	δ_3	δ_4	TER	CONF	AIR.	z_0	$\Delta\theta_R$
⊙	0.68	1	NONE	-12	0	0	-12	1	17	F-4	0.03	0
⊡	0.70	1	NONE	-12	0	0	-12	1	17	F-4	0.03	0
△	0.72	1	NONE	-12	0	0	-12	1	17	F-4	0.03	0
■	0.70	1	NONE	-12	0	0	-12	1	17	FLIGHT TEST		

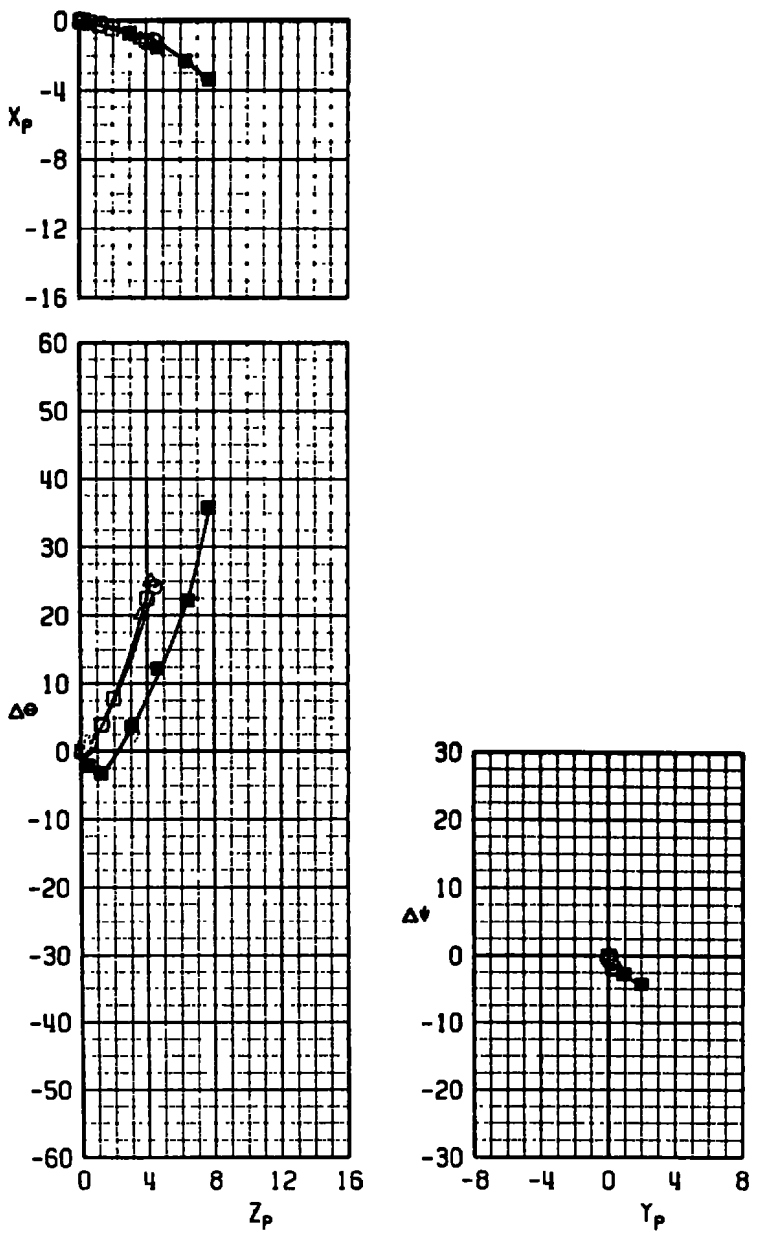

b. Displacement

Figure 38. Concluded.

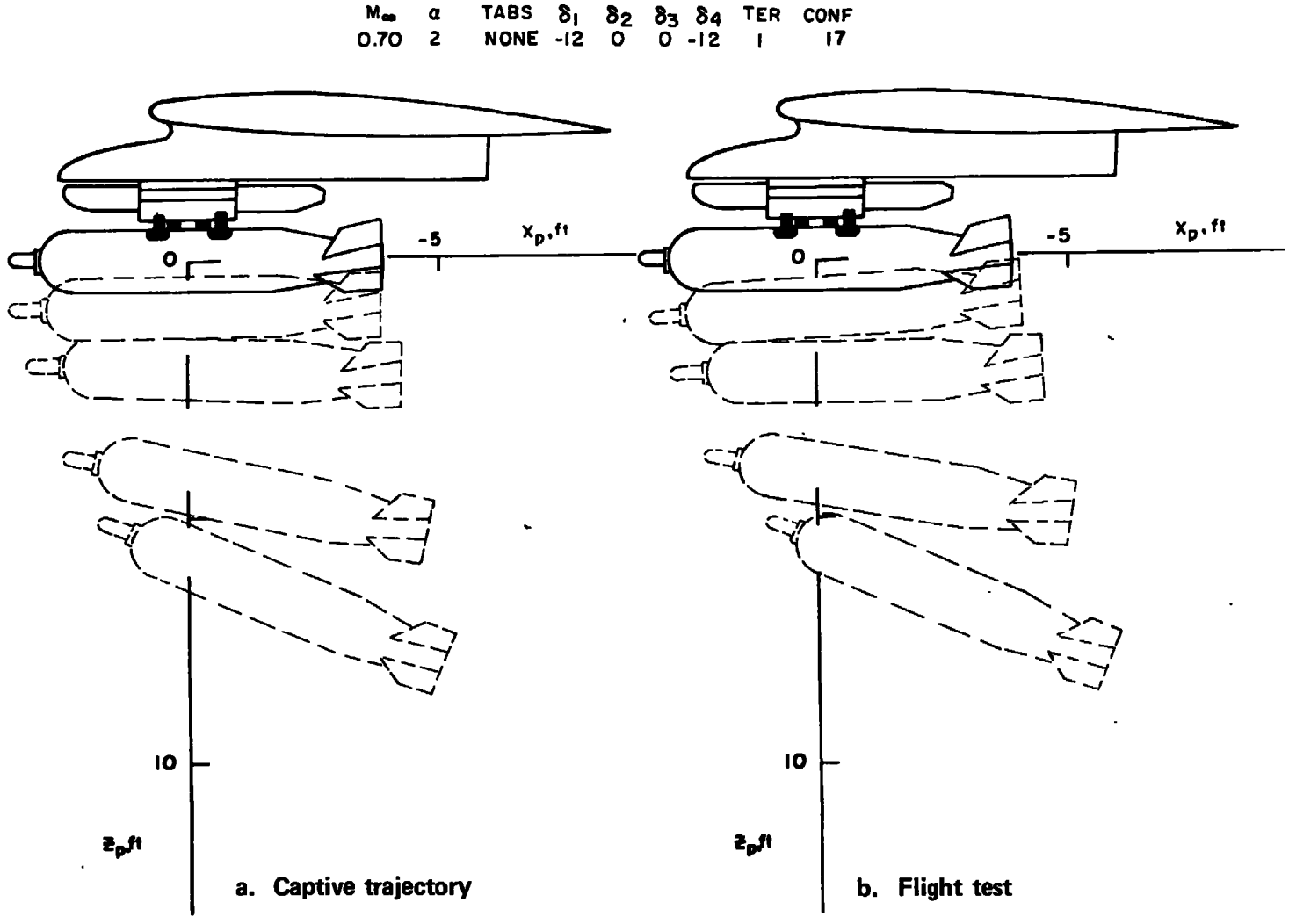

Figure 39. Illustration of wind tunnel captive trajectory and flight test separation trajectories of the MVB with canted fins, $M_\infty = 0.70$.

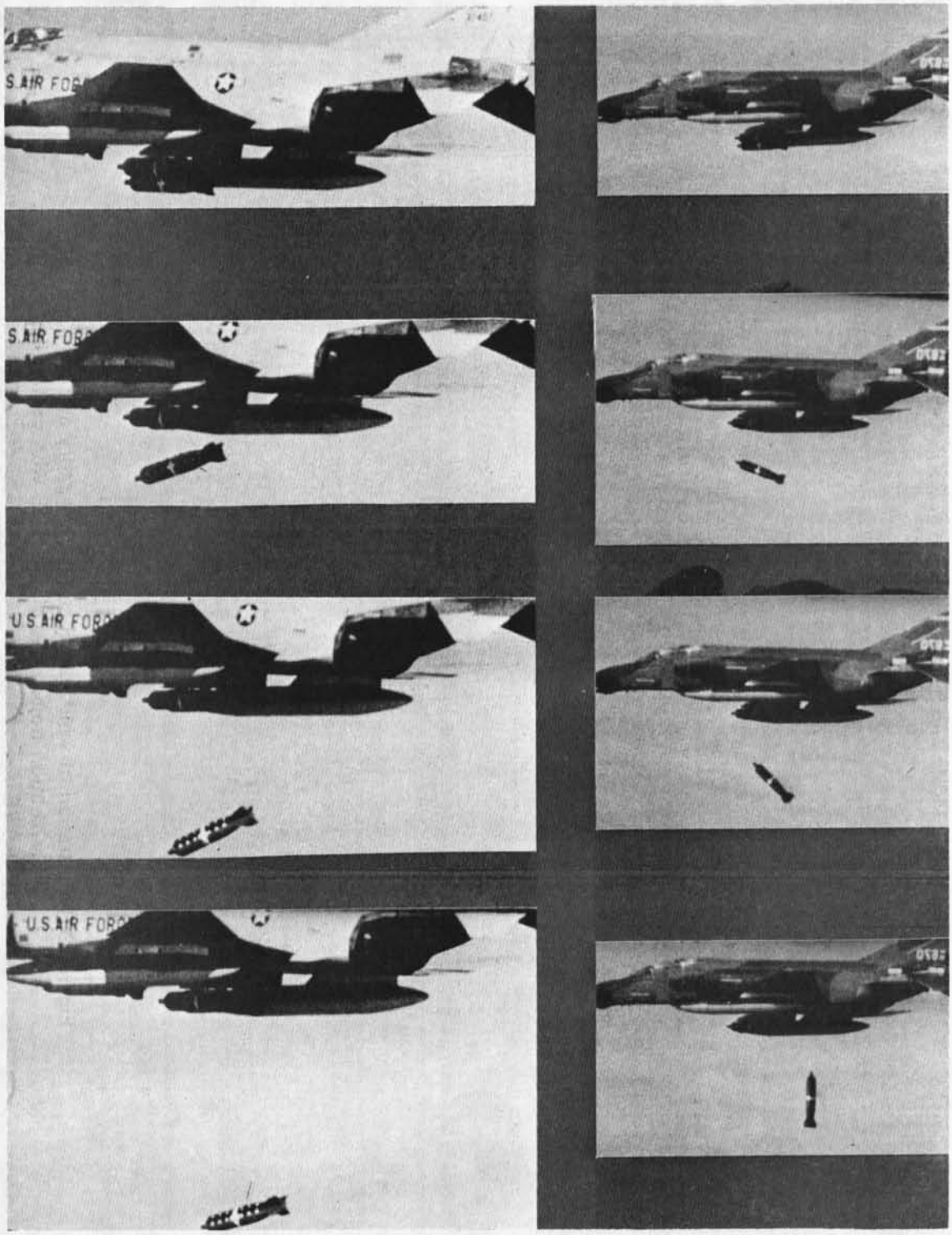

a. Uncanted fins, no tabs

b. Two fins canted, no tabs

Figure 40. Release sequence of the MVB at M_∞ = 0.70.

SYM	M_∞	α	TABS	δ_1	δ_2	δ_3	δ_4	TER CONF	AIR.	z_0	$\Delta\theta_R$
⊙	0.90	0	NONE	0	0	0	0	1	15	F-4	0.35	0
⊡	0.90	0	NONE	0	0	0	0	1	15	F-4	0.03	-40
●	0.90	0	NONE	0	0	0	0	1	15	FLIGHT TEST		

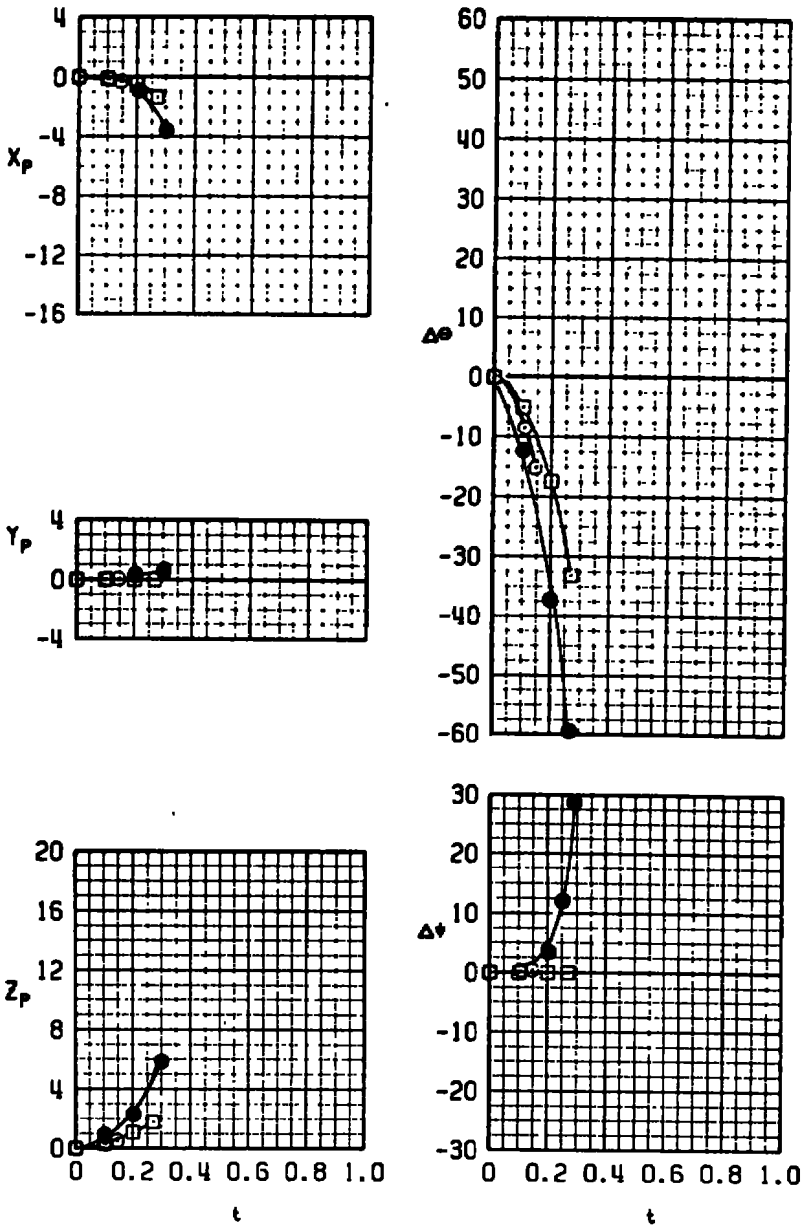

a. Time

Figure 41. Wind tunnel captive trajectory and flight test separation trajectories of the MVB with uncanted fins, M_∞ = 0.90.

SYM	M_∞	α	TABS	δ_1	δ_2	δ_3	δ_4	TER	CONF	AIR.	Z_0	$\Delta\theta_R$
⊙	0.90	0	NONE	0	0	0	0	I	15	F-4	0.35	0
⊡	0.90	0	NONE	0	0	0	0	I	15	F-4	0.03	-40
●	0.90	0	NONE	0	0	0	0	I	15	FLIGHT TEST		

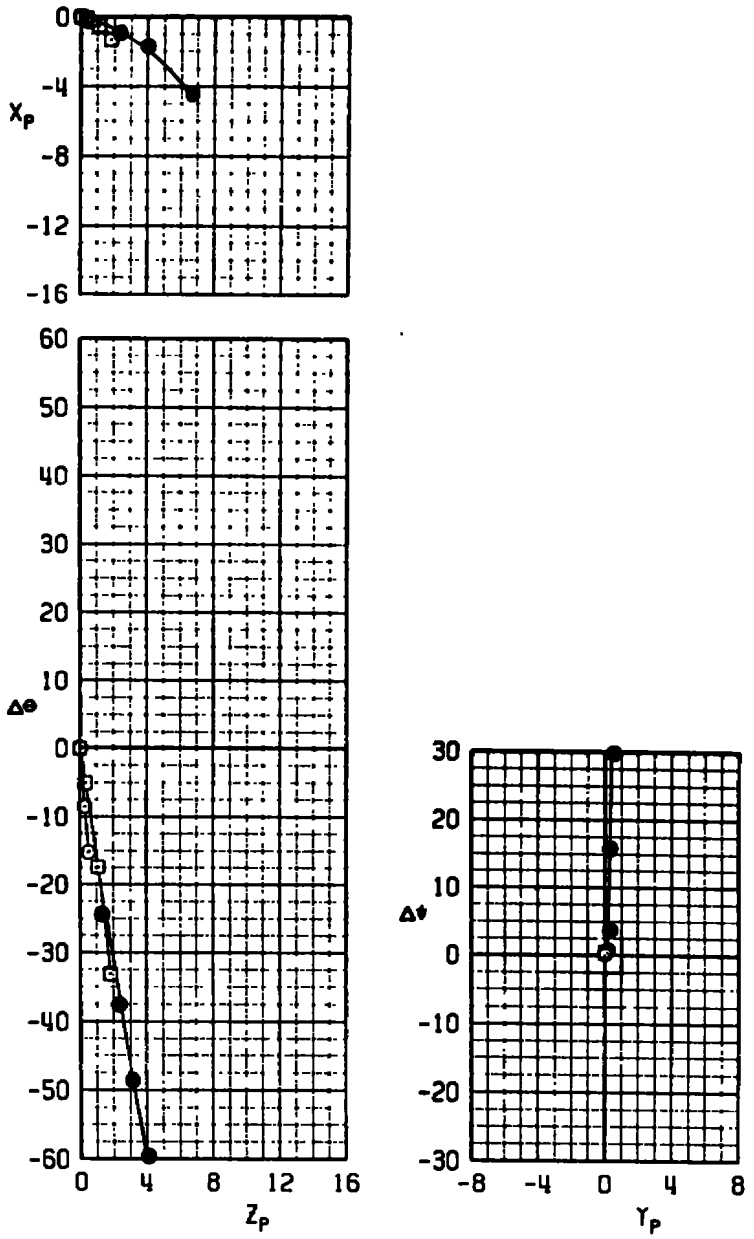

b. Displacement

Figure 41. Concluded.

M_∞	α	TABS	δ_1	δ_2	δ_3	δ_4	TER	CONF
0.90	0	NONE	0	0	0	0	1	15

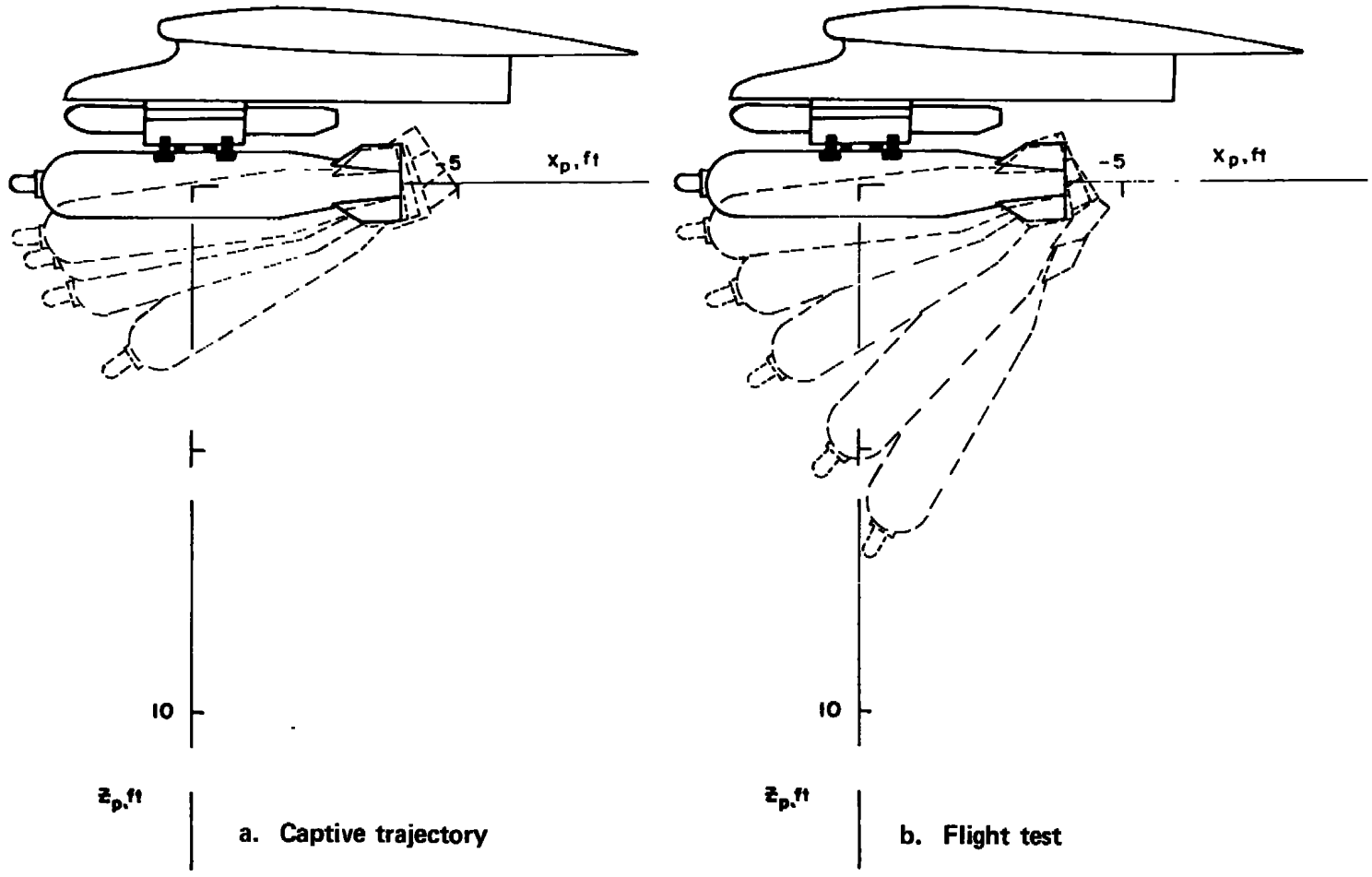

Figure 42. Illustration of wind tunnel captive trajectory and flight test separation trajectories of the MVB with uncanted fins, M_∞ = 0.90.

SYM	M_∞	α	TABS	δ_1	δ_2	δ_3	δ_4	TER	CONF	AIR.	z_0	$\Delta\theta_R$
⊙	0.88	0	NONE	-12	0	0	-12	1	17	F-4	0.35	0
⊡	0.90	0	NONE	-12	0	0	-12	1	17	F-4	0.03	0
■	0.90	0	NONE	-12	0	0	-12	1	17	FLIGHT TEST		
■	0.90	0	NONE	-12	0	0	-12	1	17	FLIGHT TEST		

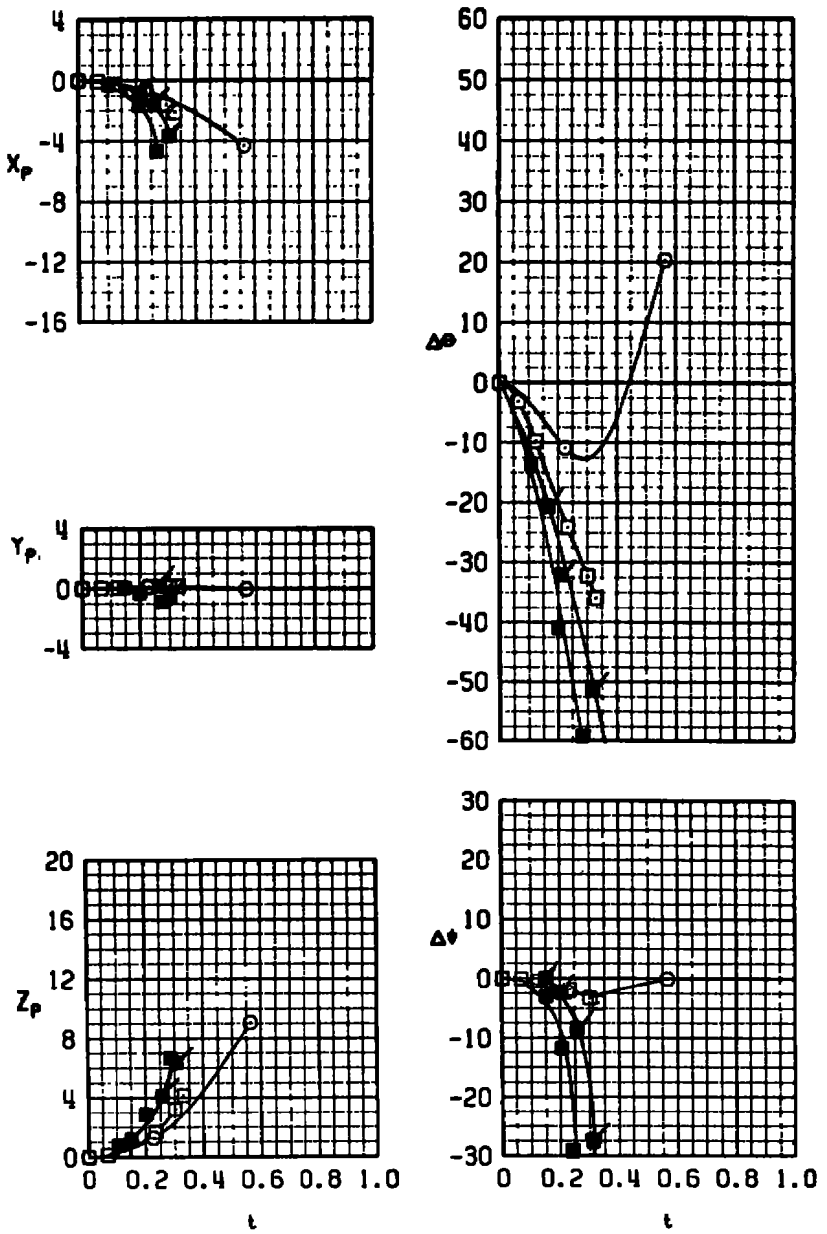

a. Time

Figure 43. Wind tunnel captive trajectory and flight test separation trajectories of the MVB with canted fins, M_∞ = 0.90.

SYM	M_∞	α	TABS	δ_1	δ_2	δ_3	δ_4	TER	CONF	AIR.	z_0	$\Delta\theta_R$
⊙	0.88	0	NONE	-12	0	0	-12	1	17	F-4	0.35	0
⊡	0.90	0	NONE	-12	0	0	-12	1	17	F-4	0.03	0
■	0.90	0	NONE	-12	0	0	-12	1	17	FLIGHT TEST		
◤	0.90	0	NONE	-12	0	0	-12	1	17	FLIGHT TEST		

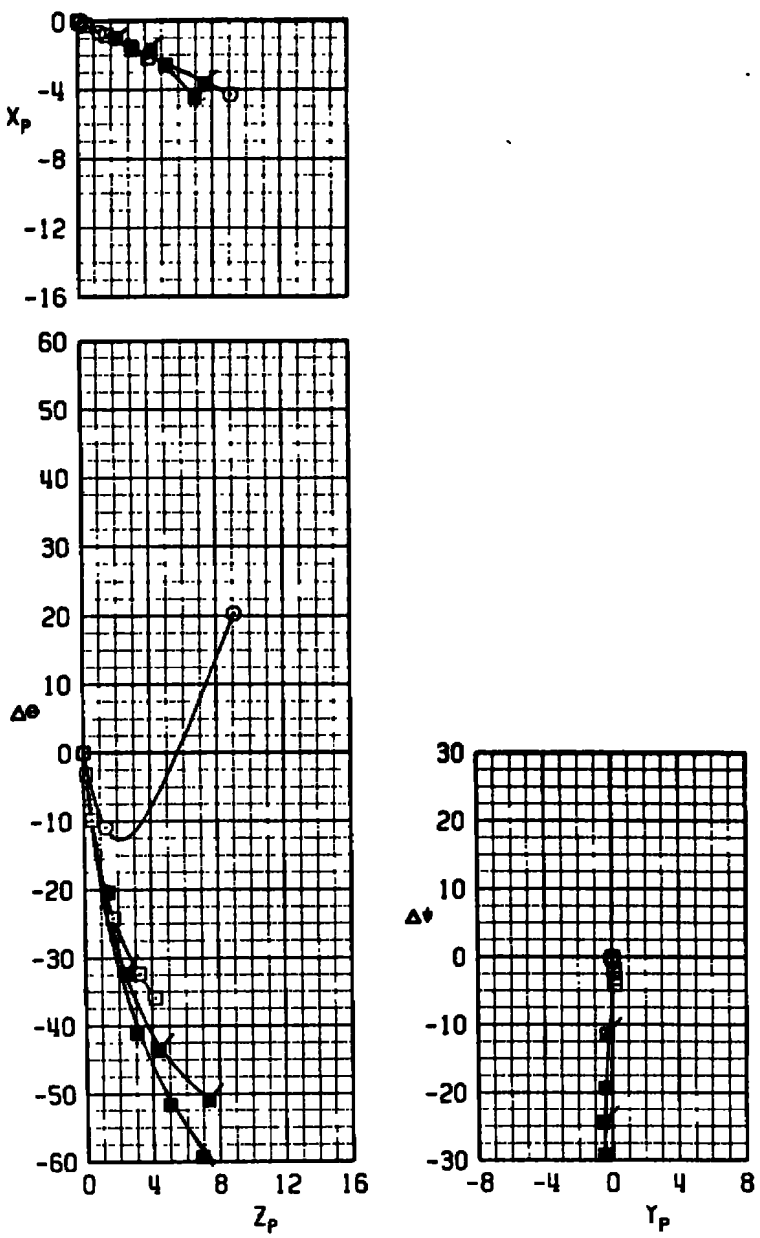

b. Displacement

Figure 43. Concluded.

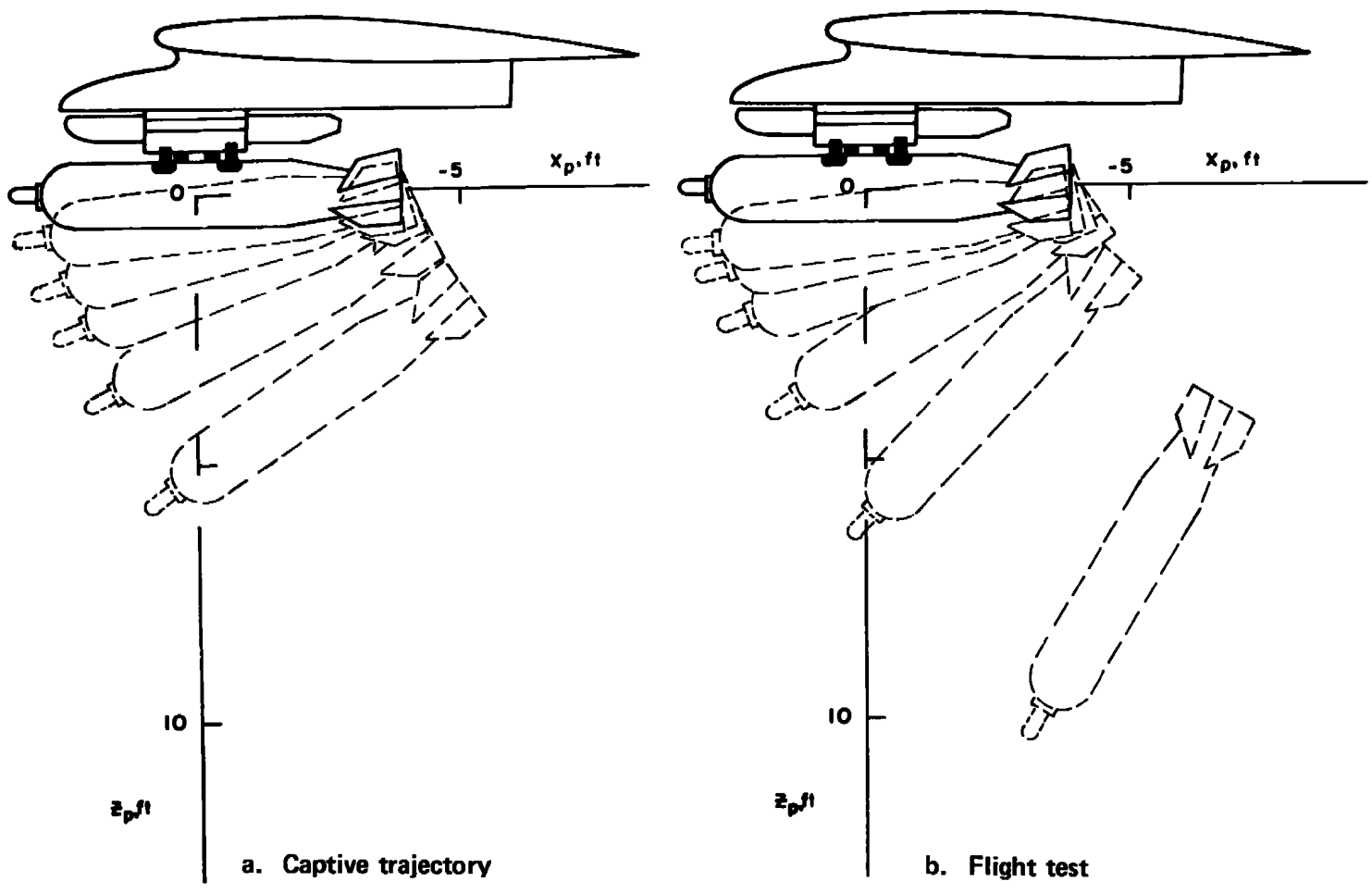

Figure 44. Illustration of wind tunnel captive trajectory and flight test separation trajectories of the MVB with canted fins, M_∞ = 0.90.

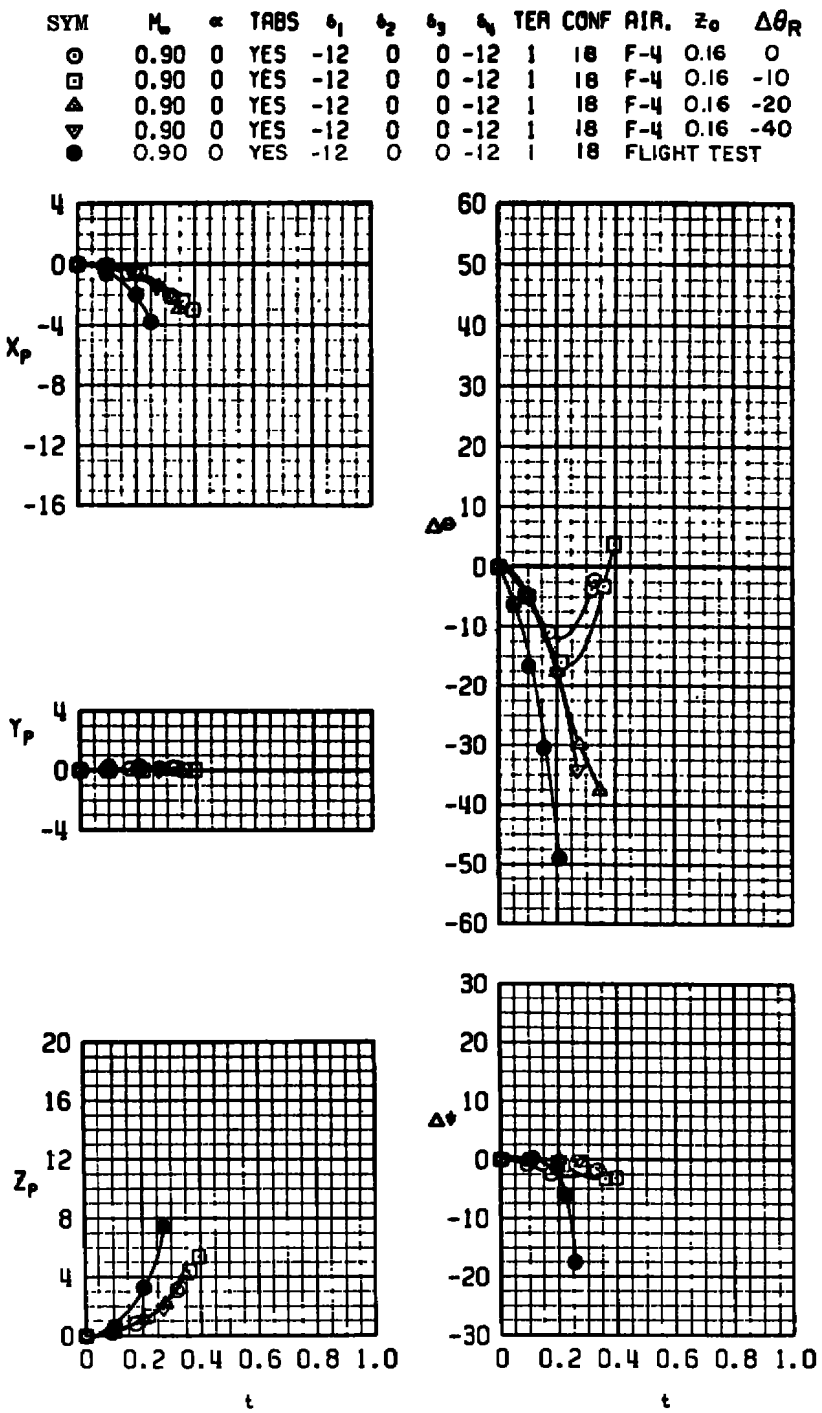

a. Time

Figure 45. Wind tunnel captive trajectory and flight test separation trajectories of the MVB with canted fins and tabs, M_∞ = 0.90.

SYM	M_∞	α	TABS	δ_1	δ_2	δ_3	δ_4	TER	CONF	AIR.	z_0	$\Delta\theta_R$
⊙	0.90	0	YES	-12	0	0	-12	1	18	F-4	0.16	0
⊡	0.90	0	YES	-12	0	0	-12	1	18	F-4	0.16	-10
△	0.90	0	YES	-12	0	0	-12	1	18	F-4	0.16	-20
▽	0.90	0	YES	-12	0	0	-12	1	18	F-4	0.16	-40
●	0.90	0	YES	-12	0	0	-12	1	18	FLIGHT TEST		

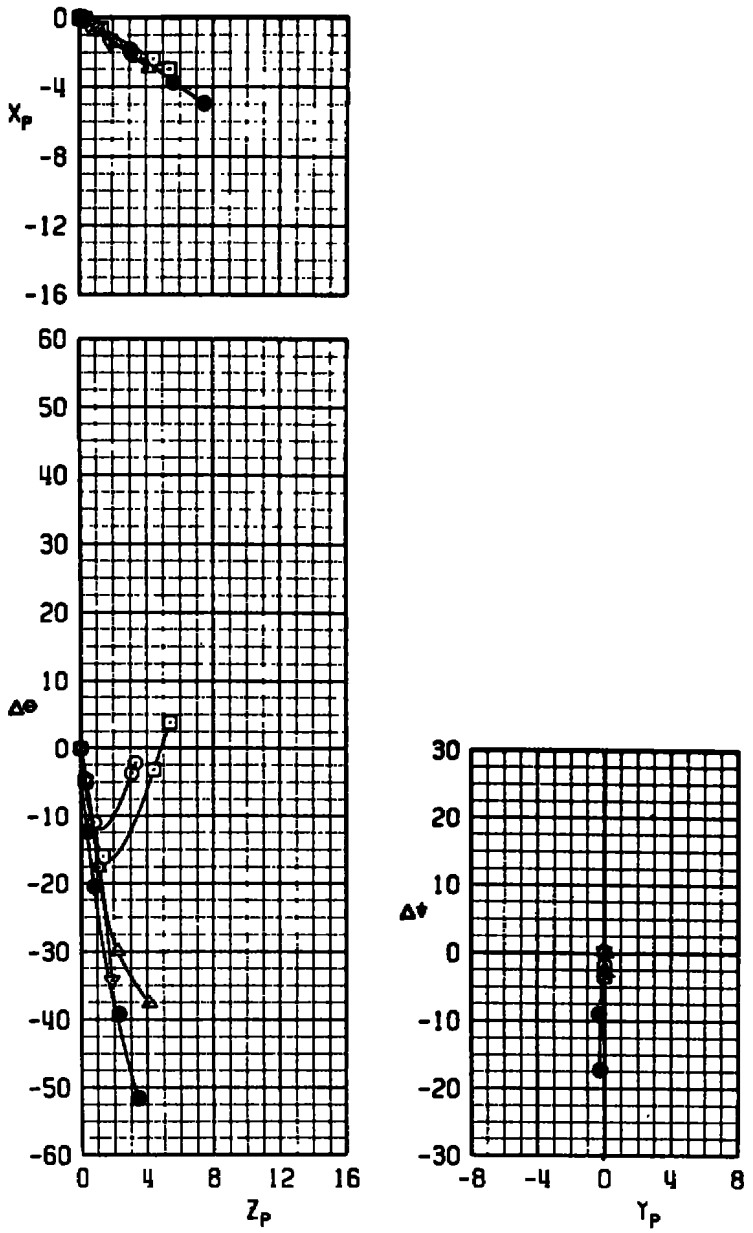

b. Displacement

Figure 45. Concluded.

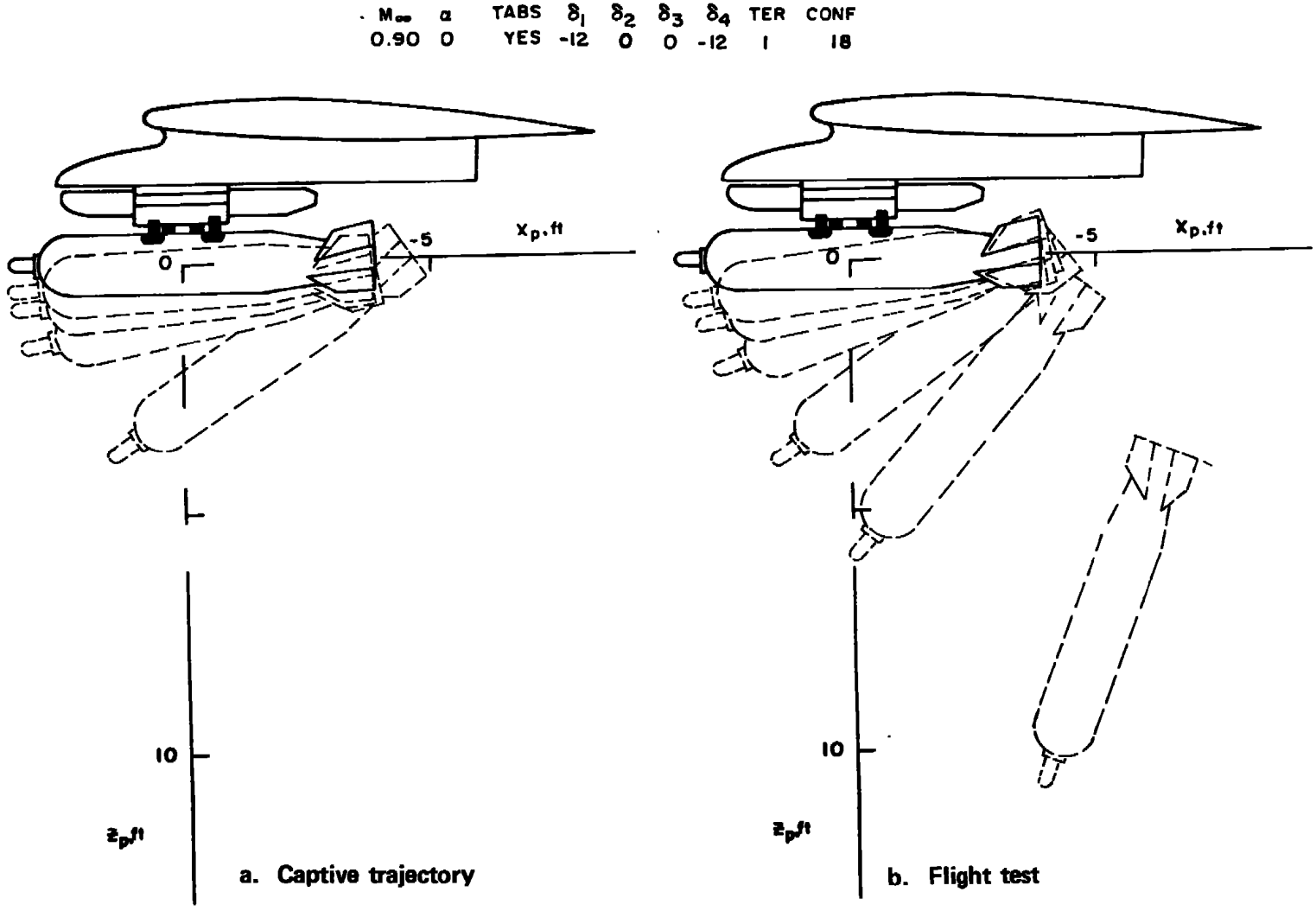

Figure 46. Illustration of wind tunnel captive trajectory and flight test separation trajectories of the MVB with canted fins and tabs, M_∞ = 0.90.

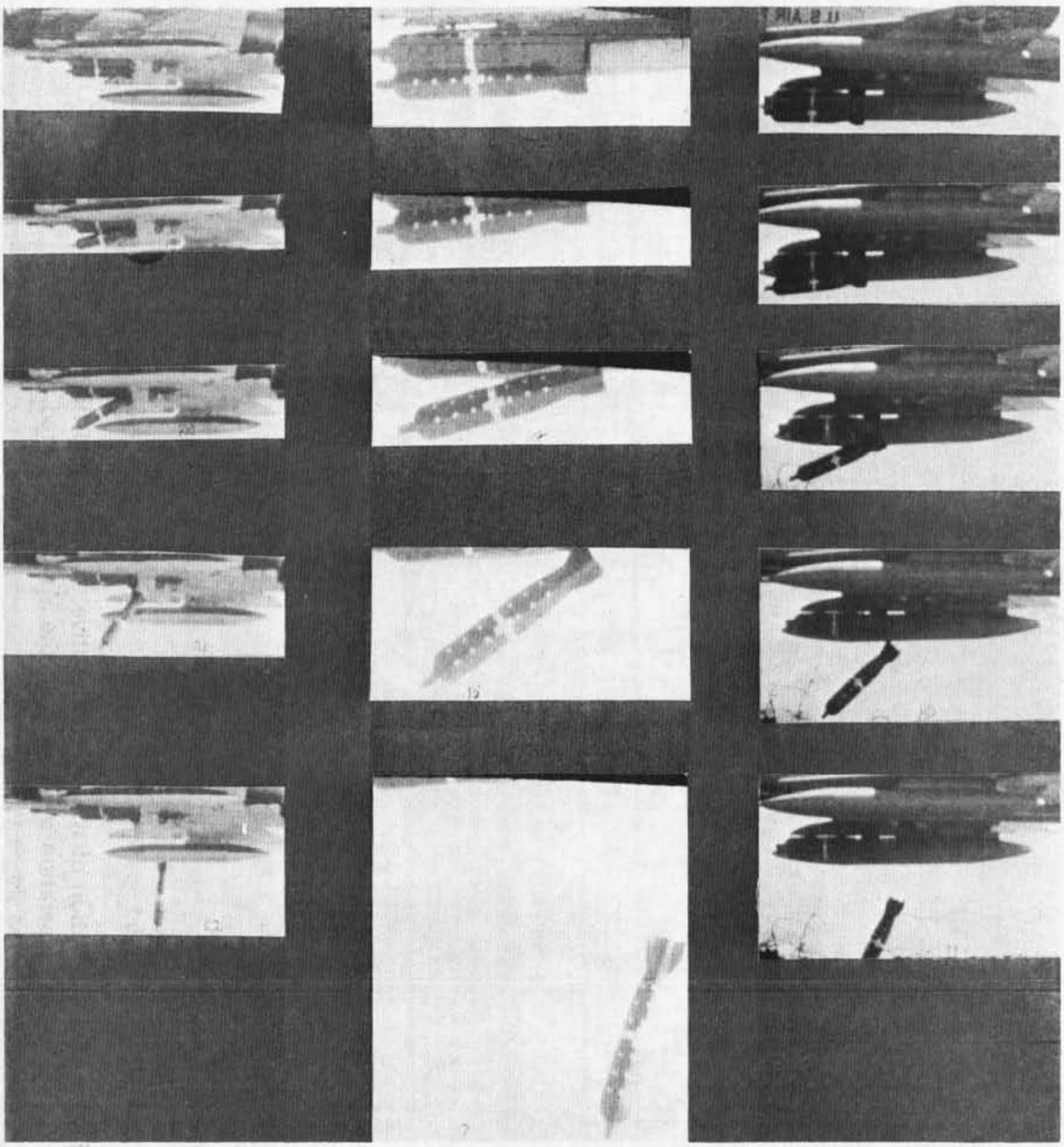

a. Uncanted fins, no tabs b. Two fins canted, no tabs c. Two fins canted, with tabs

Figure 47. Release sequence of the MVB at M_∞ = 0.90.

SYM	M_∞	α	TABS	δ_1	δ_2	δ_3	δ_4	TER	CONF	AIR.	z_0	$\Delta\theta_R$
⊙	1.02	0	NONE	0	0	0	0	1	15	F-4	0.03	-40
⊡	1.02	1	NONE	0	0	0	0	1	15	F-4	0.03	-40
△	1.02	0	NONE	0	0	0	0	1	15	F-4	0.35	0
▲	1.02	0	NONE	0	0	0	0	1	15	FLIGHT TEST		

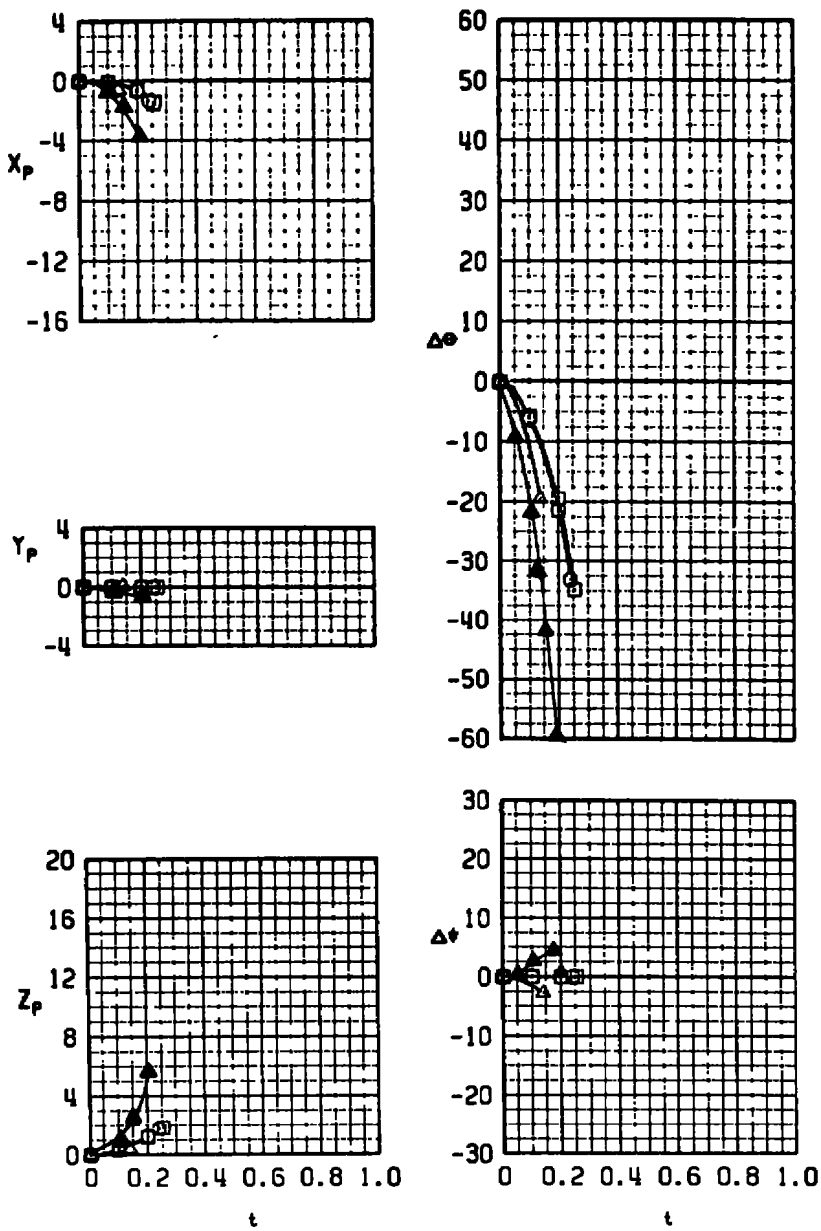

a. Time

Figure 48. Wind tunnel captive trajectory and flight test separation trajectories of the MVB with uncanted fins, No. 1 TER station, M_∞ = 1.02.

SYM	M_∞	α	TABS	δ_1	δ_2	δ_3	δ_4	TER	CONF	AIR.	z_0	$\Delta\theta_R$
⊙	1.02	0	NONE	0	0	0	0	1	15	F-4	0 03	-40
⊡	1.02	1	NONE	0	0	0	0	1	15	F-4	0.03	-40
△	1.02	0	NONE	0	0	0	0	1	15	F-4	0 35	0
▲	1.02	0	NONE	0	0	0	0	1	15	FLIGHT TEST		

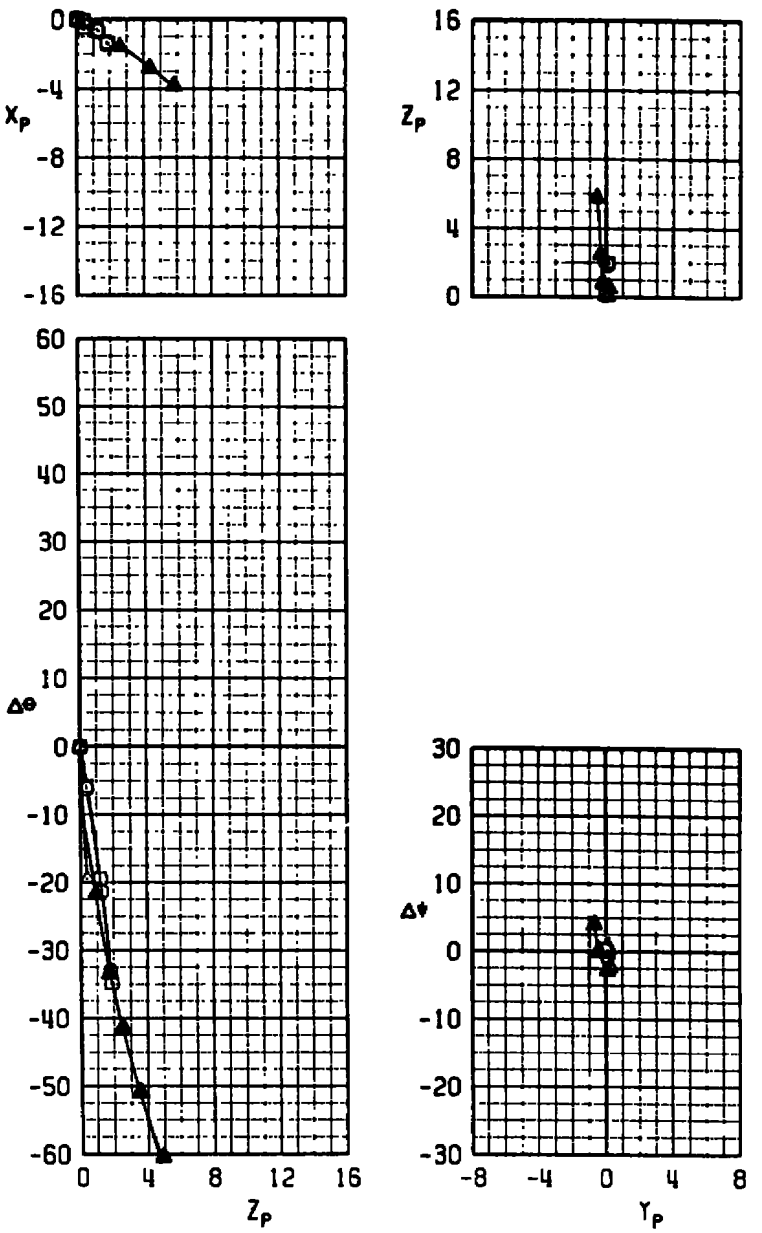

b. Displacement

Figure 48. Concluded.

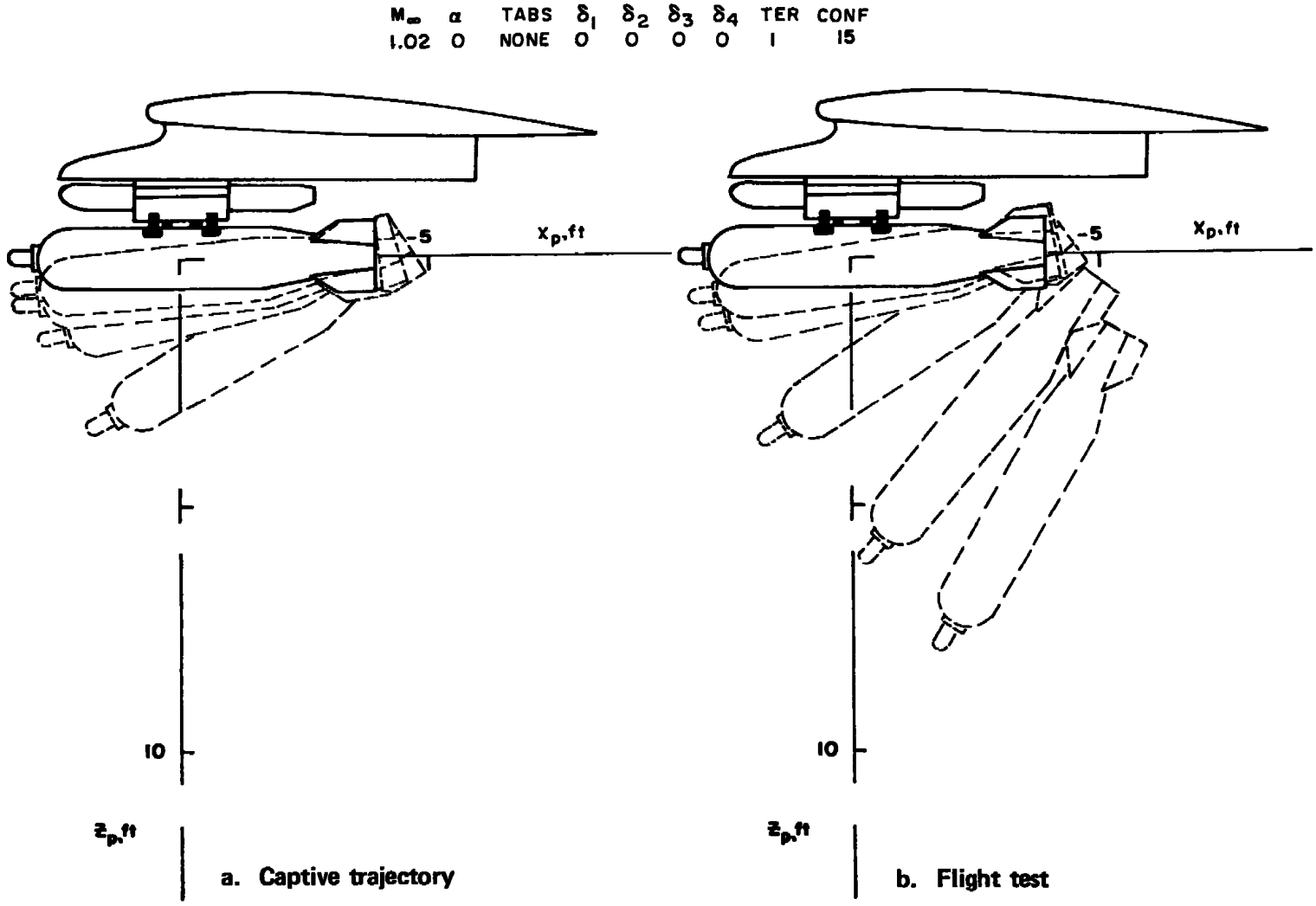

Figure 49. Illustration of wind tunnel captive trajectory and flight test separation trajectories of the MVB with uncanted fins, No. 1 TER station, M_∞ = 1.02.

SYM	M_∞	α	TABS	δ_1	δ_2	δ_3	δ_4	TER	CONF	AIR.	z_0	$\Delta\theta_R$
⊙	1.00	0	NONE	0	0	0	0	2	16	F-4	0.01	0
⊡	1.02	0	NONE	0	0	0	0	2	16	F-4	0.01	0
△	1.04	0	NONE	0	0	0	0	2	16	F-4	0.01	0
■	1.02	0	NONE	0	0	0	0	2	16	FLIGHT TEST		

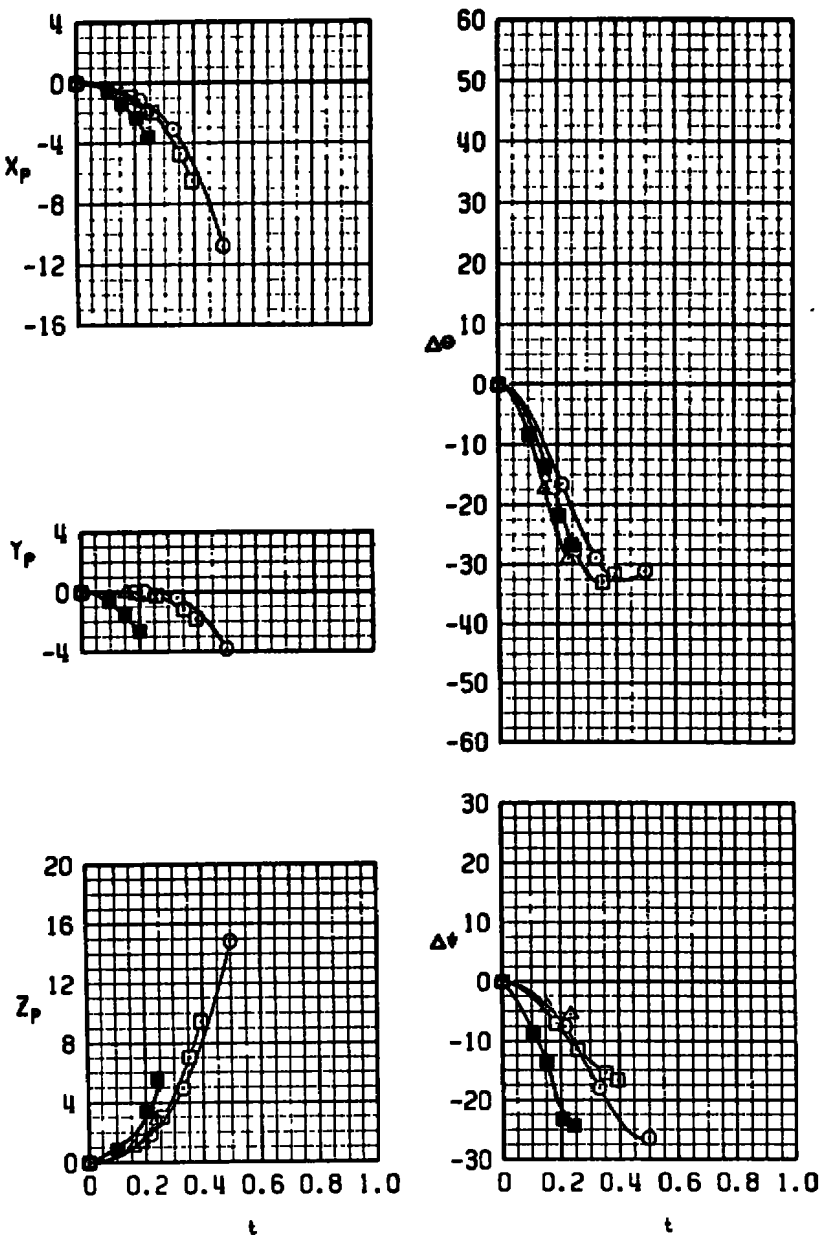

a. Time

Figure 50. Wind tunnel captive trajectory and flight test separation trajectories of the MVB with uncanted fins, No. 2 TER station, M_∞ = 1.02.

SYM	M_∞	α	TABS	δ_1	δ_2	δ_3	δ_4	TER	CONF	AIR.	z_0	$\Delta\theta_R$
⊙	1.00	0	NONE	0	0	0	0	2	16	F-4	0.01	0
⊡	1.02	0	NONE	0	0	0	0	2	16	F-4	0.01	0
△	1.04	0	NONE	0	0	0	0	2	16	F-4	0.01	0
■	1.02	0	NONE	0	0	0	0	2	16	FLIGHT	TEST	

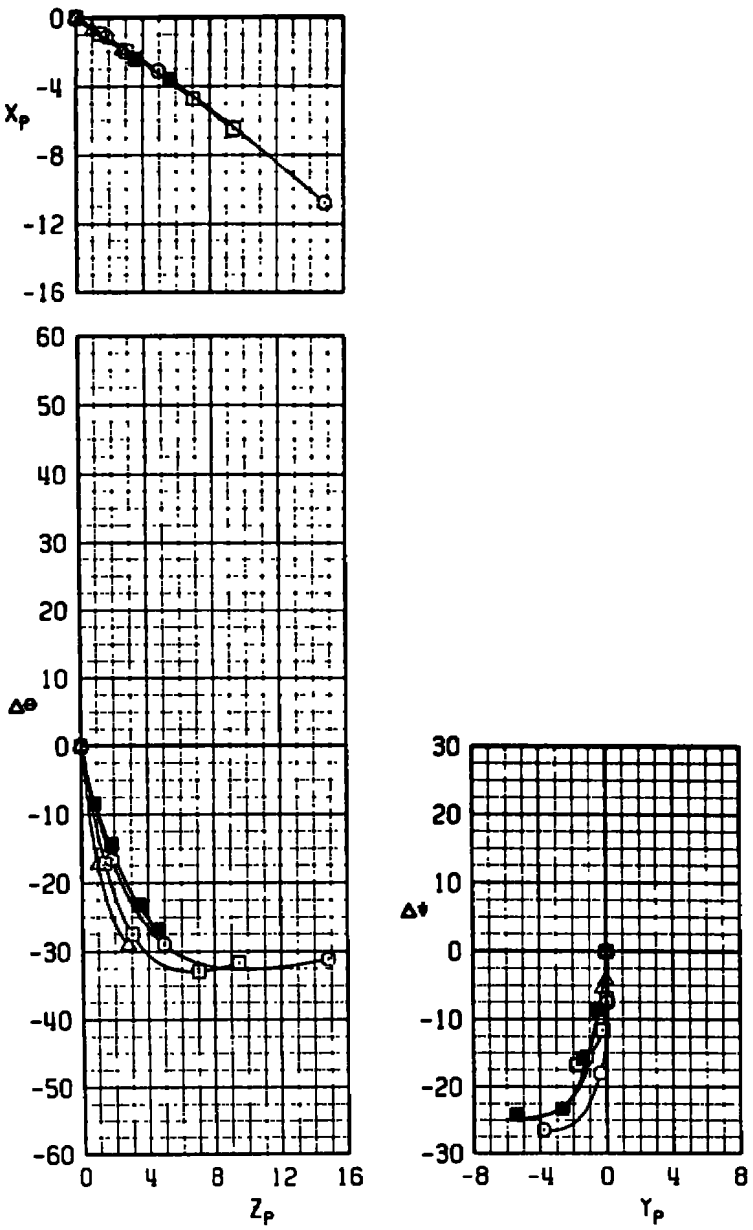

b. Displacement

Figure 50. Concluded.

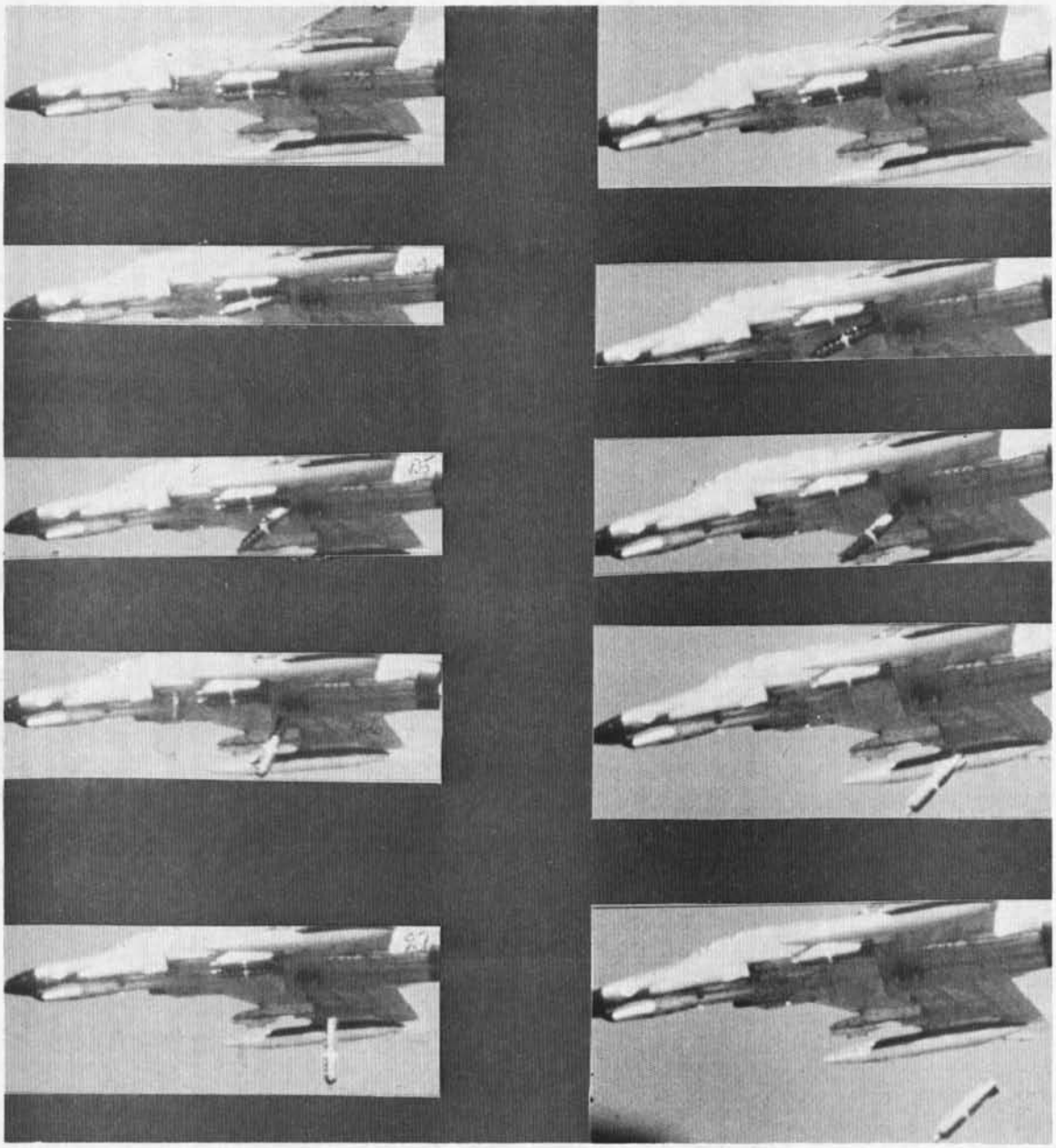

a. TER station No. 1 b. TER station No. 2

Figure 51. Release sequence of the MVB with uncanted fins, no tabs, M_∞ = 1.02.

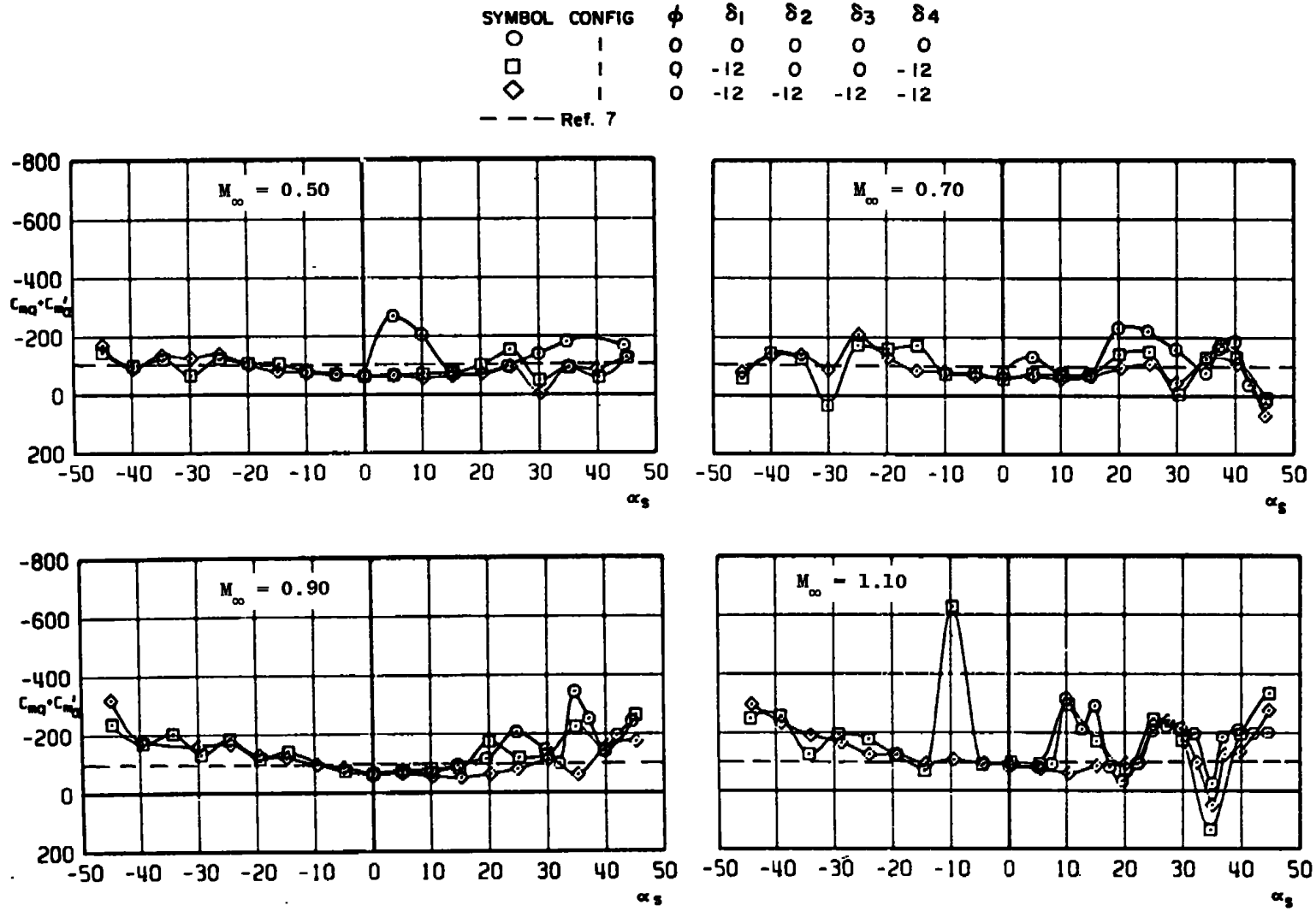

a. No tabs

Figure 52. Effects of angle of attack on the pitch-damping derivative of the MVB.

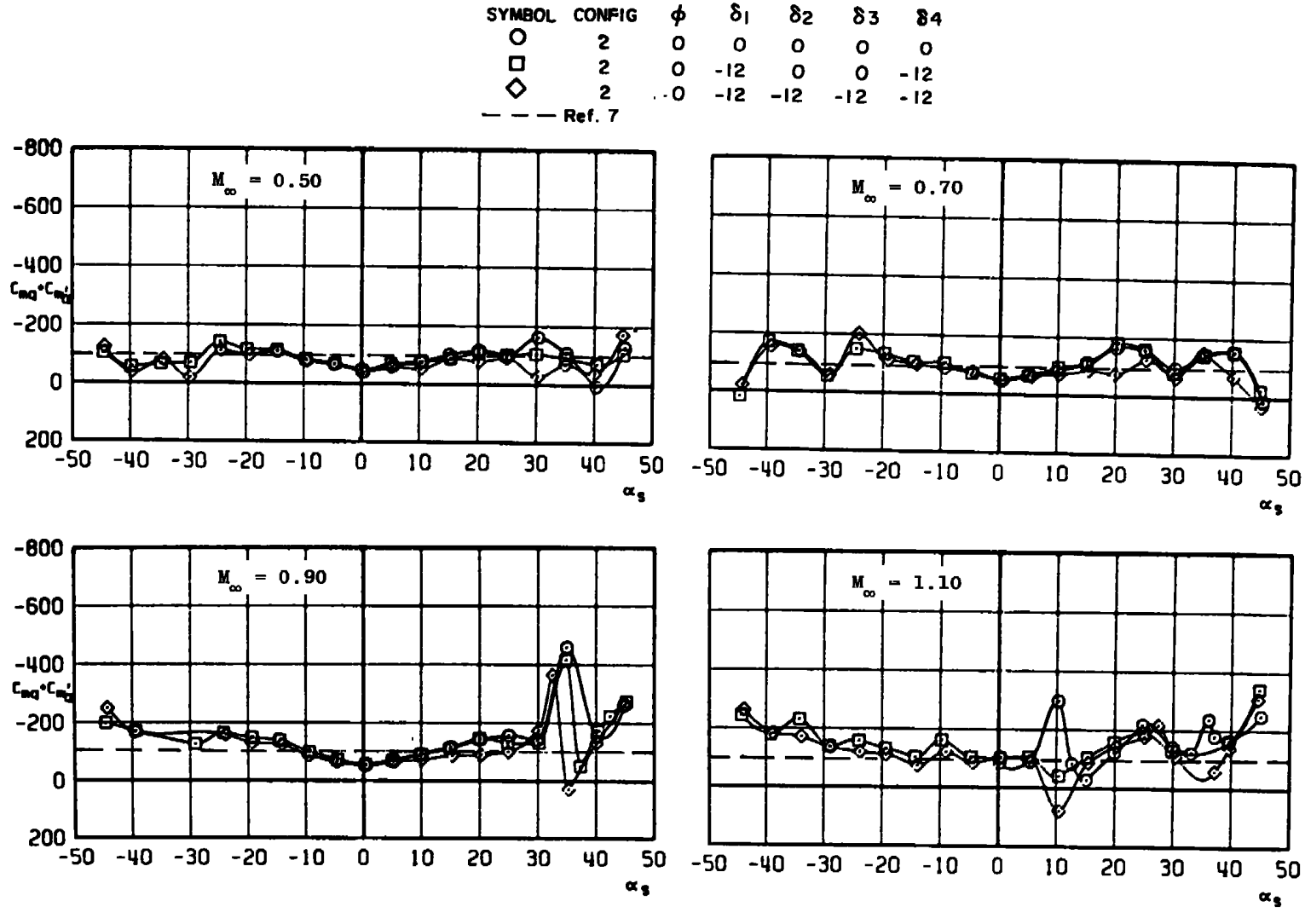

b. With tabs

Figure 52. Concluded.

Table 1. Full-Scale Store Parameters

Parameter Set No.	S	b	$\bar{m}$	I_{yy}/I_{zz}	X_{cg}	C_{m_q}/C_{n_r}	F_{z_1}	F_{z_2}	X_{L_1}	X_{L_2}	Z_E
1	1.396	1.333	24.86	65.0/65.0	3.042	-24.0/-24.0	1,200	—	-0.173	—	0.255
2	↓	↓	↓	↓	3.042	-100/-100	↓	—	↓	—	↓
3	↓	↓	↓	↓	2.708	-24.0/-24.0	↓	—	↓	—	↓
4	↓	↓	↓	↓	2.708	-100/-100	↓	—	↓	—	↓
5	↓	↓	↓	↓	2.708	-100/-100	↓	—	-0.505	—	↓
6	↓	↓	↓	↓	3.042	-24/-24	1,500	1,500	0.833	-0.8333	0.342
7	↓	↓	26.64	77.3/77.3	3.130	-75/-75	1,200	—	-0.083	—	0.255
8	↓	↓	26.57	↓	3.141	-100/-100	↓	—	-0.073	—	↓
9	↓	↓	26.57	↓	3.130	-125/-125	↓	—	-0.083	—	↓
10	↓	↓	26.45	↓	3.135	-125/-125	↓	—	-0.083	—	↓
11	↓	↓	26.45	76.8/76.8	3.115	-125/-125	↓	—	-0.100	—	↓
12	↓	↓	26.01	77.3/77.3	3.069	-100/-100	↓	—	-0.145	—	↓
13	↓	↓	26.636	77.3/77.3	3.052	-125/-125	↓	—	-0.162	—	↓
14	↓	↓	26.356	77.8/77.8	3.083	-125/-125	↓	—	-0.132	—	↓

Table 2. Identification of Captive Trajectory Test Configurations and Test Conditions for F-4C Aircraft

Config No.	Tail Config	M_∞	α, deg	H, ft	Pylon Station	TER Config	Trajectory Condition	Parameter Set No.	Run Identification No.
1	$\delta_1=\delta_2=\delta_3=\delta_4=0$ No Tabs	0.50	4	5,000	8	Sta 1: Metric Sta 2, 3: Dummies	Initiated from Carriage Position	1	3
↓	↓	0.50	8	20,000	↓	↓	↓	↓	4
		0.70	2	5,000					9
		0.70	2	20,000					10
		0.90	0	5,000					11
		0.90	↓	20,000					12
		1.10		5,000					15
		1.10		20,000					14
2	$\delta_1=\delta_2=\delta_3=\delta_4=-3$ No Tabs	0.50	4	5,000					19
↓	↓	0.50	8	20,000					20
		0.70	2	5,000					23
		0.70	2	20,000					24
		0.90	0	5,000					25
		0.90	↓	20,000					26
		1.10		5,000					28
		1.10		20,000					27
3	$\delta_1=\delta_2=\delta_3=\delta_4=-6$ No Tabs	0.50	4	5,000					31
↓	↓	0.50	8	20,000					32
		0.70	2	5,000					33
		0.70	2	20,000					34
		0.90	0	5,000					36
		0.90	↓	20,000					37
		1.10		5,000					39
		1.10		20,000					38
4	$\delta_1=\delta_2=\delta_3=\delta_4=-9$ No Tabs	0.50	4	5,000					43
↓	↓	0.50	8	20,000					44
		0.70	2	5,000					47
		0.70	2	20,000					48
		0.90	0	5,000					49
		0.90	↓	20,000					50
		1.10		5,000					56
		1.10		20,000	↓		↓	↓	57
4A	$\delta_1=\delta_2=\delta_3=\delta_4=0$ No Tabs	0.50	4	5,000	—		Initiated at Lanyard of 1.5 ft	1 (F_{Z_1} - 0)	140
4A	$\delta_1=\delta_2=\delta_3=\delta_4=0$ No Tabs	0.50	8	20,000	—	↓	Initiated at Lanyard of 1.5 ft	1 (F_{Z_1} - 0)	143

Table 2. Continued

Config No.	Tail Config	M_∞	α, deg	H, ft	Pylon Station	TER Config	Trajectory Condition	Parameter Set No.	Run Identification No.
4A	$\delta_1=\delta_2=\delta_3=\delta_4=0$ No Tabs	0.70	2	5,000	—	Sta 1: Metric Sta 2, 3: Dummies	Initiated at Lanyard of 1.5 ft	1 (F_{Z_1} - 0)	145
4A	$\delta_1=\delta_2=\delta_3=\delta_4=0$ No Tabs	0.70	2	20,000	—		Initiated at Lanyard of 1.5 ft	1 (F_{Z_1} - 0)	146
4A	$\delta_1=\delta_2=\delta_3=\delta_4=0$ No Tabs	0.90	0	20,000	—		Initiated at Lanyard of 1.5 ft	1 (F_{Z_1} - 0)	149
5	$\delta_1=\delta_2=\delta_3=\delta_4=-12$ No Tabs	0.50	4	5,000	8		Initiated from Carriage Position	1	61
↓	↓	0.50	8	20,000	↓		↓	↓	62
		0.70	2	5,000					65
		0.70	2	20,000					66
		0.90	0	5,000					67
		0.90	↓	20,000					68
		1.10		5,000					72
		1.10		20,000					69
5A	$\delta_1=\delta_2=\delta_3=\delta_4=0$ No Tabs	0.50	4	5,000	—		Initiated at Lanyard of 1.5 ft	1 (F_{Z_1} - 0)	141
↓	↓	0.50	8	20,000	↓		↓	↓	144
		0.70	2	20,000					147
		0.90	0	5,000					151
		0.90	↓	20,000					153
		1.10		5,000					157
		1.10		20,000					156
6	$\delta_1=\delta_2=\delta_3=\delta_4=-12$ No Tabs	0.90		5,000	8	Sta 1: Empty Sta 2: Metric Sta 3: Dummy	Initiated from Carriage Position		78
6	↓	↓		20,000	8	Sta 1: Empty Sta 2: Metric Sta 3: Dummy	↓		79
7				5,000	2	Sta 1: Empty Sta 2: Empty Sta 3: Metric			81
7	↓			20,000	2	Sta 1: Empty Sta 2: Empty Sta 3: Metric			80
8	4 Fins at 0 Cant No Tabs			5,000	8	Sta 1: Empty Sta 2: Metric Sta 3: Dummy			84
8	4 Fins at 0 Cant No Tabs			20,000	8	Sta 1: Empty Sta 2: Metric Sta 3: Dummy			85
9	4 Fins at 0 Cant No Tabs	↓	↓	5,000	2	Sta 1: Empty Sta 2: Empty Sta 3: Metric	↓	↓	87

Table 2. Continued

Config No.	Tail Config	M_∞	α, deg	H, ft	Pylon Station	TER Config	Trajectory Condition	Parameter Set No.	Run Identification No.
9	4 Fins at 0 Cant No Tabs	0.90	0	20,000	2	Sta 1: Empty Sta 2: Empty Sta 3: Metric	Initiated from Carriage Position	1	86
10	$\delta_1=\delta_4=-12$ $\delta_2=\delta_3=0$ Tabs	0.50	4	5,000	8	Sta 1: Metric Sta 2, 3: Dummies			208
		0.50	8	20,000					209
		0.70	2	5,000					211
		0.70	2	20,000					210
		0.90	0	5,000					213
		0.90		20,000					214
		1.10		5,000					220
		1.10		20,000					218
11	$\delta_1=\delta_4=-6$ $\delta_2=\delta_3=0$ Tabs	0.50	4	5,000					195
		0.50	8	20,000					196
		0.70	2	5,000					198
		0.70	2	20,000					197
		0.90	0	5,000					200
		0.90		20,000					202
		1.10		5,000					205
		1.10		20,000					204
12	$\delta_1=\delta_4=-9$ $\delta_2=\delta_3=0$ Tabs	0.50	4	5,000					54
		0.50	8	20,000					55
		0.70	2	5,000					57
		0.70	2	20,000					56
		0.90	0	5,000					71
		0.90		20,000					60
		1.10		5,000					72
		1.10		20,000					73
13	$\delta_1=\delta_4=-9$ $\delta_2=\delta_3=0$ No Tabs	0.50	4	5,00					165
		0.50	8	20,000					168
		0.70	2	5,000					173
		0.70	2	20,000					171
		0.90	0	5,000					181
		0.90	0	20,000					185
		1.10	0	5,000					192

Table 2. Continued

Config No.	Tail Config	M_∞	α, deg	H, ft	Pylon Station	TER Config	Trajectory Condition	Parameter Set No.	Run Identification No.
13	$\delta_1=\delta_4=-9$ $\delta_2=\delta_3=0$ No Tabs	1.10	0	20,000	S	Sta 1: Metric Sta 2, 3: Dummies	Initiated from Carriage Position	1	188
14	↓	0.90	↓	5,000	↓	↓	↓	5	143
↓	↓	↓	↓	20,000	↓	↓	↓	1	146
↓	↓	↓	↓	20,000	↓	↓	↓	2	147
↓	↓	↓	↓	20,000	↓	↓	↓	5	148
↓	↓	1.10	↓	5,000	↓	↓	↓	1	151
↓	↓	↓	↓	↓	↓	↓	↓	2	160
↓	↓	↓	↓	↓	↓	↓	↓	3	153
↓	↓	↓	↓	↓	↓	↓	↓	4	161
↓	↓	0.50	8	20,000	↓	↓	↓	4	127
↓	↓	0.50	8	20,000	↓	↓	↓	5	128
↓	↓	0.70	2	5,000	↓	↓	↓	1	132
↓	↓	0.70	2	20,000	↓	↓	↓	2	131
↓	↓	0.90	0	5,000	↓	↓	↓	1	134
↓	↓	↓	↓	↓	↓	↓	↓	2	135
↓	↓	↓	↓	↓	↓	↓	↓	3	138
↓	↓	↓	↓	↓	↓	↓	↓	4	141
↓	$\delta_1=\delta_4=-12$ Tabs	0.50	4	↓	↓	↓	↓	1	119
↓	↓	↓	↓	↓	↓	↓	↓	2	120
↓	↓	↓	↓	↓	↓	↓	↓	3	121
↓	↓	↓	↓	↓	↓	↓	↓	4	122
↓	↓	↓	↓	↓	↓	↓	↓	5	123
↓	↓	↓	8	20,000	↓	↓	↓	1	124
↓	↓	↓	8	20,000	↓	↓	↓	2	125
↓	↓	↓	8	20,000	↓	↓	↓	3	126
14A	$\delta_1=\delta_2=\delta_3=\delta_4=0$ Tabs	↓	4	5,000	↓	Sta 1: Metric Sta 2, 3: $\delta_1=\delta_2=\delta_3=\delta_4=-9$ Tabs	Initiated at Lanyard of 1.5 ft	1	234
↓	↓	↓	4	5,000	↓	↓	↓	2	233
↓	↓	↓	8	20,000	↓	↓	↓	1	231
↓	↓	↓	8	20,000	↓	↓	↓	2	230
↓	↓	0.70	2	5,000	↓	↓	↓	1	228
↓	↓	0.70	2	20,000	↓	↓	↓	1	229
↓	↓	0.90	0	5,000	↓	↓	↓	1	226
↓	↓	0.90	0	5,000	↓	↓	↓	2	225
↓	↓	0.90	0	20,000	↓	↓	↓	1	224

Table 2. Continued

Config No.	Tail Config	M_∞	α, deg	H, ft	Pylon Station	TER Config	Trajectory Condition	Parameter Set No.	Run Identification No.
14A	$\delta_1=\delta_2=\delta_3=\delta_4=0$ Tabs	0.90	0	20,000	8	Sta 1: Metric Sta 2, 3: $\delta_1=\delta_2=\delta_3=\delta_4=-9$ Tabs	Initiated at Lanyard of 1.5 ft	2	223
↓	↓	1.10	↓	5,000	↓	↓	↓	1	222
		↓		20,000				1	221
				5,000				5	155
				20,000				1	154
				20,000				2	158
				20,000				5	156
15	$\delta_1=\delta_2=\delta_3=\delta_4=0$ No Tabs	0.48	4.0	5,000		Sta 1: Metric Sta 2, 3: Dummies	Initiated from Carriage Position ($\Delta\theta_R$ = 0°)	7	7
↓	↓	0.48	3.0	↓	↓	↓	↓	↓	69
		0.50	4.0						9
		0.50	4.0						14
		0.70	1.0					8	64
		0.72	2.0					8	30
		0.72	1.0					8	31
		0.90	1.0				↓	9	32
	$\delta_1=\delta_2=\delta_3=\delta_4=0$ No Tabs	0.90	1.0				Initiated from Carriage Position ($\Delta\theta_R$ = -40)	↓	44
	↓	↓	0				Initiated from Carriage Position ($\Delta\theta_R$ = -40)		36
			0				Initiated from Carriage Position ($\Delta\theta_R$ = 0)		38
			-1.0				Initiated from Carriage Position ($\Delta\theta_R$ = 0)		39
		↓	-1.0	↓			Initiated from Carriage Position ($\Delta\theta_R$ = -40)	↓	40
		1.02	-1.0	4,500			↓	10	46
		↓	0	4,500				↓	45
			0	5,000					47
			1.0	5,000					50
↓	↓	↓	0	5,000	↓	↓	Initiated from Carriage Position ($\Delta\theta_R$ = 0)	↓	53

Table 2. Concluded

Config No.	Tail Config	M_∞	α, deg	H, ft	Pylon Station	TER Config	Trajectory Condition	Parameter Set No.	Run Identification No.
15	$\delta_1=\delta_2=\delta_3=\delta_4=0$ No Tabs	1.02	-1.0	5,000	8	Sta 1: Metric Sta 2, 3: Dummies	Initiated from Carriage Position ($\Delta\theta_R$ = 0)	10	54
16	↓	↓	1.0	↓	↓	Sta 1: Empty Sta 2: Metric Sta 3: Dummy	↓	11	71/74
↓	↓	↓	0	↓	↓	↓	↓	↓	72
↓	↓	↓	-1.0	↓	↓	↓	↓	↓	73
↓	↓	1.04	0	↓	↓	↓	↓	↓	75
↓	↓	1.00	0	↓	↓	↓	↓	↓	76
17	$\delta_1=\delta_4=-12$ $\delta_2=\delta_3=0$ No Tabs	0.68	1.0	↓	↓	Sta 1: Metric Sta 2, 3: Dummies	↓	12	79
↓	↓	0.70	1.0	↓	↓	↓	↓	12	80/99
↓	↓	0.72	1.0	↓	↓	↓	↓	12	81
↓	↓	0.80	0	↓	↓	↓	↓	13	82
↓	↓	0.80	0	↓	↓	↓	↓	↓	83
↓	↓	0.90	1.0	↓	↓	↓	($\Delta\theta_R$ = -40)	↓	84
↓	↓	↓	1.0	↓	↓	↓	($\Delta\theta_R$ = 0)	↓	85
↓	↓	↓	0	↓	↓	↓	($\Delta\theta_R$ = 0)	↓	93
18	$\delta_1=\delta_4=-12$ $\delta_2=\delta_3=0$ Tabs	↓	1.0	↓	↓	↓	Initiated from Carriage Position ($\Delta\theta_R$ = 0)	14	105/106
↓	↓	↓	-1.0	↓	↓	↓	Initiated from Carriage Position ($\Delta\theta_R$ = 0)	↓	107/110
↓	↓	↓	0	↓	↓	↓	Initiated from Carriage Position ($\Delta\theta_R$ = 0)	↓	121
↓	↓	↓	↓	↓	↓	↓	($\Delta\theta_R$ = -10)	↓	111
↓	↓	↓	↓	↓	↓	↓	($\Delta\theta_R$ = -20)	↓	115
↓	↓	↓	↓	↓	↓	↓	($\Delta\theta_R$ = -40)	↓	122

Table 3. Identification of Captive Trajectory Test Configurations with Test Conditions for A-7D Aircraft

Config No.	Tail Config	M_∞	α, deg	H, ft	Pylon Station	Pylon Config	Trajectory Condition	Parameter Set No.	Run Identification No.
19	$\delta_1=\delta_4=-12$ $\delta_2=\delta_3=0$ No Tabs	0.50	6	5,000	8	Sta 8: Metric Sta 6, 7: Dummies	Initiated from Carriage Position	6	78
19	$\delta_1=\delta_4=-12$ $\delta_2=\delta_3=0$ No Tabs	0.70	4						79
19	$\delta_1=\delta_4=-12$ $\delta_2=\delta_3=0$ No Tabs	0.90	2						84
20	$\delta_1=\delta_4=-12$ $\delta_2=\delta_3=0$ Tabs	0.50	6						5
20	$\delta_1=\delta_4=-12$ $\delta_2=\delta_3=0$ Tabs	0.70	4						9
20	$\delta_1=\delta_4=-12$ $\delta_2=\delta_3=0$ Tabs	0.90	2						12
21	$\delta_1=\delta_4=-12$ $\delta_2=\delta_3=0$ No Tabs	0.50	6		7	Sta 7: Metric Sta 6: Dummy Sta 8: Empty			90
21	$\delta_1=\delta_4=-12$ $\delta_2=\delta_3=0$ No Tabs	0.70	4						91
21	$\delta_1=\delta_4=-12$ $\delta_2=\delta_3=0$ No Tabs	0.90	2						107
22	$\delta_1=\delta_4=-12$ $\delta_2=\delta_3=0$ Tabs	0.50	6						18
22	$\delta_1=\delta_4=-12$ $\delta_2=\delta_3=0$ Tabs	0.70	4	5,000					19
22	$\delta_1=\delta_4=-12$ $\delta_2=\delta_3=0$ Tabs	0.90	2						24
23	$\delta_1=\delta_4=-12$ $\delta_2=\delta_3=0$ No Tabs	0.50	6		6	Sta 6: Metric Sta 7, 8: Empty			65
23	$\delta_1=\delta_4=-12$ $\delta_2=\delta_3=0$ No Tabs	0.70	4						66
23	$\delta_1=\delta_4=-12$ $\delta_2=\delta_3=0$ No Tabs	0.90	2						73
24	$\delta_1=\delta_4=-12$ $\delta_2=\delta_3=0$ Tabs	0.50	6						28

Table 3. Continued

Config No.	Tail Config	M_∞	α, deg	H, ft	Pylon Station	Pylon Config	Trajectory Condition	Parameter Set No.	Run Identification No.
24	δ_1-δ_4=-12 δ_2-δ_3=0 Tabs	0.70	4	5,000	6	Sta 6: Metric Sta 7, 8: Empty	Initiated from Carriage Position	6	33
24	δ_1-δ_4=-12 δ_2-δ_3=0 Tabs	0.90	2	↓	6	Sta 6: Metric Sta 7, 8: Empty	Initiated from Carriage Position	6	29
25	δ_1-δ_4=-12 δ_2-δ_3=0 No Tabs	0.50	6	↓	2	Sta 1: Metric Sta 2-6: Dummies Pylon 1, 3: Empty	↓	2	77
25	δ_1-δ_4=-12 δ_2-δ_3=0 No Tabs	0.70	4	↓	↓	↓	↓	↓	80
25	δ_1-δ_4=-12 δ_2-δ_3=0 No Tabs	0.90	2	↓	↓	↓	↓	↓	83
26	δ_1-δ_4=-12 δ_2-δ_3=0 Tabs	0.50	6	↓	↓	↓	↓	↓	4
26	δ_1-δ_4=-12 δ_2-δ_3=0 Tabs	0.70	4	↓	↓	↓	↓	↓	6
26	δ_1-δ_4=-12 δ_2-δ_3=0 Tabs	0.90	2	↓	↓	↓	↓	↓	14
27	δ_1-δ_4=-12 δ_2-δ_3=0 No Tabs	0.50	6	↓	↓	Sta 1: Empty Sta 2: Metric Sta 3-6: Dummies Pylon 1, 3: Empty	↓	↓	103
27	δ_1-δ_4=-12 δ_2-δ_3=0 No Tabs	0.70	4	↓	↓	↓	↓	↓	104
27	δ_1-δ_4=-12 δ_2-δ_3=0 No Tabs	0.90	2	↓	↓	↓	↓	↓	100
28	δ_1-δ_4=-12 δ_2-δ_3=0 Tabs	0.50	6	↓	↓	↓	↓	↓	17
28	δ_1-δ_4=-12 δ_2-δ_3=0 Tabs	0.70	4	↓	↓	↓	↓	↓	20
28	δ_1-δ_4=-12 δ_2-δ_3=0 Tabs	0.90	2	↓	↓	↓	↓	↓	23
29	δ_1-δ_4=-12 δ_2-δ_3=0 No Tabs	0.50	6	↓	7	Sta 1, 2: Empty Sta 3: Metric Sta 4-6: Dummies Pylon 6, 8: Empty	↓	↓	111
29	δ_1-δ_4=-12 δ_2-δ_3=0 No Tabs	0.70	4	↓	7	Sta 1, 2: Empty Sta 3: Metric Sta 4-6: Dummies Pylon 6, 8: Empty	↓	↓	112

Table 3. Continued

Config No.	Tail Config	M_∞	α, deg	H, ft	Pylon Station	Pylon Config	Trajectory Condition	Parameter Set No.	Run Identification No.
30	$\delta_1=\delta_4=-12$ $\delta_2=\delta_3=0$ Tabs	0.50	6	5,000	7	Sta 1, 2: Empty Sta 3: Metric Sta 4-6: Dummies Pylon 6, 8: Empty	Initiated from Carriage Position	2	45
30	$\delta_1=\delta_4=-12$ $\delta_2=\delta_3=0$ Tabs	0.70	4	↓	7	Sta 1, 2: Empty Sta 3: Metric Sta 4-6: Dummies Pylon 6, 8: Empty	↓	↓	46
30	$\delta_1=\delta_4=-12$ $\delta_2=\delta_3=0$ Tabs	0.90	2	↓	7	Sta 1, 2: Empty Sta 3: Metric Sta 4-6: Dummies Pylon 6, 8: Empty	↓	↓	49
31	$\delta_1=\delta_4=-12$ $\delta_2=\delta_3=0$ No Tabs	0.50	6	↓	2	Sta 1-3: Empty Sta 4: Metric Sta 5, 6: Dummies Pylon 1, 3: Empty	↓	↓	151
31	$\delta_1=\delta_4=-12$ $\delta_2=\delta_3=0$ No Tabs	0.70	4	↓	↓	↓	↓	↓	154
31	$\delta_1=\delta_4=-12$ $\delta_2=\delta_3=0$ No Tabs	0.90	2	↓	↓	↓	↓	↓	158
32	$\delta_1=\delta_4=-12$ $\delta_2=\delta_3=0$ Tabs	0.50	6	↓	↓	↓	↓	↓	52
32	$\delta_1=\delta_4=-12$ $\delta_2=\delta_3=0$ Tabs	0.70	4	↓	↓	↓	↓	↓	56
32	$\delta_1=\delta_4=-12$ $\delta_2=\delta_3=0$ Tabs	0.90	2	↓	↓	↓	↓	↓	57
33	$\delta_1=\delta_4=-12$ $\delta_2=\delta_3=0$ No Tabs	0.50	6	↓	7	Sta 1-4: Empty Sta 5: Metric Sta 6: Dummy Pylon 6, 8: Empty	↓	↓	152
33	$\delta_1=\delta_4=-12$ $\delta_2=\delta_3=0$ No Tabs	0.70	4	↓	↓	↓	↓	↓	153
33	$\delta_1=\delta_4=-12$ $\delta_2=\delta_3=0$ No Tabs	0.90	2	↓	↓	↓	↓	↓	158
34	$\delta_1=\delta_4=-12$ $\delta_2=\delta_3=0$ Tabs	0.50	6	↓	↓	↓	↓	↓	53
34	$\delta_1=\delta_4=-12$ $\delta_2=\delta_3=0$ Tabs	0.70	4	↓	↓	↓	↓	↓	54
34	$\delta_1=\delta_4=-12$ $\delta_2=\delta_3=0$ Tabs	0.90	2	↓	↓	↓	↓	↓	58

Table 3. Continued

Config No.	Tail Config	M_∞	α, deg	H, ft	Pylon Station	Pylon Config	Trajectory Condition	Parameter Set No.	Run Identification No.
35	$\delta_1=\delta_4=-12$ $\delta_2=\delta_3=0$ No Tabs	0.50	6	5,000	2	Sta 1-5: Empty Sta 6: Metric Pylon 1, 3: Empty	Initiated from Carriage Position	2	110
35	$\delta_1=\delta_4=-12$ $\delta_2=\delta_3=0$ No Tabs	0.70	4	↓	↓	↓	↓	↓	113
35	$\delta_1=\delta_4=-12$ $\delta_2=\delta_3=0$ No Tabs	0.90	2						114
36	$\delta_1=\delta_4=-12$ $\delta_2=\delta_3=0$ Tabs	0.50	6						44
36	$\delta_1=\delta_4=-12$ $\delta_2=\delta_3=0$ Tabs	0.70	4						47
36	$\delta_1=\delta_4=-12$ $\delta_2=\delta_3=0$ Tabs	0.90	2						48
37	$\delta_1=\delta_4=-12$ $\delta_2=\delta_3=0$ No Tabs	0.50	6			Sta 1: Metric Sta 2, 3: Dummies Pylon 1, 3: Empty			64
37	$\delta_1=\delta_4=-12$ $\delta_2=\delta_3=0$ No Tabs	0.70	4						67
37	$\delta_1=\delta_4=-12$ $\delta_2=\delta_3=0$ No Tabs	0.90	2						70
38	$\delta_1=\delta_4=-12$ $\delta_2=\delta_3=0$ Tabs	0.50	6						27
38	$\delta_1=\delta_4=-12$ $\delta_2=\delta_3=0$ Tabs	0.70	4						32
38	$\delta_1=\delta_4=-12$ $\delta_2=\delta_3=0$ Tabs	0.90	2						31
39	$\delta_1=\delta_4=-12$ $\delta_2=\delta_3=0$ No Tabs	0.50	6						129
39	$\delta_1=\delta_4=-12$ $\delta_2=\delta_3=0$ No Tabs	0.70	4						131
39	$\delta_1=\delta_4=-12$ $\delta_2=\delta_3=0$ No Tabs	0.90	2						133
40	$\delta_1=\delta_4=-12$ $\delta_2=\delta_3=0$ No Tabs	0.50	6		7				120

Table 3. Concluded

Config No.	Tail Config	M_∞	α, deg	H, ft	Pylon Station	Pylon Config	Trajectory Condition	Parameter Set No.	Run Identification No
40	$\delta_1=\delta_4=-12$ $\delta_2=\delta_3=0$ No Tabs	0.70	4	5,000	7	Sta 1: Empty Sta 2: Metric Sta 3: Dummy Pylon 6, 8: Empty	Initiated from Carriage Position	2	121
40	$\delta_1=\delta_4=-12$ $\delta_2=\delta_3=0$ No Tabs	0.90	2	↓	↓	↓	↓	↓	126
41	$\delta_1=\delta_4=-12$ $\delta_2=\delta_3=0$ Tabs	0.50	6						37
41	$\delta_1=\delta_4=-12$ $\delta_2=\delta_3=0$ Tabs	0.70	4						38
41	$\delta_1=\delta_4=-12$ $\delta_2=\delta_3=0$ Tabs	0.90	2						41
42	$\delta_1=\delta_2=\delta_3=\delta_4=0$ Tabs	0.50	6						144
42	$\delta_1=\delta_2=\delta_3=\delta_4=0$ Tabs	0.70	4						145
42	$\delta_1=\delta_2=\delta_3=\delta_4=0$ Tabs	0.90	2						148
43	$\delta_1=\delta_4=-12$ $\delta_2=\delta_3=0$ No Tabs	0.50	6		2	Sta 1, 2: Empty Sta 3: Metric Pylon 1, 3: Empty			119
43	$\delta_1=\delta_4=-12$ $\delta_2=\delta_3=0$ No Tabs	0.70	4						122
43	$\delta_1=\delta_4=-12$ $\delta_2=\delta_3=0$ No Tabs	0.90	2						123
44	$\delta_1=\delta_4=-12$ $\delta_2=\delta_3=0$ Tabs	0.50	6						36
44	$\delta_1=\delta_4=-12$ $\delta_2=\delta_3=0$ Tabs	0.70	4						39
44	$\delta_1=\delta_4=-12$ $\delta_2=\delta_3=0$ Tabs	0.90	2						40
45	$\delta_1=\delta_2=\delta_3=\delta_4=0$ Tabs	0.50	6						143
45	$\delta_1=\delta_2=\delta_3=\delta_4=0$ Tabs	0.70	4						146
45	$\delta_1=\delta_2=\delta_3=\delta_4=0$ Tabs	0.90	2	↓	↓	↓	↓	↓	147

Table 4. Identification of Static Stability Test Conditions for the 0.05-Scale MVB Model

Tail Config	δ_1	δ_2	δ_3	δ_4	M_∞	α, deg	Fin Hinge Line	Fuze	Fin Gap	Run Indentification No.
No Tabs	0	0	0	0	0.50	-20 to 20	5	None	None	91
↓	↓	↓	↓	↓	0.70	↓	↓	↓	↓	95
					0.90					96
					1.10					98
	-3	-3	-3	-3	0.50					102
					0.70					103
					0.90					104
					1.10					105
	-6	-6	-6	-6	0.50					108
					0.70					109
					0.90					110
					1.10					111
	-9	-9	-9	-9	0.50					114
					0.70					118
					0.90					121
↓	↓	↓	↓	↓	1.10	↓	↓	↓	↓	124

Table 4. Continued

Tail Config	δ_1	δ_2	δ_3	δ_4	M_∞	α, deg	Fin Hinge Line	Fuze	Fin Gap	Run Indentification No.
No Tabs	-12	-12	-12	-12	0.50	-20 to 20	5	None	None	128
↓	↓	↓	↓	↓	0.70	↓	↓	↓	↓	133
↓	↓	↓	↓	↓	0.90	↓	↓	↓	↓	134
↓	↓	↓	↓	↓	1.10	↓	↓	↓	↓	136
Tabs	0	0	0	0	0.50	-30 to 30	↓	↓	↓	19
↓	↓	↓	↓	↓	0.70	↓	↓	↓	↓	21
↓	↓	↓	↓	↓	0.90	↓	↓	↓	↓	25
↓	↓	↓	↓	↓	1.10	↓	↓	↓	↓	26
↓	-6	↓	↓	-6	0.50	↓	↓	↓	↓	32
↓	↓	↓	↓	↓	0.70	↓	↓	↓	↓	33
↓	↓	↓	↓	↓	0.90	↓	↓	↓	↓	34
↓	↓	↓	↓	↓	1.10	↓	↓	↓	↓	36
↓	-9	↓	↓	-9	0.50	↓	↓	↓	↓	40
↓	↓	↓	↓	↓	0.70	↓	↓	↓	↓	41
↓	↓	↓	↓	↓	0.90	↓	↓	↓	↓	42
↓	↓	↓	↓	↓	1.10	↓	↓	↓	↓	43
↓	-12	↓	↓	-12	0.50	↓	↓	↓	↓	3

Table 4. Concluded

Tail Config	δ_1	δ_2	δ_3	δ_4	M_∞	α, deg	Fin Hinge Line	Fuze	Fin Gap	Run Indentification No.
Tabs	-12	0	0	-12	0.70	-30 to 30	5	None	None	4
Tabs	↓	↓	↓	↓	0.90	-30 to 30	↓	↓	↓	5
Tabs	↓	↓	↓	↓	1.10	-30 to 30	↓	↓	↓	7
No Tabs	↓	↓	↓	↓	0.50	-30 to 30	↓	↓	↓	252
↓	↓	↓	↓	↓	0.70	↓	↓	↓	↓	253
↓	↓	↓	↓	↓	0.90	↓	↓	↓	↓	254
↓	↓	↓	↓	↓	0.50	↓	↓	FMU-56	↓	247
↓	↓	↓	↓	↓	0.70	↓	↓	↓	↓	248
↓	↓	↓	↓	↓	0.90	↓	↓	↓	↓	249
↓	0	↓	↓	0	0.70	+4 to -52	8	↓	Yes	149
↓	0	↓	↓	0	0.90	+4 to -44	↓	↓	↓	150
↓	0	↓	↓	0	1.02	+4 to -44	↓	↓	↓	151
↓	-12	↓	↓	-12	0.70	+4 to -52/ -4 to +56	↓	↓	↓	141/145
↓	↓	↓	↓	↓	0.90	+4 to -36/ -4 to 44	↓	↓	↓	142/146
Tabs	↓	↓	↓	↓	0.70	+4 to -52/ -4 to 52	↓	↓	↓	132/137
Tabs	↓	↓	↓	↓	0.90	4 to -32/ +4 to -36	↓	↓	↓	134/138

Table 5. Identification of Static Stability Test Conditions for the 0.25-Scale MVB Model

Tail Config	δ_1	δ_2	δ_3	δ_4	M_∞	α, deg	ϕ, deg	Fin Hinge Line	Fuze	Fin Gap	Run Indentification No.
Tabs	0	0	0	0	0.50	-6 to 26	0	5	None	Yes	13
↓	↓	↓	↓	↓	0.50	↓	180	↓	↓	↓	14
					0.70		0				15
					0.70		180				16
					0.90		0				17
					0.90		0				18
					0.90		180				19
					1.10		0				20
					1.10		180			↓	21
No Tabs					0.50		0			None	32
↓					0.70		↓			↓	33
					0.90						34
					1.10						35
Tabs					0.50						38
↓					0.70						39
					0.90						40
					1.10				↓		41
↓	↓	↓	↓	↓	0.50	↓	↓	↓	FMU-56	↓	44

Table 5. Continued

Tail Config	δ_1	δ_2	δ_3	δ_4	M_∞	α, deg	ϕ, deg	Fin Hinge Line	Fuze	Fin Gap	Run Indentification No.
Tabs	0	0	0	0	0.70	-6 to 26	0	5	FMU-56	None	45
↓	0	↓	↓	0	0.90	↓	0	↓	↓	↓	46
↓	0	↓	↓	0	1.10	↓	0	↓	↓	↓	47
↓	-12	↓	↓	-12	0.50	↓	0, 180	↓	↓	↓	50
↓	↓	↓	↓	↓	0.70	↓	↓	↓	↓	↓	51
↓	↓	↓	↓	↓	0.90	↓	↓	↓	↓	↓	52
↓	↓	↓	↓	↓	1.10	↓	↓	↓	↓	↓	55
↓	↓	↓	↓	↓	0.50	↓	↓	↓	None	↓	58
↓	↓	↓	↓	↓	0.70	↓	↓	↓	↓	↓	59
↓	↓	↓	↓	↓	0.90	↓	↓	↓	↓	↓	60
↓	↓	↓	↓	↓	1.10	↓	↓	↓	↓	↓	61
No Tabs	↓	↓	↓	↓	0.50	↓	↓	↓	↓	↓	64
↓	↓	↓	↓	↓	0.70	↓	↓	↓	↓	↓	65
↓	↓	↓	↓	↓	0.90	↓	↓	↓	↓	↓	66
↓	↓	↓	↓	↓	1.10	↓	↓	↓	↓	↓	69
No Fins	—	—	—	—	0.50	↓	0	↓	↓	↓	72
No Fins	—	—	—	—	0.70	↓	0	↓	↓	↓	73
No Fins	—	—	—	—	0.90	↓	0	↓	↓	↓	74

Table 5. Continued

Tail Config	δ_1	δ_2	δ_3	δ_4	M_∞	α, deg	ϕ, deg	Fin Hinge Line	Fuze	Fin Gap	Run Indentification No.
No Fins	---	---	---	---	1.10	-6 to 26	0	5	None	None	75
Tabs	0	0	0	0	0.50	↓	0, 180	↓	FMU-56	Yes	78
↓	↓	↓	↓	↓	0.50	↓	45, -135	↓	↓	↓	79
↓	↓	↓	↓	↓	0.70	↓	0 180	↓	↓	↓	80
↓	↓	↓	↓	↓	0.70	↓	45, -135	↓	↓	↓	81
↓	↓	↓	↓	↓	0.90	↓	0, 180	↓	↓	↓	82
↓	↓	↓	↓	↓	0.90	↓	45, -135	↓	↓	↓	83
↓	↓	↓	↓	↓	1.10	↓	0, 180	↓	↓	↓	84
↓	↓	↓	↓	↓	1.10	↓	45, -135	↓	↓	↓	85
↓	-12	↓	↓	-12	0.50	↓	0, 180	↓	↓	↓	88
↓	↓	↓	↓	↓	0.50	↓	90, -90	↓	↓	↓	89
↓	↓	↓	↓	↓	0.70	↓	0, 180	↓	↓	↓	90
↓	↓	↓	↓	↓	0.70	↓	90, -90	↓	↓	↓	91
↓	↓	↓	↓	↓	0.90	↓	0, 180	↓	↓	↓	92
↓	↓	↓	↓	↓	0.90	↓	90, -90	↓	↓	↓	93
↓	↓	↓	↓	↓	1.10	↓	0, 180	↓	↓	↓	94
↓	↓	↓	↓	↓	1.10	↓	90, -90	↓	↓	↓	95
↓	↓	↓	↓	↓	0.50	↓	0, 180	↓	None	↓	98

Table 5. Continued

Tail Config	δ_1	δ_2	δ_3	δ_4	M_∞	α, deg	ϕ, deg	Fin Hinge Line	Fuse	Fin Gap	Run Indentification No.
Tabs	-12	0	0	-12	0.70	-6 to 26	0, 180	5	None	Yes	99
Tabs	-12	↓	↓	-12	0.90	↓	0, 180	↓	None	↓	104
Tabs	-12	↓	↓	-12	1.10	↓	0, 180	↓	None	↓	105
No Tabs	0	↓	↓	0	0.50	↓	0	↓	FMU-56	↓	108
↓	↓	↓	↓	↓	0.50	↓	45	↓	↓	↓	109
↓	↓	↓	↓	↓	0.70	↓	0	↓	↓	↓	110
↓	↓	↓	↓	↓	0.70	↓	45	↓	↓	↓	111
↓	↓	↓	↓	↓	0.90	↓	0	↓	↓	↓	112
↓	↓	↓	↓	↓	0.90	↓	45	↓	↓	↓	113
↓	↓	↓	↓	↓	1.10	↓	0	↓	↓	↓	118
↓	↓	↓	↓	↓	1.10	↓	45	↓	↓	↓	119
↓	↓	↓	↓	↓	0.50	↓	0	↓	None	↓	122
↓	↓	↓	↓	↓	0.50	↓	45	↓	↓	↓	125
↓	↓	↓	↓	↓	0.70	↓	0	↓	↓	↓	126
↓	↓	↓	↓	↓	0.70	↓	45	↓	↓	↓	127
↓	↓	↓	↓	↓	0.90	↓	0	↓	↓	↓	128
↓	↓	↓	↓	↓	0.90	↓	45	↓	↓	↓	129
↓	↓	↓	↓	↓	1.10	↓	0	↓	↓	↓	130

Table 5. Continued

Tail Config	δ_1	δ_2	δ_3	δ_4	M_∞	α, deg	ϕ, deg	Fin Hinge Line	Fuze	Fin Gap	Run Indentification No.
No Tabs	0	0	0	0	1.10	-6 to 26	45	5	None	Yes	131
↓	-12	↓	↓	-12	0.50	↓	0	↓	↓	↓	134
↓	↓	↓	↓	↓	0.50	↓	180	↓	↓	↓	135
↓	↓	↓	↓	↓	0.70	↓	0	↓	↓	↓	136
↓	↓	↓	↓	↓	0.70	↓	180	↓	↓	↓	137
↓	↓	↓	↓	↓	0.90	↓	0	↓	↓	↓	138
↓	↓	↓	↓	↓	0.90	↓	180	↓	↓	↓	139
↓	↓	↓	↓	↓	1.10	↓	0	↓	↓	↓	140
↓	↓	↓	↓	↓	1.10	↓	180	↓	↓	↓	141
↓	↓	↓	↓	↓	0.50	↓	0, 180	↓	FMU-56	↓	144
↓	↓	↓	↓	↓	0.50	↓	45, -135	↓	↓	↓	145
↓	↓	↓	↓	↓	0.50	↓	90, -90	↓	↓	↓	146
↓	↓	↓	↓	↓	0.70	↓	0, 180	↓	↓	↓	147
↓	↓	↓	↓	↓	0.70	↓	45, -135	↓	↓	↓	148
↓	↓	↓	↓	↓	0.70	↓	90, -90	↓	↓	↓	149
↓	↓	↓	↓	↓	0.90	↓	0, 180	↓	↓	↓	150
↓	↓	↓	↓	↓	0.90	↓	45, -135	↓	↓	↓	151
↓	↓	↓	↓	↓	0.90	↓	90, -90	↓	↓	↓	152

Table 5. Continued

Tail Config	δ_1	δ_2	δ_3	δ_4	M_∞	α, deg	ϕ, deg	Fin Hinge Line	Fuze	Fin Gap	Run Indentification No.
No Tabs	-12	0	0	-12	1.10	-6 to 26	0, 180	5	FMU-56	Yes	153
↓	↓	0	0	↓	1.10	↓	45, -135	↓	↓	↓	154
		0	0		1.10		90, -90				155
		-12	-12		0.50		0, 180				158
		↓	↓		0.70		0, 180				159
					0.90		↓				160
					1.10				↓		161
					0.50				None		164
					0.70				↓		165
					0.90						166
					1.10						167
Tabs					0.50						170
↓					0.70						171
					0.90		↓				172
					1.10		180				173
					1.10		0		↓		174
					0.50		0, 180		FMU-56		177
↓	↓	↓	↓	↓	0.70	↓	0, 180	↓	FMU-56	↓	178

Table 5. Concluded

Tail Config	δ_1	δ_2	δ_3	δ_4	M_∞	α, deg	ϕ, deg	Fin Hinge Line	Fuze	Fin Gap	Run Indentification No.
Tabs	-12	-12	-12	-12	0.90	-6 to 26	0, 180	5	FMU-56	Yes	179
↓	↓	-12	-12	↓	1.10	↓	↓	↓	FMU-56	↓	180
↓	↓	0	0	↓	0.50	↓	↓	↓	FMU-110	↓	183
↓	↓	↓	↓	↓	0.70	↓	↓	↓	↓	↓	188
↓	↓	↓	↓	↓	0.90	↓	↓	↓	↓	↓	189
↓	↓	↓	↓	↓	1.10	↓	↓	↓	↓	↓	190
↓	0	↓	↓	0	0.50	↓	0	↓	↓	↓	197
↓	↓	↓	↓	↓	0.70	↓	↓	↓	↓	↓	198
↓	↓	↓	↓	↓	0.90	↓	↓	↓	↓	↓	199
↓	↓	↓	↓	↓	1.10	↓	↓	↓	↓	↓	200
Tabs Faired In	↓	↓	↓	↓	0.50	↓	↓	↓	FMU-56	↓	203
↓	↓	↓	↓	↓	0.50	↓	45	↓	↓	↓	204
↓	↓	↓	↓	↓	0.70	↓	0	↓	↓	↓	205
↓	↓	↓	↓	↓	0.70	↓	45	↓	↓	↓	206
↓	↓	↓	↓	↓	0.90	↓	0	↓	↓	↓	207
↓	↓	↓	↓	↓	0.90	↓	45	↓	↓	↓	208
↓	↓	↓	↓	↓	1.10	↓	0	↓	↓	↓	209
↓	↓	↓	↓	↓	1.10	↓	45	↓	↓	↓	210
No Tabs	↓	↓	↓	↓	0.50	↓	0	↓	None	None	213
↓	↓	↓	↓	↓	0.50	↓	45	↓	↓	↓	214
↓	↓	↓	↓	↓	0.70	↓	0	↓	↓	↓	215
↓	↓	↓	↓	↓	0.70	↓	45	↓	↓	↓	216
↓	↓	↓	↓	↓	0.90	↓	0	↓	↓	↓	217

Table 6. Dynamic Stability Test Configurations and Test Conditions for the 0.075-Scale MVB Model

Config	α, deg	ϕ, deg	δ_1	δ_2	δ_3	δ_4	Mach No. 0.50	0.70	0.90	1.10
1	0→45	0	0	0	0	0	3	4	5	6
1	0→45	45	0	↓	↓	0	14	13	12	11
1	-45→45	0	-12	↓	↓	-12	19	20	21	22
2	0→45	0	0	↓	↓	0	30	29	28	27
2	-5→45	45	0	↓	↓	0	35	36	37	38
2	-45→45	0	-12	↓	↓	-12	46	45	44	43
1	-45→45	↓	-12	-12	-12	-12	51	52	53	54, 57
2	-45→45	↓	-12	-12	-12	-12	65	64	63	62
3	-5→45	↓	—	—	—	—	70	71	72	73
4	-5→45	↓	0	0	0	0	81	80	79	78
4	-45→45	↓	-12	0	0	-12	86	87	88	89

Configuration	Description
1	Body + Fins + FMU-56 Fuze
2	Body + Fins + FMU-56 Fuze + Tabs
3	Body Alone
4	Body + Fins

Table 7. Typical Uncertainties for Force and Moment Coefficient Data and Trajectory Data

Force and Moment Coefficient Data

δC_N	δC_Y	δC_A	δC_m	δC_n
±0.08	±0.04	±0.02	±0.04	±0.04

Captive Trajectory Data

t, sec	δX_p	δY_p	δZ_p	$\delta\theta$	$\delta\psi$
0.2	±0.02	±0.01	±0.003	±0.20	±0.10

NOMENCLATURE

BL	Aircraft buttock line from plane of symmetry, in., model scale
b	Store reference dimension, ft, full scale
C_A	Store axial-force coefficient, axial force/$q_\infty S$
$C\ell$	Store rolling-moment coefficient, rolling moment/$q_\infty Sb$
$C\ell_p$	Store roll-damping derivative, $dC\ell/d(pb/2V_\infty)$
C_m	Store pitching-moment coefficient, referenced to the store cg, pitching moment/$q_\infty Sb$
C_{m_α}	Rate of change of C_m with angle of attack, per radian
C_{m_q}	Store pitch-damping derivative, $\partial C_m/\partial(qb/2V_\infty)$
$C_{m_{\dot\alpha}}$	Store pitch-damping derivative, $\partial C_m/\partial(\dot\alpha b/2V_\infty)$
C_N	Store normal-force coefficient, normal force/$q_\infty S$
C_{N_α}	Rate of change of C_N with angle of attack, per radian
C_n	Store yawing-moment coefficient, referenced to the store cg, yawing moment/$q_\infty Sb$
C_{n_r}	Store yaw-damping derivative, $dC_n/d(rb/2V_\infty)$
C_Y	Store side-force coefficient, side force/$q_\infty S$
FS	Aircraft fuselage station, in., model scale
F_{Z_1}	Forward ejector force, lb
F_{Z_2}	Aft ejector force, lb
H	Pressure altitude, ft
H.L.	Fin hinge line
I_{xx}	Full-scale moment of inertia about the store X_B axis, slug-ft^2
I_{xz}	Full-scale product of inertia in the store X_B - Z_B plane, slug-ft^2

I_{yy} Full-scale moment of inertia about the store Y_B axis, slug-ft^2

I_{zz} Full-scale moment of inertia about the store Z_B axis, slug-ft^2

M_∞ Free-stream Mach number

$\overline{m}$ Full-scale store mass, slugs

p Store angular velocity about the X_B axis, radians/sec

p_∞ Free-stream static pressure, psfa

q Store angular velocity about the Y_B axis, radians/sec

q_∞ Free-stream dynamic pressure, psf

Re_d Reynolds number based on model diameter

r Store angular velocity about the Z_B axis, radians/sec

S Store reference area, ft^2, full scale

t Real trajectory time from initiation of trajectory, sec

V_∞ Free-stream velocity, ft/sec

WL Aircraft waterline from reference horizontal plane, in., model scale

X_P Separation distance of the store cg parallel to the pylon axis system X_P direction, ft, full scale measured from the prelaunch position

X_{cg} Full-scale cg location, ft, from nose of store

X_{L_1} Forward ejector location relative to the store cg, positive forward of store cg, ft, full scale

X_{L_2} Aft ejector location relative to the store cg, positive forward of store cg, ft, full scale

X_{NP} Neutral point location, $X_{cg} - (C_{m_\alpha}/C_{N_\alpha})b$, in.

Y_P Separation distance of the store cg parallel to the pylon axis system Y_P direction, ft, full scale measured from the prelaunch position

Z_E Ejector stroke, ft

Z_o Initial offset of store from carriage position, ft, full scale

Z_P Separation distance of the store cg parallel to the pylon-axis system Z_P direction, ft, full scale measured from the prelaunch position

a Aircraft model angle of attack relative to the free-stream velocity vector, deg

$\dot{a}$ Time rate of change of angle of attack, radians/sec

a_s Store model angle of attack relative to the free-stream velocity vector, deg

δ Fin deflection angle, deg

$\Delta\theta$ Angle between the store longitudinal axis and its projection in the X_P-Y_P plane, positive when store nose is raised as seen by the pilot, deg

$\Delta\psi$ Angle between the projection of the store longitudinal axis in the X_P-Y_P plane and the X_P axis, positive when the store nose is to the right as seen by the pilot, deg

$\Delta\phi$ Angle between the store lateral axis and the intersection of the Y_B-Z_B and X_P-Y_P planes, positive for clockwise rotation when looking upstream, deg

$\Delta\theta_R$ Angle at which store is released from pivotal motion, deg

FLIGHT-AXIS SYSTEM COORDINATES

Directions

X_F Parallel to the free-stream wind vector, positive direction is forward as seen by the pilot

Y_F Perpendicular to the X_F and Z_F directions, positive direction is to the right as seen by the pilot

Z_F In the aircraft plane of symmetry and perpendicular to the free-stream wind vector, positive direction is downward

The flight-axis system origin is coincident with the aircraft cg and remains fixed with respect to the aircraft during store separation. The X_F, Y_F, and Z_F coordinate axes do not rotate with respect to the initial flight direction and attitude.

STORE BODY-AXIS SYSTEM COORDINATES

Directions

X_B Parallel to the store longitudinal axis, positive direction is upstream in the prelaunch position

Y_B Perpendicular to the store longitudinal axis, and parallel to the flight-axis system X_F-Y_F plane when the store is at zero roll angle, positive direction is to the right looking upstream when the store is at zero yaw and roll angles

Z_B Perpendicular to both the X_B and Y_B axes, positive direction is downward as seen by the pilot when the store is at zero pitch and roll angles

The store body-axis system origin is coincident with the store cg and moves with the store during separation from the airplane. The X_B, Y_B, and Z_B coordinate axes rotate with the store in pitch, yaw, and roll so that mass moments of inertia about the three axes are not time-varying quantities.

PYLON-AXIS SYSTEM COORDINATES

Directions

X_P Parallel to the store longitudinal axis when in the carriage position on the aircraft, positive direction is forward as seen by the pilot

Y_P Perpendicular to the X_P axis and parallel to the flight-axis system X_F-Y_F plane, positive direction is to the right as seen by the pilot

Z_P Perpendicular to both the X_P and Y_P axes, positive direction is downward

The pylon-axis system origin is coincident with the store cg in the prelaunch carriage position. The axes are rotated with respect to the flight-axis system by the prelaunch yaw and pitch angles of the store. Both the origin and the direction of the coordinate axes remain fixed with respect to the flight-axis system throughout the trajectory or survey.